THE EFFECT OF MINOR ADDITION ELEMENTS ON THE CORROSION BEHAVIOUR OF BARE AND COATED STEELS

ISOLDA COSTA

A Thesis submitted to the

UNIVERSITY OF MANCHESTER

for the degree of

DOCTOR OF PHILOSOPHY

in the Faculty of Technology

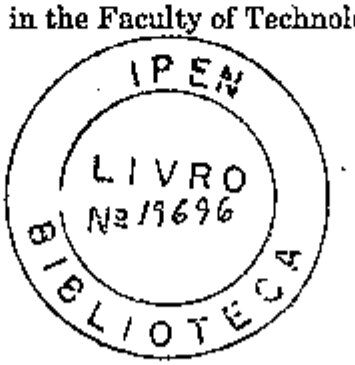

Corrosion and Protection Centre

UMIST

1991

Oriel Coll

James David Scantlebury

Declaration

I declare that no part of the work presented in this Thesis has previously been submitted to this or another University, in support of an application for any other degree of qualification.

Isolda Costa

ISOLDA COSTA

ABSTRACT

Corrosion tests were carried out to investigate the effect of small differences in the composition of steels on their corrosion behaviour when bare and coated. Tests were performed in near neutral media and using various electrochemical techniques. The steels chosen for the study included two types of steels, namely, mild steels and low alloy steels. Batches of these types of steels, originating from two different manufacturers, were used. As a background to the study, the electrochemical characteristics of the bare steels were determined. This included measuring their polarization resistance, full polarization curves, and electrochemical impedance responses. The results indicated slight differences in electrochemical behaviour.

Long term immersion tests of coated steels, low-alloy steels and mild steels, were also carried out to study the anti-corrosion properties of the coated system in a solution containing 3.5% wt sodium chloride. A clear alkyd lacquer of approximately 30 μm thickness, was chosen as the coating in order to facilitate the monitoring of the corrosion features. Visual observation of the corrosion characteristics of the surface was carried out simultaneously with the measurement of the corrosion potential and electrochemical impedance measurements of the coated steel specimens.

The corrosion resistance of the coated steels, immersed in near neutral solutions, showed small differences in behaviour which seemed to be related to the microstructural characteristics of the steel. However, no significant differences were found between the corrosion behaviour of the two types of steels used, mild steel and low-alloy steel types, with similar inclusion contents.

Furthermore, cabinet tests with wet and dry cycles were undertaken on scribed specimens. Two aggressive atmospheres were used in these tests. In one

test the corrosion performance of the steels with larger heterogeneity contents was superior to that of the steels with less inhomogeneities. However, the other test did not distinguish the various coated specimens in terms of their corrosion behaviour.

In order to elucidate the phenomena occurring at the coating-substrate interface, Auger Spectroscopy and XPS analysis were performed on coated specimens after the test was terminated. The identification of aggressive species and products of the corrosion process at the interface was possible through the use of these two techniques. There was some indication that the delamination was a result of the cathodic process around the anodic site.

To my parents

ACKNOWLEDGEMENTS

The author would like to thank Dr. G.E. Thompson and Professor G.C. Wood of the Corrosion and Protection Centre, U.M.I.S.T., for providing research facilities, and the "Conselho Nacional de Pesquisas e Desenvolvimento Científico e Tecnológico" (CNPq), and "Instituto de Pesquisas Energéticas e Nucleares" (IPEN/CNEN), Brazil, for the financial support provided.

The author also wishes to express her gratitude to:

Dr. J.D. Scantlebury, her supervisor, for his help and encouragement through this work.

Dr. S.E. Faidi for his interest in her work, useful suggestions, friendship, and for kindly reading this thesis.

Mr. J.L.Rossi for his patience, encouragement, and helpful discussions on the metallurgical aspects of this research.

Dr. J. Walton, Dr B. Bethume, and D. Moore for help with the surface analysis.

Her past and present colleagues of D-6 for their help and friendship.

Her friends in Manchester who contributed to an unforgettable stay.

CONTENTS

CHAPTER 1

PRINCIPLES OF CORROSION AND CORROSION PROTECTION BY ORGANIC COATINGS

1.1 - Introduction

The corrosion of metals may be defined as the degradation of the metallic material through chemical or electrochemical reactions of the metal with its environment[1]. The physical and chemical properties of the products of these reactions are important since they may both influence the subsequent rate of metal dissolution. If the corrosion products formed are adherent, compact and protective, the corrosion rate will slow down or eventually stop. However, most of the corrosion products are soluble and form away from the metal interface, so that, they cannot provide effective protection. Thus, the metal in a corroding environment continues to dissolve until it is consumed, or until it loses its mechanical properties.

The cost of corrosion, including measures for protection against corrosion, is very high in any industrial country. It is estimated to be around 3 % of the Gross National Product. Besides, corrosion causes a waste of natural resources, pollution of the environment and may have deleterious influence on metallic structures and on the safety of people[1]. Corrosion control can be achieved by various methods. These include modification of the environment (using scavengers, inhibitors, etc), modification of the metal (by addition of alloying elements or heat treatment), modification of the electrode potential metal/corrosive environment (by cathodic or anodic protection), and modification of the metal/environment interface (by the application of a protective coating on the metal).

The present study is concerned with the effect of minor alloying elements on the corrosion behaviour of steel substrates, bare and coated, and under various testing conditions.

1.2 - Principles of the corrosion of mild steel and low-alloy steel

Carbon steel and low-alloy steels as a group represent by far the most widely used structural metallic materials due to their availability at low cost, combined with their excellent mechanical properties and ease of fabrication. Unfortunately, carbon steels are not very resistant to corrosion, reacting rapidly with oxygen and water and forming a non protective corrosion product.

Although unalloyed steels corrode at high rates in aggressive atmospheres, the presence of only a few hundredths per cent of copper has a large effect in lowering weight losses. Copper additions over 0.2 %, however, are less effective. In the case of steels alloyed with nickel, copper additions up to 1 % are decidedly helpful in increasing atmospheric corrosion resistance. Chromium is especially helpful in decreasing the amount of corrosion occurring during long exposure periods[2]. For particular applications, the use of reduced weight of the low-alloy steel, combined with its high strength can narrow or eliminate the difference in total cost between these steels and carbon steel.

There have been only very few systematically designed programs to investigate the effect of alloying elements on the corrosion resistance of bare steels to aqueous solutions. Far less is known about the effect of minor alloying elements in diverse steels on their corrosion behaviour when coated and under fully immersed conditions.

The corrosion of steel in aqueous solutions consists of two main reactions, the anodic oxidation of iron and the cathodic reduction of non metallic species[3]. In aqueous environments the predominant corrosion process is electrochemical, that is, metallic wastage occurs by anodic dissolution[4]. The same is also true for

the corrosion of metals in moist air. The basic corrosion mechanism is similar in both situations.

Thermodynamic considerations offer fundamental predictions about the possibility or impossibility of a corrosion reaction. However, they are only applicable to chemical or electrochemical systems when these are in equilibrium. No information is thus given about the rate at which a corrosion reaction proceeds.

1.2.1 - Potential-pH diagrams

The equilibrium of a corrosion reaction is determined by two important factors, the potential and the pH of the electrolyte to which the metal is exposed.

A very useful form of presentation of both, the potential dependent and pH dependent equilibria, was produced by Pourbaix[7] in the form of E_H/pH diagrams, often called Pourbaix diagrams. In these diagrams, the two parameters E_H and pH are plotted for the various equilibria on normal cartesian coordinates with E_H as vertical axis or ordinate, and pH as horizontal axis or abscissa.

In the E_H/pH diagram the two reduction reactions, hydrogen evolution and oxygen reduction, are represented by sloping lines, and they are shown in the diagram of Figure 1.1 as the lines (ab) and (cd). Hydrogen evolution is possible only at potentials below the line (ab), and only above the line (cd) is oxygen reduction possible. So there is a domain of the E_H/pH diagram in which the electrolysis of water is not thermodynamically possible.

The E_H/pH diagram for iron

While iron can dissolve to Fe^{2+}, iron can also undergo other reactions with water. In order to account for all the likely corrosion phenomena, it is necessary to know what products are possible.

The full diagram for iron is quite complex, since many equilibria are involved, but fortunately a useful simplified diagram can be obtained from a consideration of the following equilibria[8]:

(i) $Fe \leftrightarrow Fe^{2+} + 2e^-$ (1.1)

(ii) $Fe^{2+} \leftrightarrow Fe^{3+} + e^-$ (1.2)

(iii) $Fe^{2+} + 3(OH)^- \leftrightarrow Fe(OH)_3 + e^-$ (1.3)

(iv) $Fe^{3+} + 3H_2O \leftrightarrow Fe(OH)_3 + 3H^+$ (1.4)

(v) $Fe + 3H_2O \leftrightarrow Fe(OH)_3 + 3H^+ + 3e^-$ (1.5)

(vi) $Fe + 2H_2O \leftrightarrow FeO_2H^- + 3H^+ + 2e^-$ (1.6)

(vii) $FeO_2H^- + H_2O \leftrightarrow Fe(OH)_3 + e^-$. (1.7)

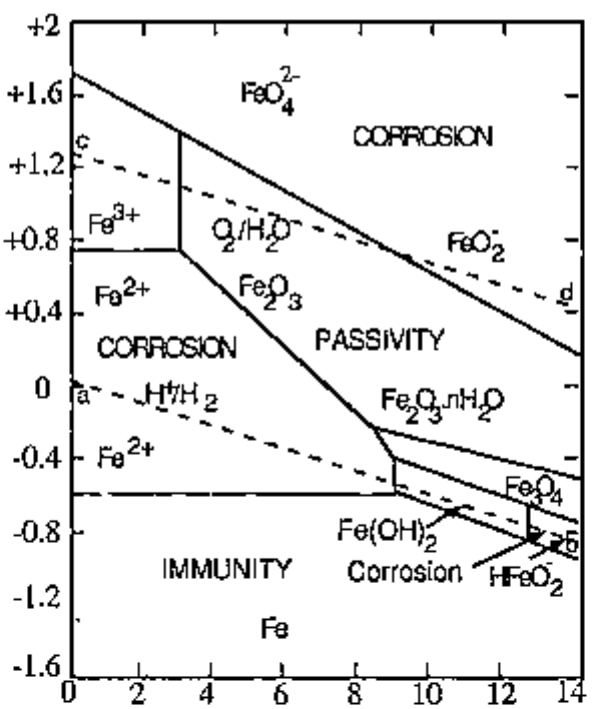

Figure 1.1 - Simplified E_H/pH diagram for Fe-H_2O[8].

Although the extension of the thermodynamic treatment to include the effects of pH represents a considerable advance in the search for a general theory of corrosion, it is important to acknowledge the limitations of the E_H/pH diagrams. The following limitations apply[8]:

(1) The thermodynamic approach excludes kinetic data.

(2) Only those equilibria concerned with metal in conjunction with water are used, so that only the hydroxyl ion (OH^-) is considered as the precipitating or complexing ion.

(3) Although the domain associated with the metal hydroxide is classified passivity, the hydroxide precipitate may not always provide a protective film, particularly if precipitation does not occur at the metal surface. Even in those cases where protection is afforded by a hydroxide film, subsequent changes in the environment may cause film failure and consequent corrosion.

(4) Highly localized pH changes at the electrode surface can occur as the result of several reactions involving the production of hydrogen ions (H^+) or hydroxyl ions. Since these may not greatly influence the bulk pH, prediction of behaviour based upon bulk pH measurements may be quite misleading.

(5) The diagrams are derived from known reactions between pure metals and pure water. In practice, corrosion problems arise from water containing dissolved salts and the additional reactions that do not occur on a pure metal.

Much more important, particularly in the case of corrosion, is a knowledge of the rates at which reactions proceed in practice, and the thermodynamic data represents only partial information about the reaction rates. The corrosion rates are in the domain of **electrode kinetics**.

1.2.2 - Electrode kinetics

The surface of a metal is in general anisotropic, because the manufacture and working of the metal distorts the metallic lattice. It allows that areas or sites in the surface are made anodic in relation to others, which are cathodic. The presence of an electrolyte on the surface gives rise to an electrochemical cell. The corrosion of iron and steel in the presence of an electrolyte solution is electrochemical in nature[1,3-5].

There are two directions in which an electrochemical reaction can proceed. At an anodic site iron leaves the lattice as ferrous ions, becomes solvated and moves away from the surface. This involves a loss of electrons, for example, in the case of iron:

$$Fe \rightarrow Fe^{2+} + 2e^- \quad (1.8)$$

and this is known as an oxidation process. The transfer of 2 electrons in equation (1.8) is not likely to occur at once. It has been suggested that this reaction might involve two steps[3]:

$$Fe \rightarrow Fe^{+} + e^- \quad \text{(r.d.s.)} \quad (1.9)$$

$$Fe^{+} \leftrightarrow Fe^{2+} + e^- \quad (1.10)$$

The equation (1.9) is considered the rate determining step (r.d.s.). The ferrous ions and hydroxyl ions concentrations, have also been found to affect the dissolution of iron, and the most probable mechanism for the iron dissolution has been suggested as[3]:

$$Fe + H_2O \leftrightarrow FeOH + H^+ + e^- \quad (1.11)$$

$$FeOH \rightarrow FeOH^+ + e^- \quad \text{(r.d.s)} \quad (1.12)$$

$$FeOH^+ + H^+ \leftrightarrow Fe^{2+} + H_2O \quad (1.13)$$

For this reaction to take place the electrons released must travel through the metal to a cathodic site where they may be discharged. The reaction which takes place at the cathode consumes the electrons generated as a result of the anodic reactions, and it is known as the reduction process.

The two most common cathodic reactions are:

(1) - the hydrogen evolution reaction;

In ***acid solutions***, the overall reaction is given by:

$$2H_3O^+ + 2e^- \rightarrow H_2 + 2H_2O \quad (1.14)$$

and in ***neutral or alkaline solutions*** by:

$$2H_2O + 2e^- \rightarrow H_2 + 2OH^- \quad (1.15)$$

(2) - the oxygen reduction reaction;

In ***acid solution***, the overall reaction is expressed as:

$$O_2 + 4H_3O^+ + 4e^- \rightarrow 6H_2O \quad (1.16)$$

and in ***neutral or alkaline solutions*** as:

$$O_2 + 4e^- + 2H_2O \rightarrow 4OH^- \quad (1.17)$$

The hydrogen evolution reaction occurs mainly in acid solutions, but sometimes also in strongly alkaline solutions. In neutral or mildly alkaline solutions the reduction of dissolved oxygen is more likely, provided that oxygen is available at the metal surface.In the hydrogen evolution reaction, the activation polarization dominates both, the anodic and cathodic processes. Concentration polarization is however observed for the oxygen reduction reaction, and this is due to the limited solubility of oxygen in water and in aqueous solutions. Corrosion rates in these media will therefore, as a rule, be limited by the diffusion rate of oxygen. If diffusion of dissolved oxygen determines the corrosion rate, we have a case of pronounced cathodic control, since, within certain limits, the corrosion current will then be independent of the slope and position of the anodic polarization curve.

After the ferrous ions have become solvated, they move away from the anodic areas and react with solvated hydroxide ions from the cathodic areas, according to:

$$Fe^{2+} + 2OH^- \rightarrow Fe(OH)_2 \quad (1.18)$$

which is a white precipitate of relatively high solubility (1.64×10^{-3} g.dm^{-3})[6]. In the presence of oxygen in solution this is oxidised to hydrated ferrous hydroxide, FeO.OH, which is sometimes written as $Fe_2O_3.H_2O$.

$$Fe(OH)_2 + 1/2\,O_2 \rightarrow FeO.OH + OH^- \quad (1.19)$$

$Fe_2O_3.H_2O$ is known as rust and is highly insoluble (4.8×10^{-8} g.dm^{-3})[6].

The composition of what is described as rust can vary considerably, but it always contains lepidocrocite, γ-FeO.OH . Although the solubility of the hydrate ferrous hydroxide is very low, the precipitate, orange in colour, is formed well

away from the metal surface, and cannot slow down the corrosion reaction by hindering the movement of ions or oxygen[2].

1.3 - Atmospheric exposure of steels

Steel surfaces exposed to the atmosphere are subjected to similar conditions to those existing in bulk solutions. Oxygen is available from the air, and anodic and cathodic areas are present on the surface. There exists a critical humidity below which corrosion is negligible and above which the amount of atmospheric corrosion increases considerably. Steel does not rust at a relative humidity of less than about 60 %. However at relative humidities greater than that , the steel surface is covered with a thin, usually invisible film of condensed or adsorbed water[1].

The polarization behaviour of metals covered with thin films of solutions indicate some significant differences from the bulk solution behaviour. The change in cathodic polarization is very important. The oxygen reduction reaction becomes much easier. This means that the thin film is capable of sustaining a significantly faster reaction than bulk solutions[9].

The presence of impurities in the atmosphere, particularly dust and sulphur dioxide, affect the atmospheric corrosion of steels. If the metal is covered by solid particles, such as dust, dirt and soot, moisture and salts are retained for a longer time[9]. Sodium chloride is an impurity which is present in any marine atmosphere. This and many other contaminants such as ammonium sulphate, will not only dissolve in the water and increase the conductivity, but chlorides may also interfere with passivation processes. Chlorides are prone to initiate localized attack resulting in pit, which may become quite deep, sometimes resulting in complete perforation[8].

The corrosion products formed on iron and mild steel when exposed to industrial atmospheres are usually rich in sulphates. Even in areas of high

atmospheric chloride contamination, it is still common to find that the major part of any corrosion product is sulphate. This is because rain will dissolve the relatively soluble chlorides leaving behind the less soluble sulphates[9]. The role of SO_2 on the mechanism of atmospheric corrosion has received much attention. There are two main proposed mechanisms. First, the electrochemical cycle[10], in which iron is gradually incorporated into rust (FeO.OH):

$$Fe \leftrightarrow Fe^{2+} + 2e^- \quad (1.20)$$

$$Fe^{2+} + 8FeO.OH^- + 2e^- \leftrightarrow 3Fe_3O_4 + 4H_2O \quad (1.21)$$

$$3Fe_3O_4 + 0.75\,O_2 + 4.5\,H_2O \leftrightarrow 9FeO\,OH \quad (1.22)$$

Secondly, the acid regeneration mechanism involving a sequence of reactions following the oxidation of SO_2 to SO_3, and its dissolution in water:

$$Fe + H_2SO_4 \rightarrow FeSO_4 \rightarrow Fe_2(SO_4)_3 \rightarrow FeO.OH + H_2SO_4 \quad (1.23)$$

Acid regeneration is considered to occur very slowly by comparison with the electrochemical cycle. Insoluble sulphate is formed and gradually removes Fe^{2+} and SO_4^{2-} from the liquid[1]. The ferrous ions produced at the anodic sites are oxidised to ferric ions by atmospheric oxygen and the resulting rust being porous and loosely bound to the surface, does not protect the steel surface from further corrosion.

Weathering steels, however, are known to develop a protective rust in mildly industrial atmosphere, and therefore would not need painting. The rust that forms on the surface of such steels has been described as an amorphous rust[11]. It seems that the protectiveness arises from the effect of the alloying elements in causing rapid nucleation of rust in the thin layers of water molecules that are on the surface. The processes occurring in a very thin layer of water molecules, produce Fe^{2+} and OH^- ions, which interact with each other because they remain close to the steel surface, and it would account for the amorphous nature of the FeO.OH. This explanation is consistent with the fact that these steels

develop protective rust layers only under the conditions specified, that is covered with a few layers of water molecules. Immersed in aqueous solutions, such steels do not seem to present very distinct differences in the corrosion rates when compared to mild steel.

1.4 - Corrosion of coated metals

The corrosion of a metal beneath a polymeric coating is an electrochemical process that follows the same principles of corrosion of a bare metal. The main difference is that the reactants often reach the metal through a solid, and in the early stages of corrosion, the small volumes of liquid involved, result in high values of pH and ion concentration.

The total corrosion process, according to Leidheiser[12], can be divided in the following components:

(1) - transport through the coating of water, oxygen, and ions;

(2) - development of an aqueous phase at the coating/metal interface;

(3) - activation of the metal surface for the anodic and cathodic reactions, and;

(4) - deterioration of the coating/metal interface bond.

Coatings generally contain defects and the corrosion process is bounded to start at the defective point. Iron dissolves at these points, that act as anodic sites, and in the case of neutral solutions, hydroxyl ions are formed at local cathodic sites. As rust builds up on the steel substrate, the permeation of oxygen through the rust layer becomes more difficult, and the site of cathodic reaction shifts to the periphery of the rust layer. The local high pH generated in the cathodic sites, at the periphery of the rust layer, disrupts the bonding between coating and the substrate with a subsequent penetration of electrolyte enlarging the area available for the cathodic reaction. Figure 1.2 illustrates schematically the corrosion processes taking place in a defective coating exposed to a corrosive

environment[13]. The pH at the periphery of the rust can be very high (12 to 13). The advancing front of adhesion loss, in the next growing stage, is considerably ahead of the corrosion development. Blistering and further corrosion results and, finally the film breaks down followed by more severe corrosion.

Three major factors that affect the tendency of a coated metal to corrode are: (1) the nature of the substrate metal,

(2) the character of the interfacial region between the coating and the substrate, and

(3) the nature of the coating.

1.4.1 - The nature of the substrate

Many authors[14-19] have studied the influence of the substrate on the corrosion behaviour of the coated system. They worked with metals of very different electrochemical properties and concluded that the corrosion performance of these painted metals was dependent on the nature of the substrate.

Tomashov and co-workers[14] tested the electrochemical behaviour of platinum, copper and iron coated with very thin (1-4 μm) insulating films, and concluded that the electrochemical nature of the metal is one of the deciding factors determining the initial deterioration of the insulating film. The rate of film deterioration was observed to increase with the more active electrode potential of the metal, in the order, platinum, copper and iron. The same authors, in a latter paper[15], stated that the electrochemical nature of the metal proper has very little effect on the stability and integrity of the coating when the metal surface is coated with insulating films without defects. The non-defective film would eliminate the possibility of the penetration of the aggressive medium to the metal surface.

However, it is well known that perfect coatings are non-existent in practice. There are always small regions where the organic coating is not in contact with the metal, and during the service lifetime of the coating, accidental defects are introduced into the coating. If the reactants are available, the corrosion reaction can occur and the electrochemical properties of the substrate are important in the corrosion reaction proceeding under the organic coating.

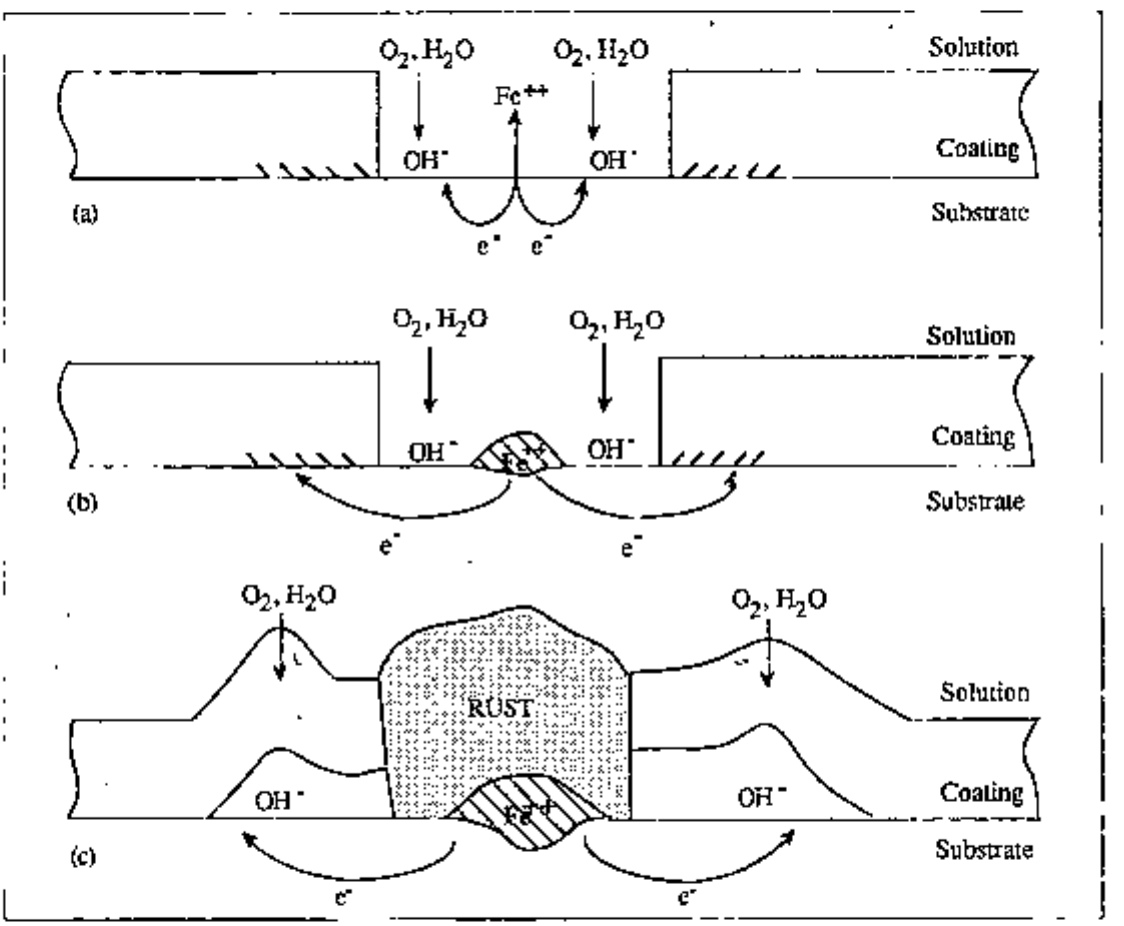

Figure 1.2 - Schematic diagram of corrosion processes that takes place in coated steel exposed to corrosive environments. (a) Initially iron dissolution and oxygen reduction occurs at adjacent and similar sites; further in the process, rust deposits, leading to the separation of cathodic and anodic sites and causing paint adhesion failure, (b) and (c)[13].

Walter[16] measured the immersion time taken for the resistive and capacitive components of sample impedance to reach selected values, of paint films (25 μm) on steel, galvanised steel, Zn/55 % Al coated steel, and aluminium immersed in 5 % NaCl solution at 50 °C. He concluded that the corrosion

performance of the painted metals was directly related to the corrosion resistance of the unpainted substrate. Kittleberger and Elm[17] also concluded that the nature of the substrate was responsible for marked differences in the susceptibility of coatings to blistering. Differences in adhesion of the paint coatings to the substrates tested were held responsible for the relative resistance to blistering. The substrates used consisted of steel, duralumin, zinc and glass, painted with zinc chromate primer plus a top coat of an alkyd paint.

Miller[18] working with an acrylic coating on aluminium, iron and steel, showed that the reactivity of the metal substrate and the type of corrosion product formed had a great influence upon the life of a protective coating. After 1000 hours test in salt spray the coating on aluminium was in good condition whereas the same coating on iron and steel panels was badly deteriorated. Koehler[19] studying the cathodic disbondment of protective organic coatings, observed that the type of coating and the type of substrate had an influence upon the cathodic disbondment. An oleoresinous coating on steel disbonded after immersion in ammonium hydroxide solution, however an epoxyphenolic coating on the same steel was not similarly disbonded. The oleoresinous coating remained firmly attached on tinplate after 24 hours exposure, but was disbonded on steel after only 4 hours immersion.

Different metals have been found to show remarkable differences in the catalytic properties for the cathodic reaction that occurs in mildly corrosive environments, namely the oxygen reduction reaction,

$$H_2O + 1/2\,O_2 + 2\,e^- \rightarrow 2\,OH^- \qquad (1.24)$$

Aluminium, for example, behaves as a very poor catalyst; tin as a moderate catalyst; and copper, iron, and zinc as excellent catalyst for this reaction. The cathodic reaction is the critical reaction in cathodic delamination. Aluminium is thus considered as a good substrate for paint for those situations where the cathodic reaction is the major mode by which the system deteriorates[20]. It has been pointed out[21] that minor addition of alloying elements to carbon steels affect

the corrosion performance of their coated systems when exposed to aggressive atmospheres.

The nature of the substrate has also been found to affect the rate of water transmission through a coating[22-30]. Many investigators[24,26,27] observed that films attached to a glass substrate absorbed less water than in the free condition, However, Funke and co-workers[28,29] found that in some cases the amount of water absorbed by attached films can be higher than that of free films. This difference in water absorption was attributed to the accumulation of water at the film/substrate interface. Holtzmann[22] compared the water permeability of adherent and free films by capacitance measurements and found that the water permeability of the adherent films was slightly lower than that of free films. The values of water uptake of supported films may however be higher than those corresponding to free films if water is allowed to accumulate at the film/substrate interface[28,29].

D'Alkaine and collaborators[30] found that the water content of attached epoxy-chromate coating on steel are higher than those of free films. The water content for films attached on glass was, however, of the same order of magnitude as of the free film. The substrate also seems to affect the transmission of ionic species through the coating. Murray[31] compared the absorption of chloride ions by an epoxy polyamide free film with the same coating on an aluminium substrate, and found that the diffusion coefficient was always higher for the film on the aluminium substrate. Kendig and collaborators[32] showed that the corrosion of the substrate enhances the development of parallel paths of ionic conduction in the coating.

The nature of the substrate also plays an important role in the ability of a coating to maintain adhesion upon contact with an aqueous environment. Walker[33,34] studied the adhesion of polyurethane and epoxy polyamide coatings to aluminium, cadmium, copper, mild steel and zinc after exposure to a water spray atmosphere. His data showed that the behaviour was a strong function of

the metal as well as the coating. The water spray reduced the adhesion of both types of coatings to cadmium, steel and zinc; it had no effect on copper coated with polyurethane but there was a major reduction for copper coated with the epoxy paint; and the adherence improved in the cases of both coatings on aluminium.

The nature of the substrate was also found to affect the resistance of films attached to it. Mayne and Mills[35] observed corrosion on D areas of an alkyd film when exposed to potassium chloride solution. The resistance of these areas when attached to an inert substrate, platinum or passivated iron, was found to be one to two order of magnitude higher than those attached to mild steel. The substrate presented no effect on the resistance of I films. The high value of resistance of the films attached to an inert substrate was attributed to a more difficult ionic diffusion in supported films.

1.4.2 - The nature of the metal/coating interface

It is very difficult to characterize the metal/polymer interface because different metals exhibit different surface chemistries and morphologies, and different polymer have, among others, different types of polar groups, different degrees of cross-linking, elemental compositions, chain segment lengths and different amounts of reactive groups. Coating components such as pigments, wetting agents, liquid component (solvents), anticorrosive components and other additives, may add further complication because some of these components may be present at the interface and play a role in the interfacial chemistry[36].

The metal/coating interface region consist however of the metal, a thin oxide film, the organic coating, and perhaps a water layer. Due to lack of sufficient experimental information, the bond between the organic coating and the substrate however is not characterized quantitatively. Another question that still remains to be answered is what happens to the nature of the bond when

water penetrates the coating and becomes available for adsorption or reaction at the interfacial region[12].

It is believed[12] that many coatings stand aggressive environments for many years, without serious deterioration, because aqueous-phase water does not form at the metal/coating interface. It is only when an aqueous phase capable of supporting the electrochemical corrosion reaction is present at the interface that the corrosion reaction can occur. Upon exposure to the atmosphere, a steel surface, prepared either by pickling or other chemical or mechanical treatment, becomes instantly coated with an oxide, 1-3 nm in thickness, in which both divalent and trivalent iron ions can be present. Surface constituents can be detected by X-ray photoelectron spectroscopy. The characterization of the metal surface before the application of the coating has been largely studied[37-40]. There has been however few studies on the chemical nature of the intact organic coating/metal substrate interfacial region, because of the difficulty in devising experimental techniques to make such study.

Iezzi and Leidheiser[37] concluded that surface contamination, mainly carbon, is an important factor in the variable paint performance observed. Its presence on localized areas interfered with the formation of the zinc phosphate pretreatment. Nitrogen was also often detected, and fluorine was detected after immersion of steel in fluorinated water. Alloying agents such as manganese, sulphur and silicon, at the surface of the steel, are not covered with an iron oxide and consequently are detectable as surface constituents by Auger spectroscopy. The coating is normally applied to such a surface and the alloying constituents, embedded abrasive and grain boundaries, provide many minute crevices and fissures which high molecular weight polymers and low surface energy materials are not able to wet completely on a nanometer scale. The metal/organic coating interface is thus likely to have non-bonded areas in which, under proper conditions, aqueous phase water can nucleate. Material with high surface

contamination fails much more rapidly than material with low surface contamination[37].

Rittèr and Kruger[40] found that an oxide exists at the interface and that the optical properties of the interface change when cathodic delamination or corrosion occurs. Leidheiser and Funke[36] stated that non-bonded areas at the interface can be originated by three major sources: voids or fissures in the metal surface; voids resulting from the lack of complete wetting of the metal by the polymer; and dynamic voids that result from the making and breaking of surface bonds by segments or polar groups in the polymer. Large voids can be detected by optical studies of transparent coatings or microscopic examination of cross-sections.

The development of new techniques for studying the interfacial region between the metal and the organic coating, is thought to be of considerable importance to major advances in organic coatings for corrosion protection. The oxide at the interface is the catalytic surface for the oxygen reduction reaction, it is also the medium through which the electrons are supplied for the oxygen reduction reaction, and it provides the bonding which results in the adherence between the coating and the metal[12].

1.4.3 - The nature of the coating

Since corrosion is an electrochemical reaction involving anodic and cathodic reactions, transport of electrons, reactants and products, the suppression of any of these processes can be used to control it. The protection mechanism offered by organic coatings is mainly a barrier effect. Thus for organic coatings to be effective, good barrier and good adhesion properties are required[41]. The barrier membrane properties of organic coatings are dependent on the following properties:

-the electrical resistance,

-the permeability to water and water vapour,

-the permeability to oxygen, and,

-the permeability to ions.

1.4.3.1 - The electrical resistance of organic coatings

One of the earliest and widest work involving estimation of resistances of organic coatings, was the work of Bacon, Smith and Rugg[42]. They studied the resistance of over 300 organic coatings applied to mild steel, and found out that the resistance of the coatings as a function of time, was directly related to the protection confered. Good protection was observed when the coating resistance, obtained by d.c. resistance measurements, was greater than $10^8\,\Omega.cm^2$. For coatings with resistance in the range of 10^6 to $10^8\,\Omega.cm^2$, the behaviour was variable, and poor protection was always observed when the d.c. resistances were less than $10^6\,\Omega.cm^2$. Figure 1.3 shows a schematic representation of their results.

Some authors[35,43-46] studied the relation between corrosion behaviour and d.c. resistance of organic coatings. Mayne and Mills[35,43-45] found that the d.c. resistance of free films is not always a good indication of the corrosion performance of the coated system, whereas a good correlation between the corrosion behaviour and the d.c. resistance of attached films seems to apply. These authors suggested that the d.c. resistance of attached films include both, the polarization resistance of the substrate[35], and the d.c ionic resistance of the coating[43]. They measured the d.c. resistance of coatings and found that different areas of a film exhibited distinct resistances[35]. Corrosion was observed at areas of low resistance in the film (10^6-$10^8\,\Omega.cm^2$), but no corrosion was seen when the coating resistance was of the order of $10^{10}\,\Omega.cm^2$ or greater. The areas of low resistance were called D-type behaviour areas, and the conductance of the film in these areas showed a direct relation to the external solution conductance. It was suggested that it is the initial breakdown under the D-areas which leads to the

observed corrosion. In their work, films with thicknesses in the range 25-40 μm were generally used, but sometimes coatings of thicknesses up to 75 μm were also analysed. They pointed out[44] that thickening the film reduces the chance of finding low resistance D-type areas. Leidheiser[46] also suggested that the boundary between the absence and presence of corrosion is of the order of 10^7 $\Omega.cm^2$. Corrosion rates would be low for coatings whose d.c. electric resistance is greater than 10^7 $\Omega.cm^2$.

1.4.3.2 - The transport properties of coatings for water, oxygen and ions

The corrosion reaction underneath the coating generally involves the cathodic reaction:

$$H_2O + 1/2\,O_2 + 2e^- \rightarrow 2OH^- \qquad (1.25)$$

Thus, oxygen and water are required to be present at the interface, along with ionic constituents that provide sufficient conductivity in the interfacial region to permit separation of the anodic and cathodic regions. All organic coatings allow the passage of water and oxygen at a rate which differ with the coating system.

The diffusion coefficient **D**, the permeability coefficient **P**, or the flux **J** through the film, provide the characteristic transport properties of coatings. The diffusion coefficient is defined as the constant in Fick's first law of diffusion:

$$dJ/dt = -D\,(dC/dx) \qquad (1.26)$$

where dJ/dt is the flux per unit time,

and dC/dx is the change in concentration with distance in the x direction.

The permeability is given by the product **D** x **S**, where **S** is the solubility coefficient of the diffusing species in the film. The flux, d**J**/dt, is the actual mass transported across the film per unit time[47].

The equilibrium concentration of water in a coating exposed to 100 % relative humidity is generally in the range 0.5 to 3 %. The flux of water through a free film 100 μm thick is typically of the order of 1-10 $mg.cm^{-2}.day^{-1}$ for many classes of coatings. If the same value applies to a coating on a metal, it can easily be seen that the flux of water through the coating is not rate-determining in the corrosion process. The rate of oxygen migration through a coating is generally much lower than that of water. In some instances, it has been shown that the flow of oxygen increases with the water content of the film, probably because the water acts to swell the polymer[47].

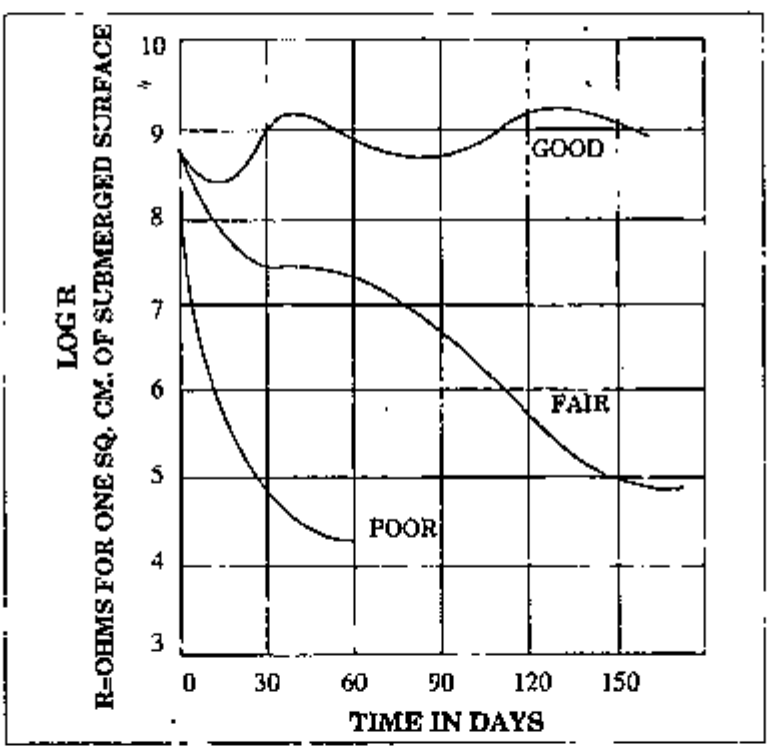

Figure 1.3 - Schematic representation of the corrosion property of organic coatings as related to their electrical resistance[42].

The permeability of organic coatings to water, water vapour, and oxygen.

Much has been written[48-54] concerning the role of permeability of coatings to water and oxygen in corrosion control by organic coatings. Mayne[51,52] showed that organic coating films are so permeable to water and oxygen that they cannot

be the rate limiting step of the corrosion process under organic coatings. He also concluded that in the absence of inhibitive pigments it is the high electrolytic resistance of organic coatings that delays corrosion. Available evidence[28,48-50], however, indicates that although the water permeability of organic coatings is generally higher than that necessary for corrosion to proceed, the oxygen permeation rate through the coating may be within or lower than that recognized for corrosion reaction of unpainted steel. These findings indicated that oxygen permeation may or may not be the rate limiting step which controls the corrosion process of coated steel[28].

The water permeability of homogeneous organic coatings is controlled by two concurrent processes, absorption and diffusion[55].

Absorption of water by organic coatings

Absorbed water molecules accommodate in the spaces within the structural matrix of the coating, and therefore, the absorption of water is affected by the structural features of the coating[55,56]. Available evidence indicates that the absorption of water tends to increase with increasing polymer polarity, and decreasing cristallinity and cross-linkage[55].

The effect of osmotic pressure of the solution on water absorption has been considerably studied[17,57,58]. It was generally found that the amount of water absorbed varied linearly with water activity for solution with water activity below 0.8, and above this value there was a substantial increase in water absorption[58]. The following explanation for this phenomena was offered by Mayne[58]. For solution with water activity below about 0.8, the water is evenly distributed throughout the polymer. When the solution water activity is greater than 0.8, water tends to accumulate at the ionogenic sites in the coating and, eventually, for water activities approaching unity, the coating turns milky, in which case water

would have been separated as a second phase visible under phase-contrast microscope.

The absorption of water is also affected by an electrical potential gradient that may drive water through a capillary or membrane under its influence. This phenomenon is known as electroendosmosis. Tests by Kittelberger and Elm[59] showed that over 90 % of the water absorbed by a linseed oil type coating under the influence of potential and concentration gradient was transferred by electroendosmotic force.

Permeation of water through organic coatings

Water permeation is known as the continuous movement of absorbed water molecules under the influence of driving forces such as concentration or potential gradient. The permeation of water through organic coatings is thus a diffusion process.

In a steady state, if **D** is essentially constant and independent on concentration, the permeability of water through coatings, **P**, will be given by the product **D x S**, where **D** is the diffusion coefficient, and **S** is the solubility coefficient of water in the film[47]. The transport of water molecules through coatings occurs by random migration through the spaces between chain-segments, so that it is affected by the structure of the polymer. The structural features which affect water permeation are basically the same as for water absorption, polymeric polarity, crystallinity, cross-linkage, and chain stiffness[55].

Water and water vapour permeation can also occur via capillaries which exist in the cross linked molecular structure of the coating. Water permeation for different coatings in sodium chloride was observed to follow Fick's diffusion equation, and the permeation rate was inversely dependent on coating thickness and directly proportional to exposure times[60]. The diffusion coefficients of water in coatings was observed to increase with water content for coatings absorbing

more than 5 %, and it was attributed to the swelling and plasticizing effect of water on the polymer. Coatings only capable of absorbing less than 5 % water showed diffusion coefficients essentially independent on water content or relative humidity[55]. Water permeability generally increases with the relative humidity of the surrounding environment or water activity of the solution, and this is attributed to a higher absorption of water at higher relative humidity. The absorbed water is believed to facilitate the permeation of water by increasing the mobility of chain segments and reducing the rigidity in the structural matrix of the coating[61].

Permeation of oxygen through organic coatings

The oxygen permeation rate for dried and homogeneous films, was found to vary linearly with the reciprocal of film thickness for various coatings[28,50]. The increase of pigment concentration led to a distinct decreasing in the rate of oxygen diffusion[28].

The permeability of organic coatings to ions

Although organic coatings do not prevent water and oxygen from reaching the metal substrate, they still prevent corrosion by interposing a high electrical resistance path between the cathodic and anodic sites. It is termed **resistance inhibition**[51,52,53].

The electrical current across organic coatings with no inhibitive pigments, is believed to consist of a flow of ions, since a mechanism of electrical conduction involving electrons is almost impossible for these types of coatings. The electrical resistance of organic coatings is thus controlled by the mechanism of ionic permeation through paint films. A linear relationship between the diffusion rate of sodium chloride and the reciprocal of the resistance of the film was found,

suggesting that the electrical resistance of a paint film is directly related to the permeation of ions[62].

Permselectivity of organic coatings

Permselectivity of organic coatings is generally attributed to the ionogenic groups within the polymer, which render the film selectively permeable to ions of opposite charge. When paint films are immersed in water or solution of electrolyte, they take up a charge. The most common ionisable group in organic coatings is the carboxyl group, consequently the paint films are selectively permeable to cations. With appreciable amounts of polyamides or similar material, however, the polymer takes up a positive charge upon immersion in aqueous solutions[63].

The characteristics of permselectivity of organic coatings, and the relationship between the concentration of external solution and ionic diffusion coefficients, have been demonstrated[60]. Available evidence[64,65] indicates that ions permeate through paint films by an ion exchange mechanism. Maitland and Mayne[64] observed a slow change in the electric resistance of paint films and associated it with the ion exchange between the cations from the solution and hydrogen ions from the carboxyl groups in the paint films. This finding was also confirmed by Cherry and Mayne[65].

A negative correlation has been shown between the ions exchange capacity and the corrosion protection efficiency of organic coatings[66,67]. Coatings with high ion exchange capacities showed poor corrosion protection and vice-versa[66]. The d.c. resistance of paint films of high ion exchange capacity was also found to drop rapidly when compared to films of low ion exchange capacities. The presence of pigments in the coating also affects the efficiency of corrosion protection, but for coatings with a same type of pigment and at the same volume concentration, the ion exchange capacity is believed to be the determining factor

for rank order of corrosion protection efficiency[67]. The ion exchange capacity of alkyd and pigmented alkyd when exposed to a corrosive environment (5 % NaCl in a salt spray chamber), was determined by Malik and Aggarwal[68]. Very slow change in the ion exchange capacity with time was associated with good corrosion protection efficiency in both cases, pigmented and unpigmented alkyd.

Ionic conduction in organic coatings

The relation between the d.c. resistance of paint films and the concentration of electrolyte has been largely demonstrated[42,64,65,68]. The changes in d.c. resistance with time of an alkyd coating on mild steel substrate were determined in distiled water and three sodium chloride solutions. The resistance was found to increase with the concentration of electrolyte in the solution[42]. Maitland and Mayne[64] observed that the change in resistance which took place when varnish films were immersed in a solution of potassium chloride was controlled by at least two processes: (1) a fast change associated with the entry of water into the film which tend to cluster around ionogenic groups, and (2) a slow change attributed to a reversible process of ion exchange between the cations from solution and the hydrogen ions from the carboxyl groups in the film.

Mayne and Scantlebury[69] studied the distribution of D and I areas in a film. They observed that I films are always free from D areas, but D films contained a mixture of D and I areas with the D areas distributed over an appreciable area of the sample. The d.c. resistance of D areas was always lower than those of I areas, and this led to the conclusion that D conduction cannot be attributed to the presence of pores unless they were of molecular dimension. D areas were also observed to be softer and have a higher percentage of swelling when exposed to solvents. The authors concluded that I and D areas are caused by difference in cross-linking density within the film. No defects or pores were observed by Mills and Mayne[43] using electron microscopy or optical microscopy,

confirming the conclusion arrived by Mayne and Scantlebury that D conduction was not due to the presence of pores.

Parks[70] studied the relative diffusion characteristics of water, Na^+ and Cl^- ions in a commercial alkyd coating, using radioactive Na-22 and Cl-36, and impedance methods to calculate the total water uptake. The diffusion coefficients for water were higher than the ones corresponding to Na^+ and Cl^- in the steady state. It was observed that water entered the coating at a much higher rate during the first 3 hours when the samples were first immersed in the electrolyte. It also appeared that the ionic diffusion occurred to a significant extent only after water had penetrated the coating. These findings indicated that water uptake precedes ionic diffusion. However, the similarity of the diffusion coefficients values suggested that the ions migrate simultaneously with the water or that all the three components follow the same types of pathway through the coating.

The application of a potential of -0.8 V vs SCE was found to cause an increase in the diffusion coefficients of Na^+ ions and water by one order of magnitude as compared to the behaviour in the absence of the applied potential. This finding supports the concept that cations reach the coating-substrate interface by diffusion through the coating[20].

1.5 - The protection of metals by organic coatings

The application of organic coatings is a widely used method for the protection of metals. The use of a coating resistant to the environment to which it is to be exposed, allows the use of substrates with desired physical and chemical properties and which for reasons of low corrosion resistance could not be possibly used in bare conditions. Leidheiser[12] proposed that there are two main mechanisms by which an organic coating protects a metal substrate: (1) serving as a barrier for the reactants, water, oxygen, and ions, and (2) serving as a container for corrosion inhibitors.

The barrier properties of organic coatings for water, oxygen and ions have been presented in the previous sections, and the conclusion reached is that, one of the most important effects in corrosion protection by organic coatings is the barrier effect of resistance inhibition. The corrosion reaction is retarded by inhibiting the ionic transport between cathodic and anodic sites within the electrochemical corrosion cell. As organic coatings typically have high resistance to ionic conductivity they offer very good barrier properties. In this type of resistance inhibition, the adhesion of the coating to the substrate plays a vital role. Once the adhesion is lost, low ionic resistive pathways are introduced underneath the coating, and corrosion can take place[71]. The effect of inhibitors on the corrosion protection by organic coatings is beyond of the scope of this thesis.

1.6 - Mechanisms of failure of organic coatings

Organic coatings are subject to degradation by environmental constituents. The main agencies by which degradation occurs are thermal, chemical, mechanical and radiant. Living organisms may also degrade paints. Deterioration takes the form of discolouration, cracking and crazing, loss of adherence to the substrate, or change in a physical property such as resistivity or mechanical strength[12].

The mechanism involved in the development of corrosion processes under protective films, needs to be investigated and understood, since these processes are the basic reasons for the initial development of corrosion on painted metallic surfaces, resulting in loss of protective properties of the paint coating and subsequent acceleration of the corrosion process on the bare metal surface. The exact mechanism by which the coating/substrate bond is broken, however, is very controversial at the present time.

There are various proposed mechanisms for coating delamination. Dissolution of substrate surface oxide or conversion coating[20], displacement of

polymer from the substrate by water[14], and saponification or other chemical degradation of the paint resin in the interfacial region[13,72], are among the mechanisms proposed. Dickie and co-workers[13,72] associated the major adhesion loss accompanying the corrosion of painted steel with the disruption of the paint interface by cathodically produced hydroxide. Leidheiser[20], however, suggested that the dissolution of the oxide is the important factor in the delamination process. Although it was not said if this oxide solubilization occurs before or after the delamination process. According to Koehler[14], cathodic delamination is a specialized form of loss of adhesion by intervening water. Despite of all the different mechanisms mentioned above, it is now known that under certain conditions, all the mechanisms proposed may be active[73].

1.7 - Adhesion of organic coatings to metallic substrates

There seems to be no general agreement to whether the adhesion of organic coatings to metallic substrate bares a crucial importance to the efficiency of corrosion protection. For many investigators[53,61,74-77] the presence of a strong bonding between coating and metal substrate is an important protection function of organic coatings, and may retard both, initiation and spreading of corrosion of metal substrate beneath the film. However, there is a second group of researchers[78,79] for whom a correlation between adhesion and the efficiency of corrosion protection does not always apply. They observed no real correlation between adhesion and corrosion resistance for some coatings.

Funke[53,74,75] considered adhesion, specially wet adhesion, to be an important factor influencing the corrosion protection of organic coatings. On the other hand, Walker[78] tested three coatings, and the two which presented highest resistance showed the lowest adhesion on water immersion. The third, a long oil alkyd, showed good adhesion properties but the worst corrosion resistance. These results were supported by Schwenk[80] who observed that adhesion loss had no adverse effect on corrosion protection of the organic coating analysed.

Funke[74] criticized the conclusions arrived by Walker[78], pointing that possibly misinterpretation of the corrosion scales used to rank protective quality of coatings, may have led to error. Walker[78] attributed the loss of adhesion of organic coatings to the metallic substrate when exposed to water, to the accumulation of water at the coating/metal interface disrupting the adhesion bonds. Walker[78] and Bullet[81] showed that the decrease of adhesion for several coatings begins in the range of 65 to 80 % R.H., while the adhesion drops rapidly at R.H. above 90 % It has been largely observed[78,80,81] that the adhesion of organic coatings to metallic substrates drops rapidly when exposed to high humidity environments or aqueous solutions

The loss of adhesion caused by water is also known as **water disbondment**. Water disbondment was defined by Leidheiser and Funke[36] as the separation that occurs between a polymer coating and a solid substrate when a moderate force, insufficient to affect the system when not exposed to water is applied during or immediately after the coating system is exposed to gaseous or liquid phase water or aqueous solutions. According to their hypothesis, water disbondment is a consequence of the formation at the metal/coating interface of a discontinuous or, in some cases, a continuous water film, several to many molecular layers in thickness. Some of the mechanisms which possibly could lead to the accumulation of water at the interface were considered. These were osmotic forces, temperature differences and chemisorption or physisorption of water. The presence of non-bonded areas at the interface can allow the accumulation of water forming a local aqueous phase, which grows laterally due to the stress exerted on the metal/coating bonds.

Water may reach the coating/metal interface within the first hours of exposure. This observation is in accord with the adhesion loss of alkyd coating observed by Bullet[81]. The adhesion of several paints to mild steel was observed to degrade rapidly within 15 minutes of exposure to water[80]. The non-permanent adhesion loss was then attributed to the absorbed water by organic coating, and

the phenomenon of recovery of adhesion on drying out after immersion was also noted[78,80,81].

The oxide and hydroxide of iron on the surface of steel have a strong affinity for water, and the presence of water adsorbed on the surface of metal has been detected by McCafferty and collaborators[82]. The water molecules on the first layer are chemically adsorbed by the hydroxide iron through hydrogen bonding, and the subsequent layers are only physically adsorbed[83]. Dickie[73] detected little or no chemical change in the organic coating associated with humidity induced adhesion loss. Water-soluble inorganic salts present as surface contaminants, however, alters the interfacial chemistry, and can lead to osmotic blistering and various corrosion related blistering and adhesion loss[84].

Although it can be concluded that for some coatings adhesion is not the predominant factor controlling corrosion, there is still very strong evidence which suggests that adhesion is a crucial factor for efficient corrosion protection.

1.8 - The influence of small differences in composition on the corrosion behaviour of steel in various environments.

The corrosion of steel is a function of both, its composition and the environment to which it is exposed. The environments considered here are various atmospheres and aqueous solutions. The compositions considered are those of mild steels, wrought irons, copper steels and low-alloy steels. The main focus will be on mild steel and low-alloy steel types, since these were the steels used in this work.

The ability of copper to reduce the corrosion rates of low-carbon was first recognized in 1900. At about the same time, nickel (3%) was also reported to be beneficial[85]. High strength alloy steels containing small additions of alloying elements were developed in the early 1930's and have been produced since for specific mechanical properties. Some of the low-alloy steels, however, contain

small amounts of alloying elements that also impart superior atmospheric corrosion resistance. The improved atmospheric resistance is due to the protective film formed on the surface upon atmospheric exposure which impairs further corrosion[86].

1.8.1 - Atmospheric exposure of bare steels

The extent of the improvement in resistance to atmospheric corrosion depends upon the composition, with the copper, nickel, chromium and phosphorus contents being particularly advantageous. The superior atmospheric corrosion resistance of these steels over that of copper steel have been extensively demonstrated[86-91].

Larrabee[86] reported that high-strength low-alloy steel lost less weight than either the low-carbon steel or the copper steel, and attributed the difference to the periodical drying of the rust films of all specimens. When these steels remained continuously moist, the superior resistance exhibited by the high-strength low-alloy steels was not observed. The rust films formed on the continuously moist surfaces were apparently not so protective as those formed on steels exposed to the atmosphere. He suggested that the nature of the film immediately adjacent to the metal would probably determine how protective the film could be, but at that time it was extremely difficult to study the very thin film by itself. LaQue[90] also attributed the superior atmospheric corrosion behaviour of the low-alloy steels to the characteristics of the corrosion products of these steels. The rust on the low-alloy steels were darker, thinner, less porous, and therefore, more protective than on plain iron and steels. It was also found that these differences in the rust coatings were apparent as soon as they started to form.

In a review[87] on the development of low-alloy steels for improved atmospheric corrosion resistance, copper, phosphorus, chromium, nickel and molybdenum were found to be the additives most commonly associated with

improving the atmospheric corrosion resistance of steels. From these elements came a series of low-alloy steel compositions known as the weathering steels having atmospheric corrosion resistance variously reported as being 5 to 8 times greater than that of plain carbon steel in many atmospheric test locations.

Larrabee and Coburn[91] reported extensive corrosion data on 270 experimental steel composition having systematic variations in copper, nickel, chromium, silicon, and phosphorus, exposed for 15.5 years at three different test site locations. They showed that while each of these addition elements individually contribute to some improvement in atmospheric corrosion resistance, the greatest improvement results from interactions among specific combinations of these alloying additions.

It has been shown[86] that the importance of differences in environment on the corrosion resistance of steels is such that in order to determine the suitability of any type of steel for use under certain conditions, tests have to be made in that particular environment. Estimations can only be made from the results of tests in other locations if the environments are similar.

1.8.2 - Atmospheric exposure of painted steels

Many workers[2,85,92-99] reported that an improvement in the corrosion resistance of steel promoted a beneficial effect on the durability of paint coatings. In some cases the the improved performance of painted high strength low-alloy steel (HSLA) as compared to painted mild steel was only found in not severe environments[85]. In more aggressive media, such as marine and certain chemical environments this difference was not observed, since the protective film was not seen to form. On the other hand, Fancutt and Hudson[99] reporting on the work of the Corrosion Committee of the Iron and Steel Institute, observed that although the performance of a painting scheme could be influenced by the basis metal, this effect was only marked in the case of highly corrosive industrial

atmospheres. In less corrosive atmospheres no pronounced difference was observed. It was also suggested that the use of low-alloy steel for a painted structure is of practical value because it reduces the corrosion rate when the paint has failed.

Copson and Larrabee[2] suggested that paints are more durable on low-alloy steel than on copper steels and much more durable than on mild steels, because any rust that forms is less voluminous on low-alloy steels, so there is less rupturing of the paint film and less moisture reaches the steel to promote further corrosion. Their specimens were tested at three locations, an industrial, a semirural and a marine atmosphere. In all of the atmospheres, low-alloy steel had the longest service life.

LaQue and Boylan[96] compared an open-hearth iron, a copper steel, and a high strength low-alloy steel coated with a pigmented baking urea-modified alkyd topcoat, with and without phosphate pretreatment. The specimens were scratched and exposed to a marine atmosphere. The open-hearth iron was the most corroded in both conditions, bare and painted. The low-alloy steel was the one to show the best results in all tests and the copper steel was intermediate. They concluded that there is a very marked advantage in using low-alloy steels, the improvement in anti-corrosion properties being even greater with the painted specimens and being most valuable in the most corrosive atmospheres. It has also been found[97] that paints applied to high strength low-alloy steels had the longest service life, with copper and carbon steels ranking in descending order. The rust formed on the low alloy steels was less voluminous, tighter, and more adherent than on the two other steels, and thus resulted in less damage to the paint film.

Chemical plant environments

Schmitt and Mathay[98] compared two high-strength low-alloy steels with carbon steels, either painted with a wash primer and a top vinyl coating or unpainted and exposed to atmospheric constituents of various chemical plant

environments. Their results showed that the corrosion resistance of the unpainted low-alloy steels was superior to that of the carbon steel in all the atmospheres tested, and they attributed these differences to different oxide films formed on the distinct steels. For the painted steels they found that where paint performance differed, the performance of the coating was always better on the low-alloy steels than on carbon steels. The same authors also concluded that the superior corrosion resistance of low-alloy weathering steels is not normally observed under immersed conditions. Low-alloy steels exhibited superior atmospheric corrosion resistance in ten different chemical plant environments, where atmospheric constituents included chlorine, sulphur, and organic compounds. The corrosion resistance was from 2 to 13 times superior to that of carbon steel. It has been pointed out[85] that the applications of low-alloy irons and steels with no protection, in process industries, can be broadened considerably when they are utilized in conjunction with corrosion preventive measures such as protective coatings, corrosion inhibitors, and cathodic protection.

1.8.3 - Full immersion tests of bare steels

It has been shown that corrosion rates obtained on specimens exposed alternately both to air and to sea water are not applicable to steel structures continuously immersed[93].

Natural waters

Although it is generally possible to characterize the atmospheric corrosion behaviour of steels with respect to few environmental categories (industrial, marine, rural), there is a general tendency, however, to believe that variations in composition from the wrought irons and cast irons to low-alloy steels produce no marked difference in immersed corrosion rates in natural waters (pH 4 to 10). Larrabee[86] concluded that in most natural waters and soils, the presence of

small amounts of alloying elements in the steel does not play a major part in determining the average corrosion rates. He reported a light superiority of a Corten® high strength low-alloy steel compared to structural copper and carbon in fresh waters of different rivers. The data also showed that the average corrosion rates decreased with time.

Leckie[85] stated that under immersed conditions in natural waters, where the corrosion rate is usually controlled by the diffusion of oxygen, carbon steels and low-alloy steels exhibit essentially the same corrosion behaviour. Chromium, nickel and copper at low concentrations showed no clear evidence of affecting corrosion resistance of steel in neutral water. Similarly residual elements contained at normal levels (silicon, manganese, sulphur, phosphorus, and carbon) were found to have no significant effect on corrosion rate in natural salt waters.

Neutral salt solutions

The presence of neutral salts in water generally tends to increase the corrosion rate of iron and steel by influencing the anodic polarization, conductivity of the solution, solubility of corrosion products, and diffusion and solubility of oxygen.

The maximum corrosion rate of steel as a function of sodium chloride concentration (occurring at 3 %) is explained in terms of the balance between the continuously decreasing oxygen solubility with increase in chloride concentration, and the initial increase in solution conductivity, giving rise to a reduction in the protectiveness of the rust films. Increasing solution conductivity permits the interaction of remote anodic and cathodic sites, such that the corrosion product is deposited away from the steel surface, rendering it non-protective[85]. Fancutt and Hudson[99] also found that the superior corrosion resistance of low-alloy steels over ordinary mild steels under atmospheric conditions was not paralleled under conditions of total immersion in sea water.

The relatively low corrosion resistance of iron and low-alloy steels under immersed conditions might be attributed to the fact that normal corrosion products of iron formed are non-adherent and offer little if any protection against continued dissolution. Also, since the corrosion of these steel types under immersed conditions in neutral solutions seems to be governed by the combined action of water and oxygen, with the cathodic reduction reaction playing a significant role in the rate controlling process, minor alloying elements would only play a small part in the corrosion process.

1.9 - General remarks

From the literature presented above, it can be said that in general there is an agreement about the superior corrosion behaviour of low-alloy steels compared to mild steels, copper steels or wrought irons under atmospheric exposure. The extent of the improvement depends upon the composition, with copper, nickel, chromium contents being particularly advantageous. On the other hand, carbon and manganese in large amounts, have been reported as detrimental to corrosion resistance[100].

It is also believed that the improved corrosion resistance of low-alloy steels, makes paint coatings more durable, since the better corrosion resistance of low-alloy steels, would result in less voluminous rust forming on these steel types as compared to carbon steels, and causing less damage to paint coatings. In aqueous neutral solutions, either natural waters or salt solutions, low-alloy steels and carbon steels uncoated, in general have been found to exhibit similar corrosion behaviour.

Much less is however known about the behaviour of low-carbon and low-alloy steels when coated and under immersed conditions. Souza[101] observed some visual differences between the corrosion features of a mild steel and a low-alloy steel, both coated with a thin film (~25 μm) of chlorinated rubber, and fully

immersed in 3.5% wt sodium chloride solution. The reasons for the differences however were not given, and a more extensive study on the behaviour of these two steels when coated and fully immersed in aqueous solutions was necessary. It was with this aim that this research was undertaken, that is, to compare the two steel types, a mild steel and a low-alloy steel, with relation to their corrosion characteristics, when bare and painted, and under immersed conditions or exposed to wet and dry cycles inside a cabinet.

In order to study the corrosion characteristics of the mild and low-alloy steel, bare or painted, various electrochemical techniques and surface analysis methods were used. A brief introduction to these techniques is presented in the next chapter.

CHAPTER 2

METHODS FOR MONITORING THE CORROSION OF BARE AND ORGANICALLY COATED METALS.

2.1 - Electrochemical methods

2.1.1 - Introduction

Since metallic corrosion, either in aqueous solutions or atmospheric exposure, is mostly an electrochemical phenomenon, electrochemical test methods are useful to assess the thermodynamics and kinetics of corrosion. The main aim of electrochemical testing of painted metals has been to find accelerated laboratory tests which can evaluate new paint systems much more quickly than by atmospheric exposure trials and/or to provide a better understanding of how a paint film protects a metal substrate[16]. The electrochemical methods used are generally divided according to the nature of the perturbing signal into d.c. and a.c. methods. These are briefly presented below.

2.1.2 - Electrochemical corrosion potential

One of the most common measurements made as an aid to understanding corrosion phenomena is the corrosion potential. The measurement of potential-time and potential-current relationships have been used extensively, both in fundamental studies and in practical testing, to provide information on the thermodynamics and kinetics of metallic corrosion[102]. In the case of coated metals, however, the high electrolytic resistance of a wetted paint film, which can be as large as $10^{10}\ \Omega.cm^2$ for a coating of average thickness, introduces experimental problems and difficulties in the interpretation of results. It is for

these reasons that this technique has rarely been used with metals protected by coatings. However, if used together with other techniques, the measurement of the corrosion potential of coated metals can provide very useful information on the corrosion behaviour of the coated system.

The corrosion behaviour of a metal can be related to the movement of the corrosion potential with time. The movement of the potentials into a more negative direction is supposed to indicate removal of surface oxide films and development of active corrosion. Whereas a shift of the potential towards more noble potentials can reflect the formation of a film and the end of corrosion[103]. Corrosion potential alone, however, cannot be used as an unambiguous indicator of corrosion, and noble potentials do not always mean reduced corrosion rates.

Many researchers[104-108] assumed that a noble potential indicates a low corrosion rate. They tried to correlate potential-time curves for specimens of painted steel fully immersed in aqueous solutions, and the durability of the paints under immersed and atmospheric exposure conditions. Over fifty different priming paints applied onto steel were examined by Haring and Gibney[104]. They measured potential-time curves, over 24 hours, for specimens totally immersed in aerated tap water, and compared their visible condition after 4 days with their condition after atmospheric exposure tests. Measured potential values ranged from +0.25 V (SCE) to -0.45 V (SCE). A number of cases gave anomalous results, with some specimens exhibiting relatively noble potentials but showing rapid breakdown. The potential-time behaviour of painted steel in sea water,distiled water, and dilute acid, over 25-50 h, were compared with the results of corrosion weight losses after sea-water spray and immersion tests over a 40-100 days period, and also led to some anomalous cases which could not be explained[105].

Zahn[106] studied the effects of different pigment and vehicle type on painted steel. He reported that negative potentials always indicated the presence, and positive potentials, the absence of corrosion. The corrosion was established by stripping the paint and examining the substrate after a period of several hundred

hours. His report was however considered by many to be too optimistic. It is believed that the actual potential values obtained in the early stages of exposure and the maximum reached cannot be related to the protective value of the paint. This would explain the poor correlation values obtained in the work presented earlier[104-106], where measurements extended over only few hours after immersion.

The work of Wormwell and Brasher[107,108] and its use of the potential-time technique is considered one of the most complete and useful studies of this technique. Steel coated with paints intended for total immersion conditions on ships' hulls were immersed in synthetic sea water, and weight loss tests were carried out simultaneously in order to correlate the changes in potential with the corrosion process, Figure 2.1. Initially after immersion, a gradual decline in potential was seen which coincided with the onset of rusting. The potential then started to move in the more positive direction, reached a peak and then moved in the negative direction. The time to pass the peak was interpreted as the useful life of the paint. It was also observed that the potential at the maximum became more positive with increasing thickness of the paint, and it was roughly a linear function of the resistance of the paint film. It was then suggested that high resistance paints might modify the measured potential by introducing an ohmic potential drop. Irregular fluctuations in the early stages of exposure, particularly for more protective paint systems, were attributed to alternating film breakdown and repair which has been observed under certain conditions on metals carrying protective oxide films[108]. Instability in the electrical measuring system could however been introduced by a high resistance between the specimen and reference electrode[109].

Mayne[110] explained the effect of coating resistance on potential measurements based on the electrolytic resistance of the coating. The Evans diagram given in Figure 2.2 can be used to illustrate the coating effect on the measured potential. In a conducting electrolyte, the measured potential of bare

steel would be given by point B, the corrosion potential, where the cathodic polarization curve CB and the anodic curve AB intersect. Due to the high electrolytic resistance of the paint, an ohmic potential drop between the anodic and cathodic areas would be introduced. If the resistances of the approaches to the anodic and cathodic points are equal, the measured potential would be equal to F, that is situated half-way between D and E. In the early stages of exposure it is supposed that the anodic areas would be situated at weak points in the air-formed film on steel. The resistance of the approach to the smaller anodes then would be higher, causing the potential F to move nearer to D than E and therefore F would be cathodic to the potential B for unpainted steel.

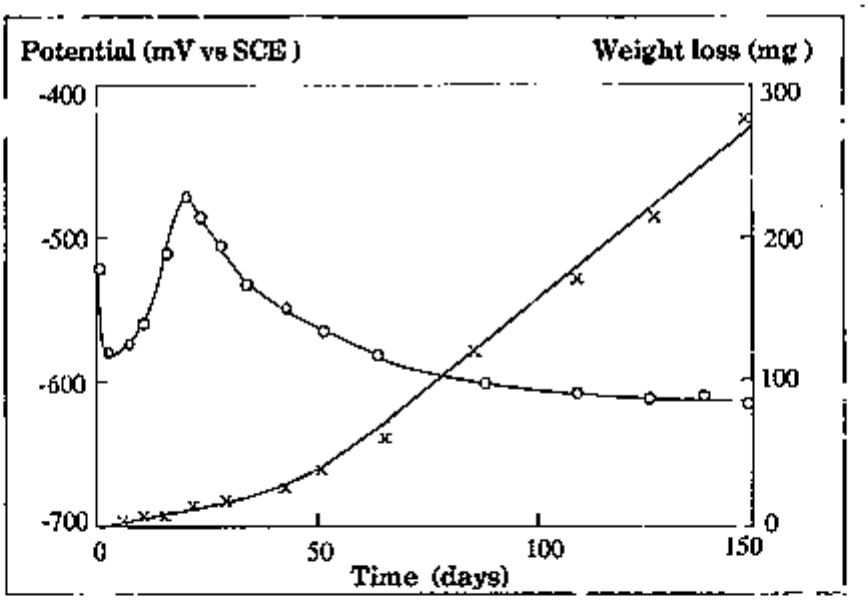

Figure 2.1 - Potential-time and weight loss curves for painted steel[107].

Yakubovitch and collaborators[111] working with paint films of thicknesses below a certain critical value (ca. 20-30 μm), observed very low electrical resistances for these paint films and attributed it to an increased number of pores and defects in the thinner films. The potentials measured were relatively negative for very thin coatings, but increased sharply when the thickness exceeded a critical value. Their results support the idea that intact, high resistance film

providing a high ohmic resistance at the anodes would shift the measured potential in a cathodic direction. The low resistance observed for thin films was related to the difficulties in preparing very thin films which are free from defects.

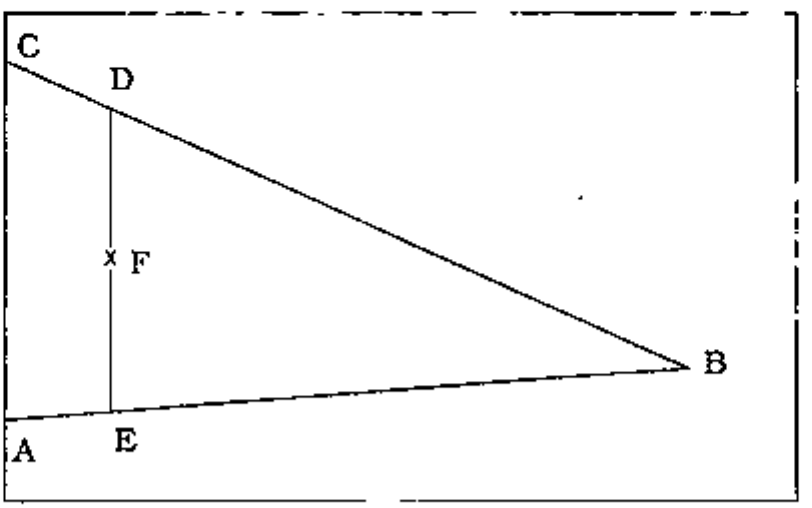

Figure 2.2 - Evans diagram of a metal corroding in a high-resistance electrolyte[110]

From the early work reported in the literature it can be said that controversies do exist on the reliability of the potential-time technique. Some authors[112] reported favourably in support of the potential-time technique, whereas others found no correlation at all between paint durability and corrosion potential[113]. Wolstenholme[114] in a review on the corrosion potential measurements and their applicability to coated metals, concluded that potential-time curves can not be considered as an "accelerated test" because although they may detect the onset of rusting, it can take a very long time after the initial immersion. He also concluded that the potential may not reflect the corrosion behaviour of a coated metal, which is affected by the resistance of the paint film. He questioned the usefulness of this technique for metals with coatings which do not confer galvanic protection and called attention to the fact that each investigator using the technique should interpret his results very carefully.

Leidheiser[12] proposed that the movement of the corrosion potential in the noble direction would reflect an increase in the cathodic/anodic surface area ratio. On the other hand, the movement of the corrosion potential in the active direction would be indicative of an increase in the anodic/cathodic surface area ratio, and a significant overall corrosion rate. In the case of steel, increasingly active potentials would mean rusting beneath the coating and a signal that the coating lifetime was limited. Increasingly positive potentials with time has also been suggested[114] as indicative that alkaline conditions, caused by the oxygen reduction reaction, are developing locally at the metal-coating interface and that delamination is of concern. Scantlebury et al[115] interpreted the positive potentials of coated metals as due to passivation supported by water in small contents at the metal-coating interface. It was suggested that either the water state or its content at the interface, might be important in determining the potential of a coated metal.

More important than the actual value of the measured potential in a certain time is the change of this potential with exposure time. The potential-time technique can be very helpful if used with other techniques so that the changes in potential can be correlated with other processes involved. Some precautions, however, have to be taken during the measurement of the corrosion potential of coated metals. In the case of high resistance coatings, a sensitive measuring equipment is necessary. Generally a voltmeter with a high input impedance ($\geq 10^{14}\,\Omega.cm^2$) is employed.

The main advantage of the potential-time technique is that it measures the electrochemical characteristics of the system without disturbing the system under investigation from its equilibrium conditions. Many other d.c. electrochemical techniques, however consist of stimulating the system by the application of current or potential, and measuring the resulting effects. These are presented in the next sections.

2.1.3 - Tafel extrapolation measurements

When corrosion occurs, current flows between individual anodes and cathodes, and this causes a change in the electrode potential of the system. Although this current cannot be measured, it can be evaluated indirectly on a metal specimen with an inert electrode and an external electrical circuit. Polarization is described as the extent of the change in potential of an electrode from its equilibrium potential caused by a net current flow to or from the electrode, galvanic or impressed[116]. Polarization can be studied by either changing the current and measuring the equivalent change in potential (galvanostatic method), or varying the potential and measuring the resultant change in the current (potentiostatic method). The corrosion rate is a function of that corrosion current. When plotted on semi-log axis, the theoretical polarization curves of both the anodic and cathodic processes, when polarized significantly from the corrosion potential, are straight lines, Tafel behaviour. The corrosion current can be measured from the intersection of the corrosion potential and either the anodic or cathodic curve, Figure 2.3. IR drops obscure Tafel behaviour. The region where the theoretical and measured curves match are called the Tafel regions. The slopes of the Tafel regions are denoted by b_a and b_c for the anodic and cathodic reactions respectively, Figure 2.3.

The main advantage of the Tafel extrapolation technique is that it provides a relatively fast quantification of the corrosion rate. It can also in certain cases provide mechanistic information.

The limitations of this technique are:

(i) it is of limited value when there is more than one cathodic reduction reaction,

(ii) in many cases it is difficult to identify a sufficient linear segment to the Tafel region, making extrapolation inaccurate,

(iii) it does not indicate local attack, only an average uniform corrosion rate,

(iv) the electrolyte resistance must be low,

(v) large currents are required to change the potentials from the corrosion potential, since currents in the Tafel region are generally one to two orders of magnitude larger on the log scale than the corrosion current[116], and

(vi) since the electrode surface is disturbed significantly, the technique cannot be employed to monitor corrosion on a specimen.

Even though the specific corrosion rate determined by Tafel extrapolation is seldom accurate, the method is still considered as a good confirmation tool[117].

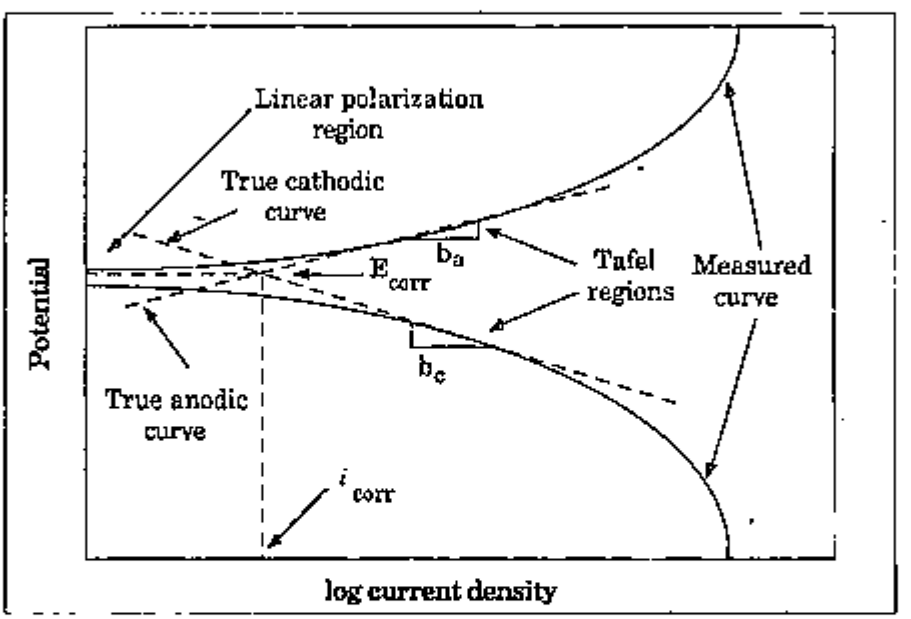

Figure 2.3 - Tafel extrapolation and linear polarization curves[116].

2.1.4 - Polarization resistance measurements

The polarization resistance, also known as linear polarization, is a method which has been widely used in determining corrosion rates in aqueous media since the publication of Stern and Geary's work[118] in 1957. This method involves obtaining a number of current versus change of potential (polarization) data in the vicinity (±10 mV) of the corrosion potential[119]. The polarization resistance, R_p, is defined as the tangent of a polarization curve at the corrosion potential, E_{corr}:

$$R_p = \left(\frac{dE}{di}\right)_{E=E_{corr}} \qquad (2.1)$$

In the case of simple, charge transfer controlled reactions, the corrosion current density, i_{corr}, is related to R_p by the Stern-Geary equation:

$$i_{corr} = \frac{b_a \cdot b_c}{2.303\,(b_a + b_c)} \cdot \frac{1}{R_p} = \frac{B}{R_p} \qquad (2.2)$$

where b_a and b_c are the Tafel slopes of the anodic and cathodic reactions, respectively. The boundary conditions for the application of this equation are[120]:

(i) charge transfer control for both anodic and cathodic partial currents,

(ii) no diffusion or resistance polarization,

(iii) the corrosion potential must have a value sufficiently far away from the redox potential of the half reactions for the possible reduction of M^{n+} ions and oxidation of the reduced component to be neglected.

The only exceptions to the limitations mentioned in conditions (i) and (ii) are corrosion systems where the partial reduction current is fully diffusion controlled, or when the anodic partial current is constant in the vicinity of the corrosion potential because of passivation. In these cases, one of the Tafel constants, b_a or b_c, is infinity, leading to slightly modified equations[120]. If the cathodic process is diffusion controlled, equation (2.2) reduces to:

$$i_{corr} = \frac{b_a}{2.303} \cdot \frac{1}{R_p} \qquad (2.3)$$

The major limitation of the polarization resistance method is that the values of the Tafel constants must be known for an accurate determination of the corrosion rate. This difficulty has been overcome by Mansfeld[121], using a technique involving curve fitting and computer analysis to obtain the values of Tafel constants and corrosion rates simultaneously. Another limitation is that the method is not sensitive to local corrosion[122].

Considerable effort has been made to improve the accuracy of this method by the use of more precise calculation[121], or by compensating the IR drop in high resistivity environments[123]. The uncompensated resistance, R_u, affects the polarization resistance, R_p. The experimental value R_p' is the sum of the true value R_p and R_u, ($R_p'=R_p+R_u$). The error caused by R_u is equal to R_u/R_p [123]. Nowadays, the polarization resistance technique is a well-established tool for measuring and monitoring corrosion.

One of the major disadvantages of this technique is that it assumes that the d.c. perturbation gives rise to a steady state condition. In reality it can take several minutes before a steady state is reached, depending on the electrochemical processes and kinetics which are controlling the corrosion. Another disadvantage is that if the conductivity of the electrolyte environment is low, then an error in the measurements can be introduced. For such systems, IR drop compensation is necessary.

Wolyneck and Escalante[124] determined the corrosion rate for carbon steel in stagnant NaCl solutions using a chronoamperometric method for obtaining polarization data. In this method the polarization potential is switched off for some minutes between two consecutive steps to allow the corroding system to recover, and the current is determined by extrapolating the data of the current decay curves to infinite time. Their data was in good agreement with weight loss and corrosion potential measurements. Azzeri and co-workers[125] applied linear polarization techniques to plain carbon and low-alloy steels in sea water. In order to avoid misleading contributions arising from the presence of solid corrosion products, their data were interpreted according to equivalent circuits representative of the steel surface behaviour in sea water. Good agreement with weight loss measurements throughout four years immersion in natural sea water was also observed.

Although polarization techniques have been used extensively for the study of bare metals, these methods are not so often employed to study the corrosion

numerous metals and alloys in various environments have been established by the potentiodynamic scan technique[128-,129].

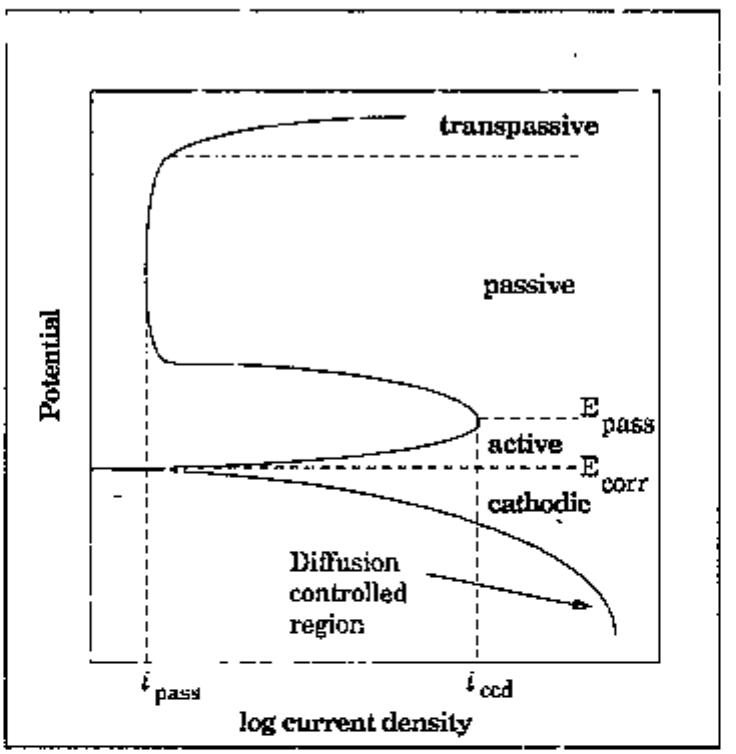

Figure 2.4 - Typical polarization curve for a metal showing active-passive behaviour. (i_{ccd} = critical current density for passivity, i_{pass} = passive current density, E_{pass} = primary passive potential and E_{corr} = freely corroding potential[116]).

Standard electrochemical direct current (d.c.) techniques to study metal/coating or film/electrolyte systems, have been found to be poorly reproducible and, in the case of nearly perfect coatings even impracticable. One of the limitations for the use of d.c. techniques with painted metals, is that the high-resistance paint film will introduce an ohmic potential drop which will be added to the true potential of the metal surface. Results that do not consider this source of error are thus invalid. Besides, large perturbation polarization may affect the electrode/coating interface leading to irreversible changes of the system concerned[18].

2.1.6 - Electrochemical impedance methods

2.1.6.1 - Introduction

Although d.c. techniques can provide useful information about the electrode-electrolyte interface, some of their limitations can be overcome by the use of electrochemical impedance techniques. First, the disturbing amplitudes employed by electrochemical impedance techniques are very small and cause only minimal perturbation of the electrochemical system. Second, electrochemical impedance measurements provide information on both electrode capacitance and charge transfer resistance, and thus reveal valuable mechanistic information. Third, measurements can be made in low conductivity media where d.c. techniques are subjected to considerable errors due to large ohmic drops. The effect of the solution resistance can be detected by electrochemical impedance techniques and thus eliminated.

In recent years the use of impedance techniques for investigations of corrosion has expanded rapidly. From a theoretical viewpoint, the impedance is considered one of the most important quantities that can be measured in electrochemistry and corrosion science[130]. Its importance lies in the fact that the current flowing across a metal/solution interface can be divided into two parts: (i) the part that follows a faradaic path when the current is part of the electrochemical reaction and which is called the charge transfer process, and (ii) the part that is non-faradaic and which establishes a charged interface, consisting of a double layer, since there is no transfer of charged particles across it. An electrode interface can then be represented as a combination of resistors and capacitors and the impedance of such an interface can be analysed with reference to an equivalent circuit, which is intended to represent the reactions taking place at the interface. The arrangement of the components in the equivalent circuit and the values related to them are intended to produce an

impedance that matches as closely as possible that of the corrosion interface under investigation[1].

The main advantages of electrochemical impedance techniques are:

(i) they often display the constituting characteristics of the system separately (charge transfer, mass transfer, surface layers),

(ii) the perturbation of the system is minor, since only very small signals which do not disturb the electrode properties are used,

(iii) corrosion rates can be measured in low conductivity media where traditional d.c. methods fail, and

(iv) polarization resistance and double layer capacitance values can be obtained in the same measurement. According to Macdonald[131], the most important advantage of this technique is the precision that can be gained by its use for mechanistic analyses, compared with other electrochemical techniques. A brief introduction to the basics of electrochemical impedance theory is presented next.

2.1.6.2 - Basics of electrochemical impedance theory

An electrode interface during an electrochemical reaction can be represented by an equivalent electrical circuit, consisting of various passive elements (resistors, capacitors and inductors). The response of the electrical circuit to an applied voltage depends upon both, the behaviour of the individual elements, and their arrangement in the circuit in relation to each other.

If an a.c. alternating potential ,E_{ac}, of the form;

$$E_{ac} = E_0 \sin(wt) \qquad (2.4)$$

where, E_o = maximum voltage amplitude,

w = angular frequency (in $rad.s^{-1}$),

t = time.

is applied across an electrical circuit, then the resulting current I_{ac} will be given by:

$$I_{ac} = E_{ac} / X \tag{2.5}$$

where X is the reactance of the specific passive element in the electrical circuit. In most cases I_{ac} is also sinusoidal and of the same frequency w, but different in amplitude and phase from E_{ac}.

$$I_{ac} = I_o \sin (wt + \emptyset) \tag{2.6}$$

where, I_o = current amplitude,

$\emptyset$ = phase shift.

The reactance of the passive elements is normally expressed as a complex quantity, using the complex number, j ($j = \sqrt{-1}$)[132]. Using this notation, the reactances of the elements are given by:

$$X_R = R \qquad \text{(for a resistor)} \tag{2.7}$$

$$X_C = 1/-jwC \qquad \text{(for a capacitor)} \tag{2.8}$$

$$X_L = jwL \qquad \text{(for an inductor)} \tag{2.9}$$

where R,C, and L, are the resistance (ohms), capacitance (farads), and inductance (henrys), respectively.

The combined effect of these reactances in the electrical circuit is known as the impedance, Z. Electrical impedance can be considered as an obstruction to flow of alternating current, and it is a vector quantity with a magnitude, or modulus, |Z|, given by:

$$|Z| = E_o / I_o , \tag{2.10}$$

and a direction, or argument $\emptyset$.

Since the impedance is a vector, it is convenient to represent it in a complex plane plot, Argand plot[132] or a Nyquist plot[133], Figure 2.5. Impedance can be expressed either as a combination of "real" (Z') and "imaginary" (Z") parts in cartesian co-ordinates, or as the impedance modulus (|Z|), and phase angle ($\emptyset$) in polar co-ordinates, that is $Z = Z' + jZ"$ or $Z = (|Z|, \emptyset)$. The two forms are related by:

$$|Z| = (Z'^2 + Z"^2)^{1/2} \tag{2.11}$$

$$\emptyset = \tan^{-1} Z''/Z' \tag{2.12}$$

and

$$Z' = |Z| \cos \emptyset \tag{2.13}$$

$$Z'' = |Z| \sin \emptyset \tag{2.14}$$

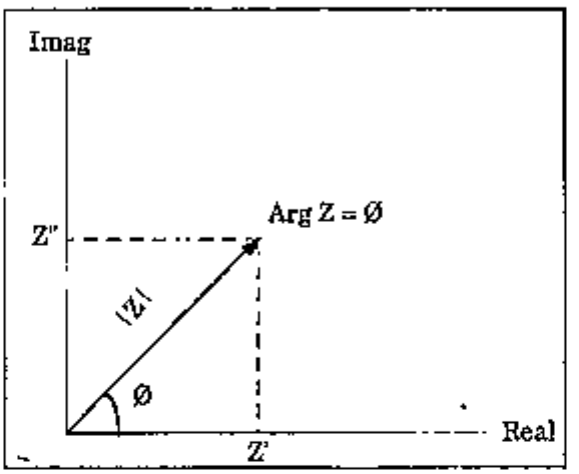

Figure 2.5 - Nyquist plot (Complex plane plot) of impedance.

The impedance of a combination of circuit elements can be calculated by the complex addition of the reactances. For a series combination of n elements, the total impedance is given by equation (2.15).

$$Z = \sum_{k=1}^{n} X_k \tag{2.15}$$

and for a parallel combination of m elements, by equation (2.16)

$$\frac{1}{Z} = \sum_{k=1}^{m} \frac{1}{X_k} \tag{2.16}$$

For systems involving parallel combinations, it is sometimes more convenient to define the admittance, Y, of the circuit, which is the reciprocal of impedance, Y = 1/Z.

The reactances of capacitors and inductors are frequency dependent, as shown by equation (2.8) and (2.9), with the following limits:

$$\text{as } w \to 0 \; : \; X_C \to -\infty \; , \quad X_L \to 0 \, .$$

$$\text{as } w \to \infty \; : \; X_C \to 0 \; , \quad X_L \to \infty \, .$$

It should be noted that in the majority of cases of interest in electrochemical work, the capacitive response occurs in the negative imaginary area. For convenience, the Nyquist plots are generally plotted as -Z'' vs Z'. In this thesis this convention will be adopted, although the imaginary axis will be only marked as Z''.

2.1.6.3 - Concept of equivalent circuit

Since the corroding electrode interface can be represented by a hypothetical electrical circuit, as has been stated in the previous section, it is useful to consider the impedance response of relevant electrical circuits, keeping in mind that this response depends upon the arrangement of the elements relative to each other, and the angular frequency of the applied voltage.

The total impedance response, Z, of a resistor and a capacitor connected in series is given by:

$$Z = R + 1/-jwC \qquad (2.17)$$

and is represented in Figure 2.6 in a complex plane plot.

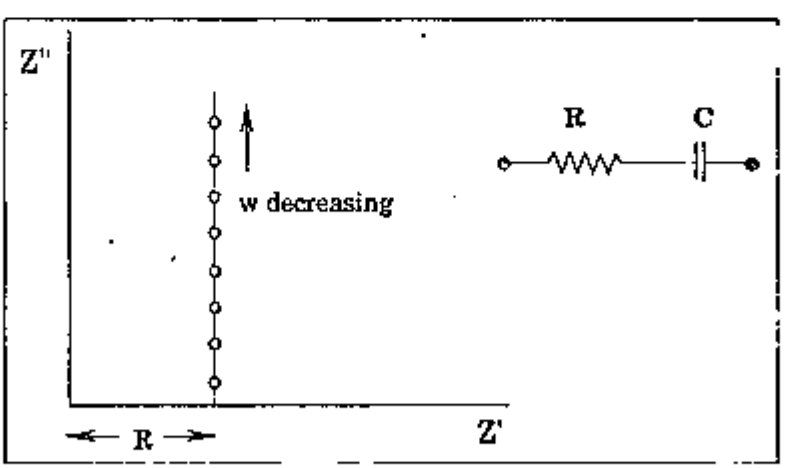

Figure 2.6 - Complex impedance plot for a series RC circuit.

In the case of a resistor and a capacitor connected in parallel, the impedance is given by:

$$\frac{1}{Z} = \frac{1}{R} + \frac{1}{\left(\frac{1}{-jwC}\right)} \tag{2.18}$$

$$Z = \frac{R}{1-jwCR} \tag{2.19}$$

If equation (2.19) is multiplied, top and bottom, by (1+ jwCR), Z may be written as:

$$Z' = \frac{R}{1+(wCR)^2} \quad \text{and} \quad Z'' = \frac{wCR^2}{1+(wCR)^2} \tag{2.20}$$

Eliminating w from both expressions in equation (2.20), a relationship between Z' and Z'' is obtained:

$$Z'^2 + Z''^2 - RZ' = 0 \tag{2.21}$$

which is the equation of a semi-circle centred on the real axis at (R/2 , 0) and whose diameter is equal to R.

Optimizing the expression for Z'' in equation (2.20), it can be shown that the maximum of the semi-circle in the positive quadrant occurs when;

$$w_{max} = \frac{1}{CR}$$

The term CR (units of seconds) is called the time constant of the circuit.

The representation of equation (2.21) on a complex plane (Nyquist) plot is shown in Figure 2.7.

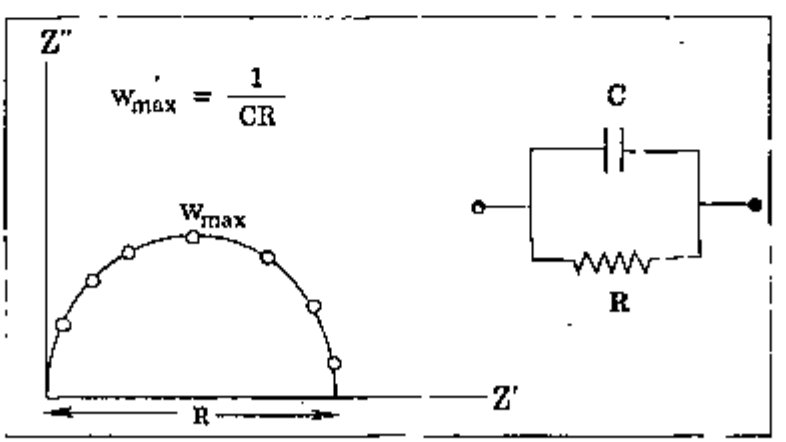

Figure 2.7 - Complex impedance plot of a resistor (R) and a capacitor(C), connected in parallel.

If to this circuit a resistor, R_s, is connected in series, the impedance response will be shifted by an amount equivalent to R_s, along the real axis. This new circuit, Figure 2.8, has been found to represent several electrochemical systems satisfactorily.

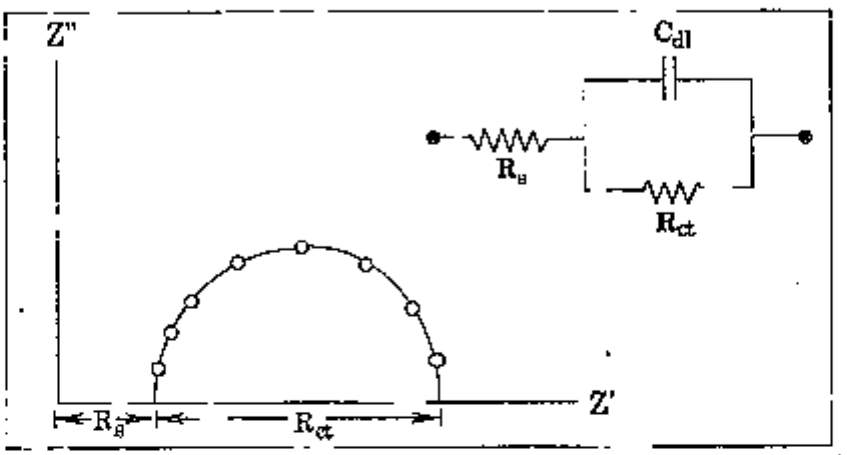

Figure 2.8 - Complex impedance plot of a resistor, R_s, connected in series with the parallel RC circuit in Figure 2.7.

The circuit elements R_s, R_{ct}, and C_{dl}, represent the solution resistance, the charge transfer resistance and the double layer capacitance, respectively. The parallel combination of R_{ct} and C_{dl} represents the corroding interface. This notation will be adopted in this thesis.

The corrosion rate, i_{corr}, is determined by the charge transfer resistance, R_{ct}, according to:

$$i_{corr} = B / R_{ct} \tag{2.22}$$

where B is a constant determined from a knowledge of the Tafel slopes, as in the Stern-Geary equation.

2.1.6.4 - Impedance of the electrode-electrolyte interface

Consider the simplest possible electrode reaction, which is a single step process, given by:

$$O + ne^- \leftrightarrow R \tag{2.23}$$

at its equilibrium, so that, at the open circuit potential, E_o, i.e., with no net current flow.

If it is assumed that the rate of the reaction (2.23) is only dependent upon the charge transfer process (single step), and the mass transport of electroactive species, and also that the disturbing potential of the working electrode is small, then the impedance of the electrode-electrolyte interface will be given by a combination of the ohmic resistance of the system (R_Ω), the effect due to the electrochemical double layer (C_{dl}), and the electrochemical reaction (R_{ct}) itself.

The ***ohmic resistance*** (R_Ω), of a system consists of the combination of the solution resistance of the electrolyte (R_s), the resistance of connecting leads, and the internal resistance of the electrodes. As the resistances of the connecting leads and electrode are usually negligible for bare metals, the ohmic resistance may be taken as the solution resistance, R_s.

The ***electrochemical double layer*** is not a perfect capacitor, but since small amplitude voltages (<20 mV) are applied to perturb the system, it can be considered as such. Its capacitance (C_{dl}), is dependent upon the permittivity of the media, ionic concentration, and its "thickness". For a perfect capacitor the relationship between the charge across the interface and the applied voltage is approximately linear.

The ***charge transfer resistance*** (R_{ct}), is defined as the resistance to electron removal or addition, and for small perturbation voltages (<20 mV), it is given by:

$$R_d = \left(\frac{\partial E}{\partial I}\right)_E \qquad (2.24)$$

The Warburg impedance

So far, only electrode reactions under activation control have been considered. In practice, however, effects due to diffusion processes are often present. These must also be considered.

The impedance due to mass transport (diffusion) of electroactive species to and from the electrode-electrolyte interface is known as ***Warburg impedance***, and is expressed by equation (2.25):

$$Z_w = \sigma w^{-1/2} - j\sigma w^{-1/2} \qquad (2.25)$$

where σ = Warburg coefficient

w = angular frequency.

At a constant potential, the Warburg coefficient is given by:

$$\sigma = \frac{RT}{z^2 F^2 \sqrt{2}} \left(\frac{1}{C_{ox} D_{ox}^{\frac{1}{2}}} + \frac{1}{C_{red} D_{red}^{\frac{1}{2}}} \right) \qquad (2.26)$$

where R = Universal gas constant,

T = Absolute temperature,

F = Faraday constant,

z = number of electrons involved,

D_{ox}, D_{red} = diffusion coefficients,

C_{ox}, C_{red} = "d.c. components" of the concentrations at the surface, controlled by the mass transport involved in d.c. process.

From equation (2.25) it can be seen that at any frequency, the real and imaginary parts are equal and proportional to $w^{-1/2}$. When plotted on a Nyquist diagram, the Warburg impedance is represented by a straight line at 45° to the axis. It should be noted that the effects of the Warburg impedance are only significant at low frequencies, and are not observed at high frequencies.

Randles[134] showed that the impedance of the electrode reaction could be represented as a combination of impedances due to charge transfer and mass transport. The impedance due to mass transport is normally represented by the Warburg impedance, Z_w. The equivalent circuit representing mixed control, charge and mass transfer, is known as Randles' equivalent circuit, and it is shown in Figure 2.9.

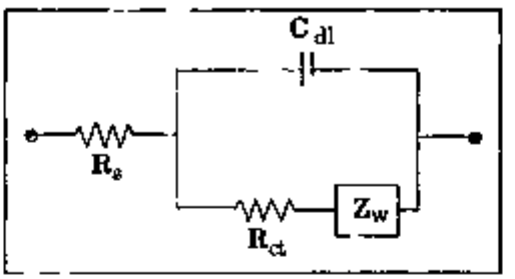

Figure 2.9 - Randles equivalent circuit[134].

The combined effects of the impedance due to charge transfer (R_{ct}), and diffusion processes (Z_w), is called Faradaic impedance. The Faradaic impedance (Z_F), at any potential is given by:

$$Z_F = R_{ct} + Z_w \tag{2.27}$$

2.1.6.5 - The Randles equivalent circuit

The total impedance of the Randles equivalent circuit which represents the simplest reaction is given by:

$$Z = R_s + \frac{1}{jwC_{dl} + \dfrac{1}{R_{ct} + \sigma w^{-1/2} - j\sigma w^{-1/2}}} \tag{2.28}$$

The analysis of the equation (2.28) can be simplified by considering the two limiting cases[135]:

(1) At high frequencies ($w \rightarrow \infty$), the relative contribution of the Warburg impedance is negligible because $\sigma w^{-1/2} \rightarrow 0$, and thus the real and imaginary parts of equation (2.28) can be expressed as:

$$Z' = R_s + \frac{R_{ct}}{1 + w^2\tau^2}, \text{ and } \quad Z'' = \frac{w\tau R_{ct}}{1 + w^2\tau^2} \tag{2.29}$$

where τ is the time constant of the system. If w is eliminated from both expressions in equation(2.29), it becomes:

$$\left(Z' - R_s - \frac{R_{ct}}{2} \right)^2 + (Z'')^2 = \left(\frac{R_{ct}}{2} \right)^2 \qquad (2.30)$$

This result is similar to the one obtained when the solution resistance, R_s, was connected in series to the parallel combination of a resistor and a capacitor, showed in Figure 2.8.

(2) At low frequencies ($w \rightarrow 0$), the contribution due to Warburg impedance becomes significant, and the semi-circle observed at high frequencies distorts. The real and imaginary parts of the impedance reduces to:

$$Z' = R_s + R_{ct} + \sigma w^{-1/2}, \text{ and } Z'' = \sigma w^{-1/2} + 2\sigma^2 C_{dl} \qquad (2.31)$$

When w is eliminated from equation (2.31), it results in a expression corresponding to a straight line with a slope 45°, given by:

$$Z' = R_s + R_{ct} - 2\sigma^2 C_{dl} + Z'' \qquad (2.32)$$

The intersection of this line with the real axis, I_{int}, occurs when:

$$I_{int} = R_s + R_{ct} - 2\sigma^2 C_{dl} \qquad (2.33)$$

The total response of the Randles equivalent circuit for real systems consists of the combination of the two limiting cases. A typical plot is shown in Figure 2.10.

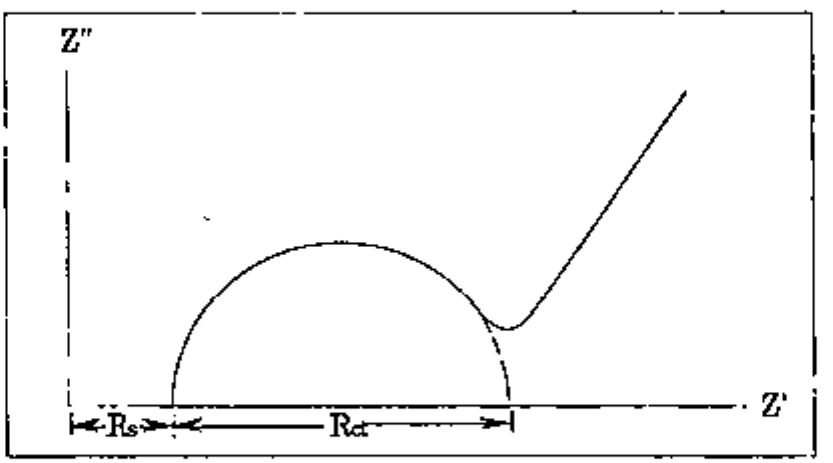

Figure 2.10 - Complex impedance plot for Randles equivalent circuit representing an electrode process under mixed control.

The relative values of R_{ct}, σ and C_{dl}, determines the actual shape of the complex impedance plot. The ratio between R_{ct}, and σ can be used as a criteria to determine whether the electrode process is under activation (charge transfer), or mass transport (diffusion) control[135].

$R_{ct}/\sigma > 10$	Activation control
$R_{ct}/\sigma < 0.1$	Diffusion control
$R_{ct}/\sigma \sim 1$	Mixed control.

2.1.6.6 - Departure from classical Warburg behaviour

According to the classical Warburg theory, the impedance due to diffusion effects is given by $Z_w = \sigma w^{-1/2} - j\sigma w^{-1/2}$, equation (2.25), presented earlier. Although this equation represents many real systems satisfactorily, it presents a pitfall at frequencies approaching zero. At this limiting condition, i.e. d.c. condition ($w \rightarrow 0$), the Warburg impedance is infinite.

$$\lim_{w \rightarrow 0} Z_w = \infty \qquad (2.34)$$

However, it is well known that the d.c. resistance of an electrochemical cell is finite, and given by the polarization resistance, R_p. In order to overcome this limitation, Sluyters[135] introduced the concept of a finite diffusion layer, replacing the infinite one used to derive the classical expression. The Warburg expression for a finite diffusion layer is given by equation (2.35):

$$Z_w = \sigma w^{-1/2} \left(\frac{\sinh(2u) + \sin(2u) - j[\sinh(2u) - \sin(2u)]}{\cosh(2u) - \cos(2u)} \right) \qquad (2.35)$$

where

$$u = \delta_N \left(\frac{2w}{D} \right)^{1/2} \qquad (2.36)$$

δ_N = thickness of the Nernst diffusion layer,

σ = Warburg coefficient.

At high frequencies, equation (2.35) reduces to the classical Warburg equation, and at low frequencies, the convection term becomes significant causing the straight line to bend towards the real axis. This complete Warburg impedance for a finite diffusion layer is plotted in Figure 2.11.

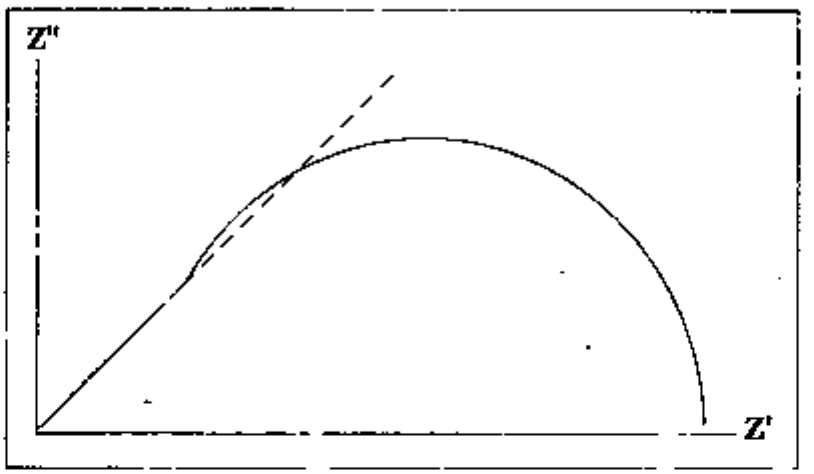

Figure 2.11 - Complete Warburg impedance for a finite diffusion layer

2.1.6.7 - Non-ideal behaviour of the electrode-electrolyte interface

The charge transfer resistance and the electrochemical double layer of the electrode-electrolyte interface have so far been assumed to behave as a perfect resistor-capacitor network. Perfect semi-circles are, however, rarely obtained in practice[136,137]. The depression, often observed, causes the centre of the semi-circle to shift below the Z'-real axis, and the value of the resistance is no longer given by the diameter of the semi-circle, but by the chord, AB, as shown in Figure 2.12. The angle that the diameter subtends with the Z-real axis, ß, is known as the depression angle.

Cole and Cole[138] assumed that the depression observed in the semi-circles was caused by a distribution in the time constant, τ, about a mean value, τ_o. Inhomogeneities on the electrode surface, leading to local variation on R_{ct}^* and C_{dl} over the surface, are considered to be the cause for the time constant dispersion.

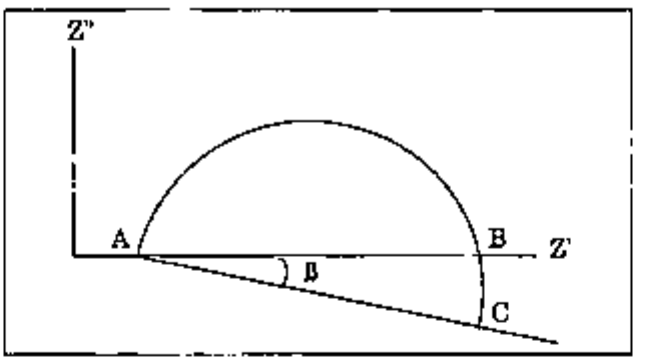

Figure 2.12 - Depressed semi-circle (for charge transfer only).

Only the simplest process, single-one step reaction, has been considered in the previous sections. However, in most practical cases, the electrode reaction is a multi-step process. The additional processes have a complex effect on the impedance response of the system. Complicated impedance responses may be produced by processes such as adsorption of intermediates, surface films, and so on. A discussion of all the processes that affect the impedance response is out of the scope of this thesis. Instead, emphasis will be given to the influence of organic coatings on the impedance of metals. It must be pointed out that, in general, the complex impedance plots originating from multi-step reactions, can be represented by a modified version of the Randles equivalent circuit.

2.1.6.8 - Painted metal equivalent circuits

An equivalent circuit model for the painted metal-electrolyte interface requires inclusion of paint film parameters to the circuit of Figure 2.8. Many workers[139-143] proposed a model similar to that shown in Figure 2.13.

Some workers[34,141] interpreted the resistor, R_{pf}, as the pore resistance due to electrolyte penetration. A more rapid solution uptake was suggested to occur at damaged areas of the film[142], or at pre-existing holes, or porous areas in the polymer with inadequate cross-linking[143]. Mikhailovskii[142] interpreted the capacitor, C_{pf}, in Figure 2.13, as the capacitance of the electric capacitor consisting of the metal, paint and electrolyte, with the paint film as a dielectric.

Kendig and collaborators[34] considered C_{pf} simply as the capacitance of the intact film, and Walter[143] as the capacitance where rapid electrolyte penetration does not occur.

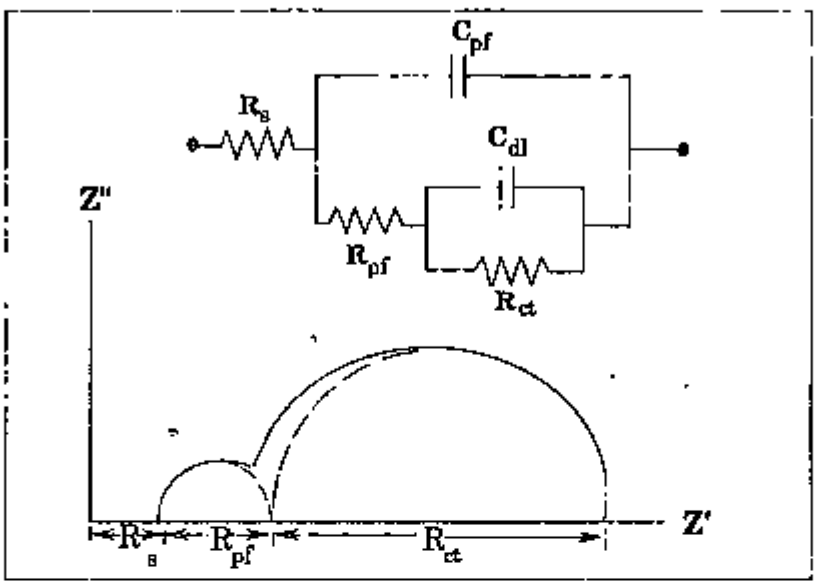

Figure 2.13 - Complex plane plot (Nyquist plot) and equivalent circuit model of a painted metal-eletrolyte interface[144].

The time constants for the paint film, τ_{pf} , and for the metal, τ_m, are given by:

$$\tau_{pf} = R_{pf} C_{pf} \quad ; \quad \tau_m = R_m C_m \tag{2.37}$$

If $\tau_{pf} > \tau_m$, the semi-circle observed at high frequencies is attributed to the paint film, which is usually the case.

The following criteria must be met if two distinct semi-circles are to be observed[144]:

$$\text{(i)} \quad 0.2 \leq (R_{ct}/R_{pf}) \leq 5 \tag{2.38}$$

$$\text{(ii)} \quad \tau_m / \tau_{pf} \geq 20 \tag{2.39}$$

According to the first criterion the two semi-circles diameter cannot be too different, and the second criterion implies that the values of w_{max} for each semi-circle cannot be too similar. When these criteria are not met, the two semi-circles

interact with each other, and the components of the equivalent electrical circuit are difficult to be separated. Figure 2.14 shows an example where one of these criteria are not met, and the two semi-circles are not distinctly separated.

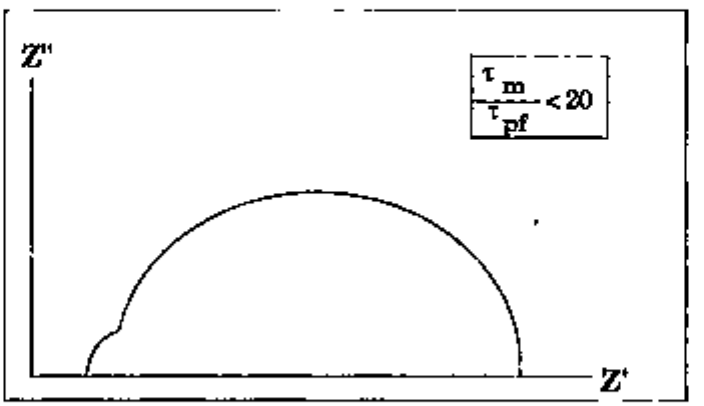

Figure 2.14 - Complex plane plot and equivalent circuit of a painted metal-electrolyte interface with an indistinct separation of the paint film and metal components.

Irregularities in the shapes of plots of practical systems should be dealt with carefully, since they can indicate the presence of other components in the equivalent circuit model. Inaccurate components values will result when the complex plane plot (Nyquist plot) is treated as if there was only one semi-circle, but in reality it is a combination of two interacting semi-circles. For the case of clear separation into two time constants, the respective component values can be obtained by treating each time constant separately. More complicated analysis will be needed for the cases of interacting semi-circles. Some methods such as iterative curve fitting, deconvolution and others, have been developed for cases where impedance data present difficulties in interpretation[144].

Diffusion processes within pores in the paint film

To account for the effects of diffusion processes within the pores in the paint film, the Warburg impedance, Z_w, is included in the circuit of Figure 2.13, placed

in series with R_{ct}. The capacitance of the double layer, C_{dl}, may[143] or may not[34] appear in parallel with $R_{ct}+Z_w$.

At $\sigma = 0$, (no diffusion process), the complex plane plot is identical to the one shown in Figure 2.13. At higher σ values, a diffusion tail begins to appear at low frequencies, attached to the second semi-circle. When σ becomes about equal to R_{ct}, the diffusion tail begins to overlap the second semicircle and subtends an angle of 45° to the Z' axis. The overlap becomes increasingly more severe at higher values of σ , and finally , the diffusion tail completely distorts the semi-circular shape of the second semi-circle, being initially greater than 45° to the Z' axis. Figure 2.15 shows the increasing effects of the diffusion on the complex plane plots (Nyquist plots) of a painted metal-electrolyte interface[144].

The values of σ can be estimated by finding a region on the Nyquist complex plane plot at low frequencies where the diffusion tail is inclined at an angle of 45° to the Z' axis. Within this region σ can be calculated from $Z'' = \sigma w^{-1/2}$ which is obtained from equation (2.25).

2.1.6.9 - Practical impedance measurements

The impedance measurement of a system consists of the application of an alternating (sinusoidal) voltage signal to the system, and the analysis of the response to this perturbation. The frequency of the alternating signal is generally varied over a large range. The input voltage and current response of the system are measured during the test. The maximum amplitude of the applied a.c. voltage must be sufficiently low to not induce damage by perturbation, but high enough to provide a measurable current at low frequency[145]. The impedance components generated are plotted either on a Nyquist (real versus imaginary) or Bode (log modulus of the impedance versus log frequency plus log phase angle versus log frequency) plot. These data normally require analysis by computer.

Early experiments were carried out using a.c. bridge methods, oscillographic methods, and phase sensitive detectors, such as lock-in amplifiers. These measurements, however, were tedious and extremely time-consuming particularly in the low frequency region of the measurements.

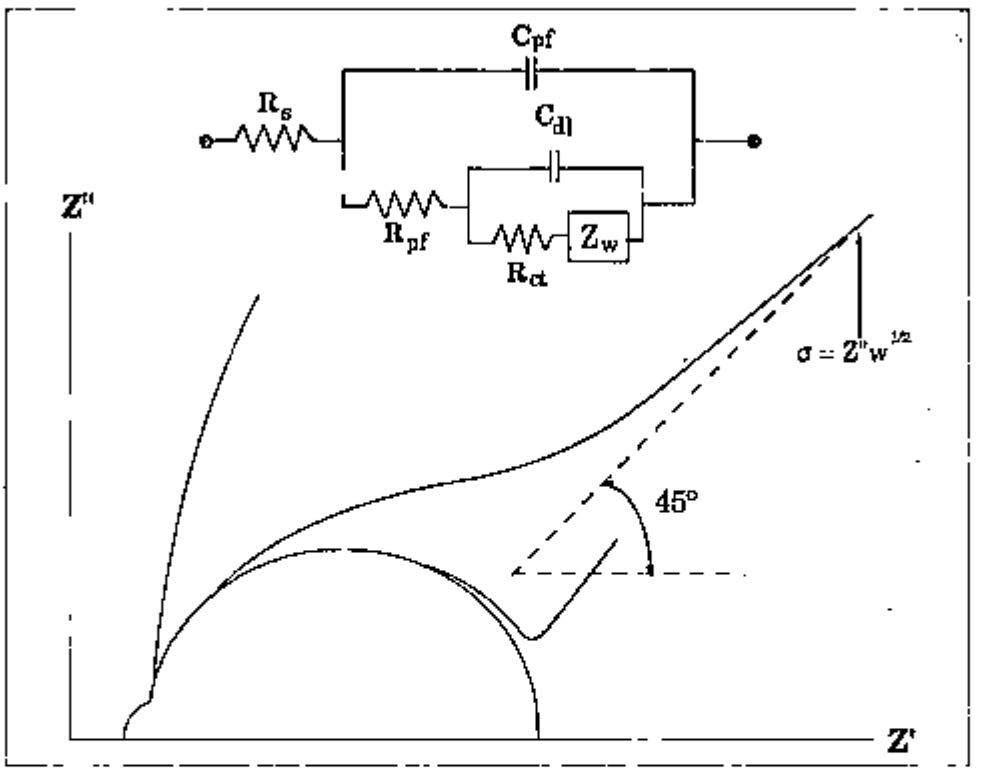

Figure 2.15 - Complex impedance plots for a painted metal-electrolyte interface in the presence of diffusion[144].

In recent years, the advent of modern digital techniques, simplified enormously the acquisition and analysis of data generated by a.c. techniques. These techniques involve the use of digital frequency response analysers, (F.R.A.). The F.R.A. consists of a programmable generator and a two channel analyser. The generator provides the disturbing sine wave, and the analyser correlates the voltage and current responses of the system. The information is fed to a microcomputer via an interface. The generator is then reset to a new frequency by the microcomputer's software, and the process is repeated. Several

arrangements can be used with the F.R.A. to obtain electrochemical impedance measurements. The two methods employed in this work are presented below.

i) Two-electrode impedance measurements

The circuit diagram for this arrangement is given in Figure 2.16. The output from the F.R.A. is applied across the cell and a counter resistor, R, in series. The resulting cell current and voltage are measured on the F.R.A. channels V_g and V_c respectively. Since the operational amplifier has a very high input impedance, the point A is a virtual earth, and therefore the current, i, flowing in the cell and the counter resistor, R, is the same[146].

From Ohm's law:

$$i = \frac{V_g}{Z_c} = \frac{V_c}{R} \qquad (2.40)$$

and the cell impedance, Z_c, is given by:

$$Z_c = \frac{V_g}{V_c} \cdot R \qquad (2.41)$$

where V_g = Output voltage of generator

V_c = Output voltage of operational amplifier

Z_c = Cell impedance

R = Counter resistor.

The F.R.A. measures the ratio V_g/V_c, and since R is known, Z_c can be calculated. For bare metals, the two working electrodes must have similar rest potential, since a large potential difference between the two electrodes introduces an additional impedance to the measurements. When two similar electrodes are used, the cell impedance will be twice the impedance of each electrode, so the impedance for unit area ($\Omega.cm^2$) is given by[146]:

$$Z = Z_c / 2 \qquad (2.42)$$

In the case of painted metals, a low impedance probe (large piece of platinum or graphite) can be used. This configuration is useful for experiments carried out at the rest potential.

The input impedance of the operational amplifiers used nowadays is of the order of 10^{14} Ω, and impedances up to 10^{12} Ω can be measured accurately if a suitable counter resistor, R, is used. The operational amplifier in Figure 2.16 is wired in a current to voltage converter model[146].

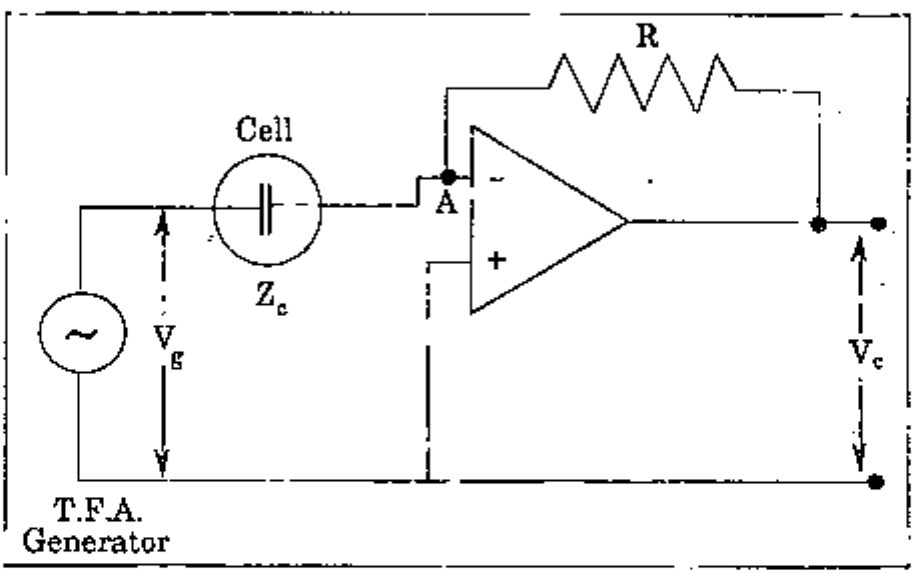

Figure 2.16 - Circuit diagram for two electrode impedance measurements.

ii) Three electrode impedance measurements

In this configuration, Figure 2.17, the generator output is connected to the external input of a potentiostat. The potentiostat is used to control the d.c. potential of the working electrode. The required working potential is set using the internal reference on the potentiostat. The F.R.A. superimposes a sine wave signal upon the fixed potential level. The a.c. signal is then applied and the measurements taken. The cell current is measured across the potentiostat's counter resistor, R, and the cell voltage is taken between the working and reference electrodes. Similarly, as in the two electrode configuration, the F.R.A. measures the ratio of the cell voltage, V_g , to the voltage across the counter

resistor, V_c. The manner in which the F.R.A. is set, only the a.c. response is analysed. The d.c. component is eliminated electronically by the F.R.A. In this arrangement, phase shifts occurring in the potentiostat at high frequencies, are minimized. If the impedance due to the counter electrode is negligible, e.g. inert electrode of relatively large area compared to working electrode, then the impedance of the system for unit area of the electrode, is:

$$Z = Z_c.A \tag{2.43}$$

where A is the area of the working electrode.

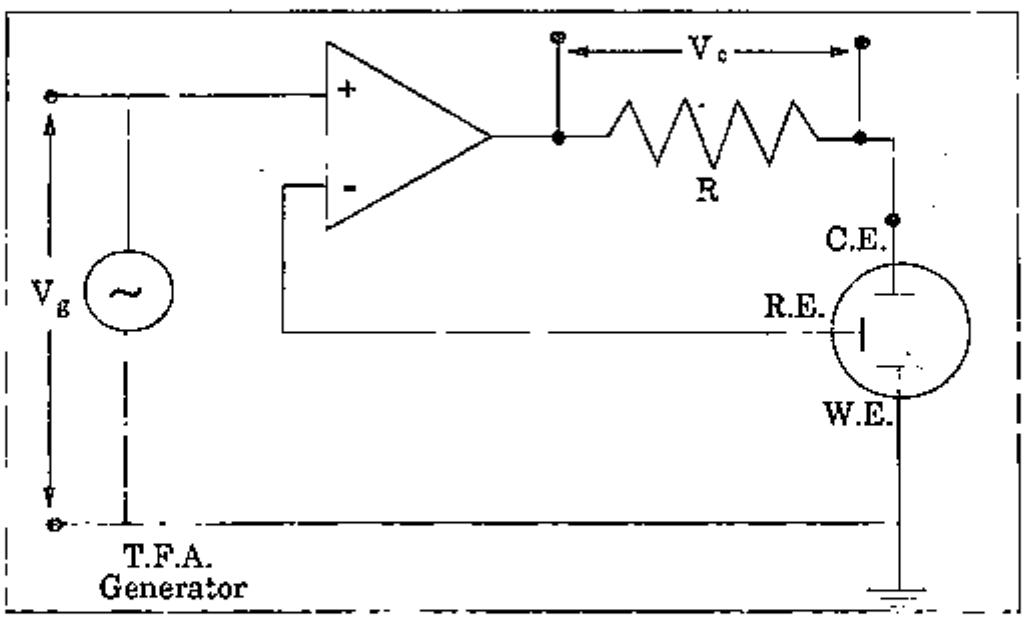

Figure 2.17 - Circuit diagram for three electrode impedance measurements.

2.1.6.10 - Graphical representation of impedance data

The complex plane plot , also known as Nyquist plot, and the Bode plot are the two most common methods of presenting data for the determination of equivalent circuit component values. In the previous sections, only complex plane plots have been presented. The complex plane plot often gives a good outline of a system. However, it has been suggested[147] that the Bode plot presents the impedance data in a clearer way. The Bode plot consists of two curves, that of the

logarithm of the modulus of the impedance, (log|Z|), and of the phase angle, Ø, plotted versus the logarithm of the frequency. A pure resistive element on such a plot is represented by a horizontal line and a constant Ø of 0°, while a pure capacitive element is a straight line of slope -1 and a constant Ø of -90°. A Warburg impedance is a straight line of slope -1/2 and a phase angle Ø of -45°.

The Bode impedance plots for some of the systems presented in the previous sections are shown in Figures 2.18 to 2.21. The regions of transition between asymptotic values correspond to those regions where the resistive and capacitive reactions have comparable values, neither being completely dominant. Their equivalents in the Nyquist plots are semi-circular sections.

The main disadvantages of the complex plane plots are:

i) the frequencies are not uniformly distributed on the plot, and

ii) since the measured values of frequency of individual points have to be displayed on the plot, this can lead to overcrowding, mainly in the high frequency region. Another disadvantage is that a change in value, for example of the capacitance, still retains the shape of a semi-circle, and the change is only noted in the different position of a given frequency on the curve. Bode plots are more suited for systems showing more than one time constant, and where one or more of these are changing. For systems with widely separated time constants, the complex plane plot will require more than one diagram to represent distinctly the various processes, as otherwise parts of the plot will be cramped[147].

The use of Bode phase diagrams as standard plots has been recommended, since all the experimental data are equally represented, and since the phase angle is a very sensitive indication of the occurrence of additional time constants in the impedance spectrum, identifying the presence of plot shape irregularities[147]. Nyquist plots are, however, believed to be easier in identifying the presence of and analysing the values of Warburg diffusion impedance[148]. Thus, both plots, Nyquist and Bode, are complementary to each other when used simultaneously.

2.1.6.11 - Limitations of electrochemical impedance techniques

Although electrochemical impedance techniques present several advantages over d.c. techniques, and these have been presented in previous sections, they are not without limitations. One of the major limitations of these techniques is that it only provides corrosion resistance, corrosion rates are not obtained. The interpretation of the impedance data is usually difficult and this is most probably the area where future work is required. Difficulties are also associated with the accuracy of the technique itself. In some cases, an appropriate model cannot be found to fit the impedance data, and in other cases even when the equivalent circuit is known, components values may not be resolved[144]. The analysis of impedance spectra is also difficult when one of the components of the model presents a very high value, or when the time constants of the various processes involved interact. In the case of painted metals, if in the initial immersion periods the nature of the painted metal is highly capacitive, the lower frequency behaviour cannot be resolved into individual components[34], or can only be resolved at longer immersion periods[140].

Inaccurate interpretation may also result because not all semi-circles and straight lines on the complex plane plot represent valid impedances[147]. The application of Kramers-Kronig relationship, (K-K) is recommended in these cases to test the validity of the impedance response[130]. For the application of (K-K), four conditions must be fulfilled: (i) causality meaning that the response of the system is due only to the perturbation applied; (ii) linearity, which requires that the impedance be independent of the magnitude of perturbation, (iii) stability which means that the system must return to its original state after the perturbation is removed, and (iv) the impedance must be finite at $w \rightarrow 0$ and $w \rightarrow \infty$, and continuous and of a finite value at all intermediate frequencies[130].

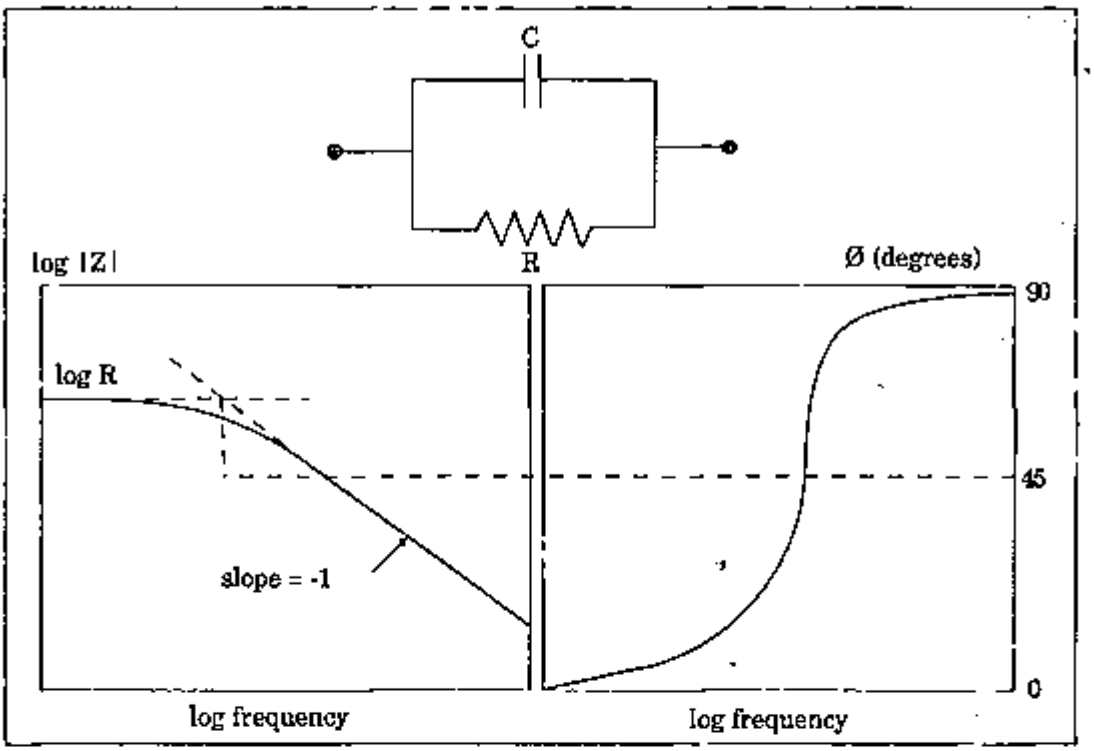

Figure 2.18 - Bode plot for a parallel RC circuit.

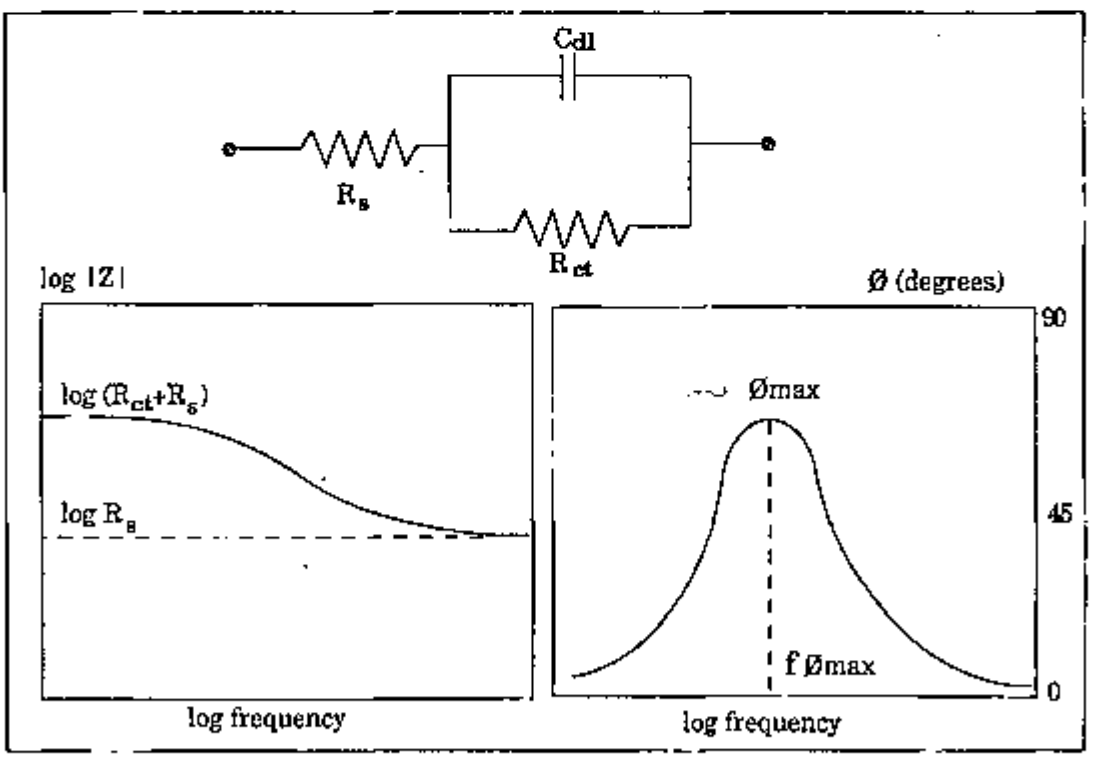

Figure 2.19 - Bode plot for a series-parallel three elements circuit.

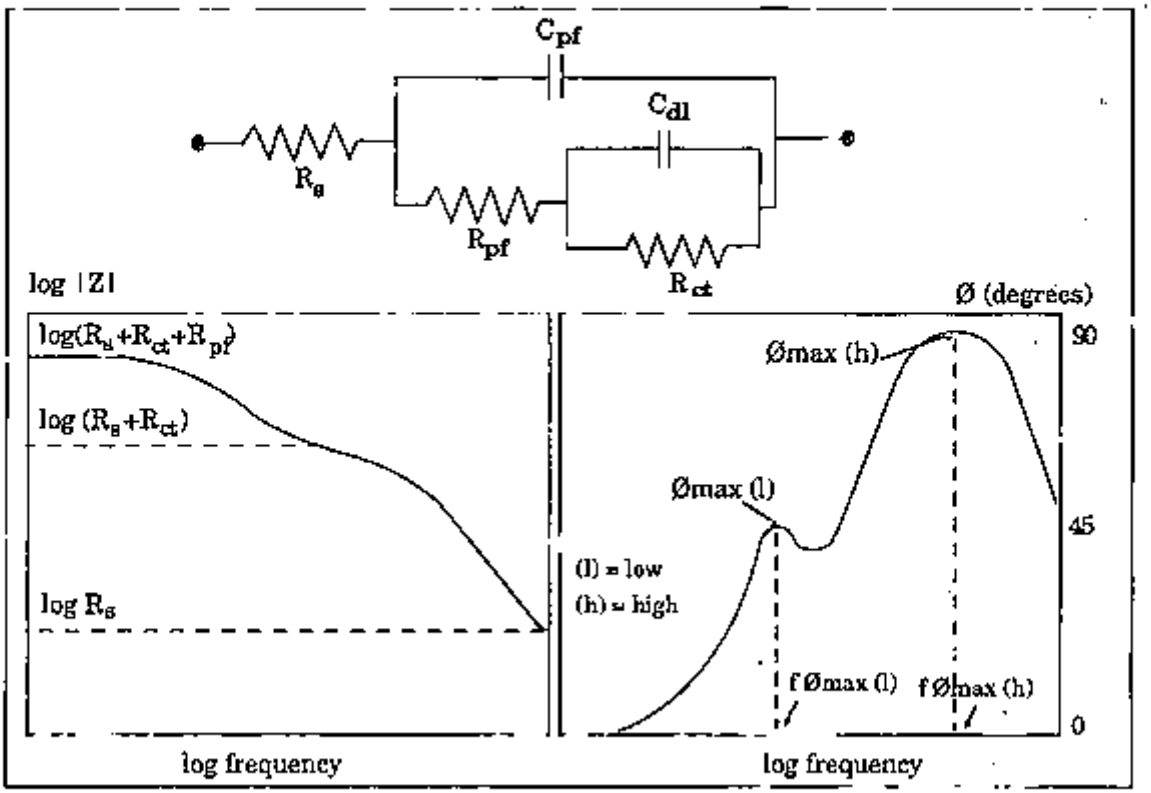

Figure 2.20 - Bode plot for a painted metal-electrolyte interface without diffusion effects.

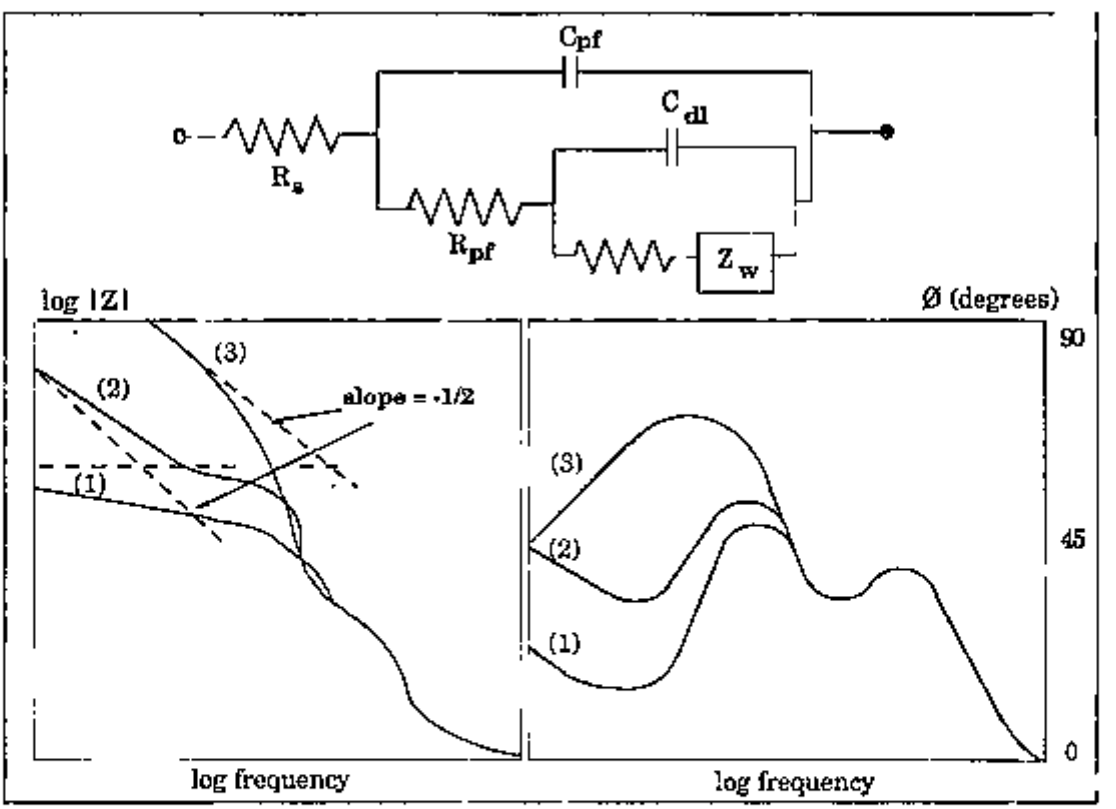

Figure 2.21 - Bode plot for a painted metal electrolyte interface showing the effect of varying diffusion coefficients on Nyquist and Bode plot shapes, $\sigma=10^5$ (1), $\sigma=10^6$ (2), $\sigma=10^7$ (3)[144].

The correct interpretation of depressed semi-circles also presents difficulties. It has been shown that two different interpretations can be applied to the same Nyquist depressed semi-circle[150]. Analysis according to Cole-Cole frequency dispersion[138] was found to give a similar plot shape to the true analysis of a model based on two heavily interacting time constants. Severely depressed semi-circles may also be interpreted either as extreme cases of Cole-Cole dispersion or as undispersed diffusion[34].

Walter[144] in a review on impedance methods for the analysis of corrosion performance of painted metals, suggested several possible causes for the dispersion in organic coated metals. These included; paint film local thickness variations, local areas of greater solution uptake leading to networks in the paint film, variations in substrate-paint adhesion, surface heterogeneity, high resistance surface films, adsorption of reactants products or intermediates species on the substrate surface, series of complex reaction steps at electrode-electrolyte interface, solid corrosion products of the substrate developing in paint film defects, porous electrodes, and surface roughness.

Complications may also arise due to inductive loops and diffusion tails which bend toward the real (Z') axis at low frequencies, and these must be considered if an accurate equivalent circuit is to model the impedance data[144]. Finally, although the time duration of the impedance test, for a frequency range of 10^3 Hz to 10^{-2} Hz, is low when compared to weight loss measurements, it is still considered long for rapidly changing systems.

2.1.6.12 - Electrochemical impedance applied to coated metals

In recent years, the large amount of work reported in the literature has shown that the electrochemical impedance technique is particularly useful in analysing interface processes, and coating performance[72,78,151-163]. If the impedance is sampled over a large frequency range, the various processes

involved in the protective action of the coating can be determined. The interpretation of the resulting impedance data allows the determination of the individual components of an equivalent electrical circuit that best approximates the behaviour of the painted metal/solution interface. Also the analysis of the changes in the component values of the circuit during immersion provides not only mechanistic information on the degradation of coatings but also a quantitative means of comparing the performance of different samples[34].

The electrochemical impedance technique has proved to be a successful tool for following the degradation of the paint film and the corrosion reaction occurring at the substrate surface[151-158]. The high frequency semi-circles, observed in Nyquist complex plane plots, have been found to represent the intact part of the coating whereas the low frequency data points have been associated with the Faradaic process occurring on the bare metal through the defects and pores in the coating[18,34,139-143].

Hepburn and co-workers[154] concluded that diffusion impedance responses for corroded painted mild steel are caused by diffusion of electroactive species through the corrosion product in the pores of the coating, and this controls the corrosion reactions in neutral solutions. According to the same authors, where soluble corrosion products are formed, diffusion control gives way to charge transfer control of corrosion reactions at the base of the pores. Callow and Scantlebury[155] also associated diffusion impedance response with the formation of insoluble corrosion products on painted metals, and Beaunier et al[156] observed a charge transfer response when soluble corrosion products formed at the base of pores in the coating.

The coated metal/solution interface has been largely described[136,140,141,160,161] as an electrical equivalent circuit reflecting a porous film behaviour. The resistance associated with the paint film resistance, is considered as a pore resistance due to electrolyte penetration. Mansfeld and collaborators[140] observed that the penetration of the coating by the electrolyte

resulted in an impedance behaviour typical of a dielectric film short-circuited by conducting electrolyte paths perpendicular and parallel to the polymer/metal interface. Titz and co-workers[162] carried out electrochemical impedance measurements to describe quantitatively perfect and imperfect coatings. They concluded that if insoluble corrosion products, formed during long-time exposure at the corrosion potential, cover the anodic area at the metal/electrolyte interface and plug the pores, the characterization of the corrosion protection by imperfect organic coatings can become difficult.

Feliu and collaborators[163] used peelable films to separate the effect of the metallic substrate from that of the film in the impedance diagrams. The metal-paint system showed only a single semi-circle whose high frequency diameter was greater than the semi-circle diameter of the free film. The semi-circle corresponding to the metal-paint system was then suggested to include both, the ionic resistance of the paint film and the polarization resistance of the corrosion reaction. Two semi-circles only appeared when the time constant corresponding to the corrosion reaction, t_2 , was much larger than the one corresponding to the ionic resistance of the film, t_1. The condition $t_2 >> t_1$ was only found to occur when the pores in the coating exceeded a critical size. Previously, Faidi and Scantlebury[164] had also found that only a high frequency semi-circle is observed when $R_1 >> R_2$, two could be seen for $R_1 > R_2$, and a low-frequency semicircle was noted for values of R_1 close to R_2, with R_1 representing the characteristics of the high resistance solution which simulated organic coatings, and R_2 the corrosion process.

2.2 - Methods for surface chemical analysis

2.2.1 - Introduction

Two spectroscopic techniques for the chemical analysis of surfaces, X-Ray Photoelectron Spectroscopy (XPS) and Auger Spectroscopy(AS), were used in this work, and the basics of these techniques are briefly presented below.

2.2.2 - X-Ray Photoelectron Spectroscopy (XPS)

X-Ray Photoelectron Spectroscopy is a powerful tool in chemical analysis and in the determination of orbital changes of both neutral and ionic species. The method utilizes the characteristic kinetic energy distribution of the photoelectrons that are ejected in the photo-ionization process. It involves the ionization of atoms or molecules in the surface of sample by a beam of monoenergetic photons with energy hv. The incident photons are produced by an X-ray source and focussed on the sample surface[165]. In this process the sample loses an electron from an inner or outer shell, according to:

$$M + hv \rightarrow M^{+}_{(E_{int})} + e \qquad (2.44)$$

where M^{+} is the resulting ion formed

E_{int} is the internal energy associated with the formed ion

e is the product photo-electron

v is the frequency of the incident photon

h is the Planck's constant.

The photoionization process is schematically represented in Figure 2.22. E_{int} includes electronic, vibrational, and rotational energy of the ions. If $E_{int} = 0$ the ion formed is in its ground state. If photo-ionization is to occur the incident photon must possess an energy higher than the lowest ionization potential, I_P, of the sample atom or molecule[165].

When monoenergetic photons are used for ionization, the kinetic energy of the photoelectrons ejected is given by:

$$E_P = hv - (I_P + E_{int}) \qquad (2.45)$$

Equation (2.45) provides the ionization potential of the sample to form its own ions in a certain energy state. Since ionization potentials, also called binding energies, are characteristic properties of atoms and molecules, the method provides a direct means for chemical analysis.

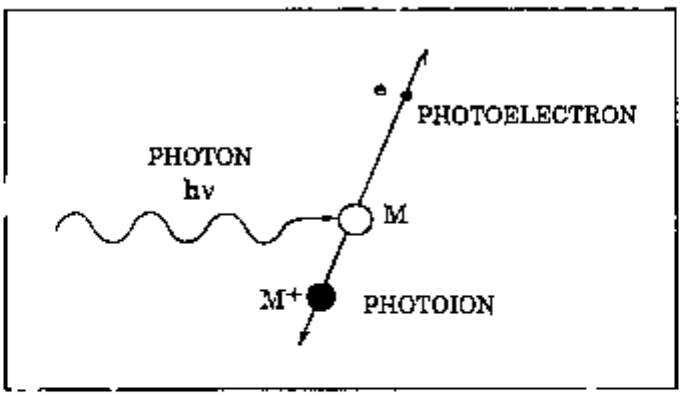

Figure 2.22 The basic photoionization process[165].

In principle, the binding energies of all the electrons in a species, from the most weakly bound to the most strongly bound may be provided by Photoelectron Spectroscopy[167]. Figure 2.23 shows the photoionization of an atom in the sample surface, by removal of a 1s electron from the K electron shell. If the binding energy associated with the orbital is less than the energy of the incident photon, ejection may occur.

The basic requirements of the technique are relatively simple consisting of a monoenergetic photon source and an electron energy analyser[165]. The recorded spectrum may serve either to identify the elements present and/or provide information about the structure of the sample[166]. A photoelectron spectrometer consists of a source of monochromatic radiation, a sample compartment where the photoelectric effect takes place, an energy analyser which can be controlled to allow only electrons of specific energy to pass, and an electron detector. The photocurrent measured by the detector is sent to some recording device, and is plotted against the setting of the energy analyser to provide the spectrum[168].

Limitations of XPS technique

One of the major drawbacks of this technique is that the incident photons cannot be focussed, thus spatial resolution within the overall area of a few millimetres square which contributes to the signal, is little or none[169].

Difficulties are also met in finding the proper area of the specimen for the analysis, or at what stage the analysis should occur. Useful information can be obscured by various factors such as contamination due to specimen handling, oxide formation upon specimen exposure to air, inappropriate cleaning procedures, and/or conditions required for the analysis (vacuum and beam effects)[170]. Control specimens and few standards are needed for a direct analysis of a corroded specimen. Another pitfall of the technique is its inability to detect hydrogen and helium .

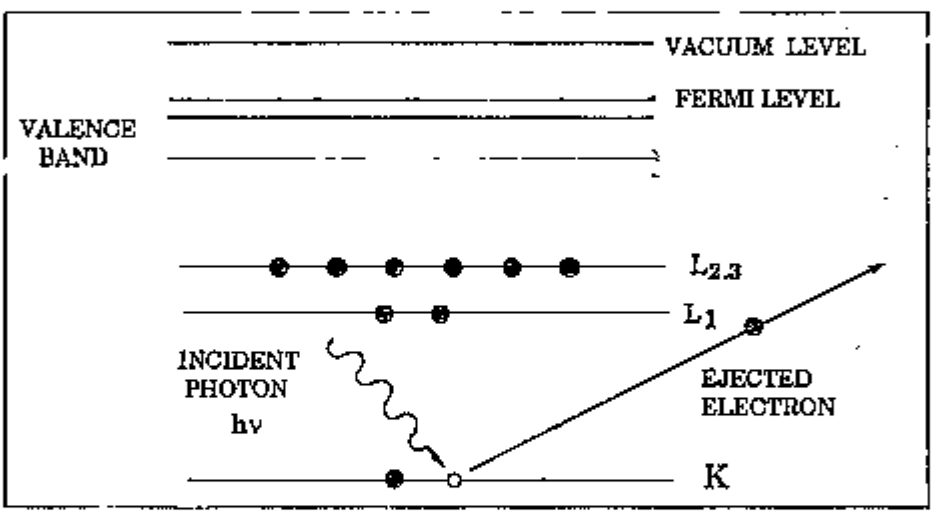

Figure 2.23 - Schematic representation of the basic photoionization process[167].

The other electron spectroscopic technique used in this work is concerned with electrons released in a secondary step following the initial ionization, known as Auger Spectroscopy.

2.2.3 - Auger Spectroscopy (AS)

In this technique, electrons are emitted from the surface of the sample from an excited state produced by an incident beam of X-ray photons or electrons. Whereas the photoionization is a one step process, the Auger process is a two-step process, and the energy of an Auger electron will depend only upon the electrons

energy levels of the states involved in the secondary process, being independent on the energy of the incident species. Thus, the electrons released in Auger Spectroscopy are determined only by the nature of the atoms from which they originated and their chemical environment, and a monochromatic source to study Auger spectra is not needed.

In Auger spectroscopy the primary process consists of the absorption of energy by the sample when bombarded, and the ejection of an electron out of an inner orbital (e.g. orbital K). The vacancy created is then filled by an electron falling back from a higher level (e.g. L_1), thereby providing sufficient energy to eject a second electron from the molecule, the "Auger electron"[171].

The energy of the Auger electron is expressed as:

$$E_A = E_K - E_{L_1} - E_{L_{2,3}} - E_{int} \qquad (2.46)$$

where the term $E_{L_{2,3}}$ represents the level from which the second electron is lost, Figure 2.24. As it can be seen, the Auger process involves transitions between three electron orbitals. The energy analysis of the Auger electron also leads to information about the energy levels of the sample[165].

Usually Auger Spectroscopy is used in conjunction with or complementary to XPS. There is, however, a marked difference between the two techniques. Whereas XPS energy is dependent on both, the incident photon energy and the electron binding energy, Auger energy results only from the electron binding energies. This difference is used to distinguish between photoelectrons and Auger electrons[171]. Since a monoenergetic beam of photons or electrons are not necessary to excite the Auger electron spectra, experimentation may be simpler than for XPS, but the interpretation of the resulting spectra is generally more difficult than for XPS because of the three-electron nature of the whole process[167].

Limitations of the Auger Spectroscopy

The same limitations concerning the handling and storing of specimens, prior to analysis, and the limitations due to vacuum requirements, encountered for XPS analysis apply to AS. The elements hydrogen and helium cannot also be detected by this technique.

Both techniques, XPS and AS, require an ultra high vacuum environment for their operation, to enable detection of emitted particles and to minimize contamination. Each has surface depth sensitivity of the order of nanometers, but is not limited to that because of depth profiling methods.

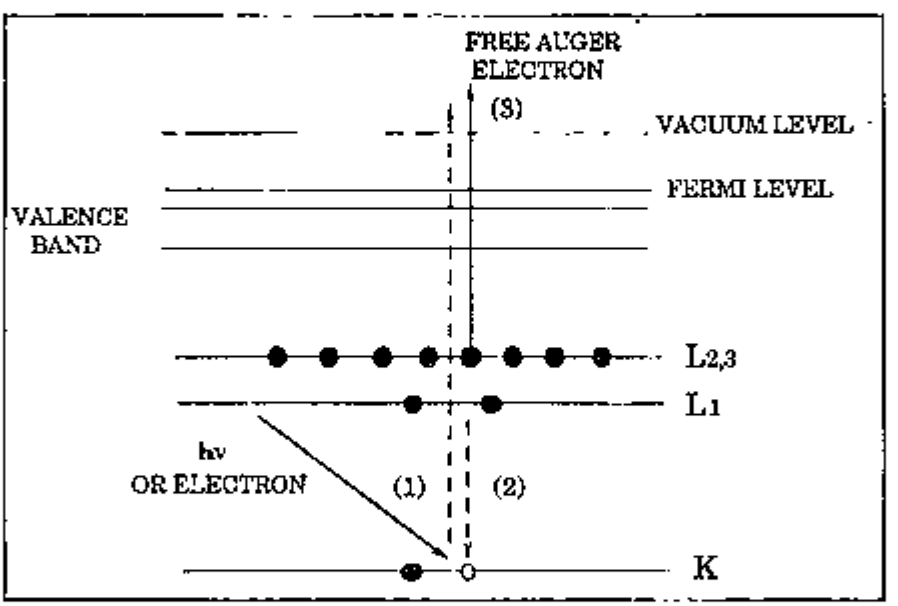

Figure 2.24 - Schematic representation of a $KL_1L_{2,3}$ process. The steps in Auger electron emission are represented by (1),(2), and (3) respectively[171].

AS and XPS techniques provide promising methods to determine the exact location of bond rupture during coating breakdown. XPS elemental analysis have been used to study the interfacial composition in corrosion-induced paint de-adhesion. Hammon and co-workers[172] determined the elemental composition of interface and surface for different coating systems, and their results suggested that polymer degradation by cathodically produced hydroxide occurs in conjunction with corrosion induced de-adhesion. Examination of the high

resolution spectra allowed identification of at least some of the products formed, and confirmed the degradation of polymer coating near the interface.

Dickie and collaborators[173] employed the XPS technique to compare mechanical and corrosion induced de-adhesion of oxidatively cross-linked polybutadiene coatings applied to bare steel. The technique allowed the distinction between the two types of induced de-adhesion. The interfacial surfaces formed by extensive cathodic polarization de-adhesion were much richer in oxidized carbon species than either the air-exposed or mechanically de-adhered surfaces, and also presented ionic residues. The localization of failure was different in both cases. The corrosion induced failure was localised closer to the substrate-coating interface than the mechanical de-adhesion, and occurred within a more highly oxidised layer of polymer adjacent to the steel surface.

CHAPTER 3

THE ELECTROCHEMICAL BEHAVIOUR OF BARE STEEL SURFACES

3.1 - Introduction

The behaviour of a coated system can be affected by the substrate and its properties. There is a general agreement that the rusting beneath organic coatings is electrochemical in nature and the mechanism is identical to that of the rusting of bare steel[21]. Even if there are some differences between the two cases, bare and coated steels, such as mass transport steps and the fact that the corrosion product is confined in a localized area beneath the coating, the knowledge of the electrochemical behaviour of the substrate can help in understanding the corrosion behaviour of these materials when subsequently coated and exposed to corrosive environments. With this aim, bare steels used in this work were tested electrochemically for their properties, near and at the corrosion potential, E_{corr}, or when these materials were far removed from E_{corr}. Tests were also carried out on the steels corroded after exposure to corrosive vapour.

For the study of the electrochemical behaviour of the steels used, various techniques were employed, including: (1) measurement of corrosion potential with immersion time, (2) linear polarization, (3) Tafel extrapolation measurements, (4) electrochemical impedance, (5) potentiodynamic polarization curves and (6) cathodic reduction curves.

3.2 - Experimental

3.2.1 - Materials

The materials used in this work corresponded to five different steels. Two of these steels were of the mild steel type, and the other three had composition typical of low alloy steels. One of the steels presented in this chapter, a low-alloy steel type, was only used in bare conditions for reasons of limited availability. The steels used in this work were provided by two different makers. Each manufacturer supplied at least a mild steel and a low-alloy steel type.

The chemical analysis of the steels studied were obtained by emission spectroscopy at the Materials Science Centre - University of Manchester/UMIST.

The elemental surface compositions of the various steels are given in Table 3.1, and their respective microstructures, obtained by optical microscopy, are shown in Figure 3.1.

TABLE 3.1 - Elemental composition of steels studied.

Steel	A-36	USI	MS	LAS I	LAS II
C	0.20	0.11	0.058	0.092	0.076
Si	0.04	0.47	0.012	0.062	0.36
Mn	0.67	0.78	0.24	0.49	0.36
S	0.028	0.010	0.012	0.009	0.009
P	0.011	0.013	0.011	0.004	0.093
Cr	...	0.50	...	1.56	0.88
Ni	0.016	0.02	0.02	0.001	0.013
Mo	...	...	0.01	...	...
Co	0.005	0.007	0.006	0.009	0.006
Cu	0.01	0.32	0.03	0.11	0.28
Ti	0.003	0.03	0.003	0.004	...
Al	0.002	0.03	0.046	...	0.035
Sn	0.004	0.006	0.013	...	0.007
Fe	balance	balance	balance	balance	balance

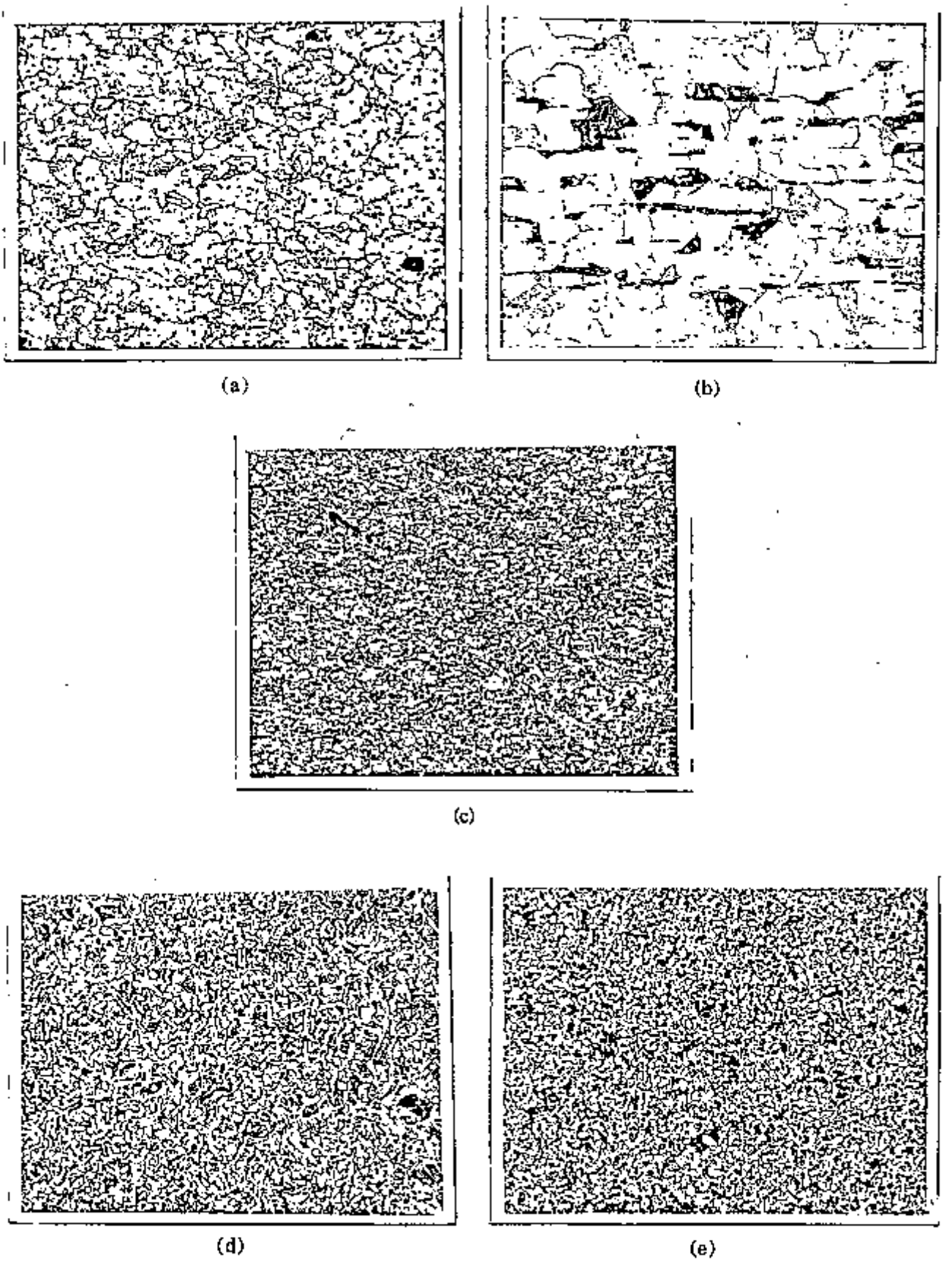

Figure 3.1 - Microstructure of steels used; (a) MS, (b) LAS I, (c) LAS II, (d) A-36 and (e) USI.

3.2.2 - Working electrode preparation.

To prepare working electrodes for electrochemical testing, steel specimens were cut to give an area of 1 cm^2. The working electrodes were prepared by soldering a piece of copper wire for electrical contact, and then cold mounting the specimens in an epoxy resin. The wire was encapsulated in a plastic tube, which was fixed to the mould with epoxy resin. The surface was polished using silicon carbide paper of grades 600, 800, and 1200, successively, rinsed in deionized water, and then hot air dried. The electrode was stored in a desiccator over silica gel for subsequent testing.

3.2.3 - Test solutions.

The test solutions used in this work were 3.5%wt sodium chloride, and 0.5M sodium sulphate. In each case the pH of the bulk solution was approximately 6. Before the tests were carried out, the test solution was aerated using an air pump for at least 1 hour. All experiments were conducted at ambient temperature.

3.2.4 - Experimental procedure.

3.2.4.1 - Electrochemical corrosion potential measurements

The electrochemical corrosion potential for the steel electrodes used was monitored relative to an external saturated calomel reference electrode, via a Luggin tube,and measured by means of a 1503-HA Thurlby digital multimeter. The corrosion potential was registered using a Servoscribe chart recorder.

3.2.4.2 - Linear polarization measurements

In order to determine the relationship between the overpotential and current in the direct vicinity of the free corrosion potential, the measurements

were taken by manually adjusting the potentiometer on a ACM Ministat potentiostat, and by taking the average value of the high and the low fluctuating current, 3 minutes after the disturbing potential has been applied.

Initially, the steel electrodes were immersed in the aerated solution tests, 3.5% wt sodium chloride and 0.5M sodium sulphate, and left for several hours, until a steady value of corrosion potential was reached. After the corrosion potential has stabilised, potentiostatic measurements were carried out by changing the potential by 5 mV steps up to 20 mV, in both the anodic and cathodic directions. For each step the potential was kept for 3 minutes. This procedure was adopted for reasons of comparison with previous work undertaken at UMIST[101]. The three electrode cell used in this experiment consisted of a platinum counter electrode, the working electrode as described above, and a saturated calomel reference electrode connected to the cell by a Luggin capillary probe. The volume of the test solution used was approximately 700 ml for each cell. Experiments were carried out at ambient temperature (22 ± 2°C). The experimental set-up for the polarization resistance measurements is shown in Figure 3.2.

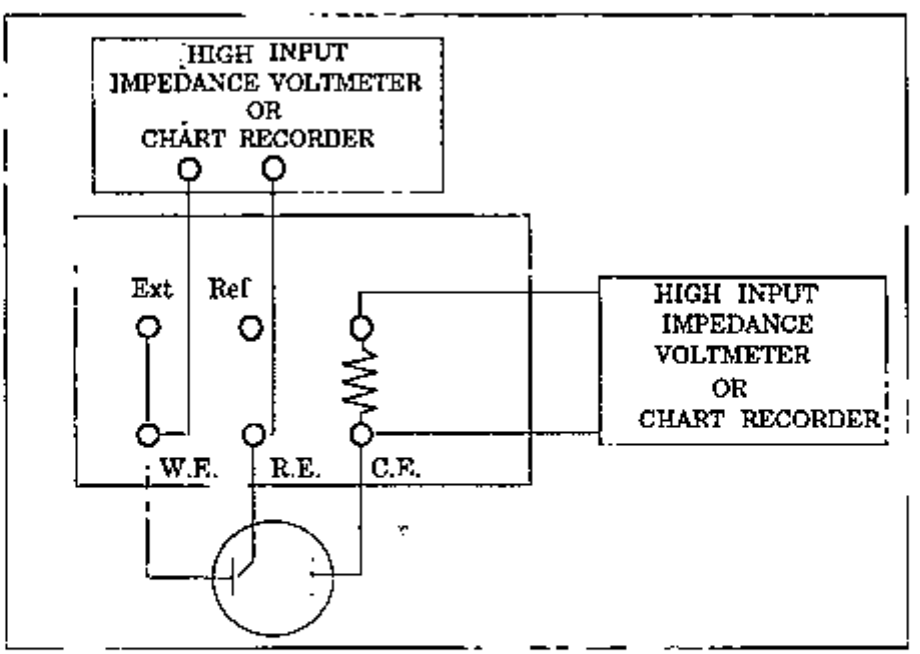

Figure 3.2 - Experimental set-up for polarization resistance experiments.

3.2.4.3 - Electrochemical impedance experiments.

A three electrode set-up was used for performing the electrochemical impedance measurements with the bare steels. The experimental set-up is outlined in Figure 3.3, and the circuit diagram for this set-up is shown in Figure 2.17. The frequency response analyser (F.R.A.) used was the Solartron 1250. A 10 mV amplitude signal was used for the analysis of bare steels. Measurements were conducted in the 10 kHz - 10 mHz range, and seven data points per decade of frequency were taken. The potentiostat used with the F.R.A. was a Thompson ministat. The F.R.A. was interfaced with a BBC microcomputer. The provided computer software was used to collect the data and control all peripheral devices, including a disk drive to store data, and an EPSON RX-80 F/T printer for the print-out of the data.

The electrochemical cell used consisted of a 1000 ml flask in which the working electrode, Luggin capillary, platinum counter electrode, and gas bubbler were placed. The volume of the solution used was the same as for the linear polarization measurements.

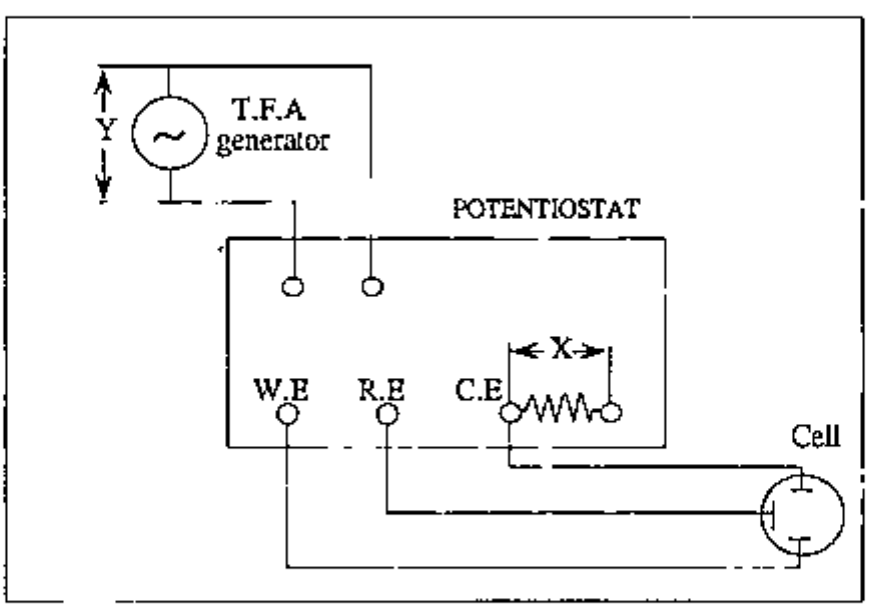

Figure 3.3 - Experimental set-up for the three electrode system impedance measurements.

3.2.4.4 - Full polarization curves

In order to obtain further kinetic data, potentiodynamic measurements were carried out for the various steels in the range -1.0 V - +1.5V (vs SCE). The tests were conducted in both 0.5 M Na_2SO_4 and NaCl 3.5% wt solutions, and by sweeping the electrode potential of the steels at a rate of 20 mV/minute.

The relationship of the overpotential and the current, i.e., the polarization curve, characterises the dependence of the rate of the cathodic and anodic reactions on the potential. This enables the investigation of the kinetics of each of these reactions which together make up the process of corrosion.

The experimental set-up used consisted of a Ministat potentiostat, supplied by ACM - England, connected to the three electrode cell. An external reference potential was provided by a Hermes sweep generator. The electrode potential between the working and reference electrodes was measured directly on a 1503-HA Thurlby Multimeter. The cell current was recorded on a Servoscribe chart recorder, as a potential drop across an appropriate counter resistor. Figure 3.4 shows schematically the potentiodynamic polarization circuit corresponding to the system described above.

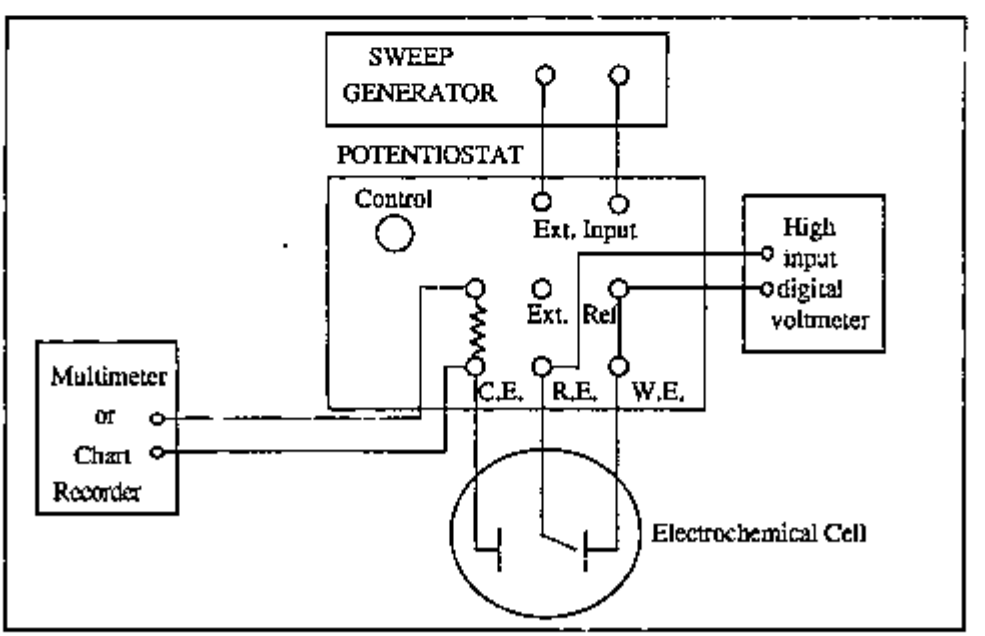

Figure 3.4 - Schematic diagram of potentiodynamic polarization circuit.

3.2.4.5 - Cathodic reduction curves

The electrochemical investigation of the various bare steels also included the cathodic reduction of corrosion products formed by exposure to a selected environment. This was achieved by preparing the specimens as described in section 3.2.2, and exposing them to the vapour phase, at 54°C, of a solution of 10^{-3} M $NaHSO_3$. The sodium hydrogen sulphite was of the reagent grade, and the solution was made up using deionized water. These exposure conditions were selected because they yield corrosion product films similar to those formed during atmospheric exposure[183]. The specimens were exposed to the vapour phase for 20 days. At the end of this time a corrosion product could be seen on the specimen surface. After removal from the vapour exposure, the specimens were immersed in a deaerated solution of 0.1M sodium sulphate, and the cathodic reduction curves were obtained galvanostatically at a current density of $1mA/cm^2$. Deaeration was accomplished by sparkling with nitrogen for 4 hours prior to sample immersion. The electrochemical potential was measured by a high input digital voltmeter which was interfaced to an HP-85 microcomputer. The current value was monitored by a multiammeter. The measurements were continued until the hydrogen evolution potential was attained. Only four steels, two of each type, were used in this test, MS, LAS II, A-36, and USI. The reproducibility of the data was established from a duplicate set of specimens.

A schematic diagram of the circuit employed for obtaining galvanostatic polarization measurements is shown in Figure 3.5. The cell uses a conventional three electrode system comprising a saturated calomel reference electrode (R.E.), a platinum counter electrode(C.E.), and the steel working electrode(W.E.).

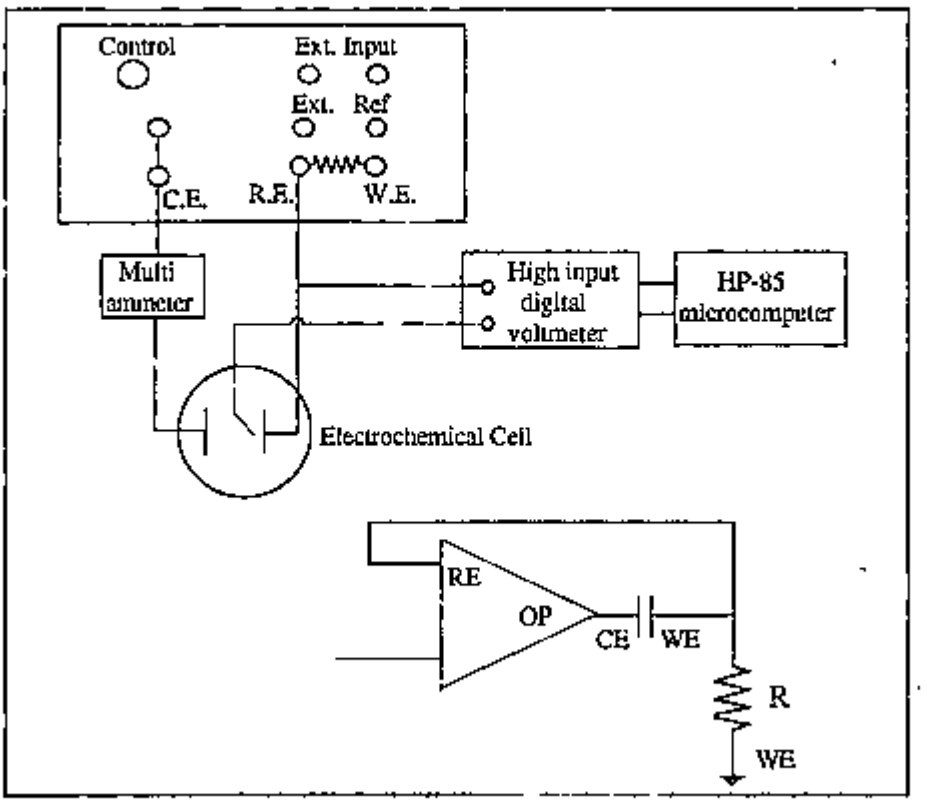

Figure 3.5 - Schematic diagram of galvanostatic polarization circuit used for cathodic reduction curves.

3.3 - Results and Discussion

3.3.1 - Electrochemical corrosion potential, E_{corr}, vs time

Typical electrochemical corrosion potential results for the different steels, upon immersion in the test solutions, are shown in Figure 3.6. Initially the steel specimens exhibited a definite starting potential (*Estart*), then slowly approached a more negative value (*Efinish*). From these records it can be seen that the corrosion potential reached a steady state after approximately 7 to 9 h. A time corresponding to 1 day immersion was then chosen as reasonable time for measuring the stable corrosion potentials of the steels studied, and also for reasons of comparison with previous work[101]. Tables 3.2 and 3.3 present the stable corrosion potentials, taken after 1 day immersion in 0.5M Na_2SO_4 and 3.5% wt NaCl respectively, for the steels used. The values are an average of at least three measurements for each steel in each condition. It can be said, based on

these data, that the stable corrosion potentials for the different steels after 1 day immersion varied little. No marked difference among the steels can be noticed when they are compared in a same solution. The corrosion potentials for the steels in 3.5% wt NaCl solution however, was always more positive by 50 to 80 mV than the corresponding potentials for steels exposed to 0.5M Na_2SO_4 solution. The reproducibility in the electrochemical potential data for the various steels was considerably high, as shown in Tables 3.2 and 3.3.

Potential measurement cannot be used alone to obtain information concerning corrosion mechanisms, but its variation with time can be of great value, if used together with other techniques.

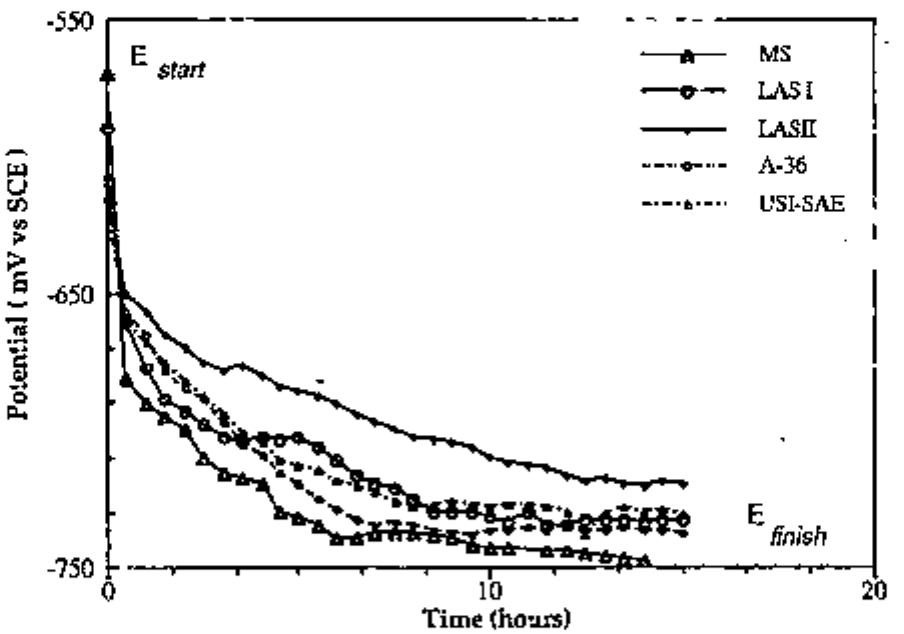

Figure 3.6 - Typical E_{corr} vs time curve for steels used upon immersion in 0.5M Na_2SO_4 solution.

TABLE 3.2 - Corrosion potential of the various steels after 1 day immersion in 0.5M Na_2SO_4.

Steel	Potential (mV vs SCE)
MS	(-753 ± 6)
LAS I	(-732± 18)
LAS II	(-720 ± 20)
A-36	(-738 ± 11)
USI	(-730 ± 5)

TABLE 3.3 - Corrosion potential of steels studied after 1 day immersion in 3.5% wt NaCl.

Steel	Potential (mV vs SCE)
MS	(-687 ± 7)
LAS I	(-660 ± 20)
LAS II	(-662 ± 13)
A-36	(-662 ± 2)
USI	(-679 ± 20)

3.3.2 - Linear polarization measurements.

Linear polarization curves were obtained for the diverse steels in 0.5M Na_2SO_4 solution, and are presented in Figures 3.7-3.11. For each test three linear polarization measurements were carried out. The values of the polarization resistance, R_p, were obtained from the tangent to a polynomial of second order that best fitted the data, at nil current density. The equations of the polynomial, and their correlation coefficient with the experimental data, are also shown in the Figures 3.7-3.11.

Table 3.4 lists the mean values of the polarization resistance, R_p, for the various steels.

TABLE 3.4 - Mean R_p values for the steels studied.

Steel	Mean R_p value ($\Omega.cm^2$)
MS	(3793±223)
LAS I	(3765±490)
LAS II	(3912±931)
A-36	(2419±393)
USI	(2402±273)

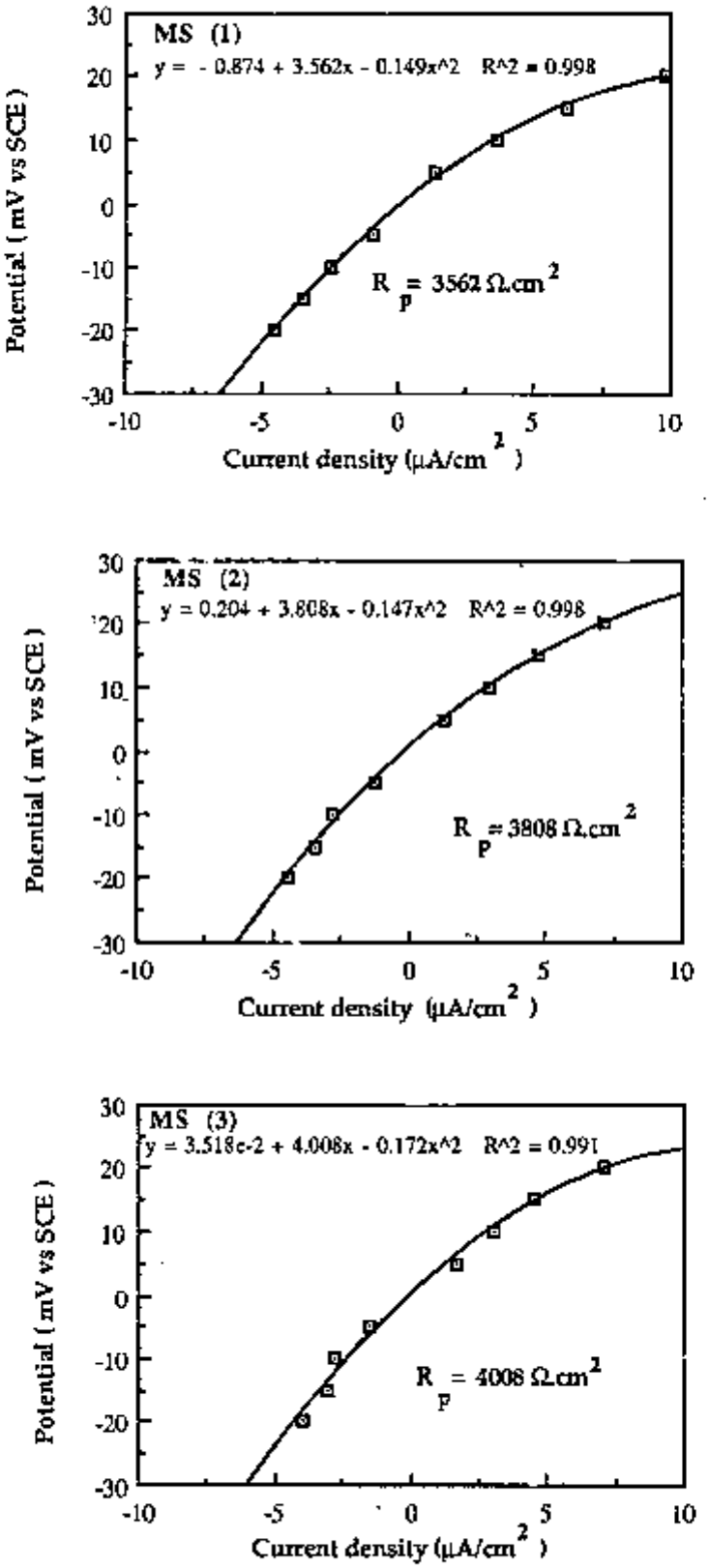

Figure 3.7 - Linear polarization curves for mild steel immersed in 0.5M Na_2SO_4 solution.

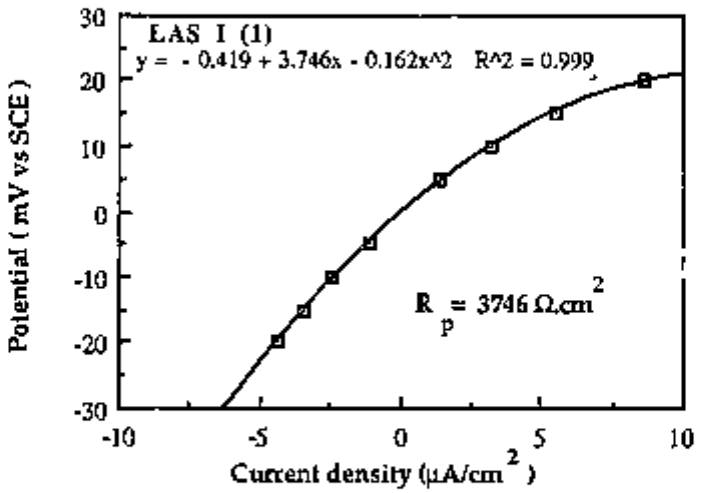

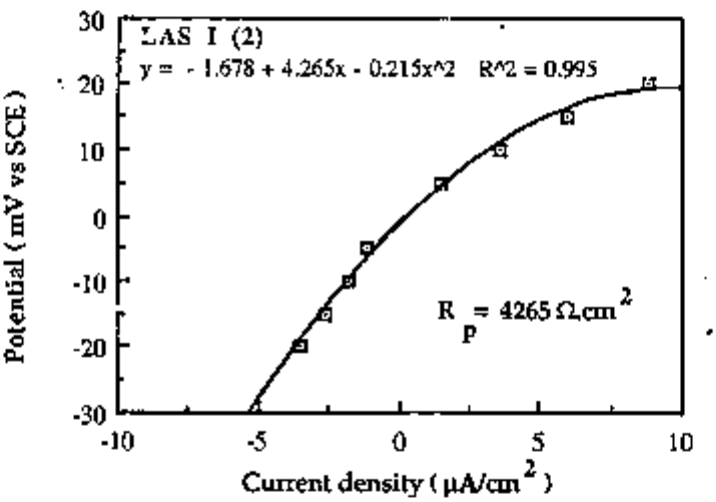

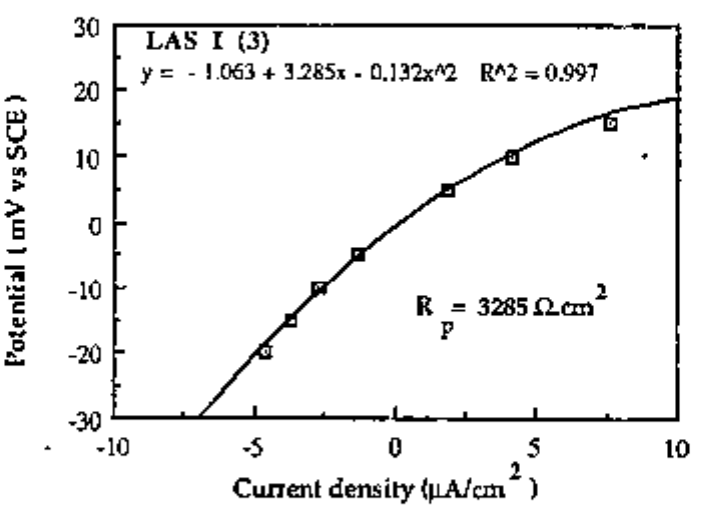

Figure 3.8 - Linear polarization curves for LAS I immersed in 0.5M Na_2SO_4 solution.

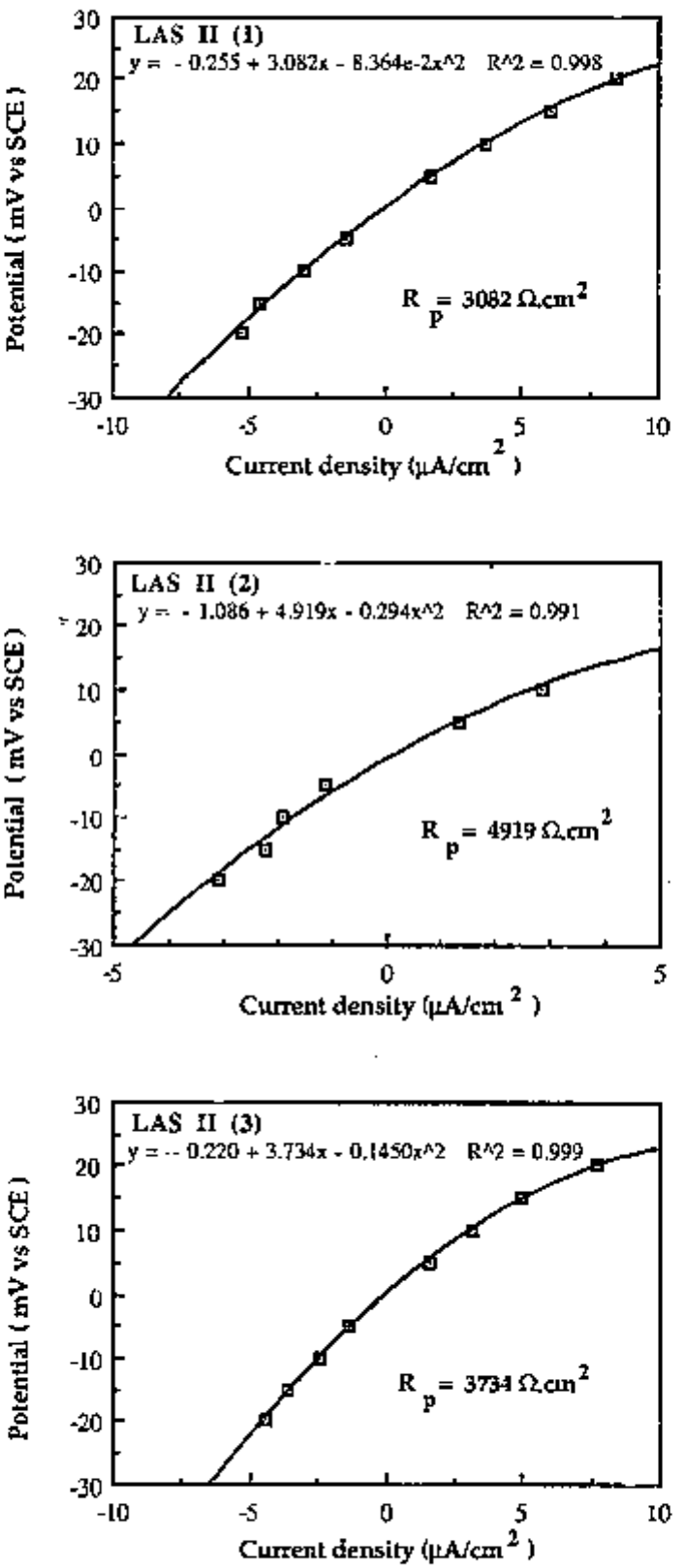

Figure 3.9 - Linear polarization curves for LAS II immersed in 0.5M Na_2SO_4 solution.

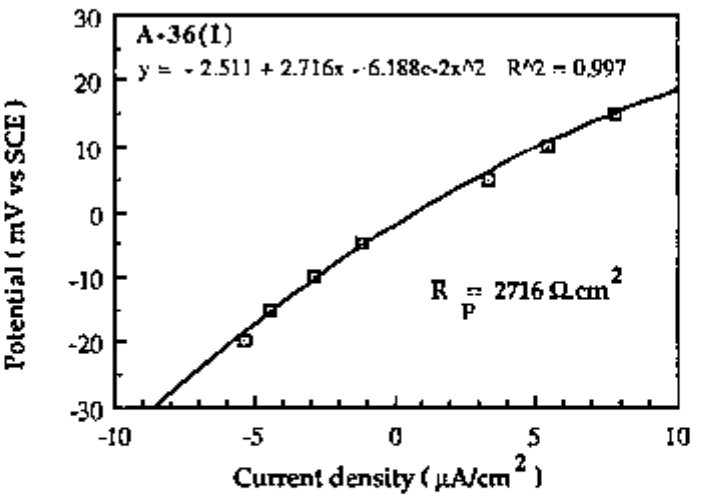

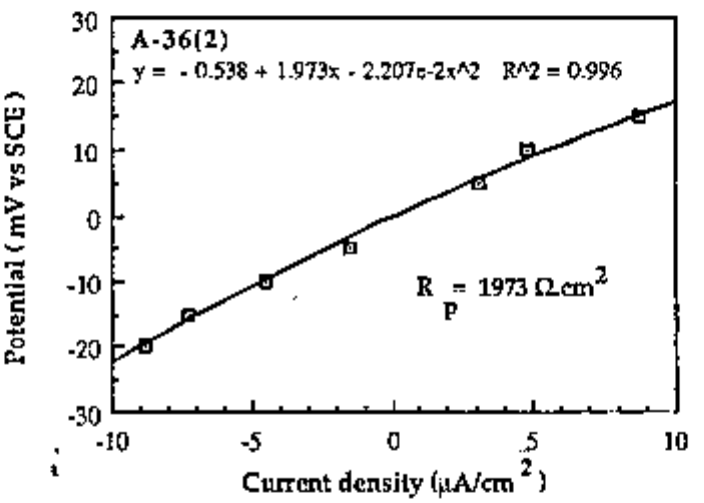

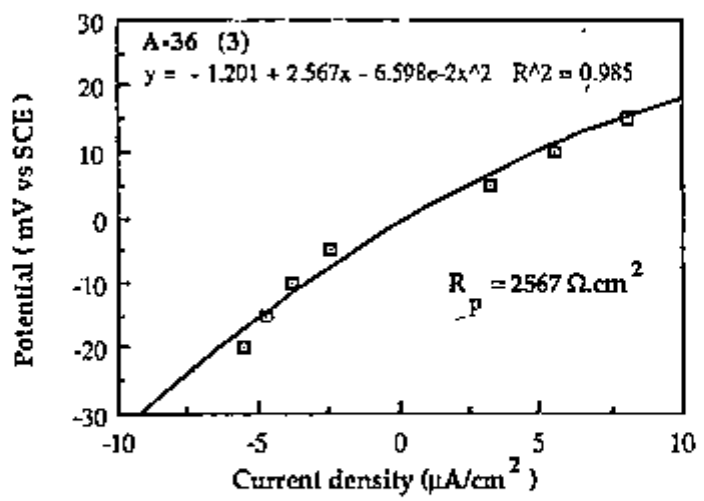

Figure 3.10 - Linear polarization curves for A-36 immersed in 0.5M Na_2SO_4 solution.

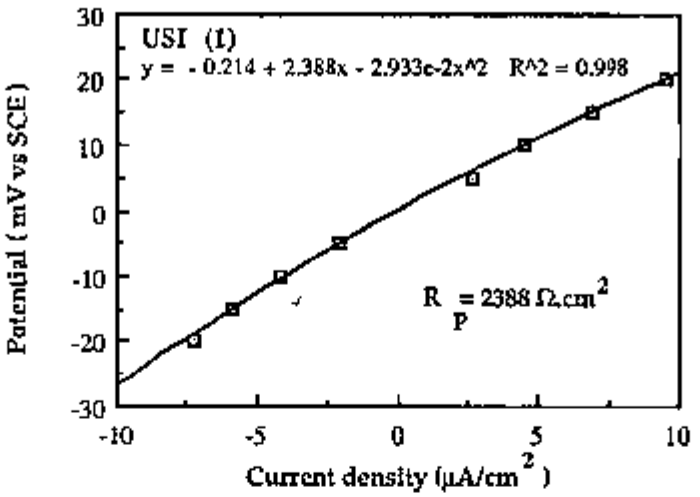

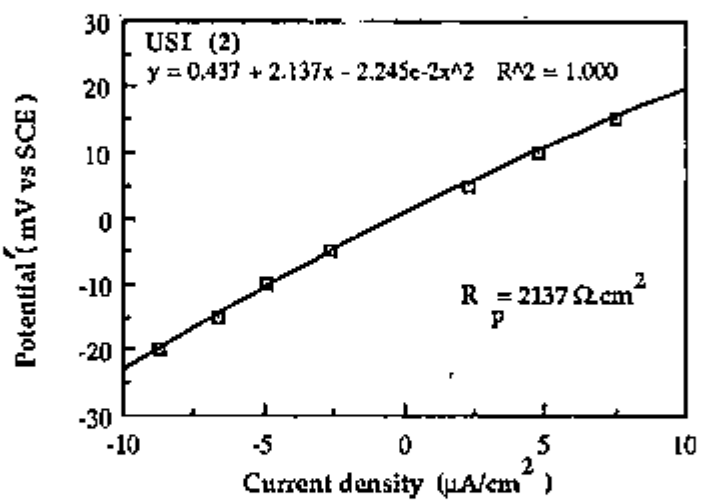

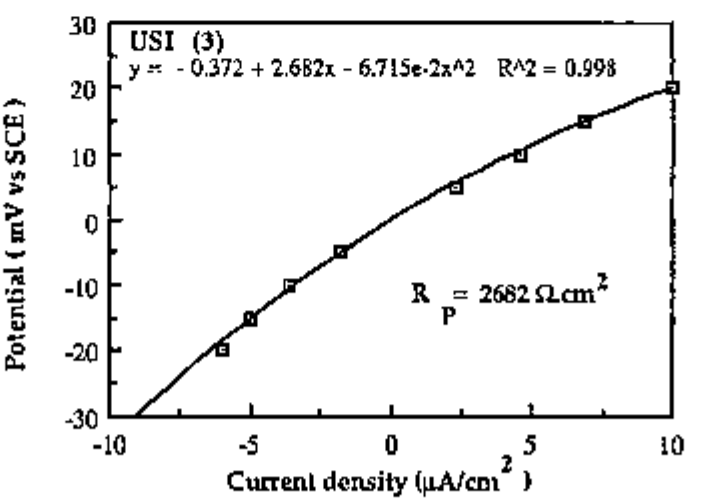

Figure 3.11 - Linear polarization curves for USI immersed in 0.5M Na_2SO_4 solution.

The main reason for undertaking linear polarization measurements in this work was to compare our results with previous results obtained at UMIST[101]. In that work[101] the steels used corresponded to A-36 and USI, and the solution used was 0.5M Na_2SO_4. Table 3.5 presents both results, our and from previous work[101], for comparison.

TABLE 3.5 - Comparison of R_p values obtained in this study with previous work[101].

Steel	R_p ($\Omega.cm^2$) this work	R_p ($\Omega.cm^2$) (from ref.[101])
A-36	(2419 ± 393)	634
USI	(2402 ± 273)	400

As can be seen from the table above, the results of this study differed significantly from the ones obtained in the previous published work[101]. In fact the values obtained were larger by factors of approximately 4 and 6, for the steels A-36 and USI, respectively. No definite explanation could be offered to account for this large difference. It should be added that the results of this work exhibited good reproducibility, and the values agree favourably with R_p data reported in the literature for steel in sodium sulphate solutions[198]. However, in the previous work[101] there is no reference to the reproducibility of their results. This prohibits a comparison of the statistics of the two sets of results. The results compared above were both calculated as the tangent at E_{corr}. In the published work[101], however, the tangent was drawn at E_{corr}, by hand, and the manner in which this is done can lead to different R_p values. Nevertheless, it is not believed that this would be the only factor to account for such large differences.

It can also be observed from the above data that the steels, A-36 and USI, produced by the same manufacturer, presented very similar results under the conditions applied, which was small perturbation (≤ 20mV) from the free corrosion potential, E_{corr}. These steels, however showed slightly lower values from the other steels studied, which all originated from another supplier. This suggests that the two type of steels used in this research, mild steel and low-alloy steel types, are not electrochemically different under conditions close to the corrosion potential. However some minor differences seem to exist between similar steels produced by different makers.

The specimens were visually examined for corrosion products in the first hours immersion and also 1 day later. It was noticed that corrosion usually started at some isolated points on the surface, Figure 3.12. The way corrosion developed after that however varied even for the same type of steel. This suggests that even in cases where the same conditions are used, such as type of steel, environment, surface finishing, other factors can still affect the corrosion behaviour of the metal. After 1 day immersion, some specimens were removed from solution and their surfaces were wiped with tissue paper to remove the brown loose corrosion product. Generalized corrosion was observed to be associated with the areas where loose corrosion product was deposited. Other areas of the specimens were covered by an adherent dark blue corrosion product, and these were generally located between the loose corrosion products and areas where no evident corrosion was seen. On those areas the surface was still metallic bright. On some of the specimens, small localized corroded spots were noted and pits were observed when their surface was re-polished. This places some doubts on the applicability of linear polarization technique in some of the cases. Linear polarization technique only leads to reliable results in cases of generalized corrosion. However, it must be said that since a fixed time of measurement, (3 min), was used for all the specimens, in this and the previous work[101], a comparison was possible.

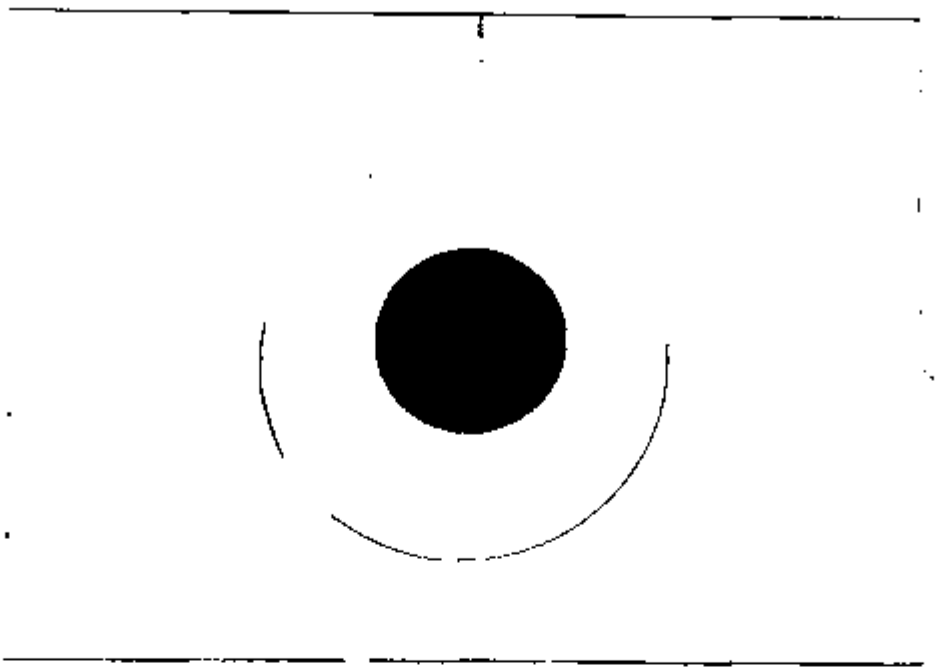

Figure 3.12 - Specimen MS after the first hours immersion in 0.5M Na_2SO_4.

3.3.3 - Tafel extrapolation measurements

In order to estimate the current density, i_{corr}, for the various steels used in this work, and to compare the values of i_{corr} obtained from different methods, Tafel extrapolation measurements were carried out. The results of Tafel extrapolation measurements, for the various steels exposed to 0.5M Na_2SO_4 are presented in Figures 3.13 to 3.17.

Tafel extrapolation measurements were taken from the regions of the polarization curves which corresponded to straight lines, on the overpotential vs log current plots. The plot of η (overpotential) vs log i, can provide the values of b_a and b_c, Tafel constants for the anodic and cathodic reaction, respectively, which are given by :

$$\eta_a = b_a \log i_a + a_a \quad \text{for the anodic reaction, and} \qquad (3.1)$$

$$\eta_c = b_c \log i_c + a_c \quad \text{for the cathodic reaction.} \qquad (3.2)$$

The corrosion current density, i_{corr}, was measured from the intersection of the linear regions of the anodic and cathodic curves, and are given in Tables 3.6 and 3.8 for the sodium sulphate and sodium chloride solutions respectively.

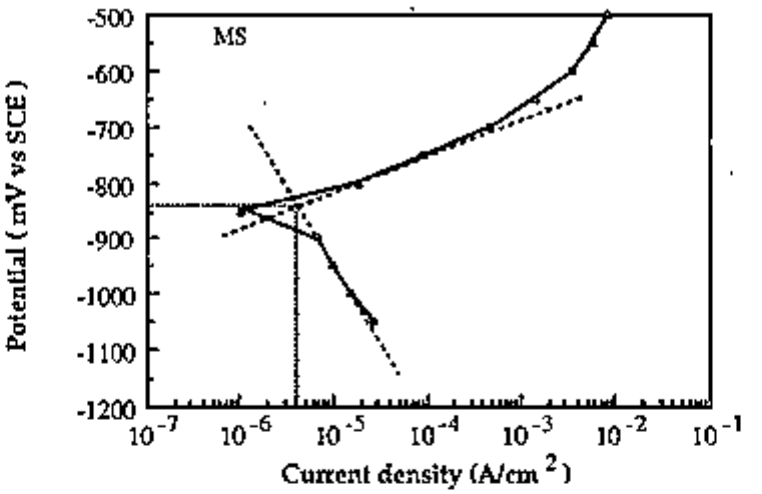

Figure 3.13 - Tafel extrapolation measurements for MS in 0.5M Na_2SO_4.

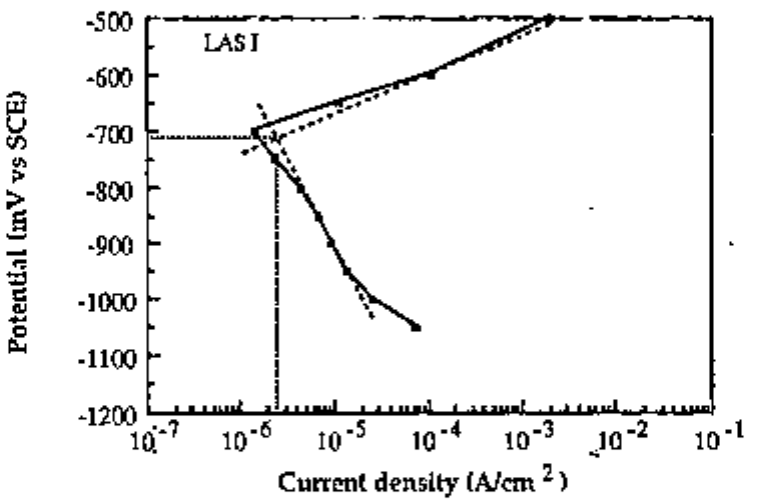

Figure 3.14 - Tafel extrapolation measurements for LAS I in 0.5M Na_2SO_4.

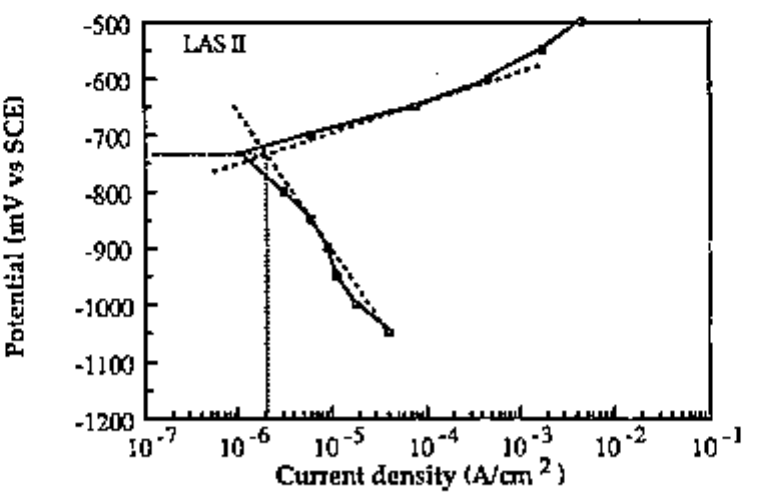

Figure 3.15 - Tafel extrapolation measurements for LAS II in 0.5M Na_2SO_4.

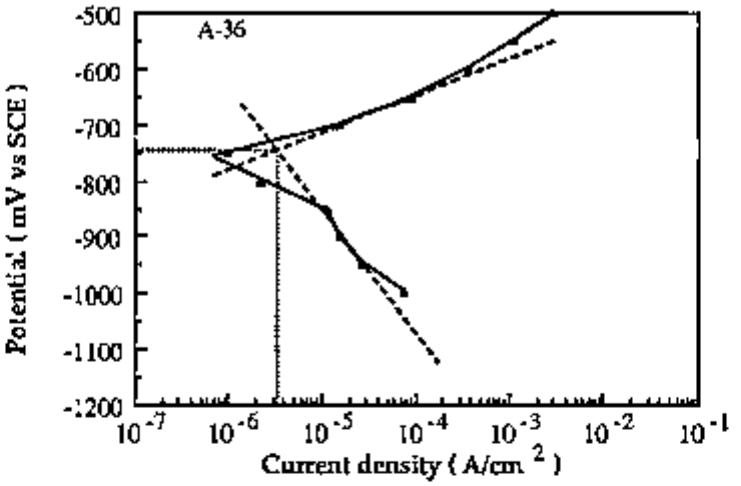

Figure 3.16 - Tafel extrapolation measurements for A-36 in 0.5M Na_2SO_4.

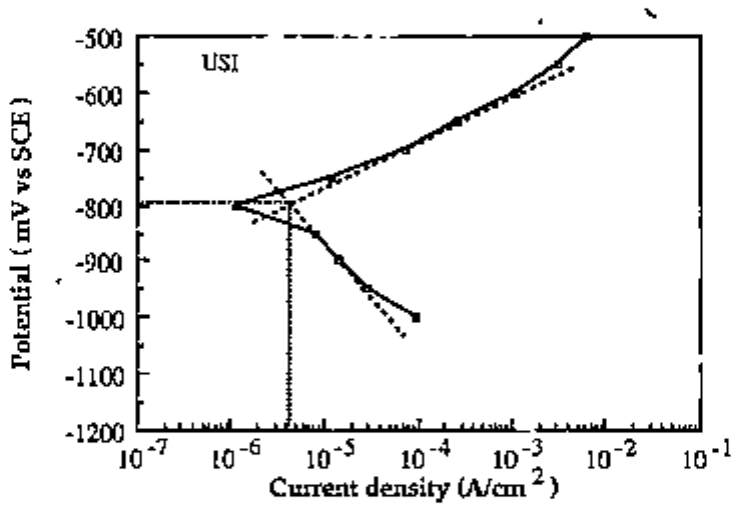

Figure 3.17 - Tafel extrapolation measurements for USI in 0.5M Na_2SO_4.

Table 3.6 gives the values of i_{corr} obtained from Tafel extrapolation measurements for various steels in 0.5M sodium sulphate solution.

TABLE 3.6 - Values obtained from Tafel extrapolation measurements in sulphate solution.

Steel	b_a (mV/decade)	b_c (mV/decade)	B (mV/decade)	i_{corr} ($\mu A/cm^2$)
MS	64	276	23	4.0
LAS I	67	310	24	2.5
LAS II	64	242	19	2.0
A-36	67	222	22	3.2
USI	74	182	23	4.2

It can be seen from the data obtained by Tafel extrapolation measurements that the values of i_{corr} were approximately the same for all the steels used. The B values of the various steels studied were also very close, and around 20 mV/decade. Thus no significant differences in the electrochemical behaviour of the steels could be deduced from the results obtained by this technique.

If it is considered that (a) no concentration or resistance polarization is present, and (b) no oxygen is present to depolarize the electrode, then i_{corr} can be obtained from:

$$i_{corr} = \frac{b_a \cdot b_c}{2.303\,(b_a + b_c)} \cdot \frac{1}{R_p} = \frac{B}{R_p} \qquad (3.3)$$

This, however, does not seem to be true for the case under investigation. Actually it was found that the anodic Tafel slopes were always lower than the cathodic ones. B_c:b_a ratios of approximately 4 were obtained for the steels MS, LAS I, and LAS II, indicating a cathodic controlled corrosion reaction (e.g. oxygen diffusion). For the other steels used, however, b_c:b_a was around 3. This suggests that for the two steels, A-36 and USI, the cathodic reaction is not as predominant over the anodic one as for the other steels. Actually a mixed controlled corrosion reaction where diffusion processes affect the corrosion rate could be operative. This is supported by the impedance data presented in the next section, 3.3.4. From impedance measurements the corrosion reaction for these two latter steels was observed to either be under diffusion or mixed (diffusion and charge transfer) control. For systems where the corrosion rate is cathodically controlled, the following equation applies[8]:

$$i_{corr} = \frac{b_a}{2.303} \cdot \frac{1}{R_p} \qquad (3.4)$$

Values of i_{corr} for the various steels were calculated from equations 3.3 and 3.4, and using the values of R_p obtained from linear polarization measurements, (Table 3.4), and these are presented in Table 3.7. The i_{corr} values obtained from Tafel extrapolation measurements are also presented in Table 3.7 for reasons of comparison .

TABLE 3.7 - i_{corr} values calculated from Linear polarization , L.P., and Tafel extrapolation, T.E., measurements .

Steel	i_{corr} (from L.P. and eq 3.3) ($\mu A/cm^2$)	i_{corr} (from L.P. and eq 3.4) ($\mu A/cm^2$)	i_{corr} (from T.E.) ($\mu A/cm^2$)
MS	6.9	9.5	4.0
LAS I	5.0	6.7	2.5
LAS II	4.3	5.3	2.0
A-36	9.1	12.9	3.2
USI	8.3	11.4	4.2

The first observation from the data presented in Table 3.7 is that the values of i_{corr} calculated using R_p mean values are generally 2 to 4 times higher when compared to i_{corr} obtained from the Tafel extrapolation measurements. If the various steels used are compared, it can also be noticed that i_{corr} values calculated from L.P. measurements were slightly larger for the steels A-36 and USI when compared to the other steels.

Tafel extrapolation measurements were also performed for the various steels in the 3.5% wt NaCl solution and their respective responses are shown in Figures 3.18 - 3.22.

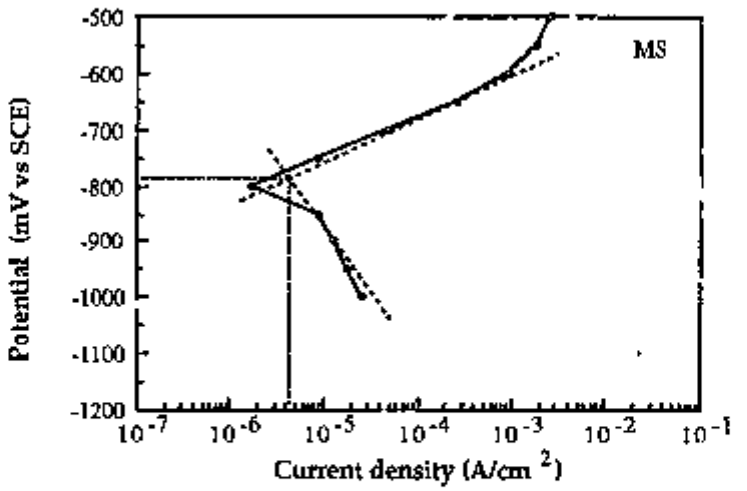

Figure 3.18 - Tafel extrapolation curves for MS in chloride solution.

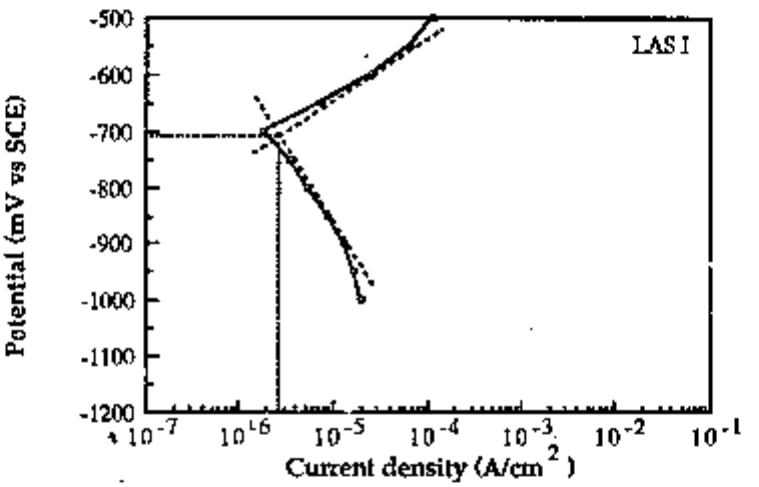

Figure 3.19 - Tafel extrapolation curves for LAS I in chloride solution.

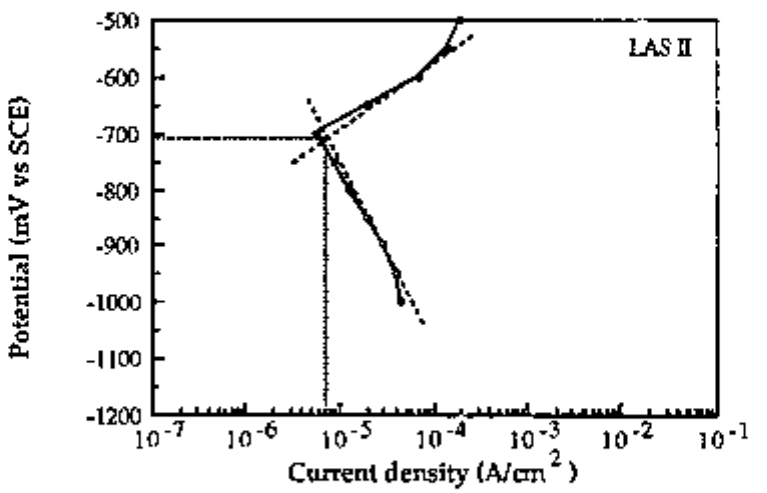

Figure 3.20 - Tafel extrapolation curves for LAS II in chloride solution.

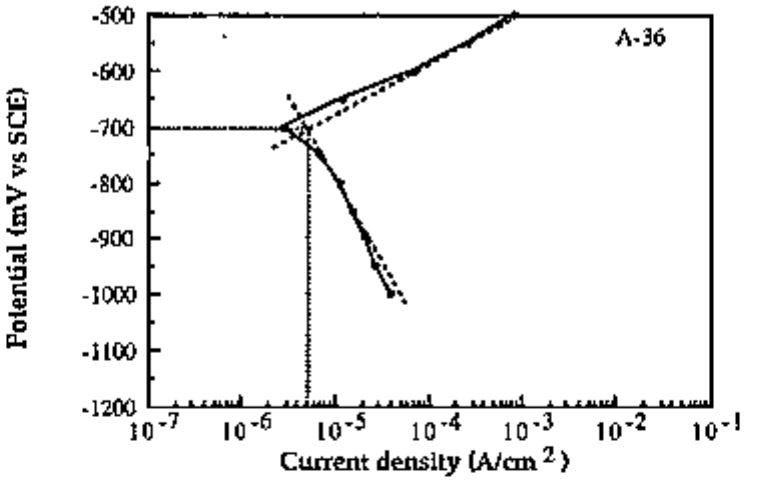

Figure 3.21 - Tafel extrapolation curve for A-36 in chloride solution.

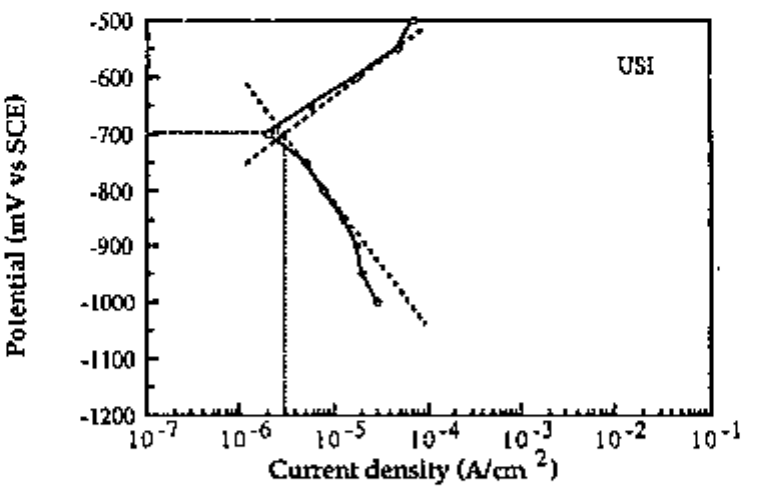

Figure 3.22 - Tafel extrapolation curves for USI in chloride solution.

Table 3.8 gives the data derived from Tafel extrapolation measurements (Figures 3.18 - 3.22).

TABLE 3.8 - Tafel extrapolation data for steels in 3.5% wt NaCl.

Steel	b_a (mV/decade)	b_c (mV/decade)	B (mV/decade)	i_{corr} ($\mu A/cm^2$)
MS	74	229	24	4.2
LAS I	108	263	33	2.7
LAS II	108	309	35	7.0
A-36	88	283	29	5.0
USI	128	220	35	3.0

The cathodic Tafel slopes are approximately 2 to 3 times higher than the anodic ones. These results suggest that the corrosion reaction is under cathodic control, since alterations in the slope of the anode line would scarcely affect the intercept. The b_a values of the low-alloy steels were all similar, but the mild steels used produced slightly smaller values. It is noted from Table above that B values of approximately 30 were generally obtained, the exception was the mild steel MS for which the value was around 20 mV/decade. However, no large difference is found in the estimated values of i_{corr} for the various steels used, and although LAS I and USI seemed to show relatively lower corrosion current densities, differences of that order could be caused by data estimation. A possible source of error is the manner in which the straight line is drawn to fit the linear region of the polarization curve.

3.3.4 - Electrochemical Impedance Measurements

The bare steels investigated in this work yield Nyquist and Bode impedance diagrams, at the corrosion potential and after 1 day immersion in 3.5% wt NaCl, as shown in Figures 3.23-3.27.

Figures 3.28-3.32 show the electrochemical impedance response of the bare steels in the 0.5M Na_2SO_4 solution, after 1 day immersion. Measurements were conducted at the corrosion potential.

A quick analysis of the impedance diagrams shown in these Figures, leads to the observation that the steels used can be divided in two groups. The steels, MS, LAS I, and LAS II, presented similar behaviour, in both solutions, which was slightly different from that exhibited by A-36 and USI. The latter, in turn, presented a similar impedance response. Since the features of the Nyquist plots of all the steels used reproduced well in the chloride solution, only three experiments were performed in this medium. Nevertheless, two types of response were noted for some of the steels in the sulphate solution. Thus, four tests were conducted for each steel in this latter solution. It can be seen, from Figures 3.23 to 3.25 and Figures 3.28 to 3.30, that in general a diffusion tail which bended towards the real axis was observed for the steels, MS, LAS I, and LAS II, in both solutions. Diffusion processes through a finite layer, could be operative in these responses. In order to compare R_p values obtained from linear polarization measurements with data obtained from impedance measurements, "R_d" values were estimated as the chord AC of the arc that best fits the impedance data and is centered below the real axis, Figure 3.33. The values of double layer capacitance, C_{dl}, were calculated from the plot of the imaginary part of the admittance, 1/Z", vs the angular frequency, w. The value of C_{dl} is equal to the slope of the curve as shown in Figure 3.34. Tables 3.9 and 3.10 give "R_d" and C_{dl} values, for chloride and sulphate solutions, respectively. The depression angle is given by ß.

The slopes of the logarithm of the modulus of the impedance, log |Z|, defined in chapter 2, vs the logarithm of angular frequency, log w, was calculated for the various steels used in the same range of frequencies, and are also presented in Tables 3.9 and 3.10.

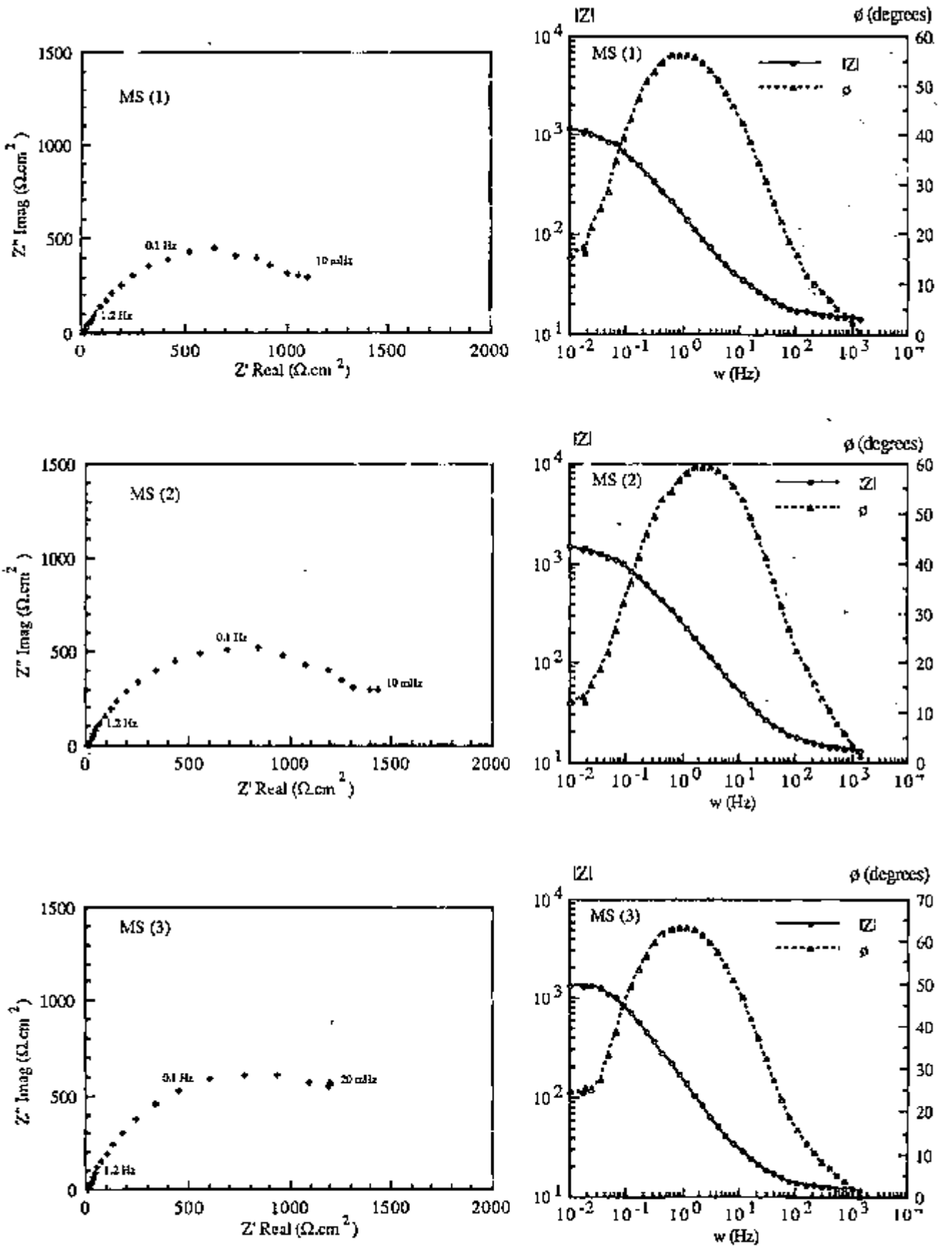

Figure 3.23 - Impedance response (Nyquist and Bode plots) of specimens MS in NaCl 3.5% wt.

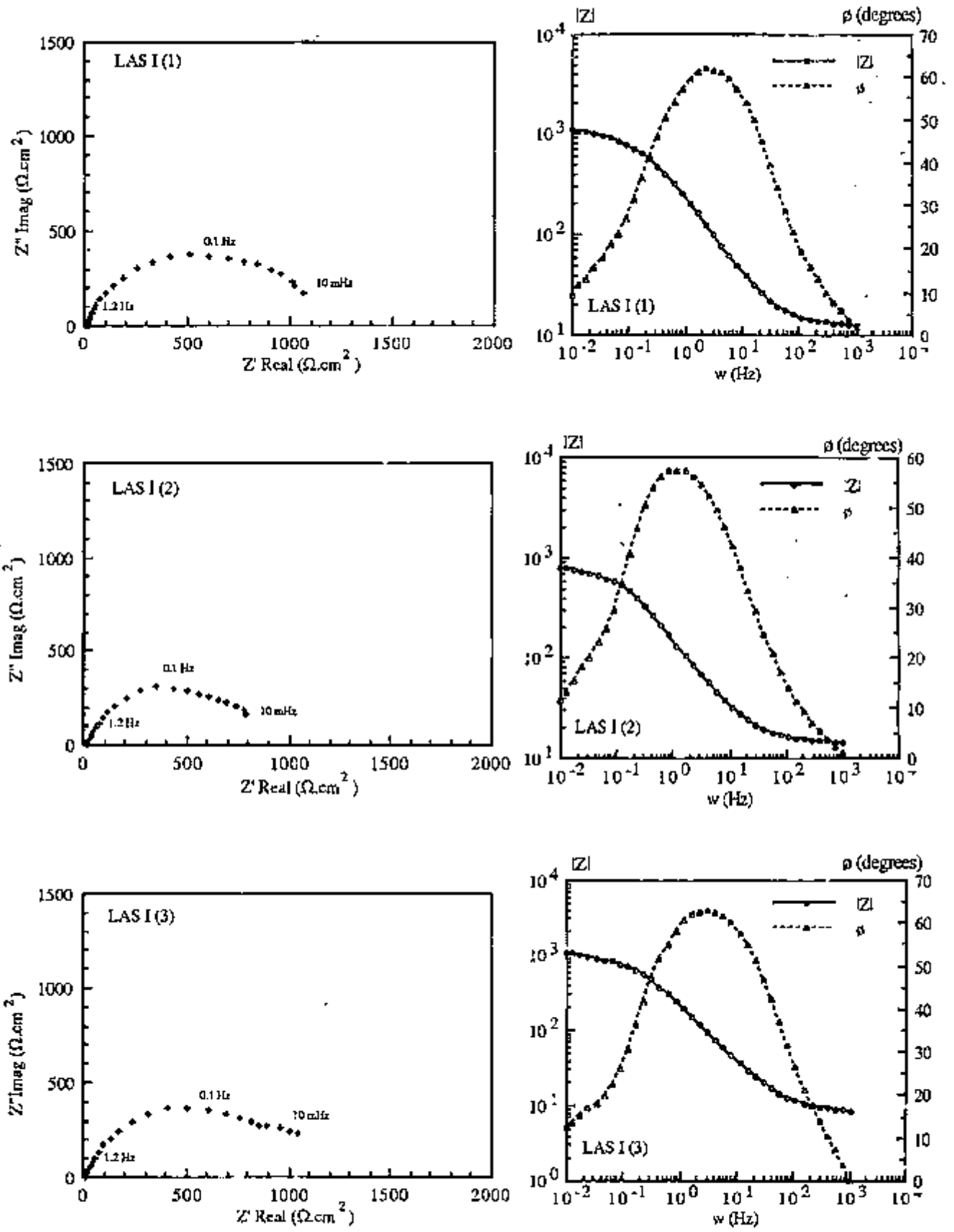

Figure 3.24 - Impedance response (Nyquist and Bode plots) of specimens LAS I in NaCl 3.5% wt.

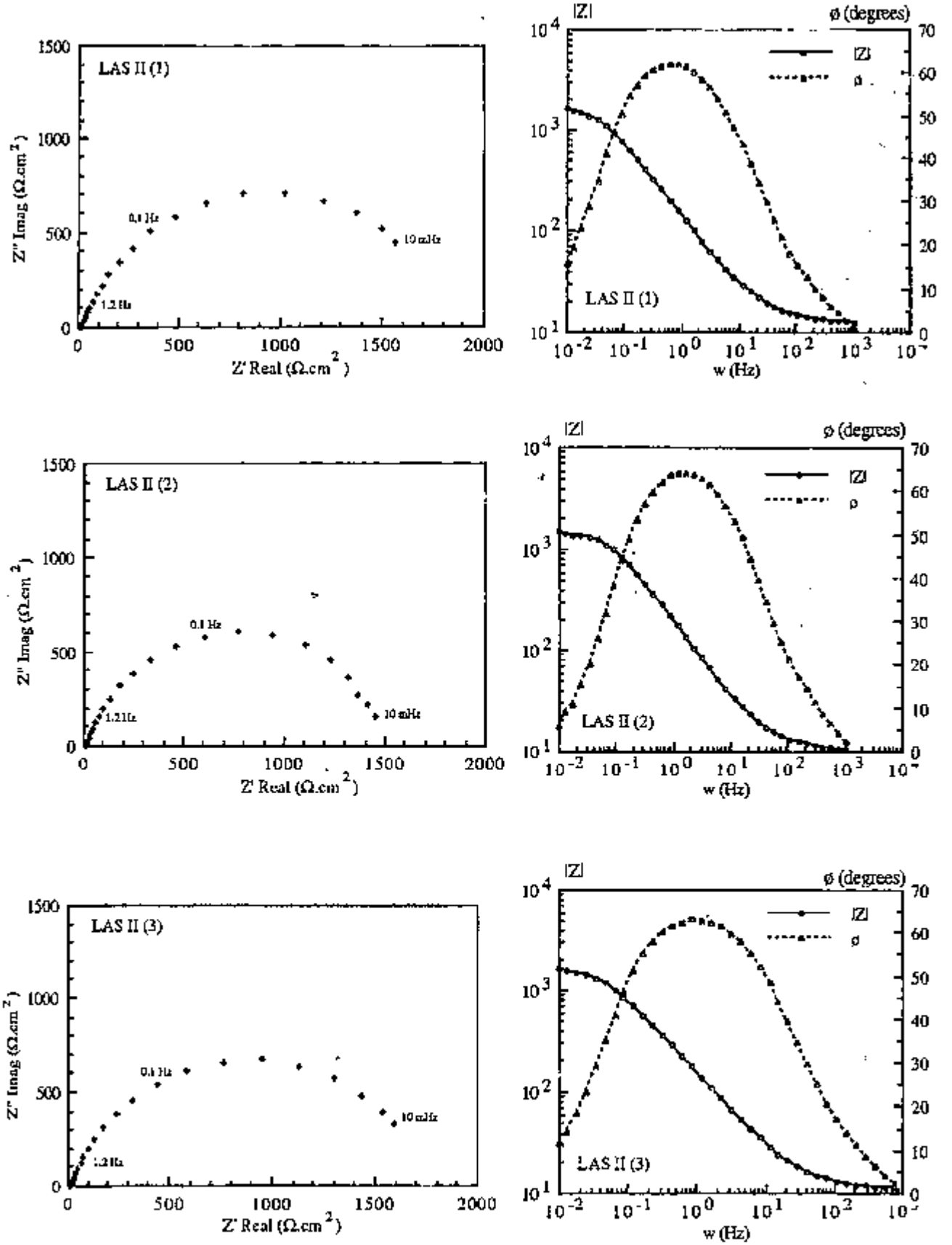

Figure 3.25 - Impedance response (Nyquist and Bode plots) of specimens LAS II in NaCl 3.5% wt.

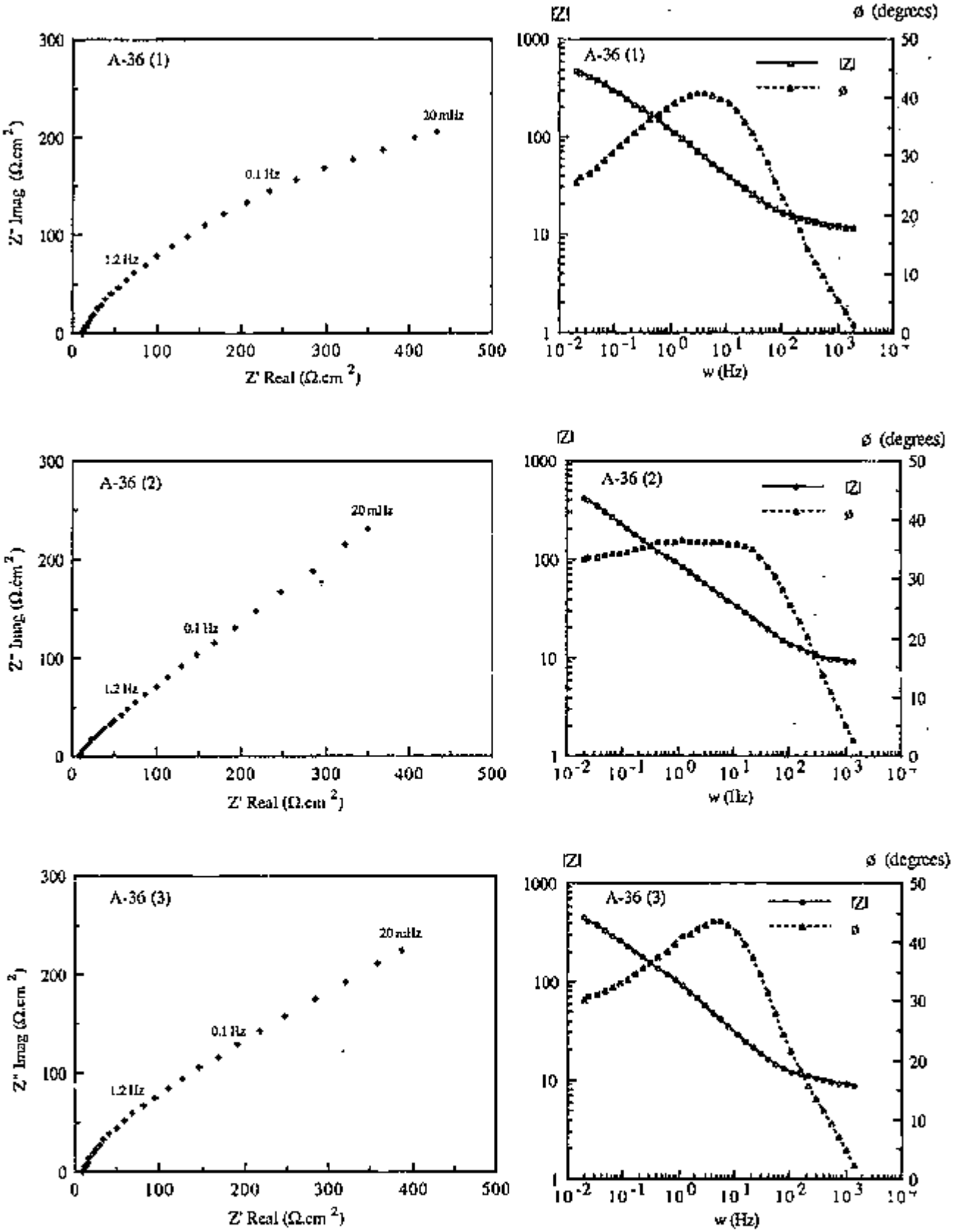

Figure 3.26 - Impedance response (Nyquist and Bode plots) of specimens A-36 in NaCl 3.5% wt.

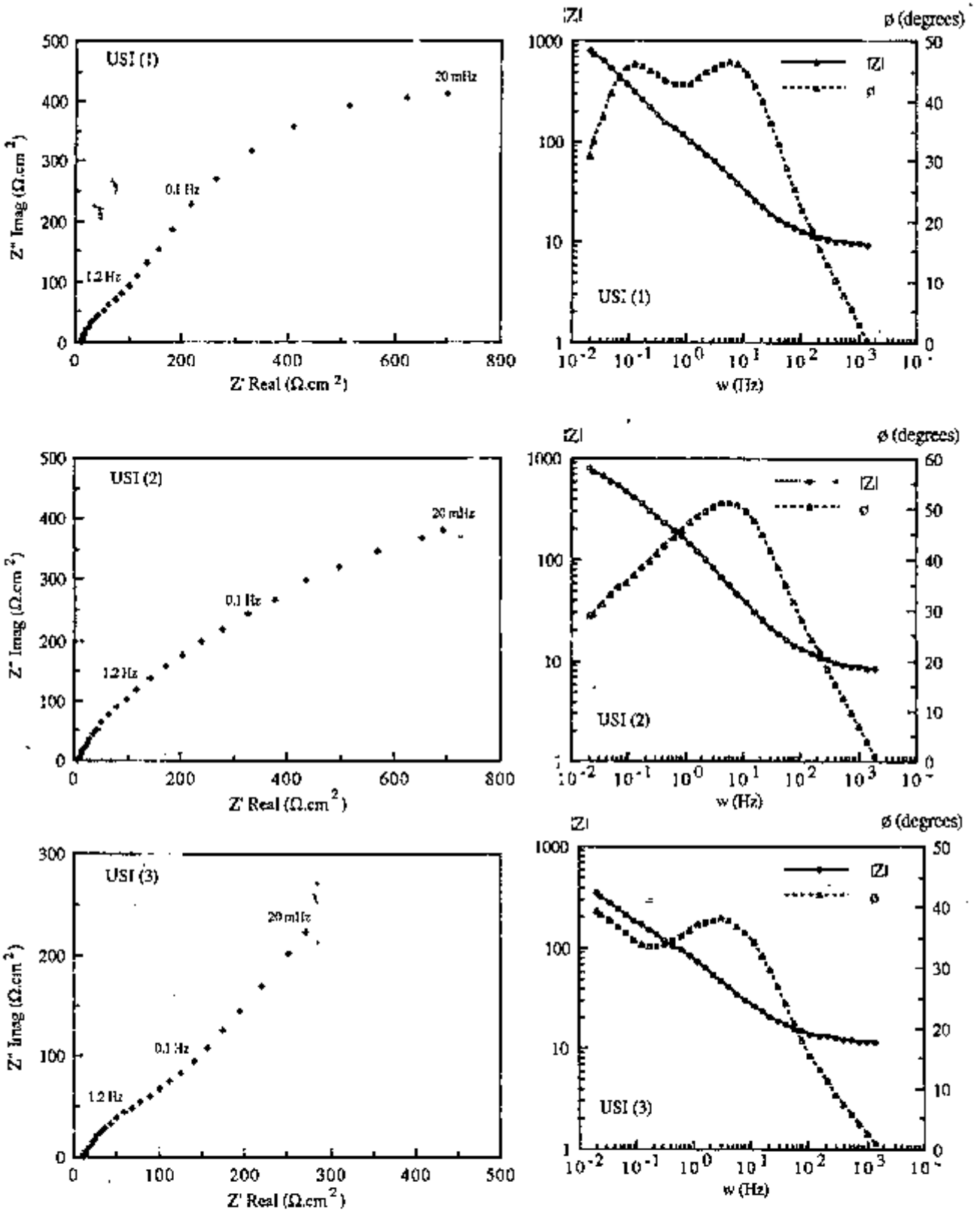

Figure 3.27 - Impedance response (Nyquist and Bode plots) of specimens USI in NaCl 3.5% wt.

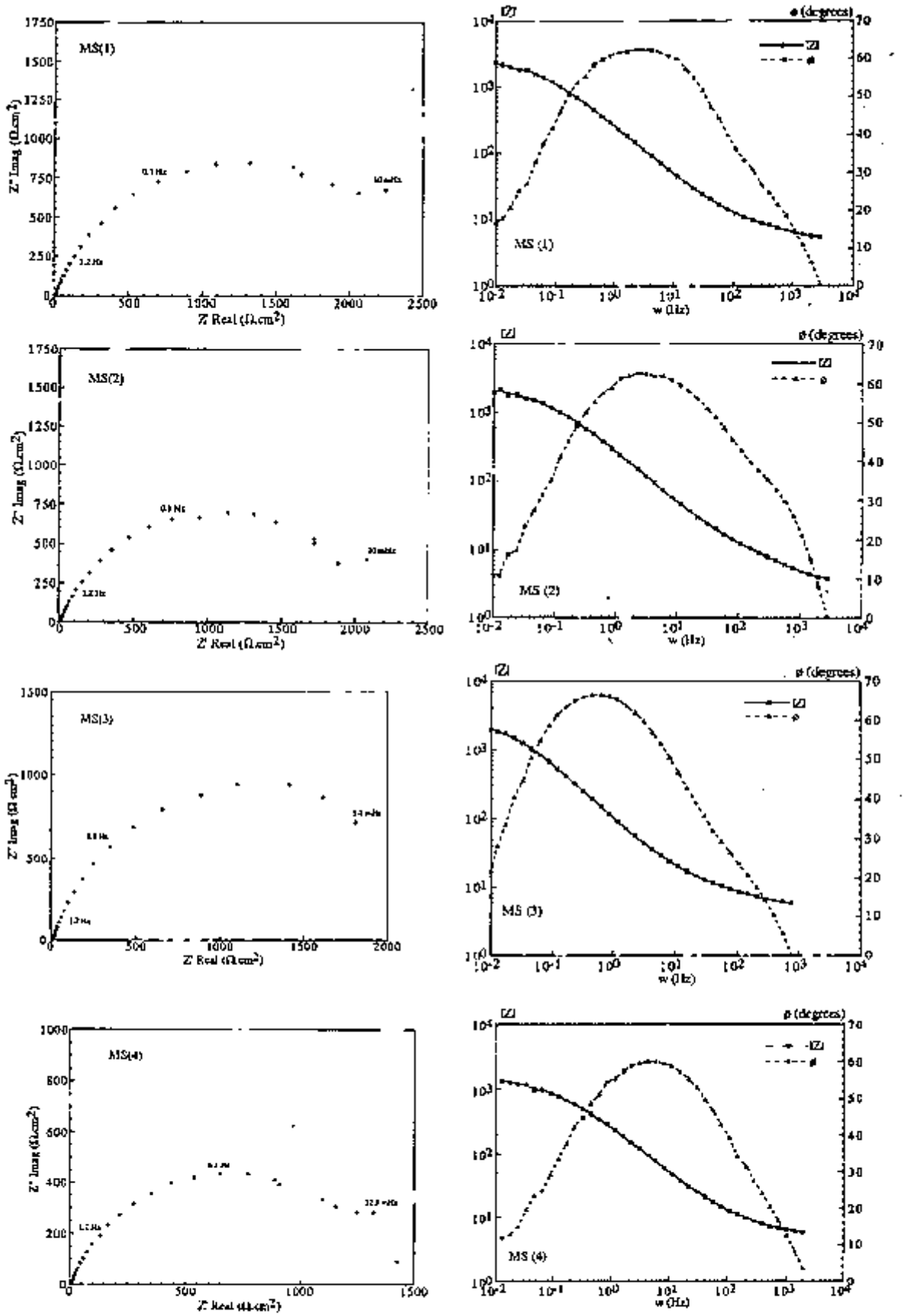

Figure 3.28 - Impedance response (Nyquist and Bode plots) of specimens MS in 0.5 M Na_2SO_4.

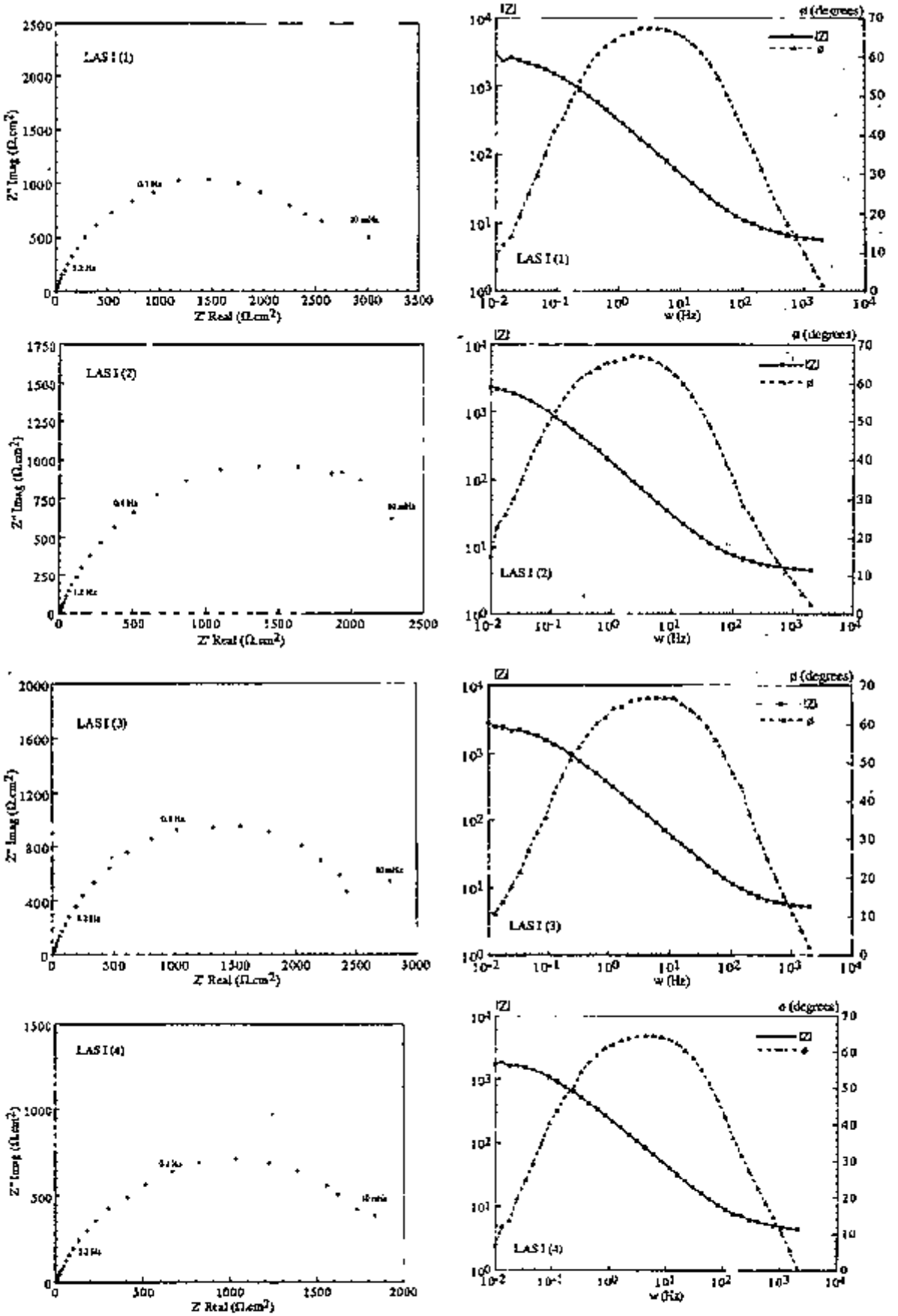

Figure 3.29 - Impedance response (Nyquist and Bode plots) of specimens LAS I in 0.5 M Na_2SO_4.

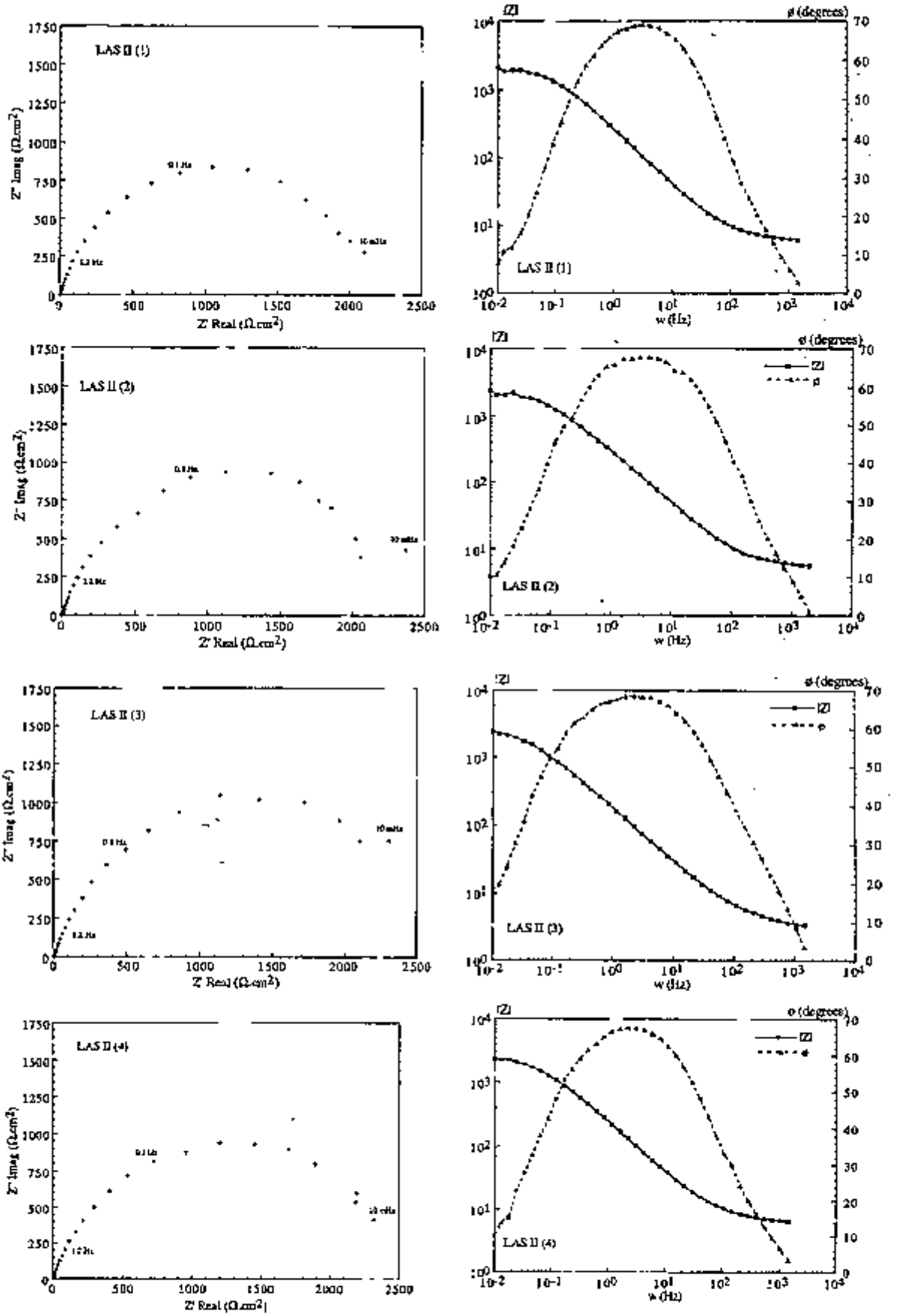

Figure 3.30 - Impedance response (Nyquist and Bode plots) of specimens LAS II in 0.5 M Na_2SO_4.

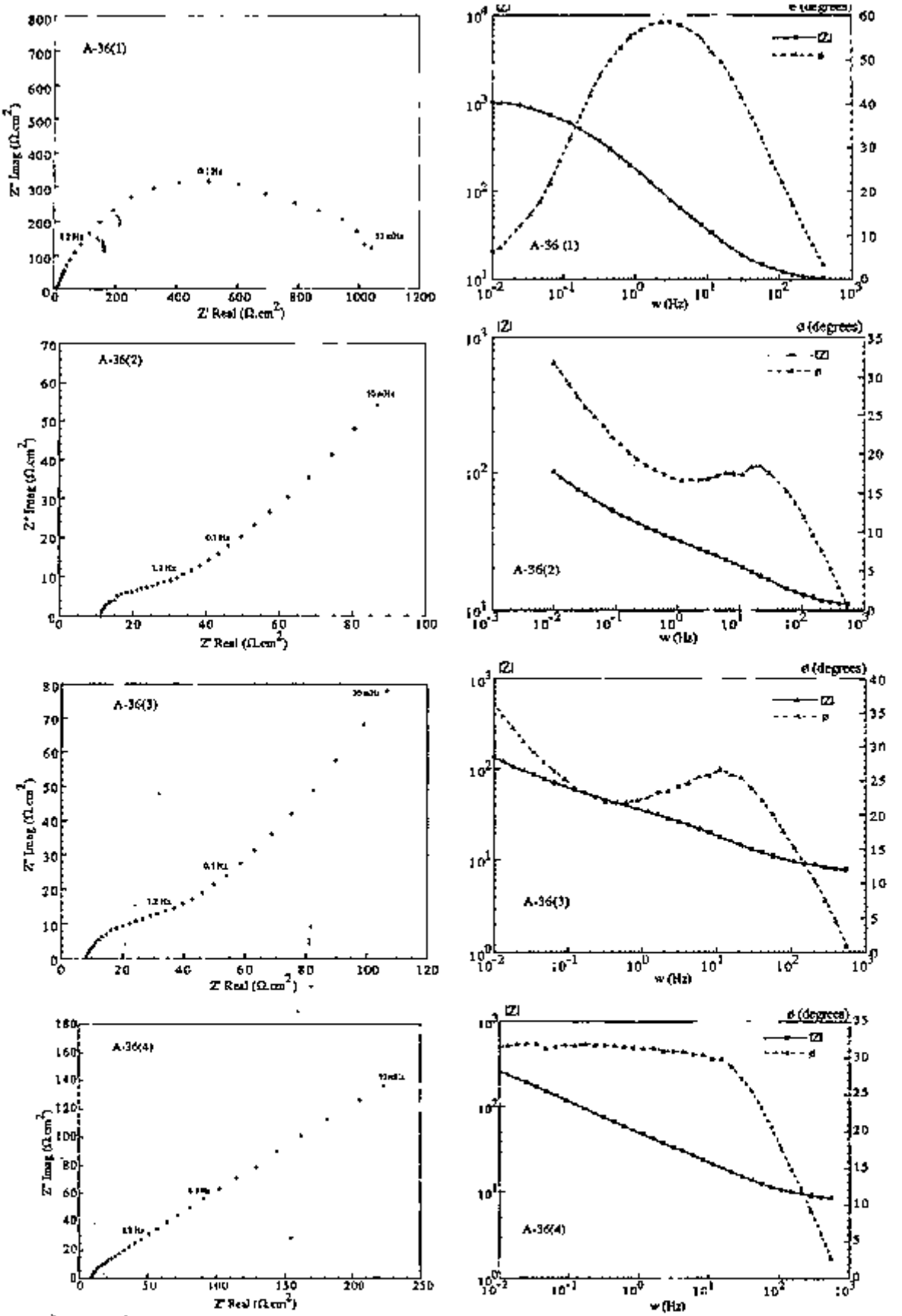

Figuro 3.31 - Impedance response (Nyquist and Bode plots) of specimens A-36 in 0.5 M Na_2SO_4.

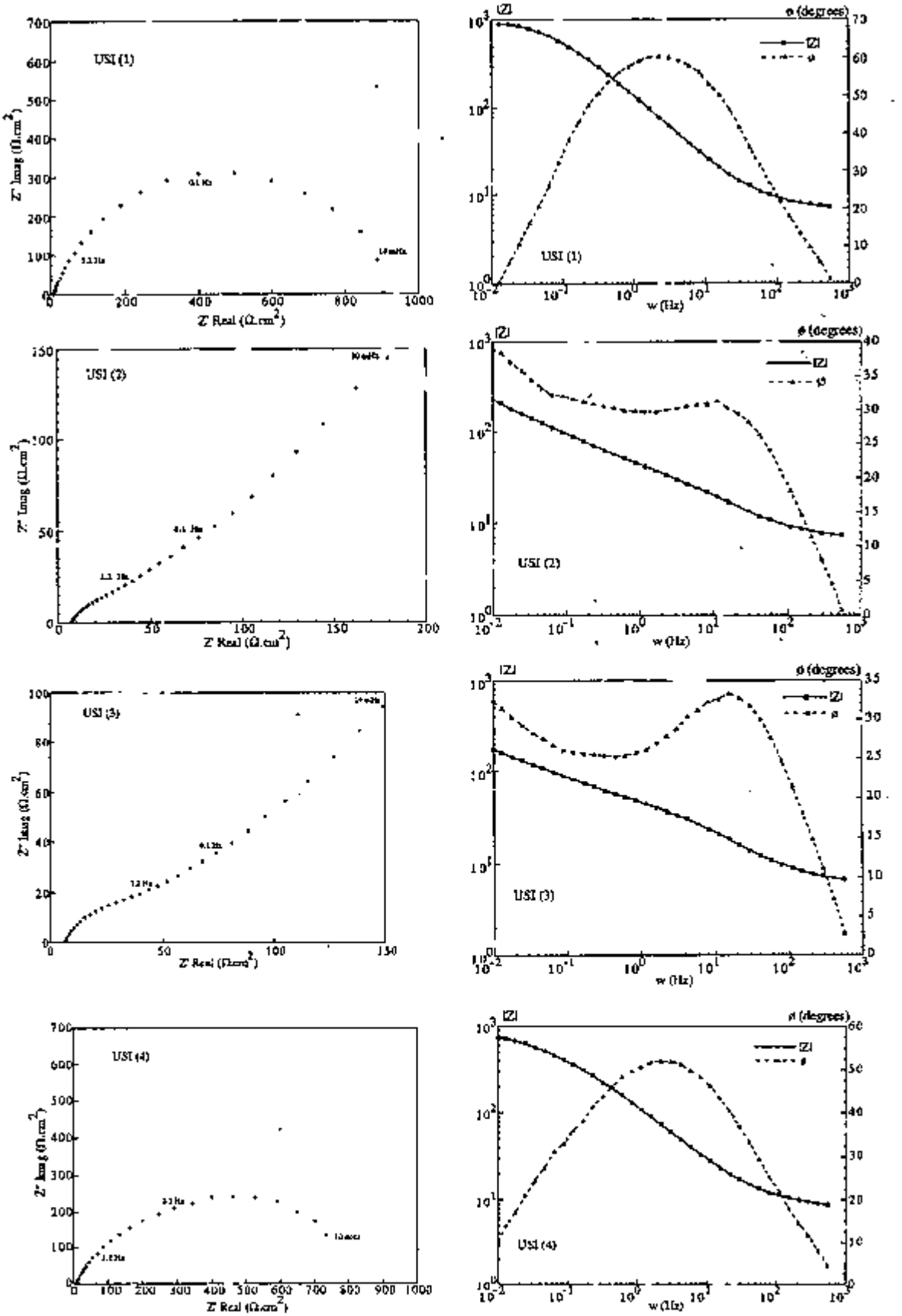

Figure 3.32 - Impedance response (Nyquist and Bode plots) of specimens USI in 0.5 M Na_2SO_4.

TABLE 3.9 - Impedance data for steels exposed in 3.5% wt NaCl solution.

Steel	"R_{ct}" ($\Omega.cm^2$)	ß (degree)	C_{dl} (mF/cm^2)	mean C_{dl} (mF/cm^2)	slope log |Z| vs log w
MS	1341 1636 1795	20 22 18	1.5 0.8 1.9	(1.4±0.5)	- 0.63 - 0.67 - 0.70
LAS I	1273 852 753	24 18 21	1.0 1.4 0.8	(1.1±0.3)	- 0.69 - 0.65 - 0.70
LAS II	1909 1568 1818	15 13 16	1.8 1.2 1.6	(1.5±0.3)	- 0.68 - 0.73 - 0.71
A-36	...	...	2.1 3.2 2.7	(2.7±0.6)	- 0.45 - 0.41 - 0.47
USI	...	...	3.3 1.7 3.9	(3.0±1.1)	- 0.50 - 0.55 - 0.42

... Indeterminate

TABLE 3.10 - Impedance data for steels studied in 0.5 M Na_2SO_4.

Steel	"R_{ct}" ($\Omega.cm^2$)	ß (degree)	C_{dl} (mF/cm^2)	mean C_{dl} (mF/cm^2)	slope log |Z| vs log w
MS	2614 2341 2500 1707	21 23 16 25	0.8 0.9 2.4 0.8	(1.2±0.8)	- 0.70 - 0.71 - 0.72 - 0.65
LAS I	2955 2909 2818 2244	18 19 18 18	0.8 1.3 0.7 0.9	(0.9±0.3)	- 0.76 - 0.76 - 0.74 - 0.71
LAS II	2341 2455 2795 2732	18 15 17 15	0.8 0.7 1.3 0.9	(0.9±0.3)	- 0.78 - 0.75 - 0.77 - 0.76
A-36	1068	22	1.1 17.5 8.0 6.3	(8.2±6.8)	- 0.66 - 0.19 - 0.26 - 0.35
USI	1024 1061	20 30	1.7 11.8 9.8 2.0	(6.3±5.2)	- 0.68 - 0.34 - 0.31 - 0.58

... Indeterminate

From Tables 3.9 and 3.10 it can be noticed that the values of "R_d" for MS, LAS I, and LAS II, calculated from the impedance diagrams are smaller, approximately 1.5 times, when compared with the values of R_p already presented in the last section. One possible reason for the difference is that with R_p evaluation, the diffusion resistance is measured as well, assuming that the solution resistance is negligible. The values of the slope of Bode plot (log |Z| vs log w), for the steels MS, LAS I and LAS II are in the range -(0.63-0.73) (sodium chloride solution), and -(0.65-0.78), (sodium sulphate solution). This supports the idea of a mixed control for the corrosion process, so that the rate of corrosion is determined by both, charge transfer and diffusion. In the cases considered, diffusion of oxygen through a porous oxide layer is believed to account for the diffusion effect in the impedance response. LAS II produced less depressed semi-circles than the other steels in both solutions, and this could be indicative of fewer interacting time constants and also less corrosion on the surface of this steel. Despite the minor differences between the steels MS, LAS I, and LAS II in both solutions, it can not be said that their impedance response is comparatively indistinguishable. Similarities among the steels produced by a same maker were observed either in the features of the impedance response diagrams, suggesting similar corrosion mechanisms, or in the values of "R_d"and C_{dl} obtained in a same solution. Capacitance values were similar in both solutions for the steels MS, LAS I and LAS II.

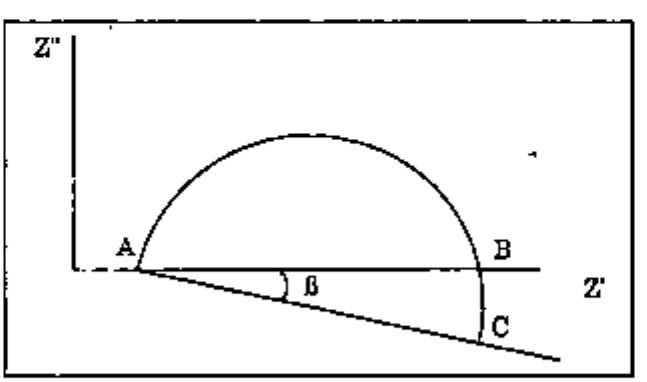

Figure 3.33 - Depressed semi-circle typical impedance response, Nyquist plot, of some steels used. R_d is estimated from the chord AC, and ß is the depression angle.

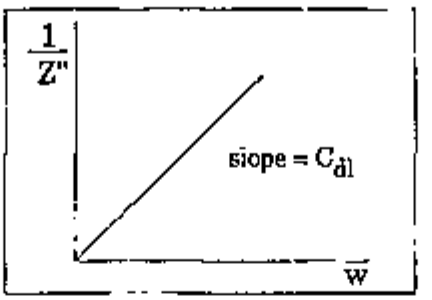

Figure 3.34 - A plot of 1/Z" versus w.

According to Juettner[184], Nyquist plots similar to the ones produced by the steels MS, LAS I, and LAS II, are the result of the simultaneous occurrence of charge transfer and transport processes in neutral aerated media. Figure 3.35 shows his "inhomogeneous surface model". In this model it is assumed that metal dissolution occurs on parts of the corroding metal which are covered with corrosion products, while oxygen reduction occurs in the pores of the oxide film. The equivalent circuit for this model consists of the charge transfer resistance R_{ct} and the transport resistances, R_{Nd} , R_{Id} and R_{Pd}, describing the Nernstian diffusion of oxygen, the inhomogeneous transport to the pores, and the diffusion of oxygen in the pores, respectively. The electrode capacitance is given by C.

Despite the similarities among the steels mentioned above, some differences were noticed among these steels and particularly the two other steels used, A-36 and USI. In sodium chloride solutions, these latter steels showed an impedance response indicative of a corrosion process under diffusion control, Bode slopes (log|Z| vs log w) were all around -0.5. The double layer capacitance of A-36 and USI steels, in this same solution, was in the range (3.7-3.9) mF/cm^2, and reproduced well for both steels. The general Nyquist plot features of this response was a partially resolved semicircle at high frequencies, and a low frequency tail which sometimes bent towards the real axis. In the sodium sulphate solution, however, two typical impedance responses were obtained for A-36 and USI. One, which was common for the steels MS, LAS I and LAS II, consisted of a large

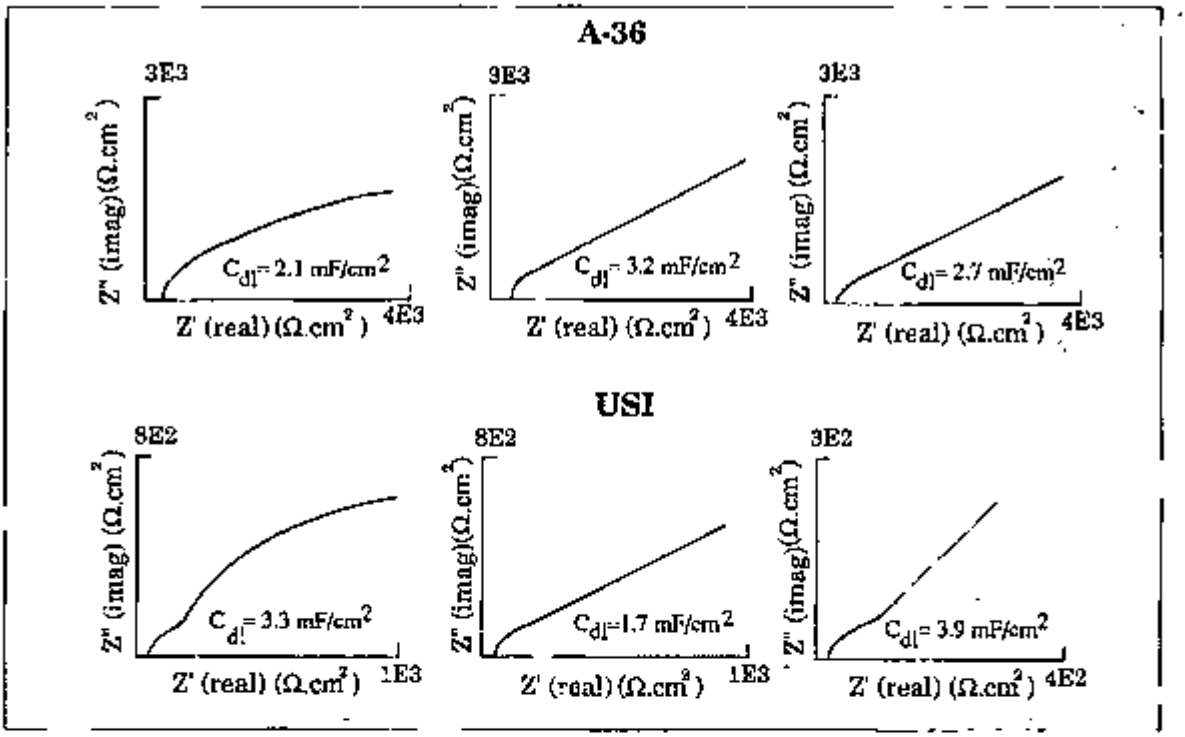

Figure 3.36 - Schematic Nyquist plots of steels, A-36 and USI, after exposure to 3.5% wt NaCl

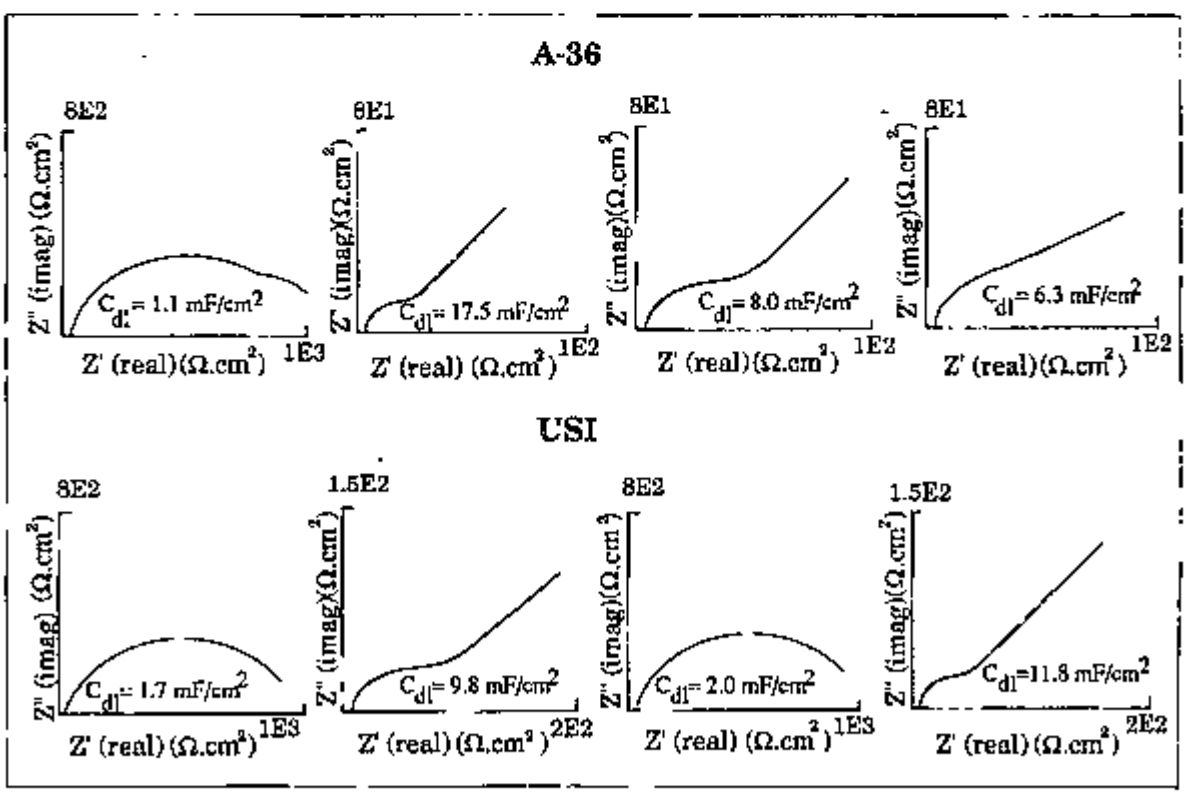

Figure 3.37 - Schematic Nyquist plots of steels, A-36 and USI, after exposure to 0.5M Na_2SO_4.

The value of the double layer capacitance, C_{dl}, for the steels A-36 and USI in the chloride solution, was around 2 times higher than for MS , LAS I and LAS II. In the sodium sulphate solution, a large variation in C_{dl} values was produced by A-36 and USI steels. The variation was associated with two different kinds of behaviour. Lower calculated capacitance values were always obtained when a particular type of response was found, which was a diffusion tail bending towards the real axis at low frequencies. On the other hand, much larger C_{dl} values were found when the Nyquist plot features corresponded to a high frequency semi-resolved semi-circle and low frequency diffusion tail.

From the impedance data shown it seems that the steels used in this study give two kinds of electrochemical impedance responses. Three steels, MS, LAS I, and LAS II, displayed similar Nyquist plots, whereas A-36 and USI, showed comparable impedance characteristics. If the two groups with similar responses are considered, it must be noticed that each group includes steels of the two types studied, either mild steel type or low-alloy steel type. Thus the evidence obtained from impedance response is that under the conditions analysed, which is fully immersed in 3.5% wt NaCl solution and 0.5M Na_2SO_4 solution, and not far removed from E_{corr}, the two types of steels used can not be differentiated. Since however two distinct behaviour were found for two groups of steel, attention must be paid to the common characteristics of the steels inside a group. The first fact that should be mentioned is that each group of steels with similar characteristics were produced by the same manufacturer. This can suggest that the history of the steel, its microstructure or composition, is affecting its electrochemical behaviour. The chemical composition of the steels is presented in Table 3.1. The elements which are present in relatively higher contents for the steels A-36 and USI, when compared to the other alloys, are mainly C an Mn, Figure 3.38. Carbon and manganese in large amounts have been found to be detrimental to corrosion resistance[100]. Also manganese in significant contents can lead to the formation of inclusions, mainly MnS, if the steel contains sulphur. 'Active' sulphide

inclusions are known as nucleating sites for pitting. Inclusions of the oxide type, generally FeO, SiO_2, Al_2O_3 and MnO, also affect the corrosion properties of steels, since they prevent the formation of passivating oxide films[6]. An analysis of the microstructure of the various steels used seemed to be necessary at this stage. This is presented in the next section.

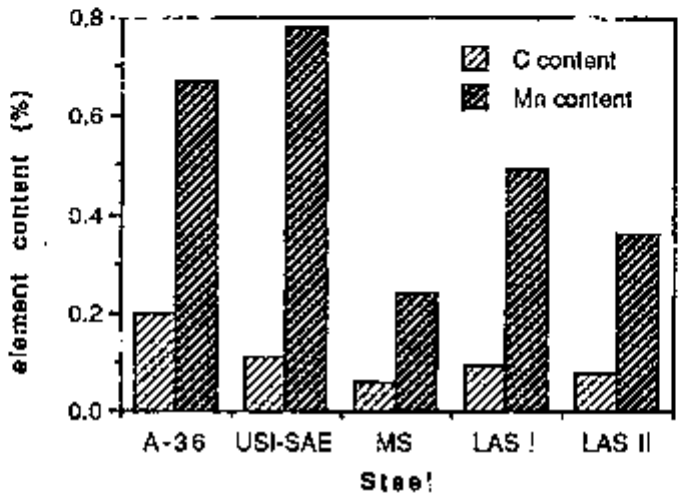

Figure 3.38 - C and Mn contents (%) of various alloys used.

Since a large variation in impedance response was observed for the steel USI in sulphate solution, more tests seemed to be required in this particular solution. Three more experiments were then conducted, and again both characteristic responses were produced, Figure 3.39. Two of the specimens showed a response, Nyquist plot , whose features corresponded to a diffusion tail bending towards the real axis, and the other, a response characteristic of a semi-resolved semi-circle at the high frequencies and a tail with a slope of 0.7 at the low frequency range. The capacitance values were calculated for the three specimens and are shown in Figure 3.39. The three specimens were then removed from the sulphate solution, re-polished and re-immersed again. This was done to check if surface finishing characteristics, mainly scratches, were responsible for the distinct behaviour. The impedance plots obtained after re-immersion of the three specimens reproduced very well the first ones, Figure 3.39. Thus the distinct

behaviour could not be attributed to a difference in the surface finishing. It could not also be related to the chemical composition, since all specimens were from the same steel.

The microstructure of the surface, inclusions content and size, of the three specimens was then examined. The two specimens which presented the same characteristic impedance response also had similar inclusions content. Nevertheless the one which produced distinct behaviour also exhibited a larger content of inhomogeneities at the surface than the other two. The characteristic of the corrosion products on the surface of the three steels was also visually observed after the impedance run was over. It was noticed that for the two steels presenting similar behaviour, diffusion tail bending towards the Z' axis, the larger proportion of the exposed area was covered by a brown and loose corrosion product which was easily removed from the surface. The rest of the specimen showed a dark blue and adherent corrosion product, which could not be removed by rubbing. However, in the case of the specimen showing an impendance response of a high frequency semicircle with a low frequency tail, the proportion of the area covered by the adherent corrosion product was larger than the area covered by loose and brown corrosion product. It is believed that the large area of adherent corrosion product exhibited by the steel USI (a) might have slowed the corrosion rate. Thus as a result, the impedance response changed from diffusion of the non-classical Warburg type to a mixed control response. This was indicated by the slope of the log |Z| vs log w plot of this specimen, USI (a), around 0.7. Charge transfer and diffusion of reactants through the porous oxide layer might have been operative. Two time constants could be separated in the impedance response corresponding to the specimen with higher proportion of adherent corrosion product, Figure 3.40. The first, related to the high frequency semi-circle, was assumed to be due to the charge transfer controlled reaction at the areas covered by the adherent corrosion product ('passivated'), and the second, to the low frequency tail, the diffusion controlled reaction at the other areas of the surface.

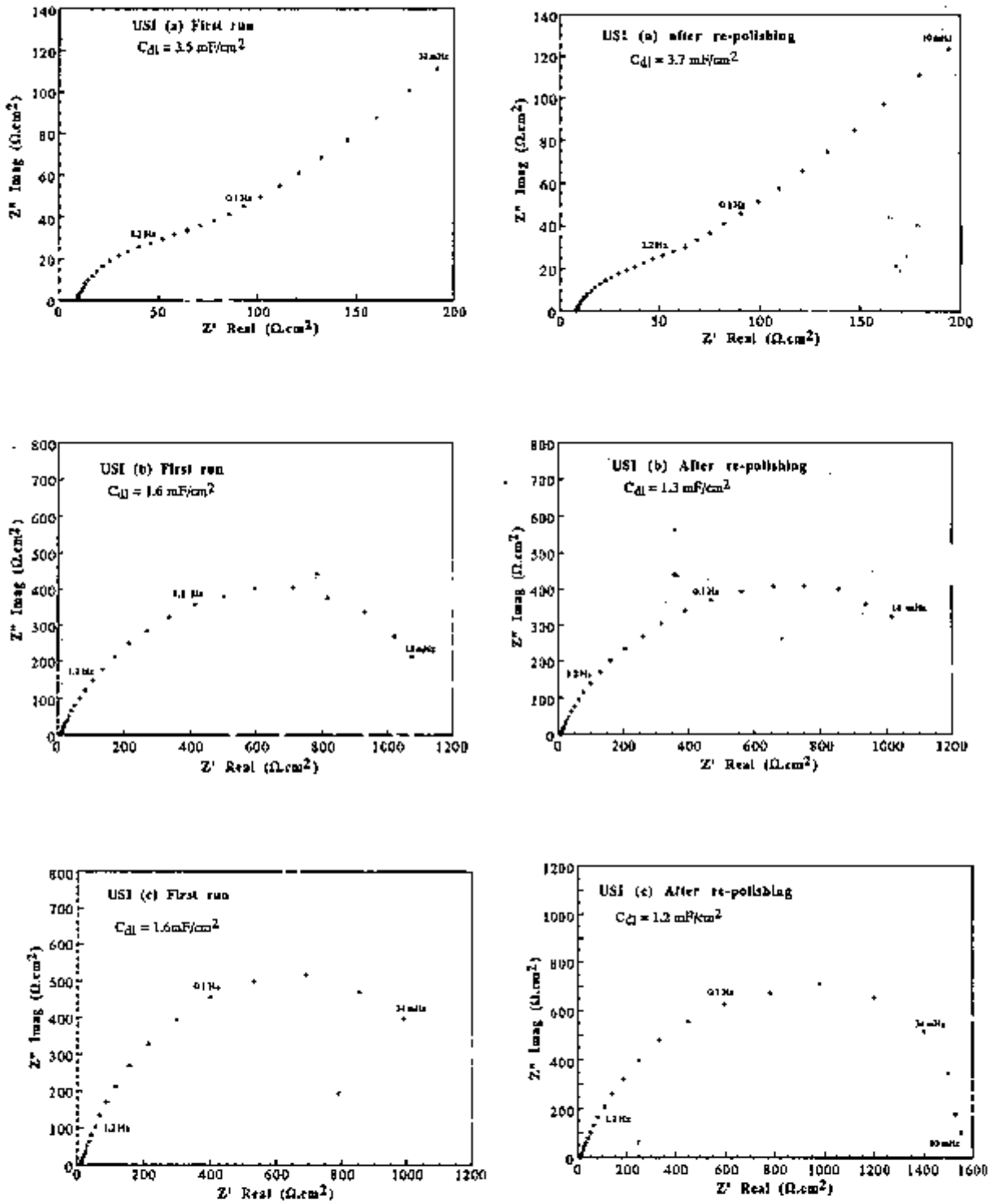

Figure 3.39 - Nyquist plots of specimens of USI steel in sulphate solution.

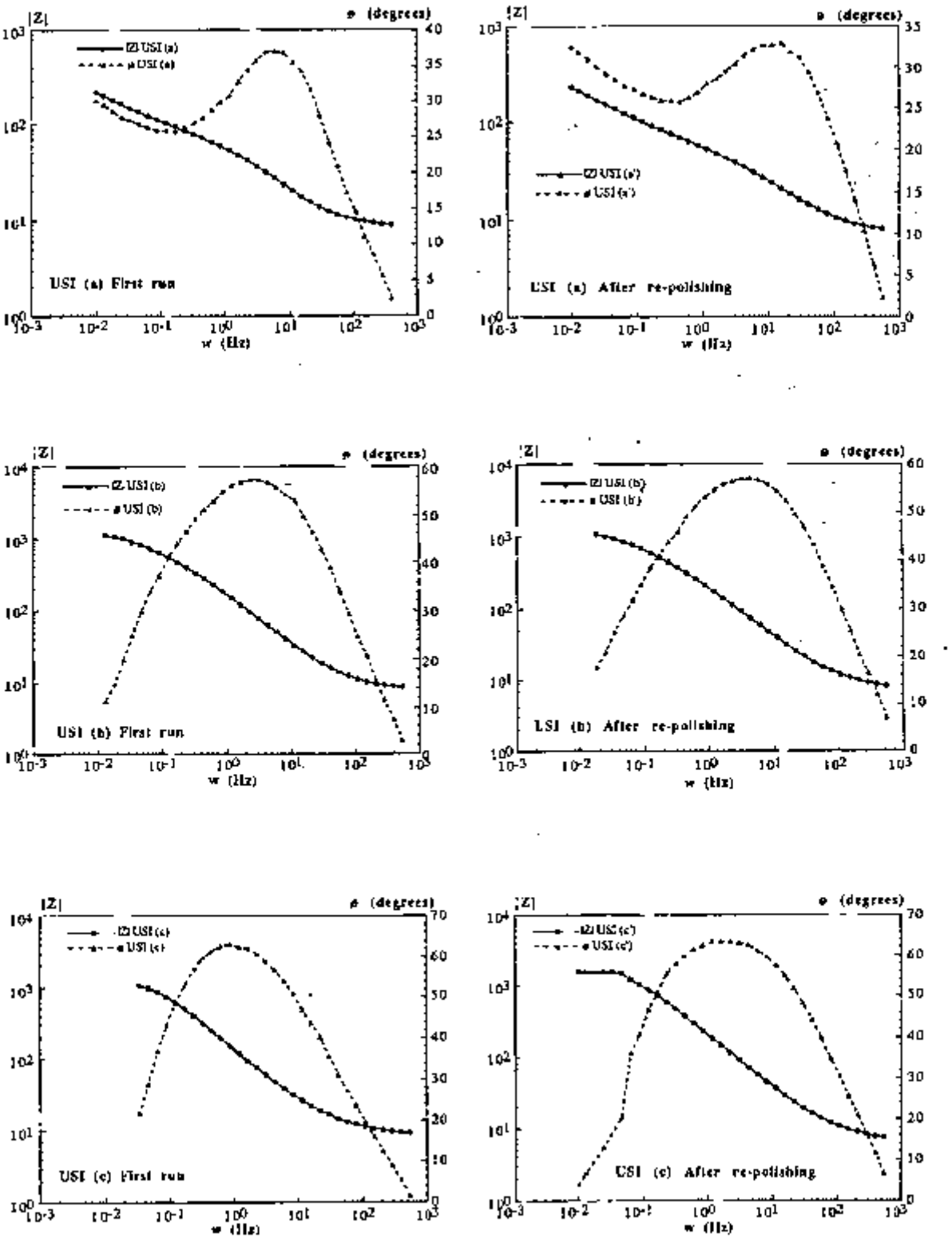

Figure 3.40 - Bode plots of specimens of USI steel in sulphate solution.

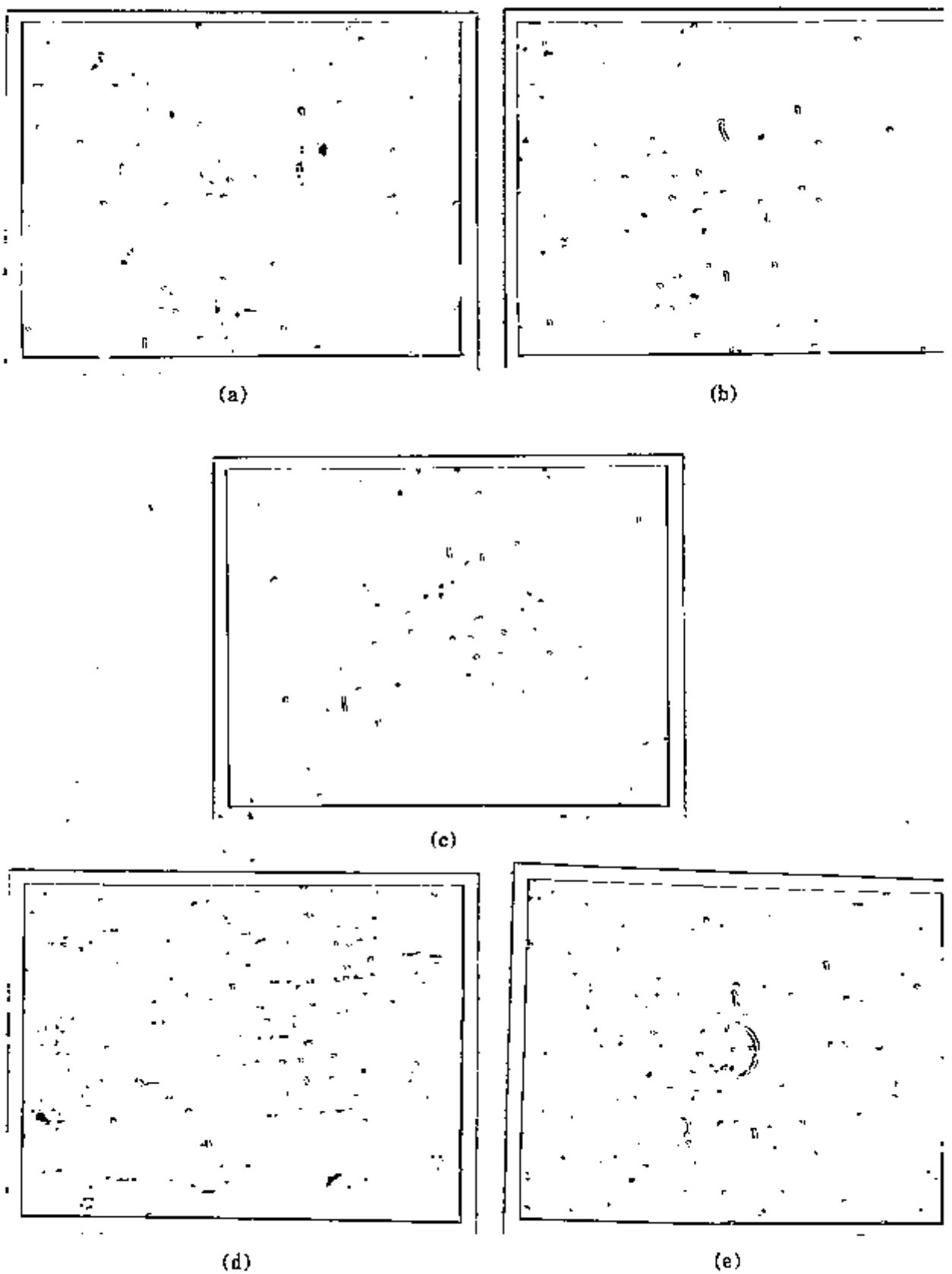

Figure 3.41 - Micrographies of steels used showing inclusions, (a) MS, (b) LAS I, (c) LAS II, (d) A-36, and (e) USI.

TABLE 3.11 - Characteristics of most common inclusions in the steels used

Steel	Average number of inclusions/cm^2	Most common types	Shape
MS	(2020±380)	mainly MnS Al_2O_3	lens round
LAS I	(1500±140)	Al_2O_3/MnS MnS/TiO_2 Al_2O_3/TiO_2/MnS	round lens round
LAS II	(1440±100)	SiO_2 Al_2O_3 Al_2O_3/MnS	round round lens
A-36	(6040±560)	mainly MnS Al_2O_3 /SiO_2/MnO	elongated round
USI	(3020±1600)	mainly SiO_2 Al_2O_3/MnS/Cu_2O TiO_2	round round round

Only techniques which cause slightly perturbation of the system from the equilibrium conditions have so far been presented. The behaviour of the steels when far removed from their corrosion potential, E_{corr} , is also of interest, and to study the electrochemical characteristics of the various steels used in this work at high polarization potentials, full polarization measurements were carried out potentiodynamically.

3.3.6 - Full polarization curves

3.3.6.1 - Sodium sulphate solution.

Potentiodynamic polarization curves in 0.5M Na_2SO_4 solution were obtained for the various steels used in this thesis and are shown in Figures 3.42 to 3.46.

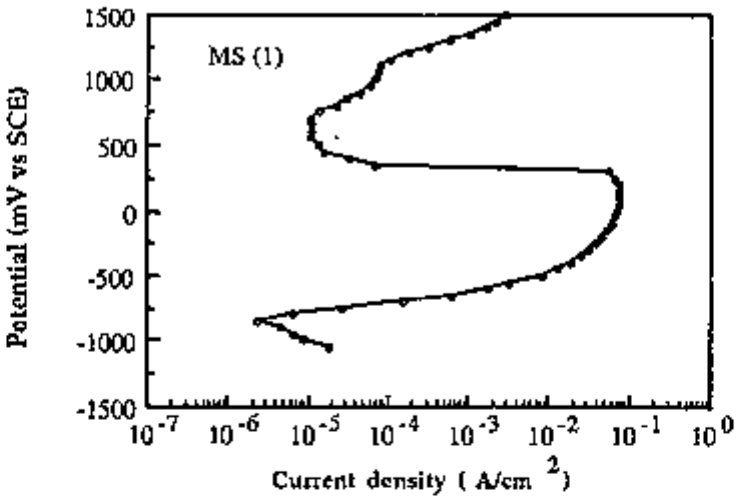

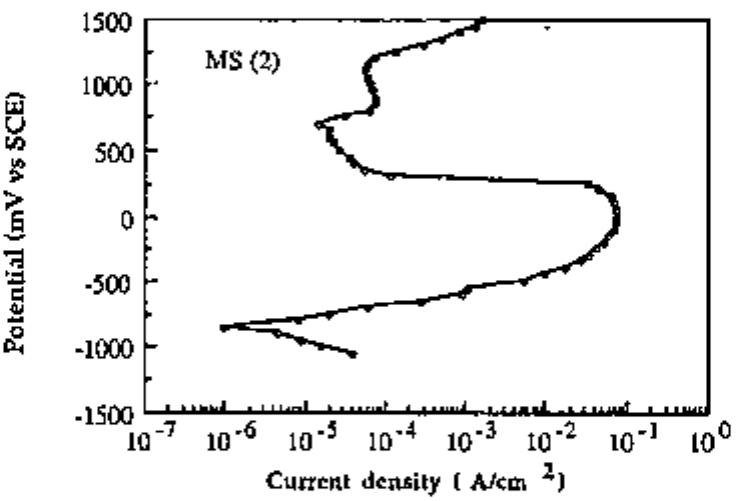

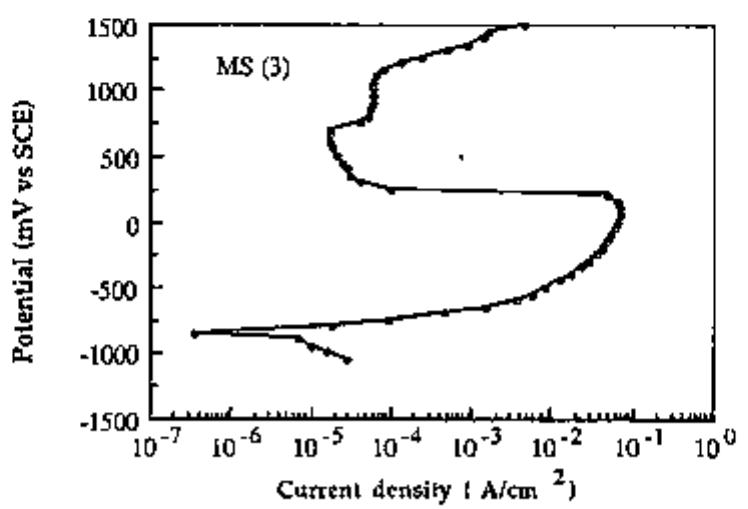

Figure 3.42 - Polarization curves of steel (MS) in 0.5M Na_2SO_4 solution.

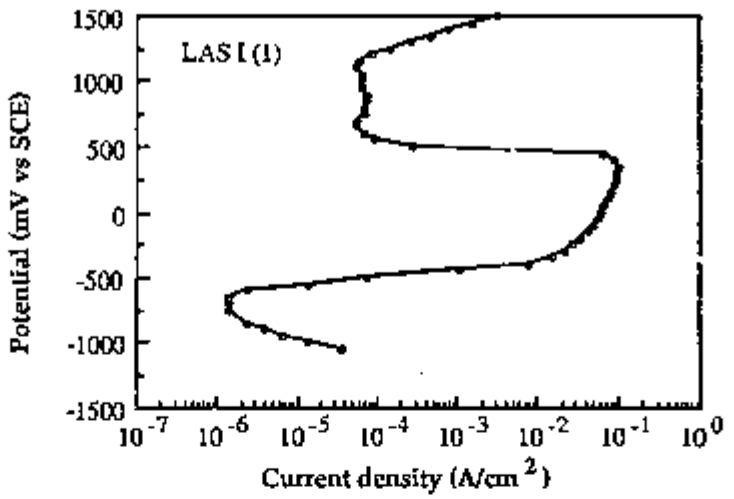

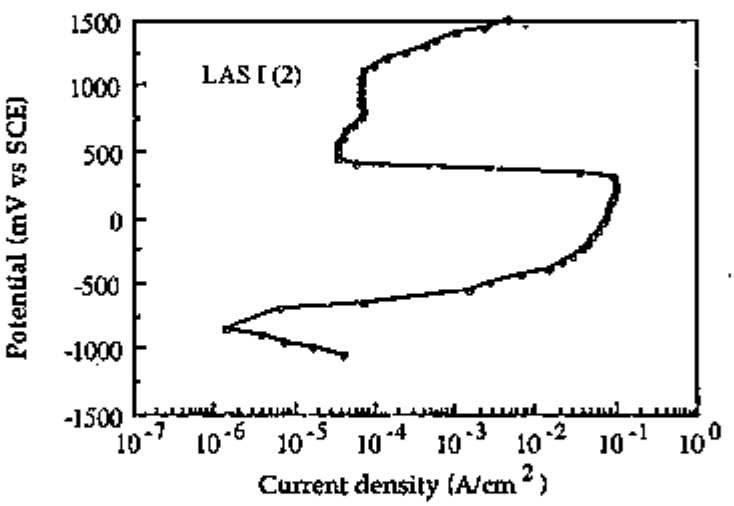

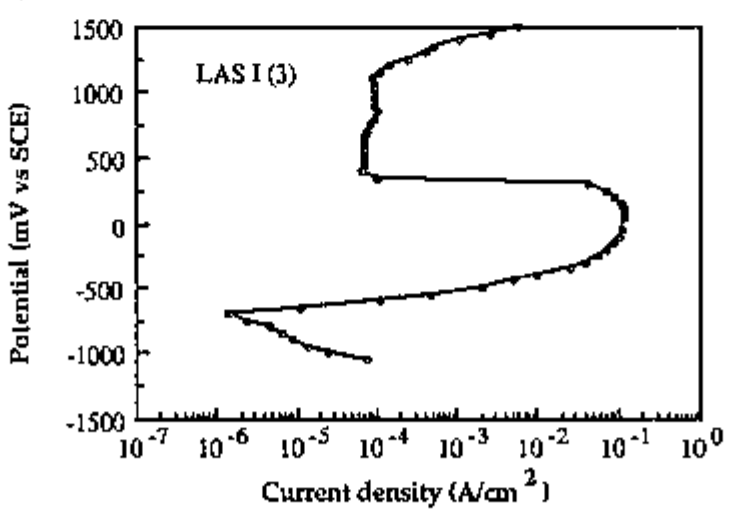

Figure 3.43 - Polarization curves of steel (LAS I) in 0.5M Na_2SO_4 solution.

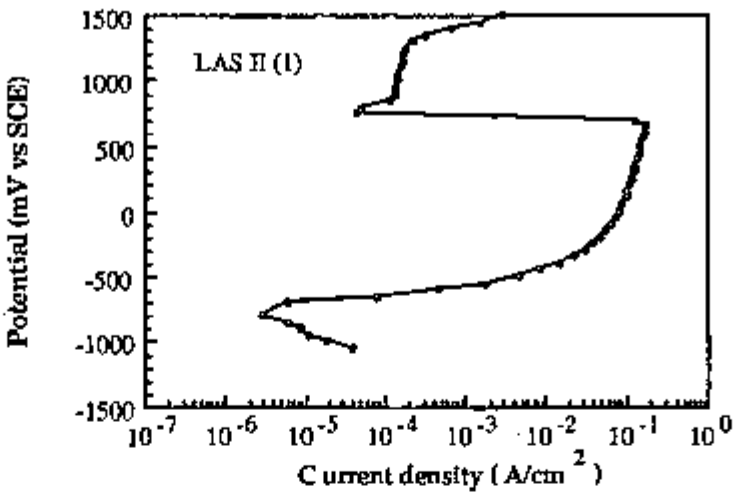

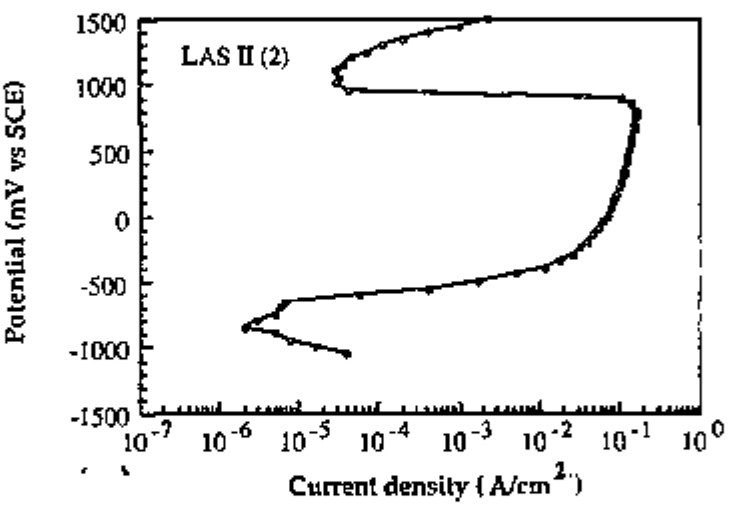

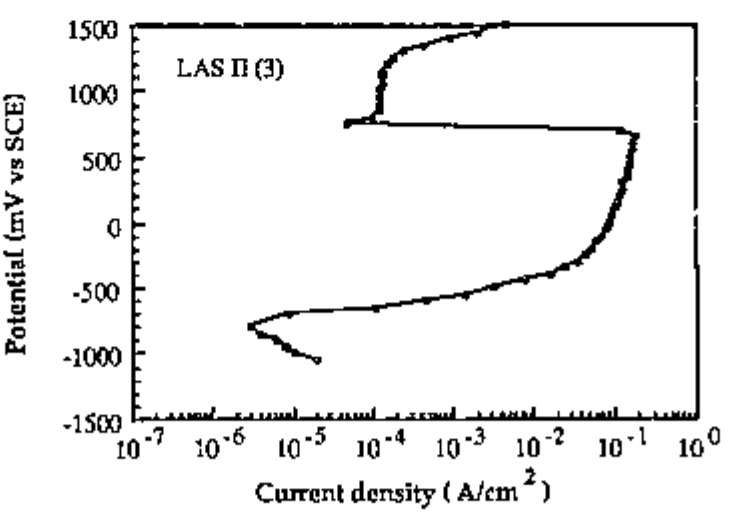

Figure 3.44 - Polarization curves of steel (LAS II) in 0.5M Na_2SO_4 solution.

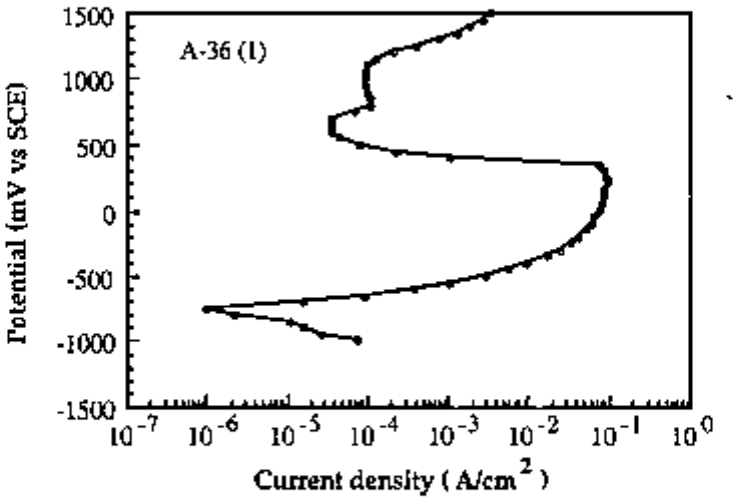

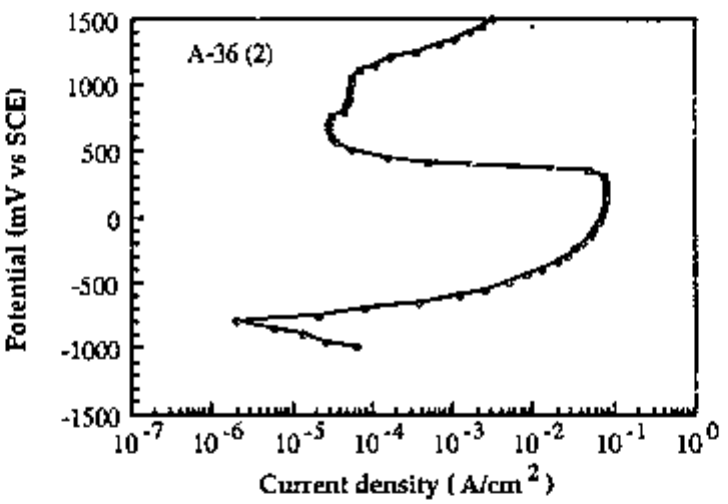

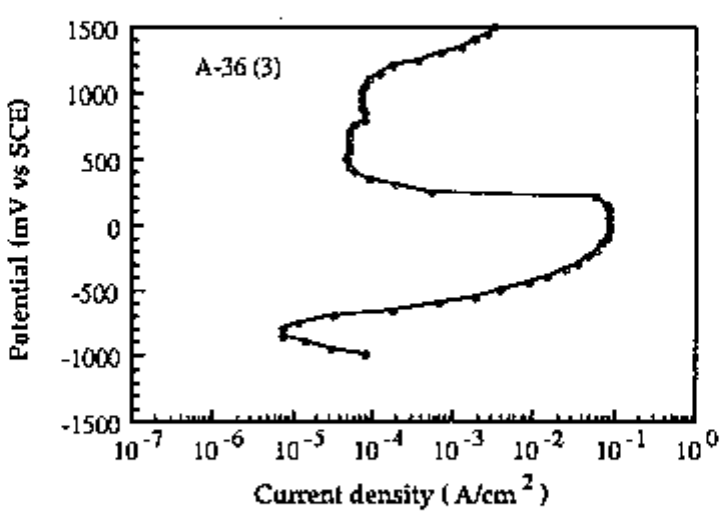

Figure 3.45 -Polarization curves of steel (A-36) in 0.5M Na_2SO_4 solution.

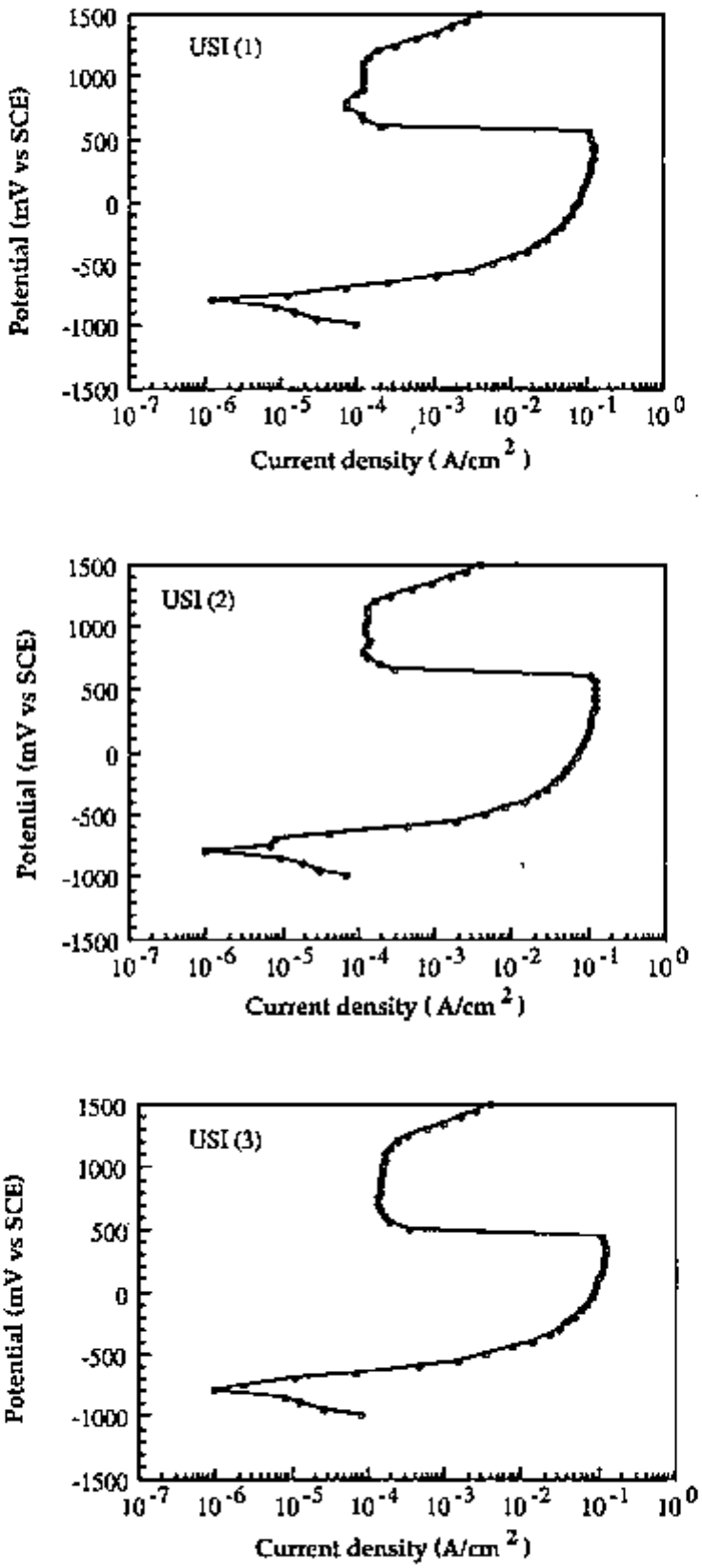

Figure 3.46 - Polarization curves of steel (USI) in 0.6M Na_2SO_4 solution.

All the steels showed an active region followed by an active-passive transition. The primary passive potentials and the corresponding current densities for passivity, i_{ccd}, were different for each material.

The values of the critical current density for passivity, i_{ccd}, primary passive potential, E_{pass}, and the current density in the passive region, i_{pass}, were obtained from Figures 3.42-3.46, and are given in Table 3.12. The current density in the passive region first reached a minimum value immediately after passivation, and then increased to a new stable value (plateau). The values of i_{pass}, given in Table 3.12, are the values obtained from the the plateau region, where it was fairly stable until the transpassivation region, or oxygen evolution started.

TABLE 3.12 - Values of i_{ccd}, E_{pass}, and i_{pass} from polarization curves.

Steel	i_{ccd} ($x10^{-2}A/cm^2$)	mean i_{ccd} ($x10^{-2}A/cm^2$)	E_{pass}	i_{pass} ($x10^{-5}A/cm^2$)	mean i_{pass} ($x10^{-5}A/cm^2$)
MS	8.0 7.8 7.0	(7.6±0.5)	250 150 150	6.3 6.0 6.0	(6.1±0.2)
LAS I	10.0 10.0 12.0	(10.7±1.2)	410 350 200	7.0 6.9 9.1	(7.7±1.2)
LAS II	17.0 17.0 18.0	(17.3±0.6)	650 660 800	15.0 3.1 15.0	(11.0±6.9)
A-36	9.5 8.0 9.0	(8.8±0.8)	300 300 150	9.3 5.8 7.0	(7.4±1.8)
USI	12.0 13.0 13.0	(12.7±0.8)	550 590 400	13.0 15.0 17.0	(15.0±2.0)

It is easily noticed from polarization curves data, that the two mild steel types passivated at lower polarization potentials, and for lower applied current densities, than all the low-alloy steel types. This is indicated by the values of E_{pass}

and i_{ccd}. In fact passivity for all the low-alloy steel types was only achieved at very high potentials and current densities. The high mean values of i_{ccd}, Table 3.12 support this observation. Thus it seems that the addition of alloying elements to the low-alloy steels shifted the active/passive transition potential towards the positive direction. An attempt was made to try to correlate the composition of the various steels used with the ease of passivation. This was done by plotting i_{ccd} versus the content of various elements in the alloy. The alloying elements considered were Cu, Cr, Si, P, Mn and C. However no standard relationship was found between these elements and the ease of reaching passivity. Thus no definite conclusion can be drawn about the effect of composition of steels studied on their passivity characteristics. An enormous number of alloys, in which each alloying element content is systematically varied whilst keeping the other alloying components would be required to study this effect further. This however was not the aim of the present study.

The passivity current density, i_{pass}, showed a direct relationship with the content of copper in the steel, Figure 3.47.

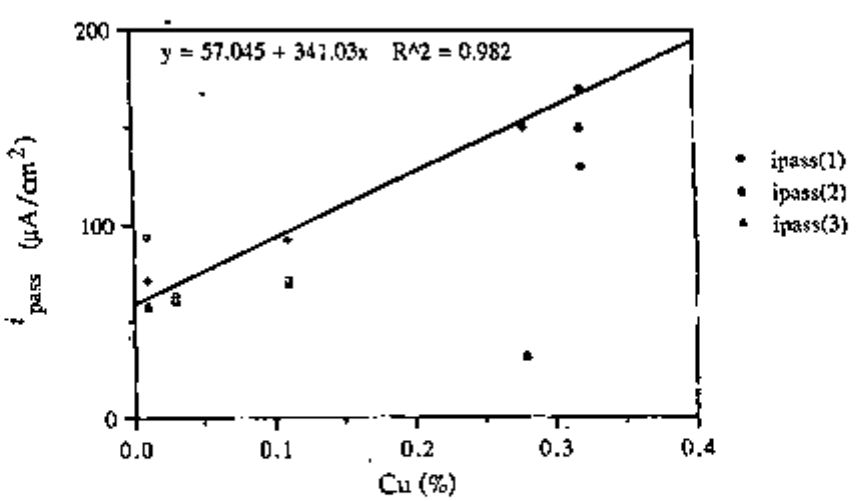

Figure 3.47 - i_{pass} vs Cu content of steels used.

It is possible that copper, even though present in small quantities, might be incorporated in the passivating film. If this occurred an increase in the electronic conductivity of the passivating film would be expected. As a result the current density in the "passive state" would also increase. It should be noted that the passive region obtained showed relatively high currents involved, 60 $\mu A/cm^2$ to 150 $\mu A/cm^2$. The appearance of the passive region is believed to be due to the precipitation of a salt layer on the surface. This is brought about by the saturation of the solution next to the metal surface with Fe^{2+} ions, which with the sulphate species combine to form a passive layer consisting mainly of iron sulphate. Once the precipitation of sulphate has occurred, the concentration of Fe^{2+} at the surface decreases, and the dissolution of iron starts again.

A dissimilar behaviour is clearly seen between mild steel types and low-alloy steel types at high anodic potentials. The difference, however, could not be easily attributed to a particular alloying element, or to a combination of them. If the inclusions type is considered, Table 3.11, a correlation seems to exist between the presence of certain inclusion types and the passivity characteristics of the steel. In the case of the mild steel types, the inclusions analysed by Scanning Electron Microscopy consisted mainly of MnS. Very few oxide type inclusions were detected for both mild steels used. On the other hand, MnS was not found alone in the low-alloy steel types. In the few cases when MnS was detected, it was always associated with oxide types, such as a duplex or even triplex type inclusion. It is probable that the predominance of oxide or duplex type inclusions in the low-alloy steel types resulted in the high passivation potential found for those steels.

It has been shown from experience that in normal carbon steels containing active sulphides, pits are nucleated by a microgalvanic effect, but they cease growing after a depth of 100 μm-200 μm is reached[197]. Sulphide inclusions are easily dissolved in acid solutions[200]. The solution inside an initiating pit is acidified by the hydrolysis of Fe^{2+} and Fe^{3+} ions generated by dissolution reactions.

Thus, conditions for dissolution of MnS type inclusions would exist, and once these have been dissolved, the matrix which has the same susceptibility to corrosion as the rest of the steel in the surface is then exposed, and the conditions for the continuation of the pit have ceased.

Even though the whole surface of the exposed specimen is dissolving very rapidly at the high anodic polarization potentials applied, it is believed that the dissolution of oxides is much more difficult. Accumulation of oxide inclusions would then result from anodic dissolution since they are nobler than the iron matrix. Consequently the rapid attack of the metal surrounding the oxide or duplex type inclusions would be accelerated even further. The conditions for an intense localized corrosion would exist and subsist for longer periods than for sulphide inclusions type.

The dissolution of the matrix surrounding the oxide inclusions, occasionally would also lead to their detachment and the exposure of the matrix. The areas surrounding small oxide inclusions can thus cause intense localized attack since they provide difficult access to the external solution, and subsequent passivation. This can explain the relatively high passivation potential for the LAS II steel, which presented the fewest inclusions content detectable by Optical Microscopy.

Situations have been reported in the literature where only duplex inclusions sulphide-oxide gave rise to intense localized attack. The single phase sulphide only dissolved to a certain extent but did not affect the matrix[196]. In the same work, an attack which produced a grid-like appearance was mentioned, and this was connected with slag inclusions in the pit bottom. That type of attack only occurred when the steel was polarized. Under freely corroding conditions, the duration of attack before the termination was too small to develop grids.

3.3.6.2 - Sodium chloride solution.

Full polarization tests were also carried out for four of the steels studied, in the sodium chloride solution, and their respective curves are shown in Figure 3.48.

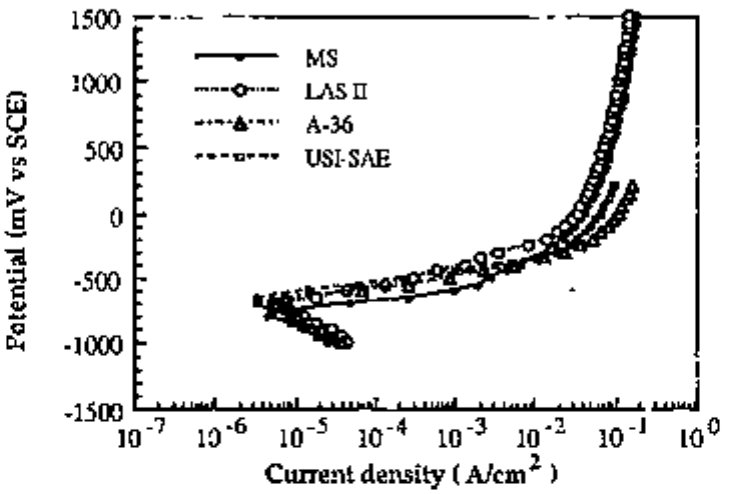

Figure 3.48 - Polarization curves of steels used in 3.5% wt NaCl.

In sulphate, passivation is achieved by the formation of a salt-type film at or near the electrode and this involves the dissolution of very large amounts of iron. Substantial changes in the solution chemistry near the electrode are required before passivation can be achieved. The passivation relies on supersaturating the solution near the electrode with Fe^{2+} ions. Since chlorides have high solubility products, the deposition of a salt-type film at the surface does not occur, and consequently 'passivity' is not attained. It is easily seen in Figure 3.48 that the characteristic shape of the active-passive transition curve disappeared entirely.

In order to identify the characteristics of the polarization curves at potentials closer to E_{corr}, the two steel types obtained from the same manufacturer were compared in Figures 3.49 and 3.50. A smaller range of polarization potential was used for this purpose. It can be noted from these Figures that the polarization curves of the low-alloy steel, LAS II, was slightly shifted to a nobler direction.

Also the anodic current density corresponding to this latter steel was usually slightly smaller than for the mild steel, MS, Figure 3.49. No such differences were however observed between A-36 and USI. The larger content of inhomogeneities at the surface of the mild steels relatively to low-alloy steels produced by the same manufacturer could have been one of the causes for the small difference found in the anodic currents. The presence of inhomogeneities at the interface of steels usually affect their localized corrosion characteristics.

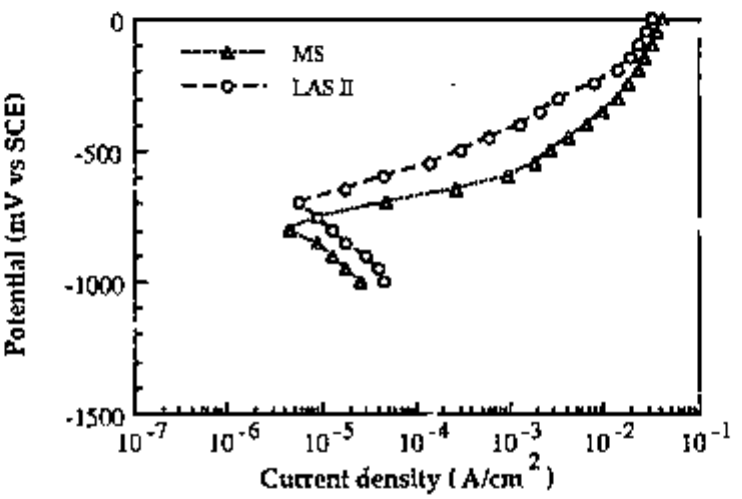

Figure 3.49 - Polarization curve of steels MS and LAS II in 3.5% wt NaCl.

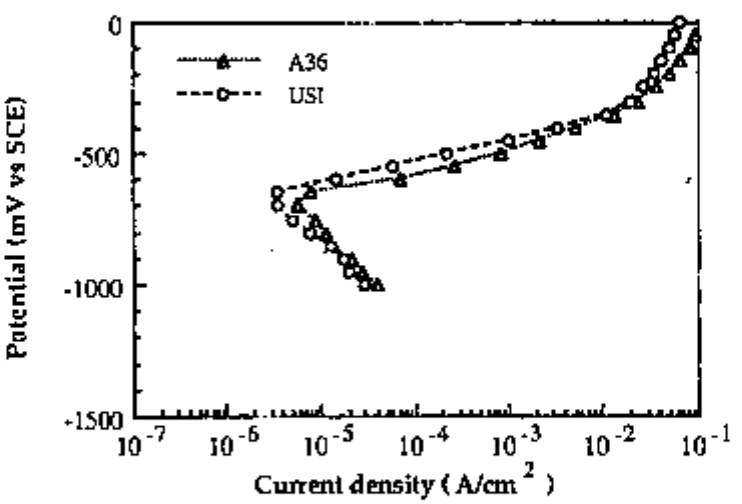

Figure 3.50 - Polarization curves of steels A-36 and USI in 3.5% wt NaCl.

3.3.6.3 - Cathodic polarization curves

Specimens of four of the steels studied, MS, LAS II, A-36 and USI, were immersed for 1 day in aerated 3.5% wt NaCl and 0.5 M Na_2SO_4 solutions. The steels were then cathodically polarized. Their responses in 3.5% wt NaCl and 0.5M Na_2SO_4 are shown in Figures 3.51 and 3.52, respectively. The corrosion product observed on the steels at the time of test was not reduced before cathodic polarization, since most of experiments presented in the previous sections of this chapter were conducted at this same condition, after 1 day exposure.

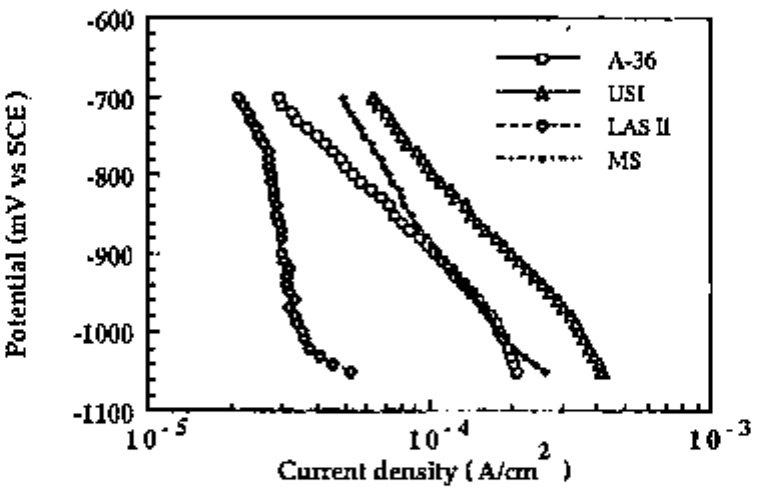

Figure 3.51 - Cathodic polarization curves for steels in 3.5% wt NaCl.

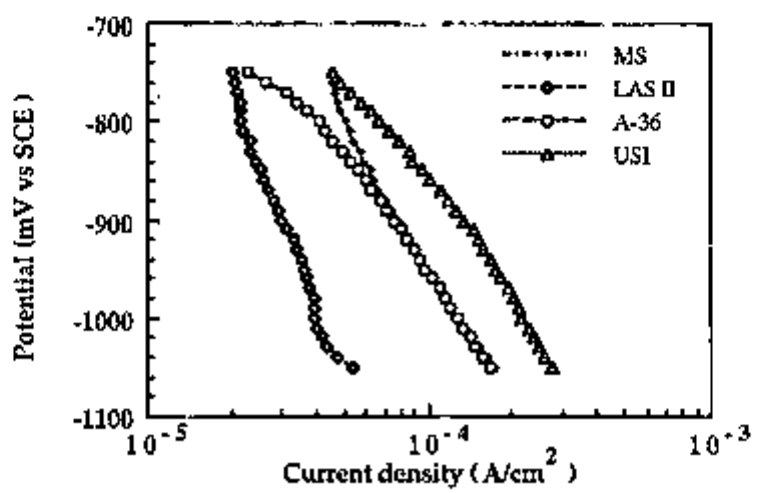

Figure 3.52 - Cathodic polarization curves for steels in 0.5M Na_2SO_4.

It is noted from Figures 3.51 and 3.52 that the shape of the cathodic polarization curves of steels obtained from the same manufacturer were much the same, indicating similar mechanisms for the cathodic reaction. At potentials close to E_{corr}, a region is seen for the steels MS and LAS II where the current density is practically constant with an increase in potential. This means that for these steels a diffusion plateau is observed at potentials near to the corrosion potential. A more uniform layer of corrosion product through which oxygen would have to diffuse to the reaction site, could be one of the probable causes for this response. The cathodic current densities of the steels A-36 and USI next to E_{corr}, were however dependent upon the applied potentials. This could indicate a mixed controlled (diffusion+charge transfer) cathodic reaction for these steels for low polarization potentials. Since these two steels had a larger number of inhomogeneities of larger sizes, than the two other steels, MS and LAS II, it is also probable that the oxide layer on the surface, not completely reduced at that range of polarized potentials, was also less uniform. Consequently as oxygen has an easier access at some areas of the surface a charge transfer process could be operative. On the other hand, at areas covered by compact oxide products, oxygen reduction is the rate controlling reaction. The lesser homogeneity of the steels A-36 and USI was clearly demonstrated when these steels were polished. The polished surface of the steels, MS and LAS II, was much brighter than the corresponding polished surface of the other two steels, A-36 and USI.

The values of cathodic current density for the various steels used varied significantly. The steel LAS II produced the lowest current densities compared to the other steels, in the whole range of polarization. It is probable that its surface is relatively not very active for the oxygen reduction reaction and the rate of cathodic reduction is low. This could be due to the more homogeneous surface of this steel when compared to the other steels used. Thus the oxygen reduction reaction is not specifically favoured in any particular region of the surface . It is

also observed from Figures 3.52 and 3.53 that the mild steel types, MS and A-36, showed very close values of cathodic current densities for potentials of approximately -850 and -900 mV vs SCE, in the sulphate and the chloride solutions respectively. The common inclusions of these two latter steels were of a sulphide type. These are cathodic relative to the matrix and electrically conductive, therefore some cathodic reaction can occur on them[8]. The highest values of cathodic current densities were produced by the steel USI. This steel is also the richest in copper. Although LAS II also contains copper (0.28%), the room temperature solubility of copper in ferrite is approximately 0.3%[183]. It is then suggested that copper in LAS II is in solid solution, whereas in the USI steel, 0.32% copper, copper could be found as precipitated particles in some areas of the surface. In fact Cu was only detected in the inclusions of the USI steel.

The oxide at the interface is the medium through which electrons are supplied for the oxygen reduction reaction[47]. Therefore the nature of the oxide is very important to the cathodic oxygen reductin reaction.

Small amounts of copper present in the iron oxide, could result in a situation where copper particles could serve as electron donator, according to:

$$Cu \quad \leftrightarrow \quad Cu^{2+} \quad + \quad 2\,e^{-} \qquad (3.5)$$

and the net effect would be the increase in the electron conductivity of the iron oxide. The electrons produced in (3.5) are available for consumption by the oxygen reduction reaction.

The Tafel slopes estimated from Figures 3.51 and 3.52, are shown in Table 3.14. These were of the order of 600 and 1100 mV/decade, for MS and LAS II, respectively. The large values of b_c for these two steels could also suggest that their cathodic reaction is under diffusion control. Lower b_c values were obtained for the two other steels.

TABLE 3.14 - Cathodic Tafel slopes estimated from Figures 3.51 and 3.52.

Steel	b_c (3.5% NaCl) (mV/decade)	b_c (0.5 M Na_2SO_4) (mV/decade)
MS	570	640
LAS II	1100	1100
A-36	350	300
USI	410	320

3.3.7 - Cathodic reduction curves.

The use of electrochemical reduction methods for the characterization of corrosion product films, has been used by Cohen[174,176], and Mayne[176] with thin oxide films, and by Okada[177] with thick rust layers formed on steel after long exposure (3 to 5 years), to industrial atmospheres. The most important corrosive constituent of industrial atmospheres, has been generally accepted to be SO_2[178]. Kesternich[179] described an apparatus combining exposure to SO_2 with continuous moistening of the surface of the specimen, and was able to prove that the same type of corrosion product formed on actual weathering was obtained in his tests. Several works after then[180-183] demonstrated that the effect of SO_2 in the presence of condensed moisture in an accelerated laboratory test, provides one of the most reliable prediction of the corrosion behaviour in an industrial atmosphere.

All the experiments presented previously in this thesis, were designed to study the electrochemical properties of steels under immersed conditions. The exposure of steels to the vapour phase of 10^{-3} M $NaHSO_3$, and subsequent cathodic reduction of corrosion products formed, however, was a laboratory accelerated test devised to predict atmospheric corrosion behaviour of bare steels in an industrial atmosphere. It was necessary to select exposure times long enough for the accumulation of corrosion products in significant quantities, so that the

various steels studied could be distinguished. Preliminary tests led to exposure times corresponding to 20 days as an acceptable time for this purpose.

The cathodic reduction curves, obtained at 1 mA/cm^2, Figures 3.53-3.56, were continued until the hydrogen evolution potential was attained, and the length of time required to reach the hydrogen evolution potential was registered as the oxide reduction time, $t_{ox.red.}$. Approximate values of $t_{ox.red.}$ were estimated from Figures 3.53-3.56 and are given in Table 3.15.

TABLE 3.15 - Oxide reduction times of corrosion products formed on steels exposed to vapour of 10^{-3} M $NaHSO_3$.

Steel	$t_{ox.red.}$ (seconds)
MS	(1) 4100 (2) 3900
LAS II	(1) 1900 (2) 2000
A-36	(1) 4700 (2) 5300 *
USI	(1) 3000 (2) 2500

* value obtained by extrapolation of the curve for times > duration of test.

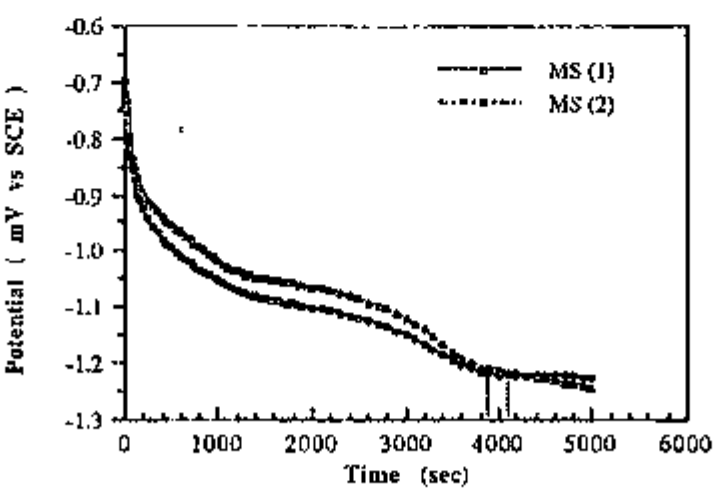

Figure 3.53 - Cathodic reduction curves of MS corroded specimens.

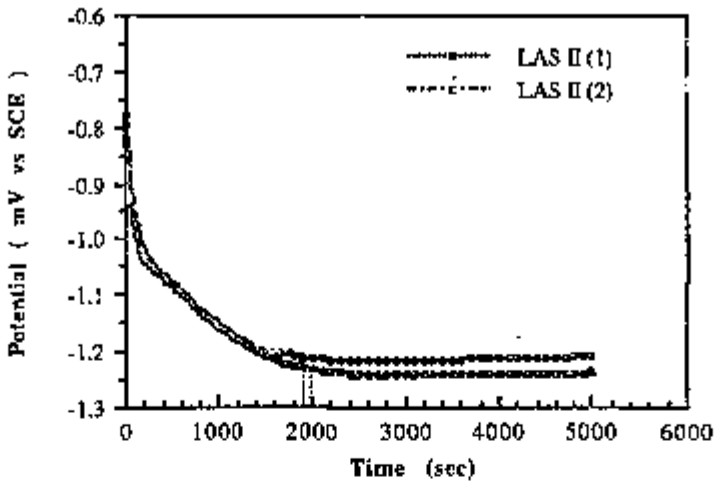

Figure 3.54 - Cathodic reduction curves of LAS II corroded specimens.

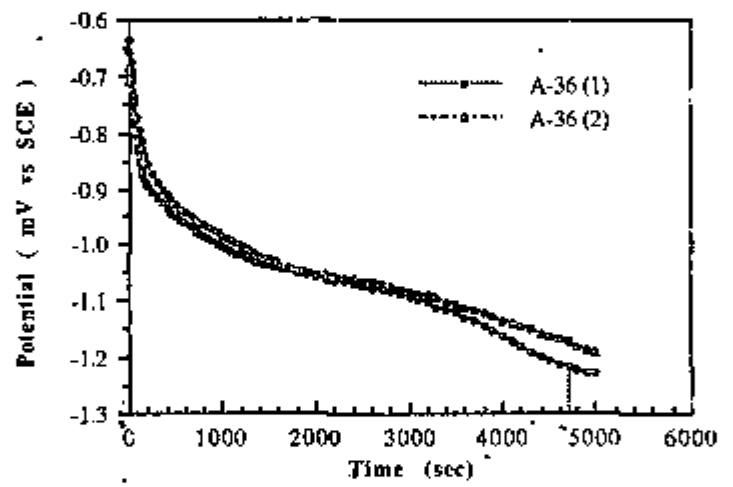

Figure 3.55 - Cathodic reduction curves of A-36 corroded specimens.

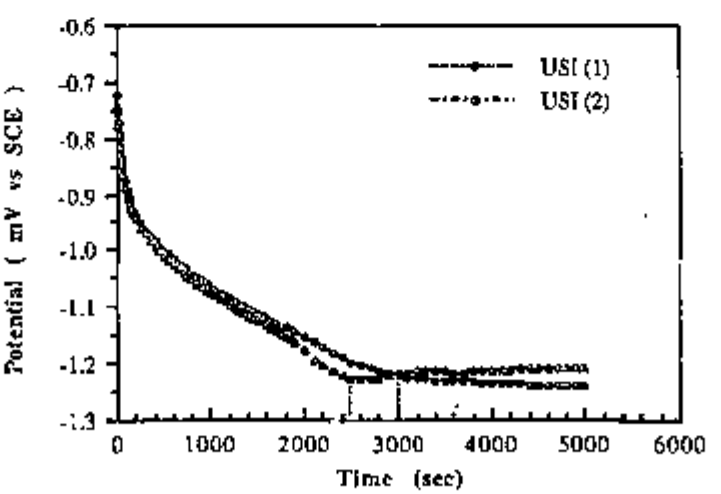

Figure 3.56- Cathodic reduction curves of USI corroded specimens.

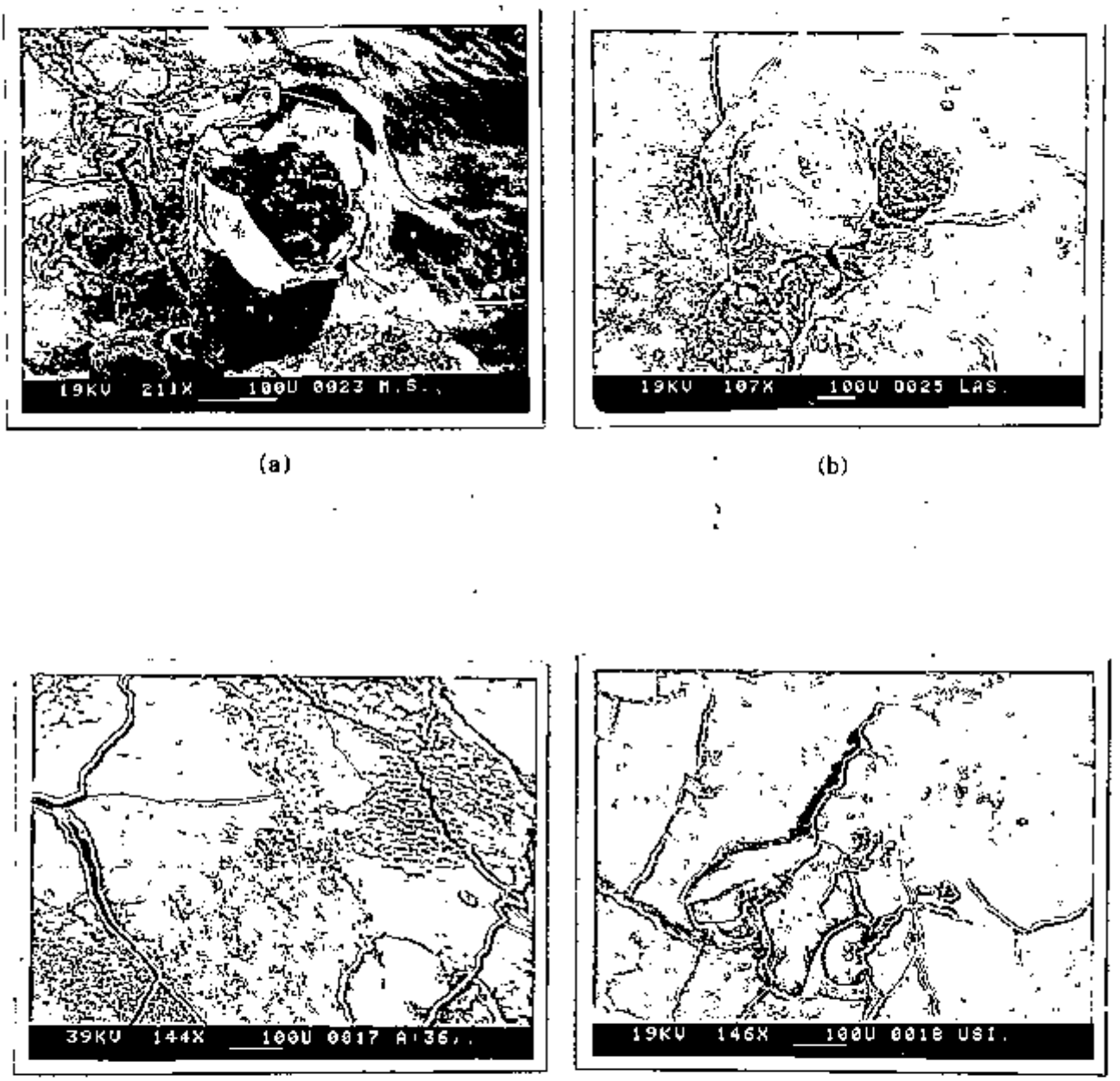

(a) (b)

(c) (d)

Figure 3.57 - Morphologies of corrosion products formed on (a) MS, (b) LAS, (c) A-36, and (d) USI steels specimens, after exposure to vapour of 10^{-3}M $NaHSO_3$ for 20 days.

3.4 - Summary

In this chapter results concerning the electrochemical behaviour of the bare steels, namely mild steel and low-alloy steel types, have been presented.

At the corrosion potential or under low polarized conditions, the steels studied were indistinguishable by type. However, some minor differences were found between steels produced by two different manufacturers. These differences were mainly detected by linear polarization resistance and electrochemical impedance techniques. The differences were probably caused by microstructure factors, both content and size of 'active' inclusions at the surface. Also, the relatively larger content of C and Mn in the steels with larger inclusions content (A-36 and USI), could also be further cause for the slightly reduced corrosion properties of these steels.

Comparable results were obtained from Tafel extrapolation measurements for all the steels. Since only small differences among the steels are noted, these differences could be attributed to experimental errors involved in the measurement. At conditions far removed from the corrosion potential, the steels were differentiated by type. The low-alloy steel types only "passivated" in sodium sulphate solutions at much higher polarization potentials, and at much larger critical current densities, i_{ccd}, than the mild steel types. Thus, the alloying elements shifted the active/passive transition towards the positive direction . The presence of inhomogeneities on the surface, nobler than the ferrite matrix, and which are not easily dissolved, are the probable reason for the high localized corrosion found for the low-alloy steels at the very high polarization potentials applied. The common inclusion types on the low-alloys steels used were mainly oxides or duplex sulphide-oxide inclusions. Sulphide inclusions were the main type of inclusion found in the mild steel types. These dissolve easier than oxide inclusion types, exposing the matrix and allowing 'passivity' to be attained. The current density at the 'passive' region, i_{pass}, was observed to increase with the Cu

content of the steel. Cu is probably enriched at the surface during dissolution of the ferrite matrix increasing the electric conductivity of the 'passive' layer, and therefore i_{pass}.

In this study, cathodic reduction of the corrosion products was also undertaken. The low-alloy steels produced less voluminous and more compact corrosion products than mild steels under exposure to the vapour phase of 10^{-3}M $NaHSO_3$. Corrosive species diffuse easier through the porous layer formed on the mild steel types, corrosion is not hindered, and consequently largest amounts of corrosion products are built up on these steels when compared to the low-alloy steels. This agrees with the work reported in the literature which states that low-alloy steels, weathering types, present better corrosion properties under atmospheric exposure than mild steels.

CHAPTER 4

THE CORROSION BEHAVIOUR OF COATED STEELS UNDER IMMERSION CONDITIONS

4.1 - Introduction

Some coating systems have been observed to perform better on low-alloy steels as compared to low carbon steels[21]. This suggests that minor changes in the composition of the steel surface could have an important effect on the protective properties of organic coatings when exposed to aggressive environments. This observation seems to be particularly true for atmospheric exposure of coated steels, since adherent and protective corrosion products which hinder further corrosion are formed on the defective areas of the coating. Nevertheless, for coated steels under immersion conditions, little is known about the effect of the small addition of alloying elements on the corrosion behaviour of the steels. Previous work carried out at UMIST[101] suggested that differences are found between two types of steels, mild steel and low-alloy steel type, when coated and fully immersed in chloride solution. Since it was not the aim of that work to study the effect of the steel composition on the corrosion properties of the coated system, a thorough study was not undertaken. On the other hand, the main purpose of the present work is to investigate the relationship, "if any", between steel composition and the corrosion behaviour of the steel when coated and immersed in sodium chloride solution.

The corrosion characteristics of four steels, two mild steel and two low-alloy steel types, were tested electrochemically in a solution containing 3.5% wt NaCl and at ambient conditions. The intent of electrochemical testing the coated

substrate was to evaluate if the substrate-coating system is affected by the nature of the substrate.

4.2 - Experimental

4.2.1 - Specimen preparation

Specimens of four of the steels studied, MS, LAS II, A-36, and USI, Table 3.1, were used in these tests. The steels were cut, and the surface was prepared by grinding with silicon carbide grit paper (up to grade 1200). The specimens were then degreased with trichloroethylene in an ultrasonic bath, hot air dried, and immediately stored in a desiccator over silica gel for at least three days before the coating was applied. The purpose of the surface preparation was to remove contaminants and aid adhesion, as well as to provide a consistent surface finish for all the substrates.

A long oil alkyd provided by Marcel Guest - Manchester was applied by flood spinning. The coated specimens were left overnight in a desiccator, before finally being cured in an oven at 40°C for four hours. The curing process occurs oxidatively. The dry thickness of the coating was measured using a digital Elcometer Minitector thickness gauge, and was found to be in the range of 20 to 30 μm. Table 4.1 presents the thicknesses of the coatings for each electrode used. The resulting coating was transparent making the observation of corrosion, blistering or delamination processes easier.

An electrical connecting wire was attached to the specimen, and the wire was encapsulated in a plastic tube fixed to the specimen with epoxy resin. The edges were blanked off using a colophony resin/beeswax mixture in the proportion 3:1. An area of 10 cm^2 was exposed to the test environment.

The alkyd coated specimens were subsequently fully immersed in aerated 3.5% wt sodium chloride solution and, in most cases, allowed to remain until the complete breakdown of the paint. During the immersion period the corrosion behaviour of the tested specimens was monitored by measuring the

electrochemical corrosion potential and the electrochemical impedance characteristics of the coated systems. Concurrently, visual observations of the steels surfaces were also made.

4.2.2 - Experimental procedure

The open circuit corrosion potential of the specimens was measured by means of a high input impedance voltmeter (approximately $10^{12}\,\Omega$), 'Keithley electrometer Model 610C'. It was measured for a time duration of approximately 15 minutes prior to each electrochemical impedance measurement. The use of a high input impedance voltmeter was necessary in order to avoid polarization of the specimen, so that the current passing between the working and reference electrode is insignificant (10^{-10}- 10^{-15}A)[185].

The electrochemical impedance measurements were performed using a 'Solartron 1250 Frequency Response Analyser', in the frequency range of 65 kHz to 20 mHz, with 7 readings per decade, and a 'Thompson Ministat' Potentiostat used as an electrochemical interface.

The measurements were carried out under potentiostatic control at the open circuit potential as a function of the exposure time. The amplitude of the exciting voltage applied varied according to the resistance of the coating film. For coatings with resistances > $1x10^7\Omega.cm^2$, the amplitude applied was 50 mV, and for lower resistance coatings the amplitude used corresponded to 20 mV. Burstein[145] stated that for relatively high resistance coatings, a comparatively high amplitude of the perturbing voltage can be applied to measure the impedance of coatings without causing significant changes to the system.

The experimental cell consisted mainly of a working electrode; a saturated calomel reference electrode, and a large graphite auxiliary electrode (surface area of approximately 158 cm^2). The graphite auxiliary electrode was built with a large area in order to avoid polarization of the specimen under analysis. For coatings showing a very high impedance (>$1x10^7\Omega.cm^2$), a two electrode

configuration consisting of the specimen working electrode and a graphite auxiliary electrode (surface area ~ 158 cm^2) was employed. In this configuration the potentiostat was used as a ZRA (zero resistance ammeter). The reproducibility of the data was established by using 5 specimens of each substrate.

TABLE 4.1 - Coating thicknesses of specimens tested in immersion in 3.5% wt NaCl.

	Coating thickness (μm)			
Specimen	MS	LAS II	A-36	USI
1	(26.5 ± 0.7)	(26.0 ± 0.2)	(24.2 ± 0.4)	(23.6 ± 0.3)
2	(23.0 ± 0.4)	(28.6 ± 0.4)	(24.6 ± 0.3)	(26.5 ± 0.2)
3	(25.7 ± 0.3)	(26.7 ± 0.4)	(23.6 ± 0.5)	(26.5 ± 0.3)
4	(23.7 ± 0.4)	(30.5 ± 0.2)	(24.4 ± 0.3)	(25.9 ± 0.4)
5	(24.6 ± 0.2)	(28.1 ± 0.5)	(24.2 ± 0.4)	(26.3 ± 0.4)

4.2.3 - Coating

The coating used in this research was a commercial long oil alkyd resin, supplied by Marcel Guest - Manchester. The main purpose for using this coating was to provide a barrier between the substrate and the test environment.

4.2.3.1 - Alkyd resins

Alkyd resins are polymeric esters prepared by the reaction of polyhydric alcohols with the mixtures of a polybasic acid and a fatty acid. The name 'alkyd' comes from combining 'al' of alcohol with the 'cid' of acid. Many of the alkyds used today employ phthalic anhydride as the main polybasic acid constituent, polyalcohols such as glycerin and pentaerythritol, and oxidizing or non-oxidizing fatty acids derived from vegetable and animal sources. Variation of the alcohol,

4.2.3.2 - Chemistry of alkyd resins

The reaction basic to all polyester resins, including alkyds, is a condensation reaction of carboxyl groups with hydroxyl groups, resulting in the formation of water and ester. This reaction follows the elementary equation for esterification[189]:

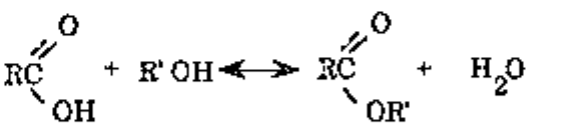

(4.2)

Since the reaction above is reversible, its completion requires removal of the water. The first product of the reaction is a monomer. Resin formation depends on the reactive sites (hydroxyls and carboxyls) of the monomers, which react with each other to form the very large molecules (polymers), which are called resins. The esters that serve as the building blocks for alkyd resins are much more complex than indicated by the equation above. The acids, typified by phthalic anhydride, contain two carboxylic acid groups. This gives them a reactive capacity or a potential functionality of two. Glycerin, the alcohol most used, contains three hydroxyl groups and, accordingly, has a functionality of three. The modifying fatty acids contain only one carboxyl group and thus a functionality of one. Multiplying the functionality of a monomer by the number of moles used gives the total functionality of that material. The total functionality of the acid components divided by the total functionality of the alcohol components is called the functionality ratio.

One of the important parameters of a polymer is the kind of chemical linkages in its structure. This feature is important because the various types of linkages differ in strength, resistance to breakdown by exposure to weathering,

water and chemicals. Alkyd resins are bound together by ester linkages, which are relatively weak.

Another basic parameter of a polymer is its molecular weight. It is generally accepted that high molecular weight favours most performance properties but reduces solubility and raises the viscosity of solutions. Fractions of low molecular weight are softer. Alkyds are low in molecular weight relative to the families of polymers. Most alkyds probably have average weights of 1,000 to 7,000, with long alkyds at the low end and short alkyds at the high end [187].

4.2.3.3 - Classification of Alkyds

The most common way of classifying alkyds is according to the oil length, which means the percentage of oil in the alkyd, based on the total non volatile components. They are designated as short, medium, long and very long oil alkyds. Alkyds that contain only the types of ingredients so far discussed are known as "pure" alkyds. In these alkyds oil length influences all properties and is the main factor that determines solubility, viscosity, flexibility and hardness. Long oil alkyds contain over 60% oil, medium oil between 40 and 60%, and short oil below 40%. Long oil alkyds are generally made with drying oils and are soluble in aliphatic solvents. They are low viscosity resins that air-dry slowly to give soft flexible films with poorer gloss retention and durability. Shorter oil length generally results in the need for aromatic solvent, giving higher viscosity resins at lower solids. Medium and short oil alkyds give hard films with good gloss retention and chemical resistance; they are less flexible than long oil alkyds and are normally dried by stoving[188].

4.2.3.4 - Use in protective coatings

Alkyd coatings have been successfully used on structural steels, tanks, bridges and the like. The protective properties include excellent resistance to

sunlight, wind, rain and mild acidic industrial environments. They also present excellent toughness, flexibility, and colour retention, but are not recommended for exposure to oxidizing agents and organic acids. They are in great demand because of their low cost, ease of application, and their excellent storage ability and versatility[189]. However, they cannot be used in alkaline environments, because the oil content is readily attacked by alkalis.

As a group, alkyds are excellent for resistance to normal atmospheric corrosive attack, have fair resistance to mild fumes of inorganic acids, and fair to good resistance to splash, spillage and fog from salt solution.

4.3 - Results and Discussion

Impedance tests were performed over extended time periods of around 500 days. In order to check if the impedance data reflected the corrosion behaviour of coated steels, the extent of corrosion was assessed visually. The corrosion potential, E_{corr}, was also monitored during these prolonged tests and the results of the various substrates are presented next. All the corrosion potentials were measured in relation to a saturated calomel reference electrode (SCE), and thus reference to this is going to be omitted in the next paragraphs.

4.3.1 - Substrate A-36

The corrosion potential, E_{corr}, and the interface features of the various immersed specimens were monitored during the long term tests, and are shown in Figures 4.2, 4.7, 4.10, 4.14 and 4.17 for the various coated A-36 substrates. Schematic impedance diagrams of these specimens at progressive times are also shown in these Figures. The reason for drawing schematic impedance diagrams together with the corrosion potential vs time curves, was to try to establish a correlation between the corrosion potential of the specimens and their impedance responses.

4.3.1.1 - Specimen A-36(1)

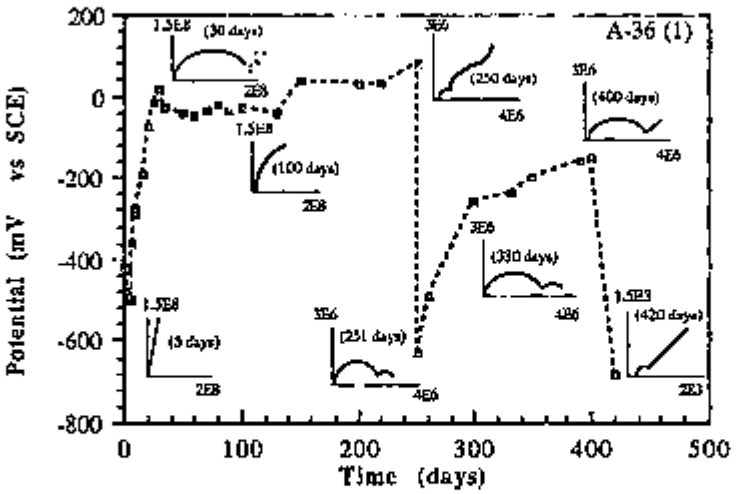

Figure 4.2 - Corrosion potential vs time and schematic Nyquist plots for specimen A-36 (1).

It can be observed from above Figure that E_{corr} was initially around -400 mV which then dropped to approximately -500 mV after five days immersion. In the following days the corrosion potential rose to nobler values (approximately +20 mV) , and then remained relatively stable until 250 days of immersion. The potential then exhibited a sharp fall to values of around -630 mV (251 days). This particular specimen was removed from solution and stored in a desiccator over silica gel for ten days, being re-immersed again afterwards. A shift to nobler potentials was observed upon re-immersion of the specimen, and also the coating resistance was found to have increased. This was caused by the drying out of the specimen. It is possible that after the drying out of this specimen re-adhesion occurred, as it is general the case when water causes loss of coating adhesion[19]. This is common in some systems, particularly for alkyd paints on steel. Between 300 and 400 days the corrosion potential did not change much, but after 420 days immersion a final drop to values of approximately -670 mV was observed. In addition, the coating resistance only decreased again after 420 days immersion. The specimen was then removed from solution since it was considered that the paint system had finally broken down.

From the electrochemical impedance measurements it was seen that between 20 and 30 days a high frequency semi-circle was obtained in the Nyquist diagram. The diameter of the high frequency semi-circle was estimated to be in the region of 200 $M\Omega.cm^2$, indicating a highly protective character of the coating. For times longer than 30 days the high frequency arc bent towards the imaginary axis, indicating an increase in the protective characteristics of the coating. This might have been due to the formation of deposits by the anodic process, which subsequently blocked the corroding spot hindering the access of corrosive species to the underlying metal.

The highly protective characteristics of this coating were maintained until 220 days of immersion. For most of that time an almost capacitive behaviour was obtained. The arc which was almost parallel to the Z" axis subsequently bent towards the real axis, after 250 days exposure. The coating resistance after this period of immersion was small enough to allow corrosion processes underneath the coating to be detected. Three time constants were easily separated at 250 days immersion, immediately before the drop in E_{corr} has occurred. A day later only two were obtained, Figure 4.3. The estimated value of R_{pf} immediately after re-immersion, was slightly larger than the coating resistance corresponding to the time of removal. Also the corrosion potential was noticed to have shifted to nobler values. After 330 days immersion, Figure 4.4(a), a flattened semi-circle was obtained, whose intercept with the real axis decreased with time until 400 days, Figure 4.4(b). Depressed semi-circles are possibly the consequence of many corroding areas on the substrate, resulting in the interaction of various time constants. At 420 days immersion the coating resistance, R_{pf}, had dropped to very small values (approximately 96 $\Omega.cm^2$), and a diffusion tail was seen in the intermediate and low frequency range, Figure 4.4(c). The test was then terminated since the coating did not protect the substrate any longer.

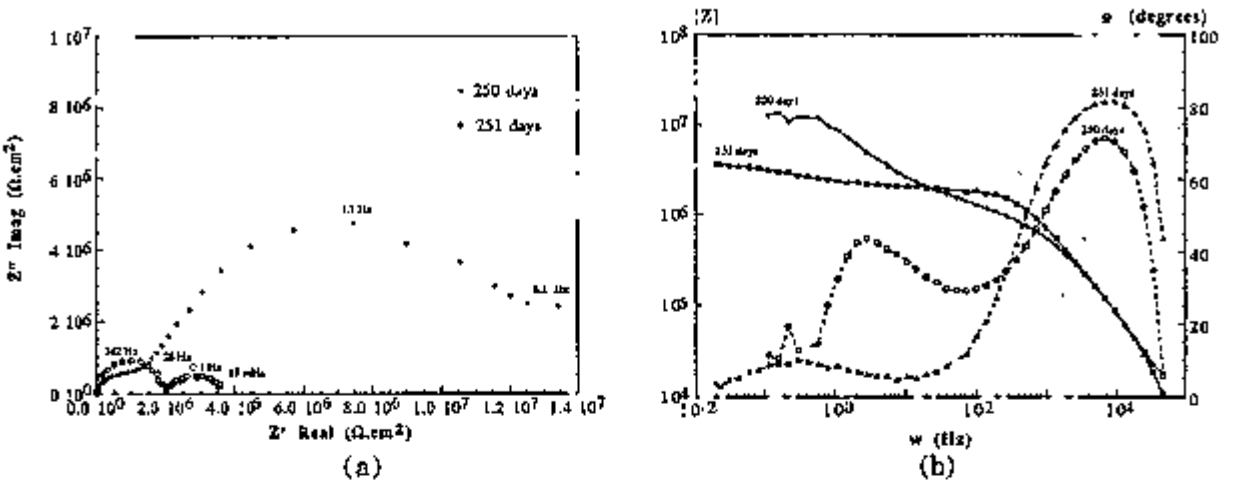

Figure 4.3 - Impedance response (a) Nyquist and (b) Bode plots for specimen A-36(1) after 250 and 251 days immersion.

The visual observation of the corrosion characteristics of the interface showed that since the first days of immersion small black and brown corrosion spots occurred and these are probably associated with the microstructure features of the specimen. The distribution of corrosion products seem to correspond to inclusions which have been elongated along the rolling direction during the fabrication process. It is worthwhile mentioning that the inclusions and their distribution along the rolling direction were easily observed on this type of steel, A-36, prior to immersion in the test solution.

A disbonded area surrounding one of the small black spots was found from the first days of immersion. The corrosion spot and disbonded area both grew with immersion time and another two black spots were noticed after 30 days testing, Figure 4.5(a). At that time, a large volume of liquid had accumulated at some areas of the interface, and new corrosion spots were starting, which became black 20 days later, Figure 4.5(b). The coating resistance was, however, too high to allow the detection of the corrosion processes at the surface. No new corrosion features appeared until 250 days, when yellowish and brownish areas were observed on the surface.

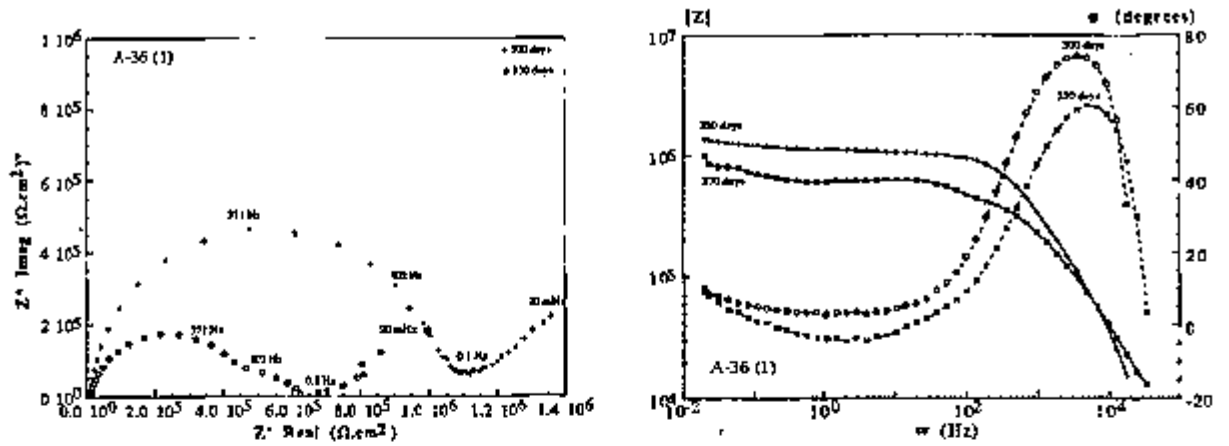

(a)

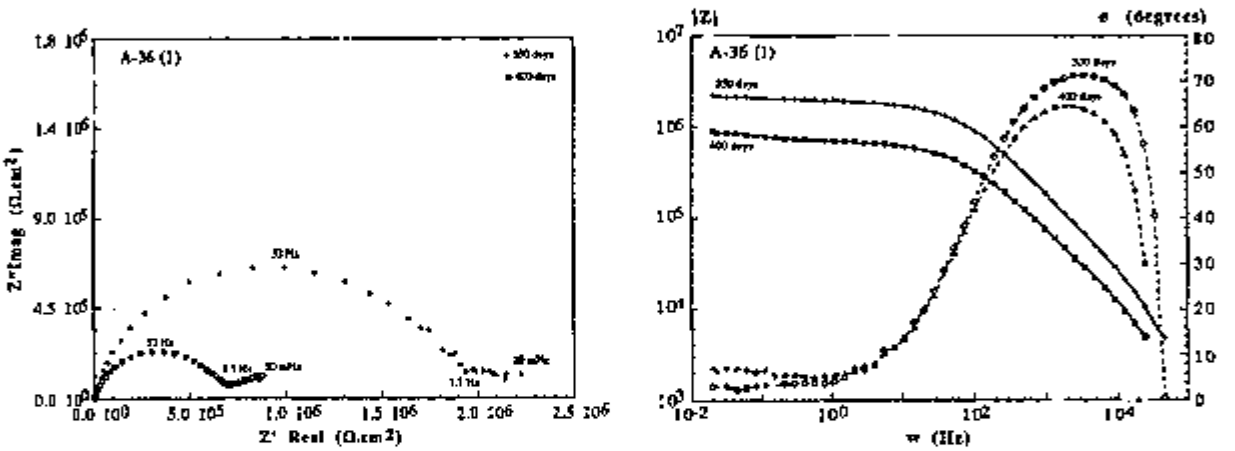

(b)

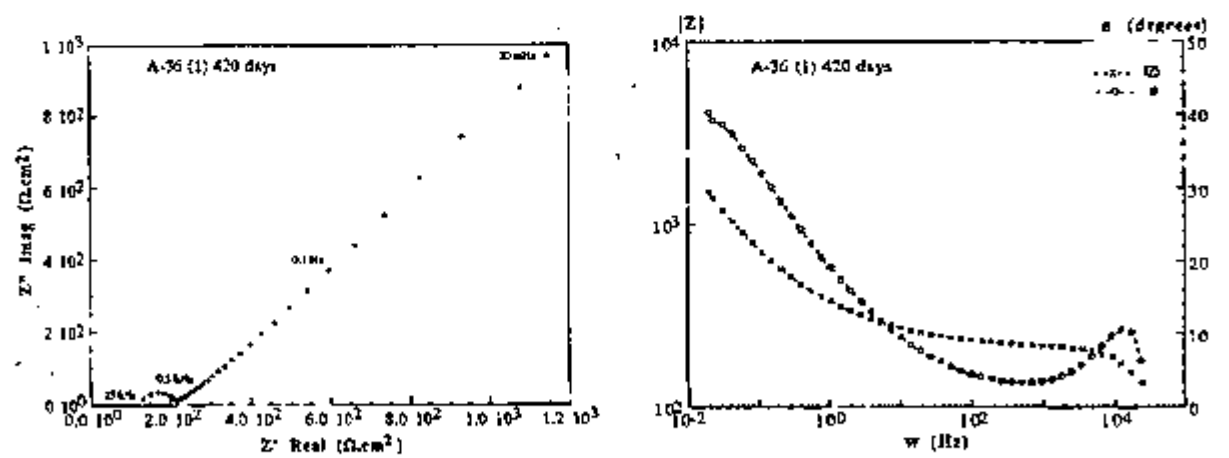

(c)

Figure 4.4 - Nyquist and Bode plots of specimen A-36(1) after (a) 300 and 330 days, (b) 350 and 400 days, and (c) 420 days exposure to 3.5% wt NaCl.

A change in the capacitance of the coating to higher values was also noted, Figure 4.6. The increase in capacitance was possibly caused by accumulation of electrolyte at the interface and in the coating. One day later when the potential had dropped to very negative values, this specimen was removed from solution. It was then allowed to dry out and as a result coating properties seemed to have been enhanced. The drying out of the specimen proved to have an effect on the coating anti-corrosion resistance, delaying the failure time which only occurred after 420 days immersion. A final and sharp increase in capacitance, to values corresponding to charge transfer processes, confirmed the failure of the coating.

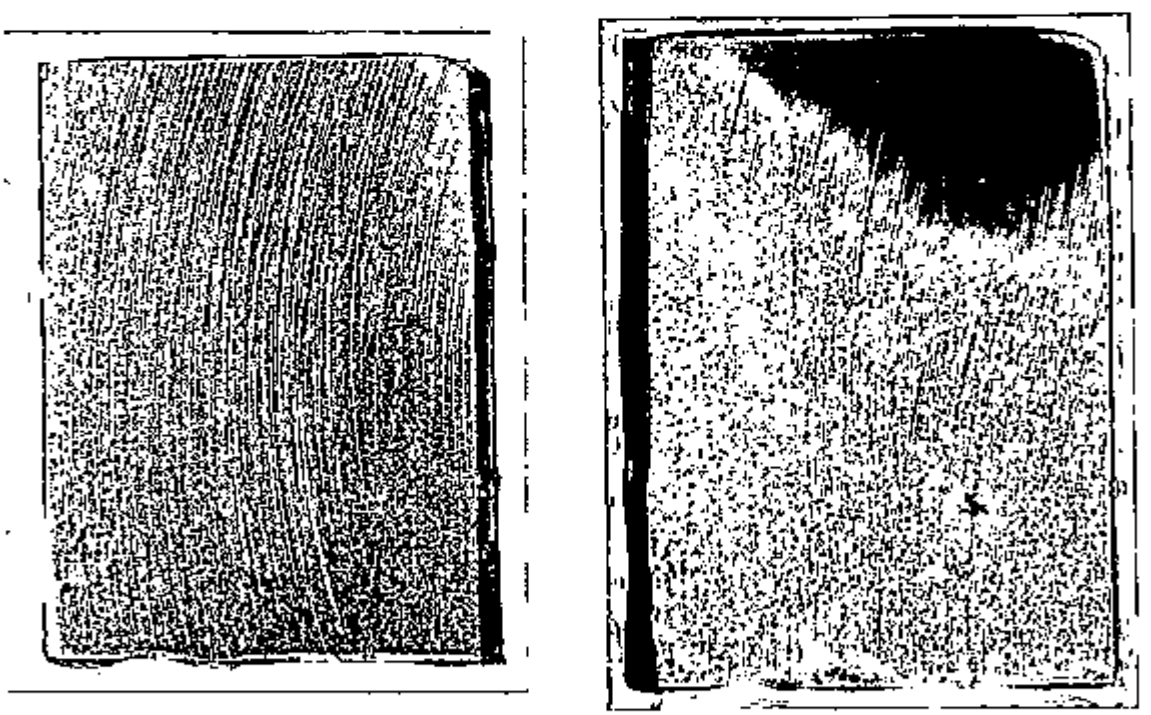

(a) (b)

Figure 4.5 - Specimen A-36(1) after (a) 30 days, and (b) 50 days immersion

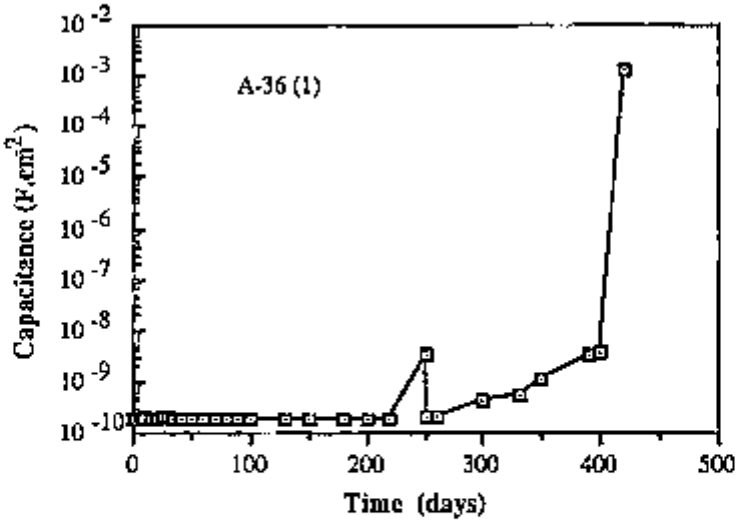

Figure 4.6 - Evolution of the coating capacitance with time for specimen A-36(1)

4.3.1.2 - Specimen A-36(2)

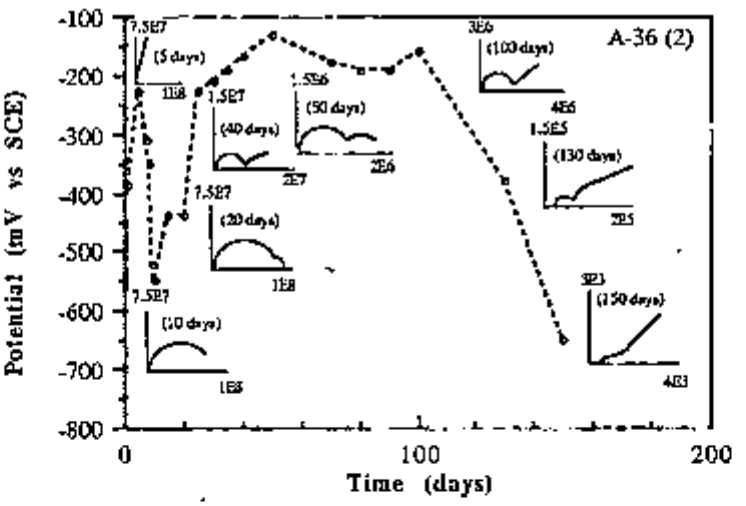

Figure 4.7 - Corrosion potential vs time and schematic Nyquist plots for specimen A-36(2).

For specimen A-36(2), the corrosion potential initially moved in the positive direction, reaching values of around -230 mV after 5 days immersion. The movement of potential into the positive direction could have been caused by the arrival of water at the interface at low contents and aiding passivation[115]. In the following days, the corrosion potential dropped to values of around -550 mV (10

days exposure). At that time, small corrosion spots were already visible on the surface. Water might have been allowed to accumulate on certain areas of the interface dissolving the oxide and allowing corrosion to start. Next, the potential shifted to more positive values, but this time it was possibly due to an increase in the ratio of cathodic to anodic area. Between 25 and 100 days immersion the corrosion potential was relatively stable. Slight oscillations occurred in the range of -130 to -230 mV. A final drop started at 100 days as the majority of the surface became active, and 50 days later the test was terminated since the coating had lost its protective characteristics.

The visual observation of this specimen showed that since the initial days of immersion a black spot and several brownish spots were present. These were also associated with microstructure characteristics of the surface. Therefore, the decrease in corrosion potential after approximately 7 days might have been caused by the initiation of corrosion at the substrate interface. The black spot increased in size in the following days, and also large volumes of liquid were allowed to accumulate on a specific area of the interface. These corrosion features were easily noted after 30 days immersion, and on that same area yellow, brown and black corrosion products were found after 50 days immersion, Figure 4.8 (a) and (b). The disbonded area corresponded then to a large proportion of the exposed surface. The fluctuations in corrosion potential observed after 5 days were possibly caused by changes in the ratio of anodic to cathodic areas.

The impedance response of this specimen during the earlier immersion days, (nearly 5 days), produced an arc almost parallel to the Z" axis, due to the highly protective characteristics of the coating. Later this arc was found to bend towards the real axis, and at 20 days immersion a high frequency semi-circle was delineated. This indicates that some deterioration of the coating was taking place. At longer immersion times until 50 days of exposure, the main trend was for the diameter of the high frequency semi-circle to decrease. Between 25 and 50

days immersion, a low frequency response became evident probably characteristic of the corrosion process. This was could be a consequence of the presence of rust spots on the specimen surface and their growth. A slight increase in the coating resistance was noticed between 50 and 100 days, and also the charge transfer controlled corrosion reaction possibly changed to a diffusion controlled one, Figure 4.9(a). Afterwards, a sharp drop in the value of the coating resistance was detected, and at 150 days immersion complete failure of coating had occurred, Figure 4.9(b) and (c).

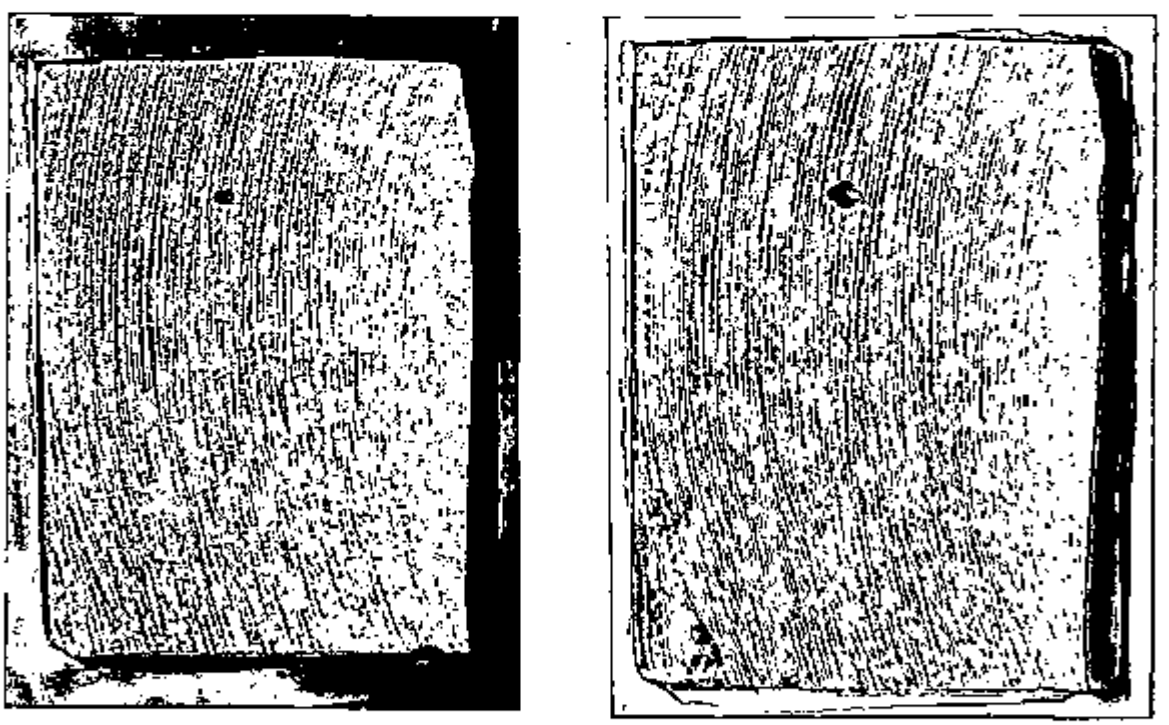

(a) (b)

Figure 4.8 - Specimen A-36(2) after (a) 30 days, and (b) 50 days exposure

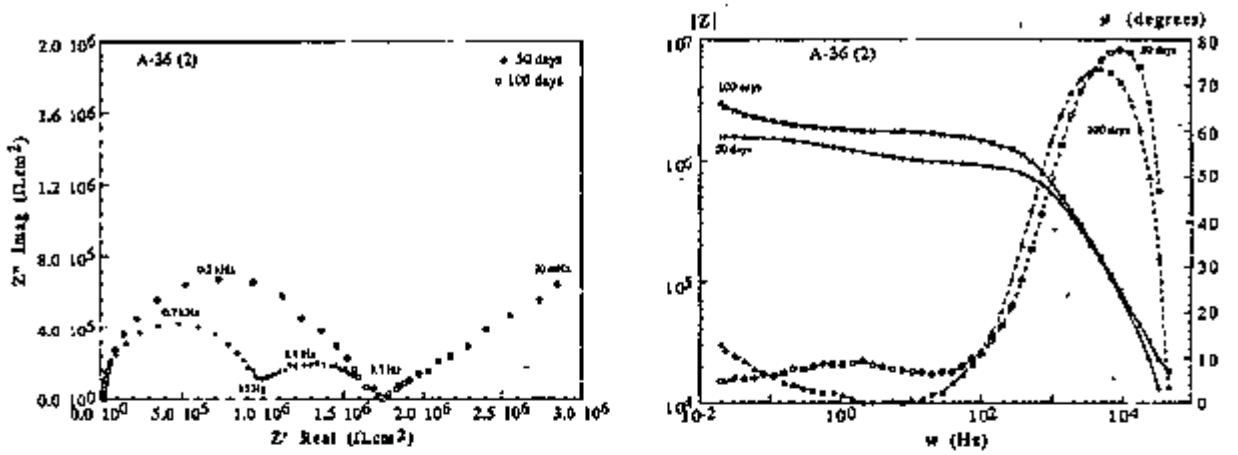

(a)

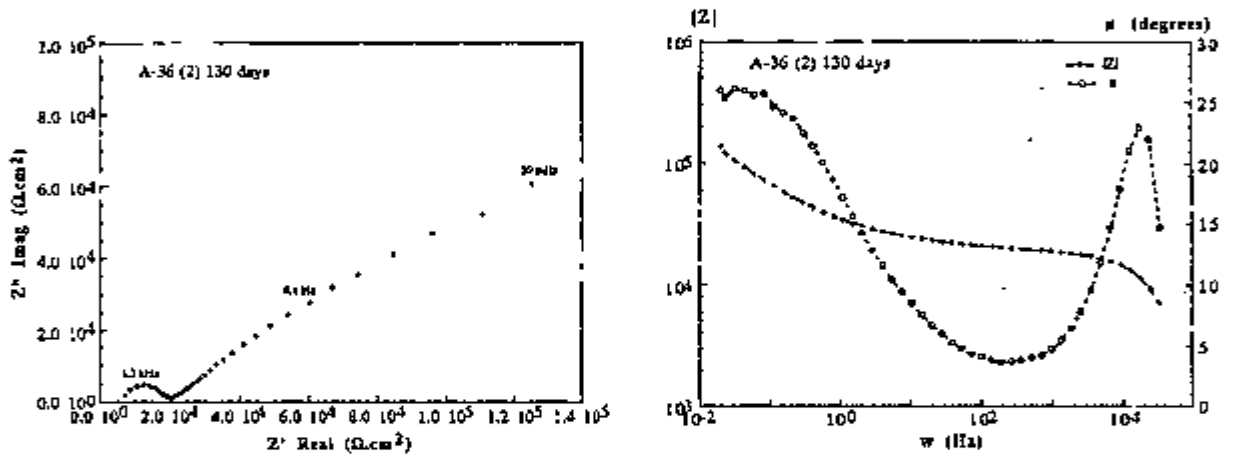

(b)

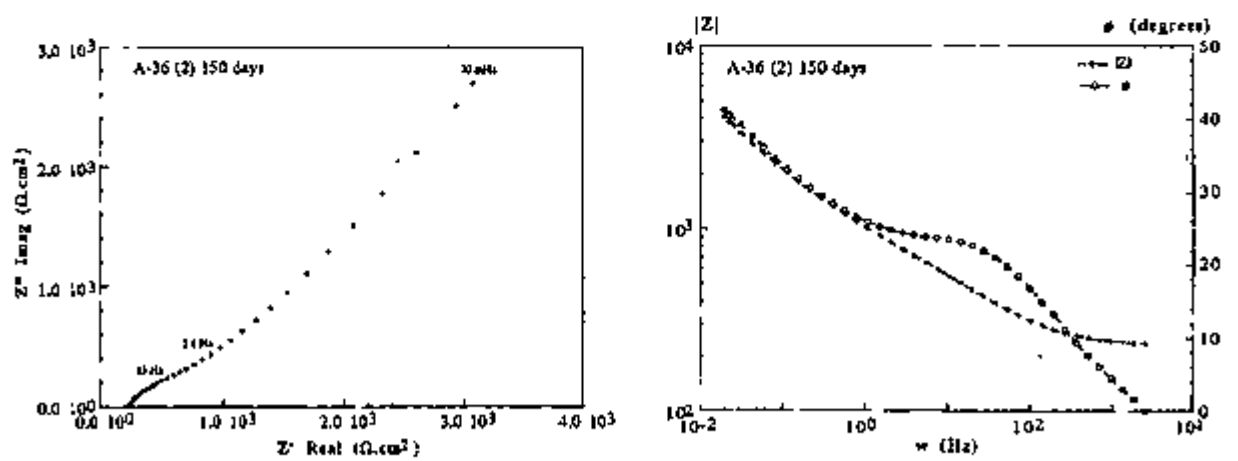

(c)

Figure 4.9 - Impedance response, Nyquist and Bode plots, of specimen A-36(2) after (a) 50 and 100 days, (b) 130 days, and (c) 150 days exposure to 3.5% wt NaCl.

4.3.1.3 - Specimen A-36(3)

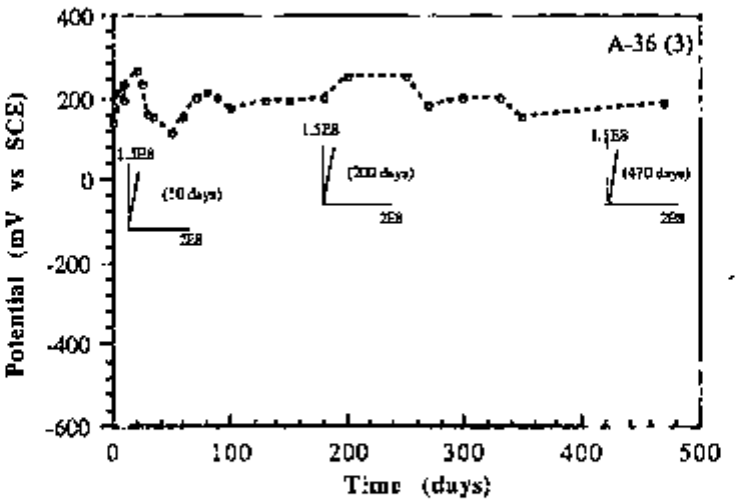

Figure 4.10 - Corrosion potential vs time and schematic Nyquist plots of specimen A-36(3).

For specimen A-36(3), the corrosion potential adopted positive values (approximately +150 mV) at the beginning of the immersion period. This then shifted to even nobler potentials attaining values of around +230 mV at 10 days immersion. The movement of E_{corr} into the positive direction might also have been the consequence of a passivation process supported by water which arrives at the interface in small quantities[115]. The highly protective characteristic of the coating was demonstrated by an impedance response typical of capacitive behaviour (ascending arc running almost parallel to the imaginary axis) which indicates that the coating film was not largely defective. This also means that there was no significant ionic transport through the coating. Very little degradation of the coating properties, as shown by the impedance measurements, was observed for this specimen even after 500 days exposure, Figure 4.11. The almost capacitive behaviour was produced by this specimen most of the immersion time The coating on this specimen could be considered as an almost "perfect coating", and as such the substrate does not have a significant effect on the behaviour of the coated system[17]. Unfortunately, perfect coatings do not normally exist in practice.

From the initial days of immersion and until the end of test, 500 days later, the surface of this specimen showed the same corrosion characteristics, which corresponded to very small brown spots uniformly distributed all over the surface and associated with microstructure features. It must be mentioned that some of the characteristics of the microstructure of this specimen was visible to the naked eye before immersion. This indicates that although corrosion was allowed to start on some spots of the surface, the highly protective character of the coating on this specimen did not allow corrosion to develop significantly. It may also suggest that once the initial corrosion spots were covered by corrosion products, the corrosion process was stifled. During the duration of test, disbonded or blistered areas were not found on the surface. The features above are illustrated in Figure 4.12. The protective character of this coating was also demonstrated by the stable values of coating capacitance obtained during the whole exposure, Figure 4.13. After the test was finished, (500 days immersion), the coating could not be easily removed from the substrate, and even its dissolution by solvents such as xylene and acetone was found to be difficult. High cross-linking of this particular coating might have been the cause of its difficult dissolution. The fact that this coating maintained its highly protective character for the whole exposure period can be explained by the probable difficulty for water to accumulate at the interface and form a continuous layer, which would cause corrosion to spread. The lack of non-bonded areas, or the presence of non-bonded areas of insufficient dimension might also have prevented the formation of a continuous aqueous phase. Since corrosion started at some small areas, corrosive species had to arrive at the interface, but once these were consumed in the corrosion reaction, their replenishment was possibly not quick enough to allow the continuation of corrosion. In addition, once the initial corroding areas were covered by corrosion products, water and oxygen access to the metal base was difficult thus stopping the corrosion process.The likely areas of corrosion initiation were at the boundary regions between inhomogeneities at the interface,

e.g. inclusions, and the metallic matrix. However, this was restricted to these small areas, due to the protective characteristics of the coating.

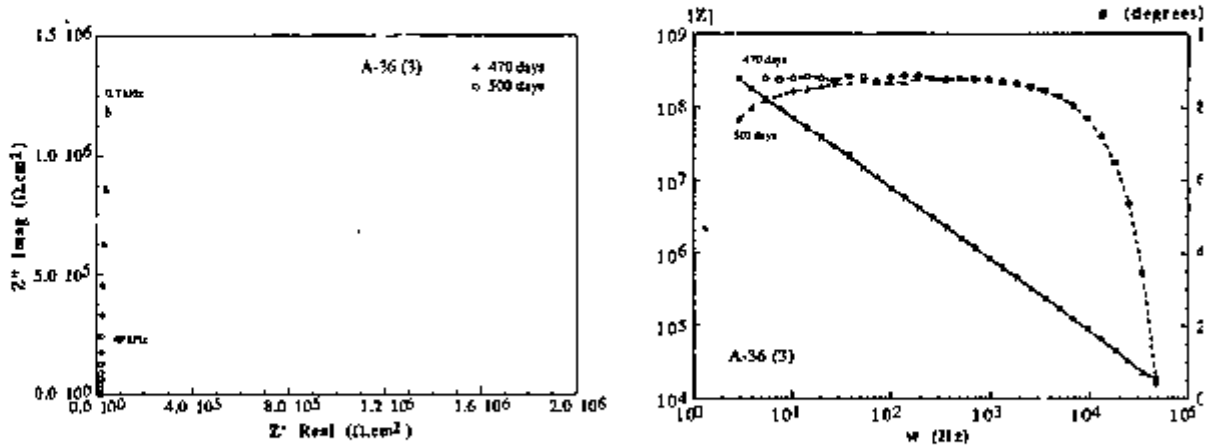

Figure 4.11 - Nyquist and Bode plots of specimen A-36(3) after 470 and 500 days immersion.

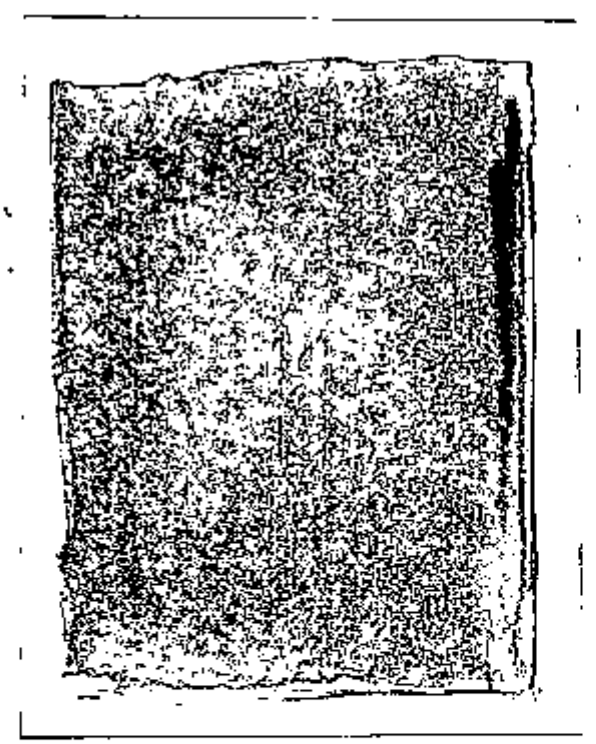

Figure 4.12 - Specimen A-36(3) after 50 days immersion.

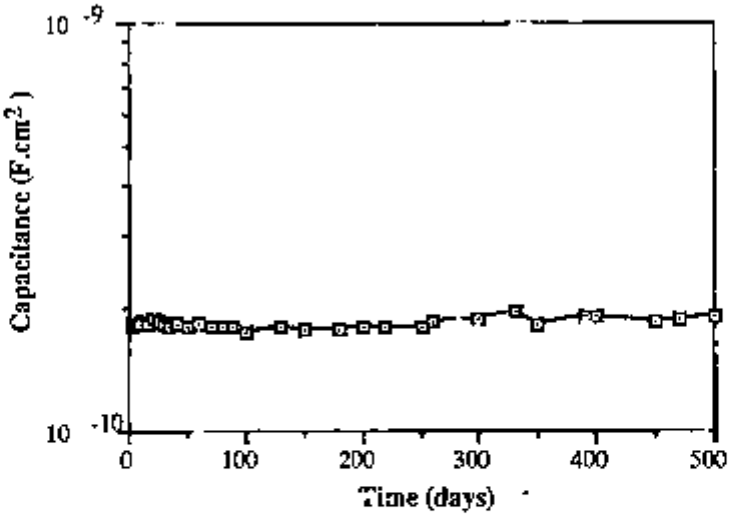

Figure 4.13 - Evolution of coating capacitance of specimen A-36(3) with immersion time.

4.3.1.4 - Specimen A-36(4)

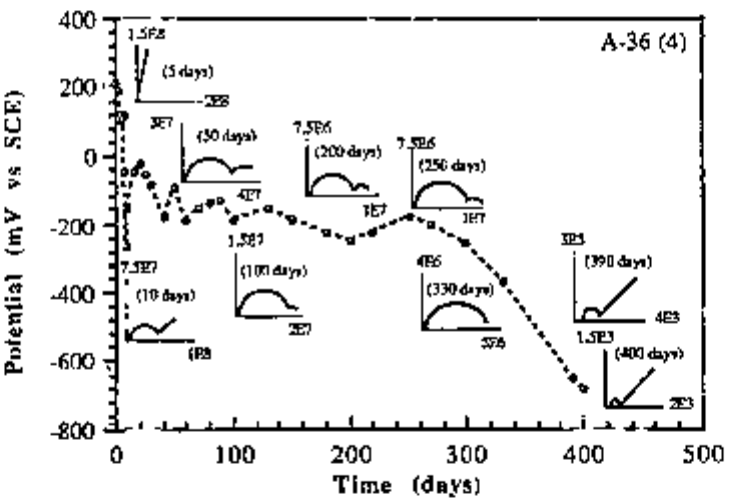

Figure 4.14 - Corrosion potential vs time and schematic Nyquist plots of specimen A-36(4).

For specimen A-36(4), the corrosion potential initially assumed positive values (approximately +210 mV), but shifted to more active potentials in the following days. A value of E_{corr} around -270 mV was obtained after 10 days immersion. This drop was accompanied by a change in the impedance response from an almost capacitive one (5 days), to one where a high frequency semi-circle could be defined (10 days). Thus, degradation of the coating was occurring since the first days of exposure. In the following days the potential increased and at 20

days immersion it was approximately -20 mV. On the Nyquist plot a tail was seen at the low frequency region, for immersion times between 10 and 40 days test, revealing the possible existence of a diffusion controlled corrosion process. The diffusion tail vanished after 40 days immersion, and was only identified again at the end of the immersion period. The visual observation of this specimen revealed the presence of a disbonded area after 10 days exposure. Therefore, the increase in E_{corr} for times longer than 8 days exposure could have been caused by an increase in the ratio of cathodic to anodic areas. From 20 to 100 days the corrosion potential fluctuated between -20 and -200 mV. After 100 days immersion, a steady and slow decrease in corrosion potential and coating resistance was noticed, Figure 4.15(a). A final and relatively sharp drop in E_{corr} and R_{pf} started at 250 days, Figure 4.15(b), and the protective characteristics of this coating failed at approximately 400 days test, Figure 4.15(c).

Characteristics of the microstructure of this specimen also seemed to have been associated with the brown corrosion spots formed during the first days of exposure. On a particular area of the surface, voluminous brown and black corrosion spots which rose from the surface were already noted from the initial immersion period. After 10 days immersion, two new black spots and an area where liquid had accumulated lifting the coating, were observed. The disbonded area enlarged in the following days, and also the two black spots continued to grow. The latter were very voluminous after 250 days. Figure 4.16 (a) and (b) illustrates the corrosion features described above after 30 and 50 days immersion, respectively. After 250 days immersion and until the end of test, 400 days, corrosion took a generalized form over the surface. Generalized corrosion started initially at the areas where liquid was observed to accumulate. The corrosion products on those areas had different colour which included blue, yellow, orange, brown and black, over increasing areas of the surface.

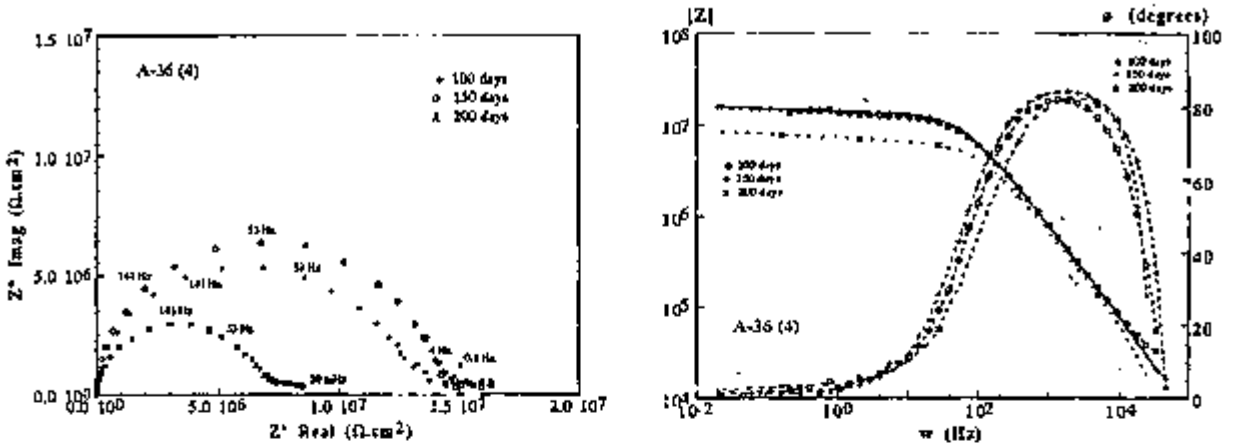

(a)

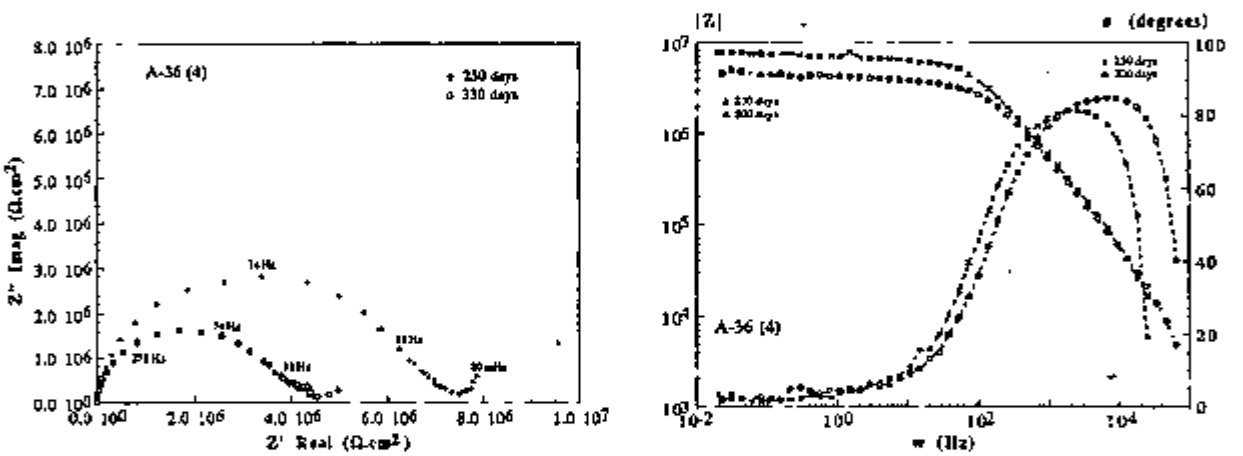

(b)

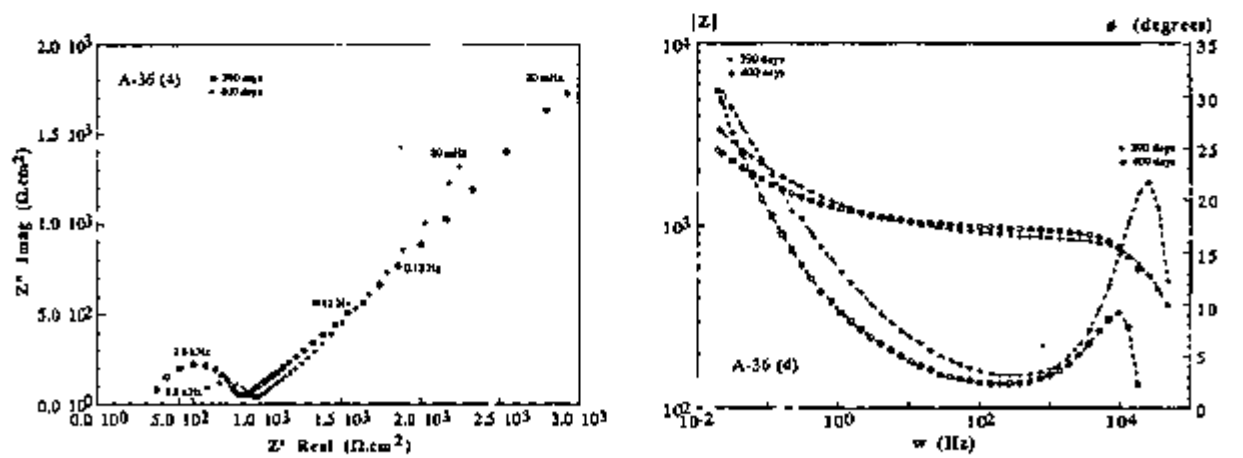

(c)

Figure 4.15 - Impedance response of specimen A-36(4) after (a) 100, 150 and 200 days, (b) 250 and 300 days, and (c) 390 and 400 days immersion.

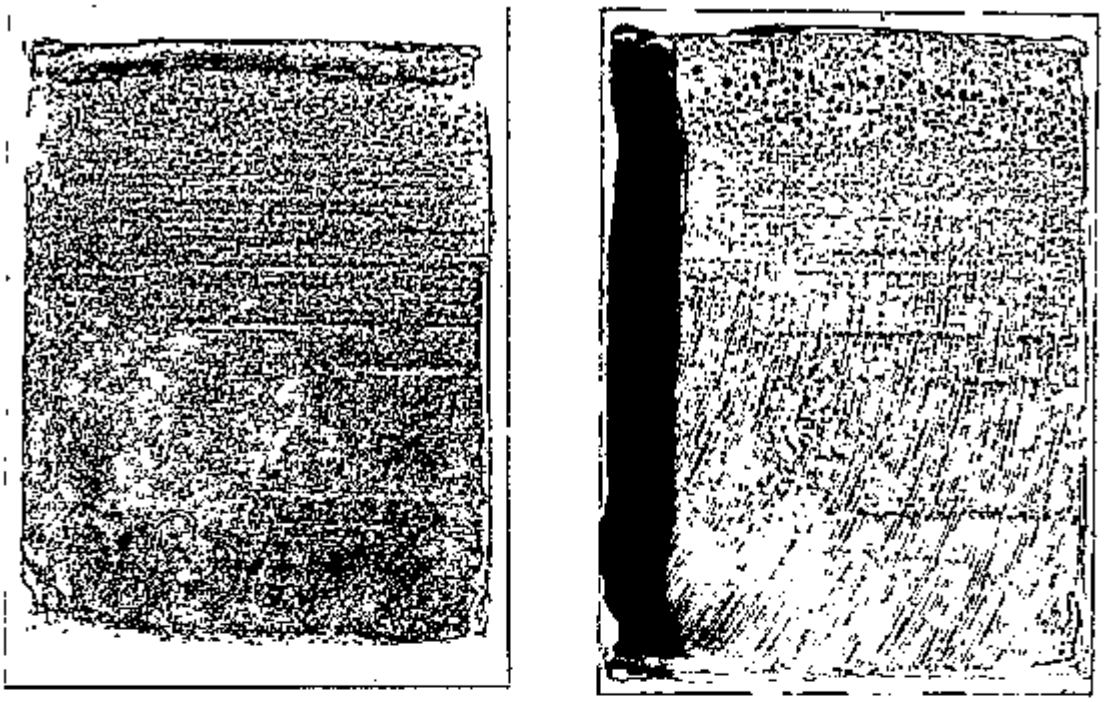

(a) (b)

Figure 4.16 - Specimen A-36(4) after (a) 30 and (b) 50 days immersion.

4.3.1.5 - Specimen A-36(5)

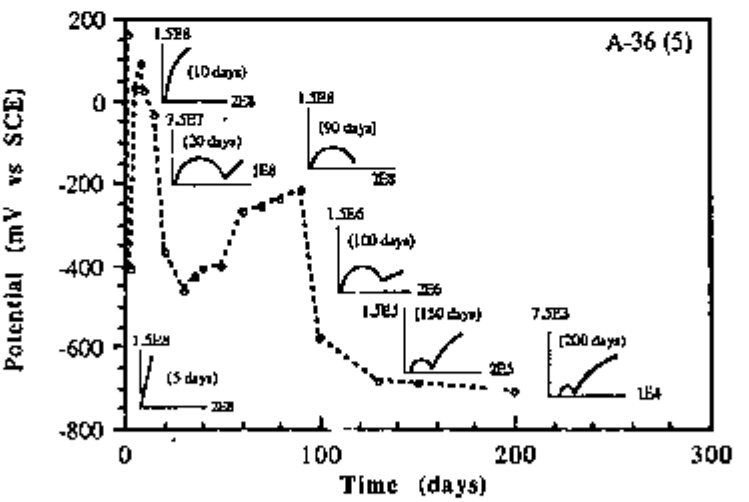

Figure 4.17 - Corrosion potential vs time and schematic Nyquist plots of specimen A-36(5).

The corrosion potential of this specimen showed significant changes in the first 30 days of immersion. Its value initially shifted from noble potentials, approximately +160 mV to more active values, around -410 mV after 3 days immersion. An increase to more positive values was then observed, and after 8 days immersion values of about +100 mV were obtained. In the following days

the corrosion potential dropped again, and E_{corr} reached values close to -450 mV after 30 days exposure. The movement of potential might have been caused by relative changes in the ratio of anodic to cathodic areas. The impedance response produced only the initial part of a semi-circle in the first days of immersion (5 days), which then started bending towards the real axis soon afterwards, (10 days). For immersion times corresponding to 20 days or longer, the high frequency semi-circle was delineated, suggesting some degradation of the insulating characteristics of the coating was occurring at that time. The corrosion potential then moved progressively to nobler values, from nearly -450 mV (30 days) to approximately -220 mV (90 days). At the end of that period a final drop in E_{corr} and R_{pf} was noted. Until 90 days immersion, the coating resistance was very high, tenths of $M\Omega.cm^2$, and thus the effects of corrosion processes underneath the coating could not be detected by impedance measurements. An exception occurred at 20 days immersion, when the coating resistance had dropped to values around 7 $M\Omega.cm^2$. At that time, mass transfer seemed to be controlling the corrosion process underneath the coating. After the diffusion tail vanished, the diameter of the high frequency semi-circle increased. This often occurs when pores or defects in the coating are blocked by corrosion products. If any corrosion process was still active underneath the coating, the high coating resistance did not permit its detection, and the high frequency semi-circle would account for both, coating resistance, R_{pf}, and polarization resistance of the corrosion reaction[163]. The charge transfer resistance cannot be seen because of the large difference between the time constants, τ, corresponding to the coating and to the corrosion process. This is a limitation of the impedance technique which has been mentioned earlier[164]. After 90 days immersion R_{pf} decreased rapidly, and values of approximately $50k\Omega.cm^2$ (150 days immersion), and $2k\Omega.cm^2$ (200 days immersion), were obtained, Figure 4.18. From 100 days until the end of the test (200 days), the low frequency data, indicated a diffusion controlled corrosion reaction at the substrate interface.

The corrosion features of this specimen during the first 5 days of immersion were similar to the ones observed for the specimens mentioned previously. The characteristics of the microstructure also seemed to be related to the small and brown corrosion products. Also two close brown and voluminous corrosion spots were noted on the surface at that time. Liquid was allowed to accumulate on a small area of the surface which was visible through the transparent coating and was causing blistering. The brown corrosion products gradually changed colour to black, increased in size, and also the disbonded area became larger, Figure 4.19 (a) and (b). After 60 days immersion the disbonded area occupied approximately one third of the total area of this specimen.

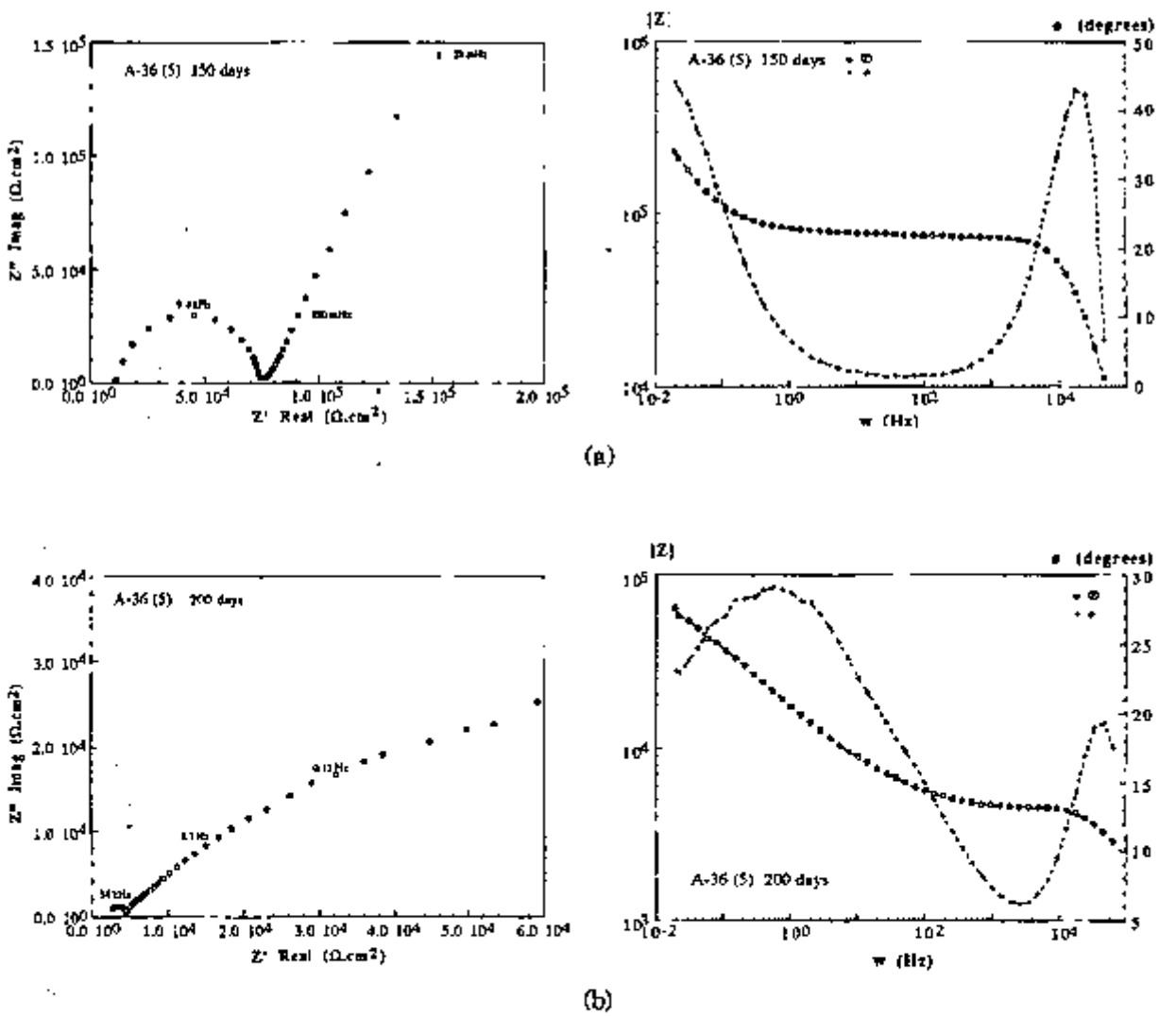

Figure 4.18 - Impedance response of specimen A-36 (5) after (a)150 and (b)200 days immersion.

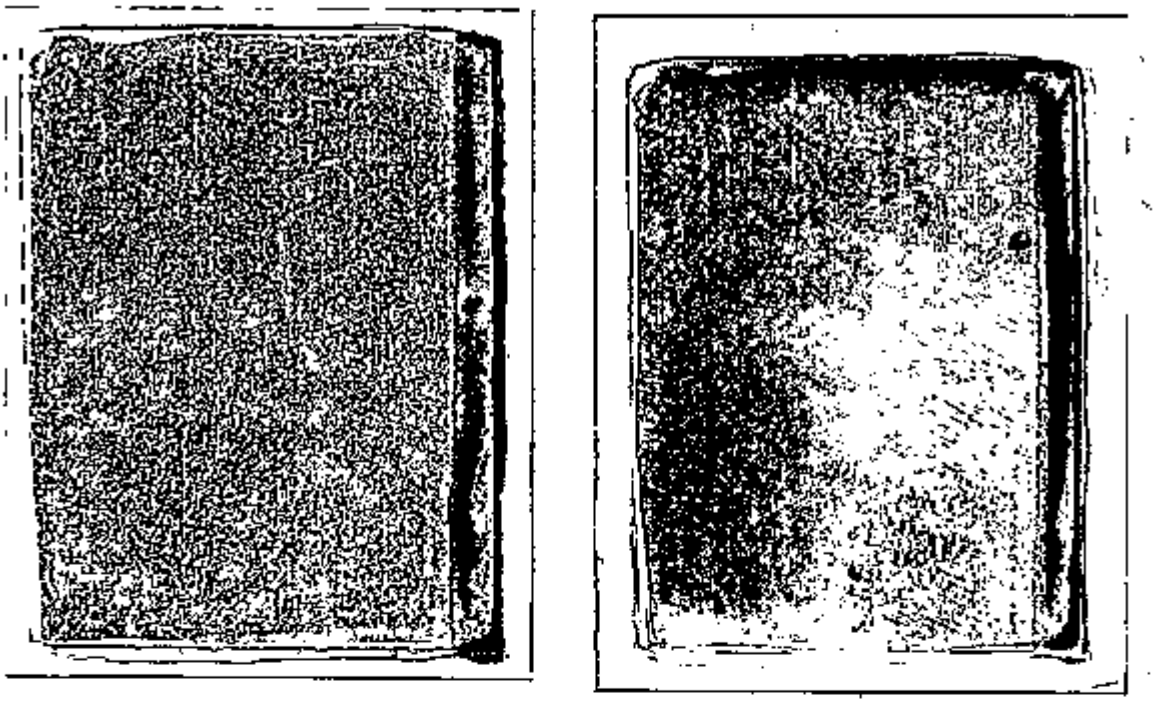

(a) (b)

Figure 4.19 - Specimen A-36 (5) after (a) 20, and (b)-50 days immersion.

4.3.2 - Substrate USI

The change of E_{corr} with time for the various coated USI steel samples used and schematic Nyquist plots are shown in Figures 4.20, 4.25, 4.29, 4.31 and 4.36.

4.3.2.1 - Specimen USI (1)

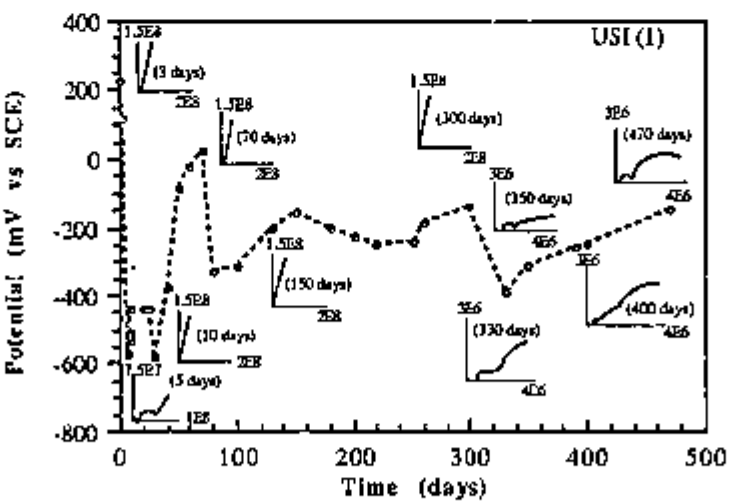

Figure 4.20 - Corrosion potential vs time and schematic Nyquist plots of specimen USI (1).

It can be seen from the previous Figure that E_{corr} decreased significantly in the first 6 days of the test, from around +230mV to nearly -570 mV. In the

following days and until 30 days immersion, it fluctuated between the latter value and approximately -440mV, when a new increase in corrosion potential occurred. The corrosion potential then reached values of approximately +20 mV (70 days), dropping again to -330mV (80 days). Values of E_{corr} around -160 mV were obtained at 150 days immersion. From that time and until 300 days of immersion it showed slight oscillations. Despite all the fluctuations in potential, the impedance response of this specimen until 300 days showed only an ascending arc almost parallel to the imaginary axis. At 5 days immersion, however, a high frequency semi-circle and a diffusion tail were distinguished in the Nyquist plot. The large drop in potential associated with the definition of the high frequency semicircle and a low frequency diffusion tail, is explained by the initiation of corrosion at the substrate. In the following days the almost capacitive response was again obtained probably as a result of the blockage of the defective corroding areas by corrosion products, hindering the access of corrosive species to the metal substrate. The corrosion potential drop after 300 days was associated with the appearance of a flattened high frequency semi-circle and an unresolved low frequency semi-circle, which bent towards the real axis (330 days), Figure 4.21(a). The flattened semicircle is usually associated with the interaction of various time constants. Actually two time constants corresponding to the high frequency range, were easily separated in the Bode plot after 390 days immersion, Figure 4.21(b) and a third time constant was easily seen for longer times of the test Figure 4.22(a-c). The high frequency semicircle still showed slight depression at that time. The coating resistance, R_{pf}, at 420 days was approximately 54 $k\Omega.cm^2$, and the faradaic processes seemed to be associated with either, a diffusion controlled (finite diffusion layer) or a mixed controlled reaction. The low frequency curve increasingly bent towards the real axis from 330 to 420 days, Figure 4.23. The coating resistance, R_{pf}, was relatively stable after 400 days immersion. When the test was interrupted, after 500 days exposure, it was nearly 50 $k\Omega.cm^2$.

The surface of this specimen was also visually examined with immersion time. A black corrosion spot and a small disbonded area around it were observed during the first days of immersion, explaining the initial drop in E_{corr} and R_{pf}. The disbonded area enlarged a little in the succeeding days, and after 20 days immersion large volumes of liquid had accumulated on some areas underneath the coating. Characteristics of the microstructure of this specimen seemed also to be associated with very small and brown corrosion spots since the early days of exposure. From 20 to 300 days, no significant changes occurred, and also new corrosion features did not appear on the surface. The enormous magnitude of the coating resistance during that period is the probable reason for this. Figure 4.24 (a) and (b) shows the features mentioned above after 30 and 50 days immersion, respectively.

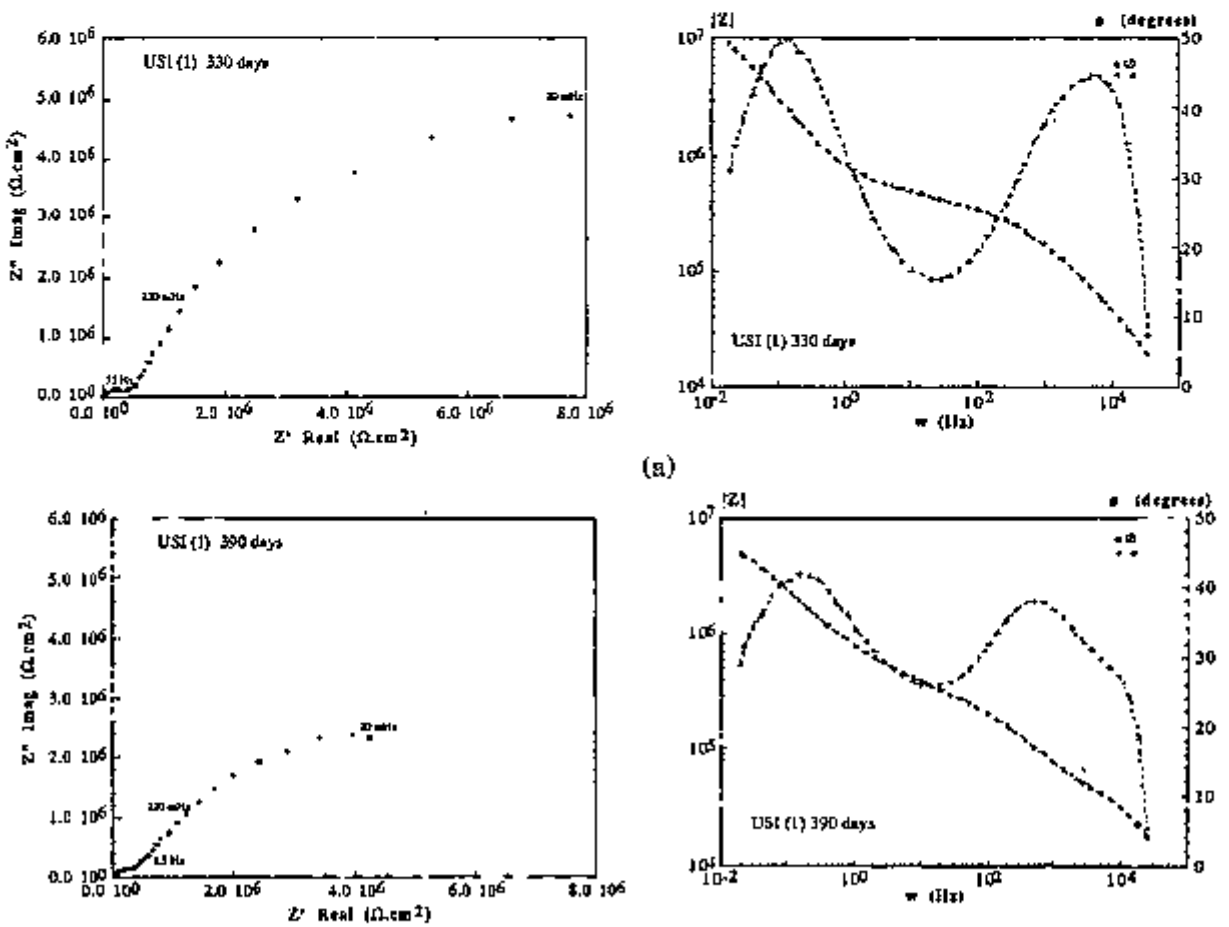

Figure 4.21 - Impedance response of specimen USI (1) after (a) 330 days and (b) 390 days immersion.

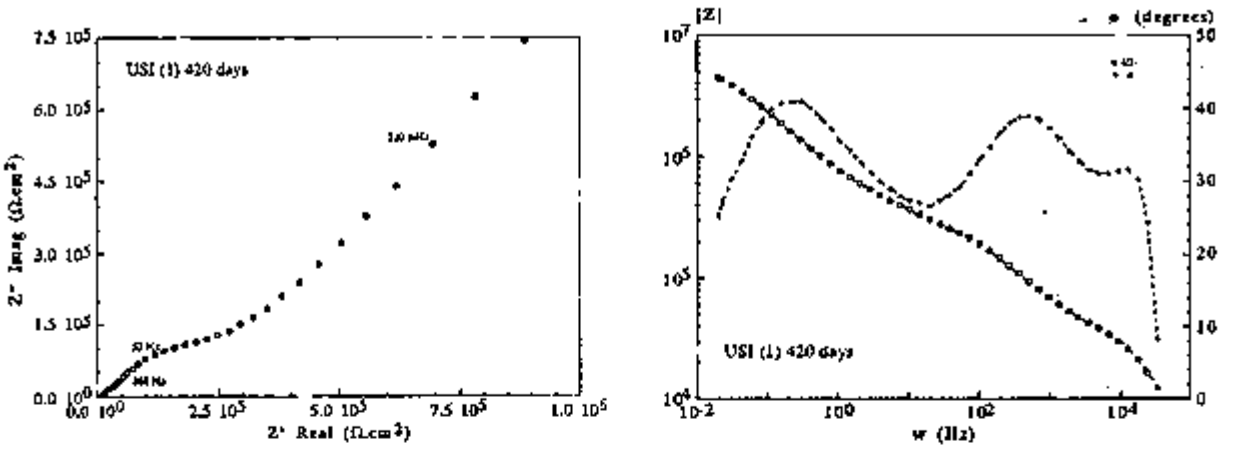

(a)

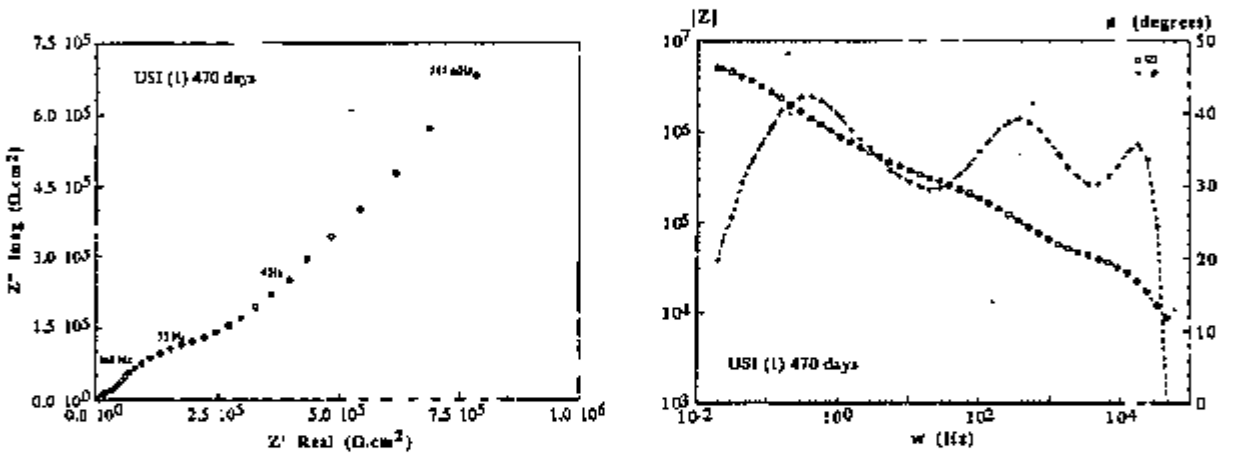

(b)

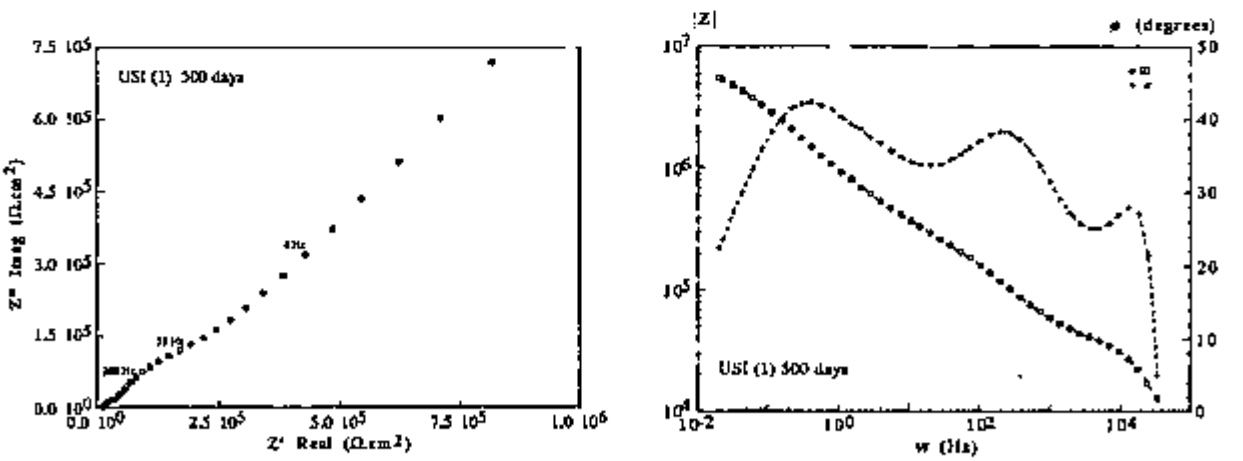

(c)

Figure 4.22 - Nyquist and Bode plots of specimen USI (1) after (a) 420 days, (b) 470 days, and (c) 500 days immersion.

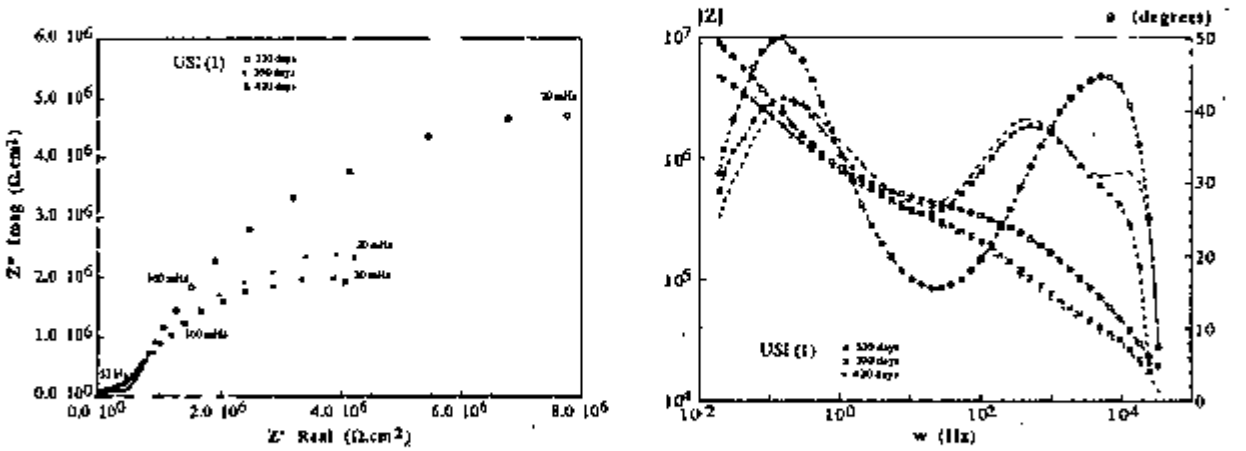

Figure 4.23 - Superimposed plots of specimen USI (1) after 330, 390, and 420 days.

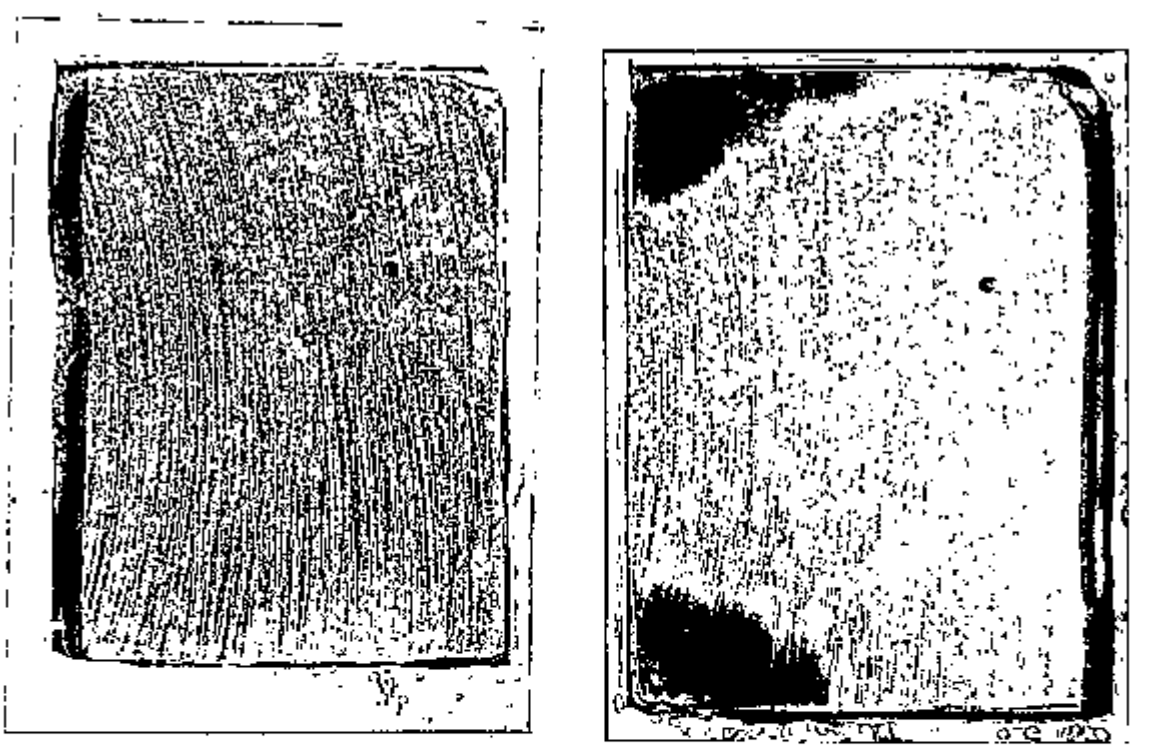

(a) (b)

Figure 4.24 - Specimen USI (1) after (a) 30 and (b) 50 days immersion.

4.3.2.2 - Specimen USI (2)

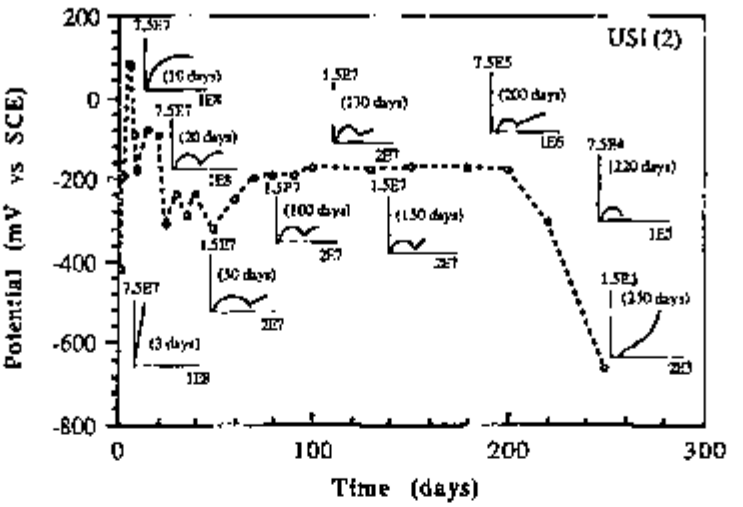

Figure 4.25 - Corrosion potential vs time and schematic Nyquist plots of specimen USI (2).

For this specimen the initial potential of approximately -400 mV was found to increase to more positive values reaching a maximum corresponding to values of around +100 mV after 5 days immersion. This was probably the result of a passivation process aided by water at small concentrations arriving at the interface[115]. In the following days and up to approximately 50 days the E_{corr} showed some fluctuations as a probable consequence of changes in the ratio anodic to cathodic areas. At 50 days immersion a movement of E_{corr} into more positive values occurred, and this was stabilised at values of approximately -200 mV until 200 days of testing when a final drop to very active values took place, and corrosion potential values close to -650 mV were obtained at 250 days of immersion.

From the above Figure it is observed that the Nyquist plot is an arc which is almost parallel to the Z'' axis in the beginning of the immersion period. In the following days it started bending towards the Z' axis. A high frequency semicircle was well defined after 20 days immersion, and the subsequent relatively fast decrease of its diameter suggested that degradation of the coating was occurring. This is indicated in Figure 4.26. The formation of new corrosion spots, increase in size of the ones which had already developed, and the fast

increase of the blistered area support the impedance response obtained. Figure 4.27 (a) and (b) show the corrosion features of this specimen, after 30 and 50 days respectively. At 50 days immersion most of the surface was blistered. Even though corrosion was evident since the initial days of exposure, the coating resistance was still very large at 130 days of the test, (approximately 10MΩ.cm^2). A sudden drop in R_{pf} values occurred after that, Figure 4.28(a) and (b), and after 250 days immersion the coating had failed completely, Figure 4.28(c).

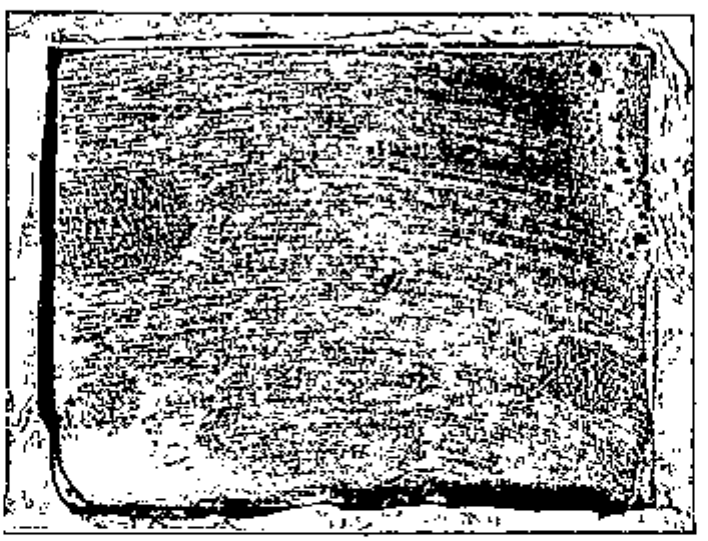

Figure 4.26 - Specimen USI (2) after 20 days immersion.

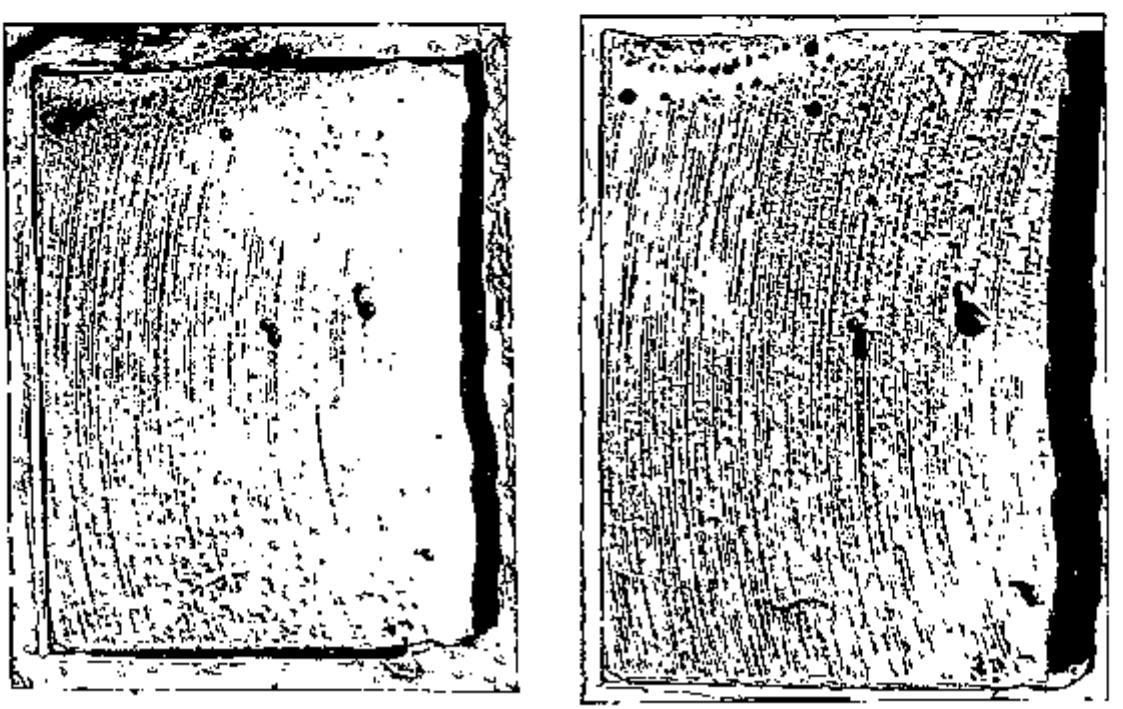

(a) (b)

Figure 4.27 - Specimen USI (2) after (a) 30, and (b) 50 days immersion.

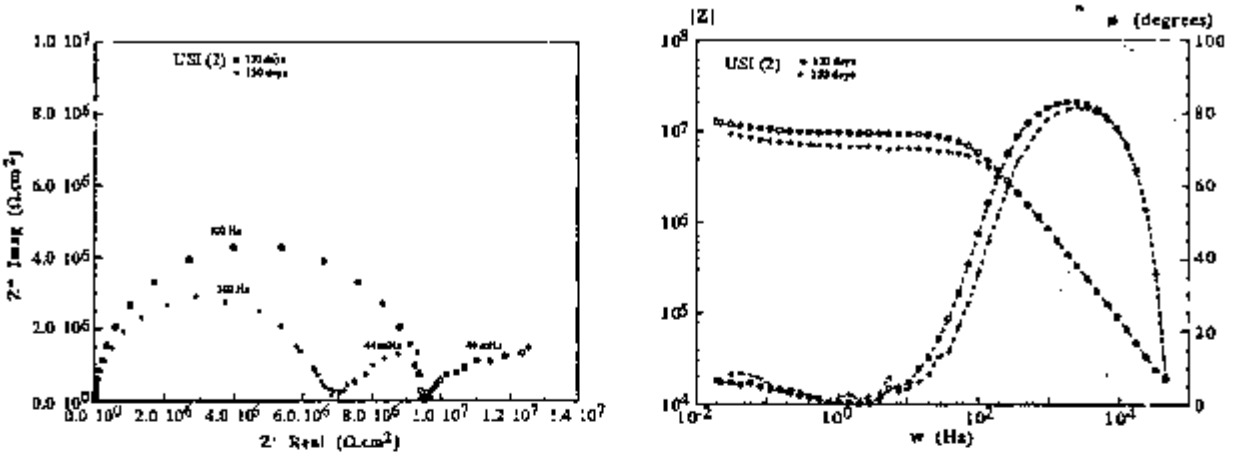

(a)

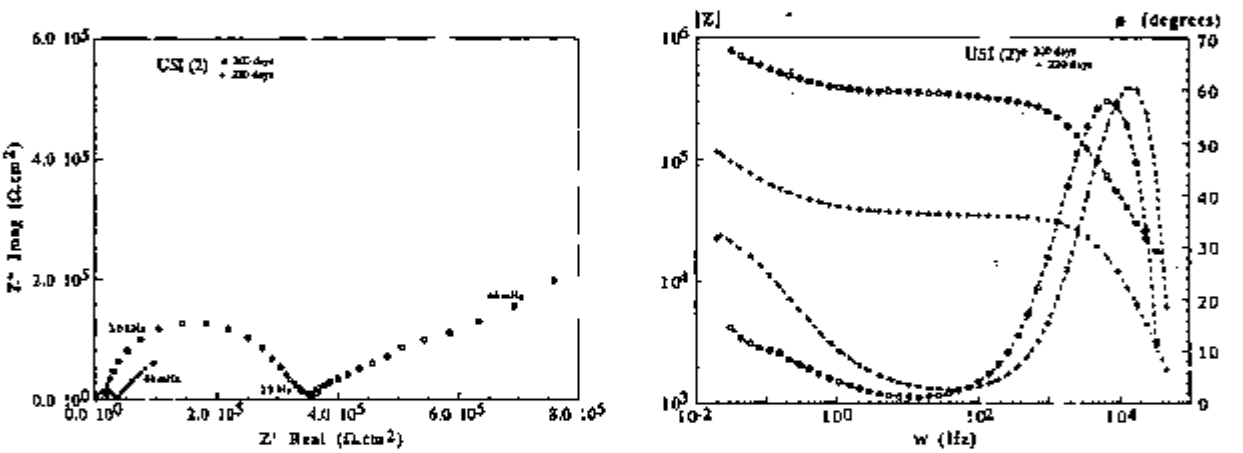

(b)

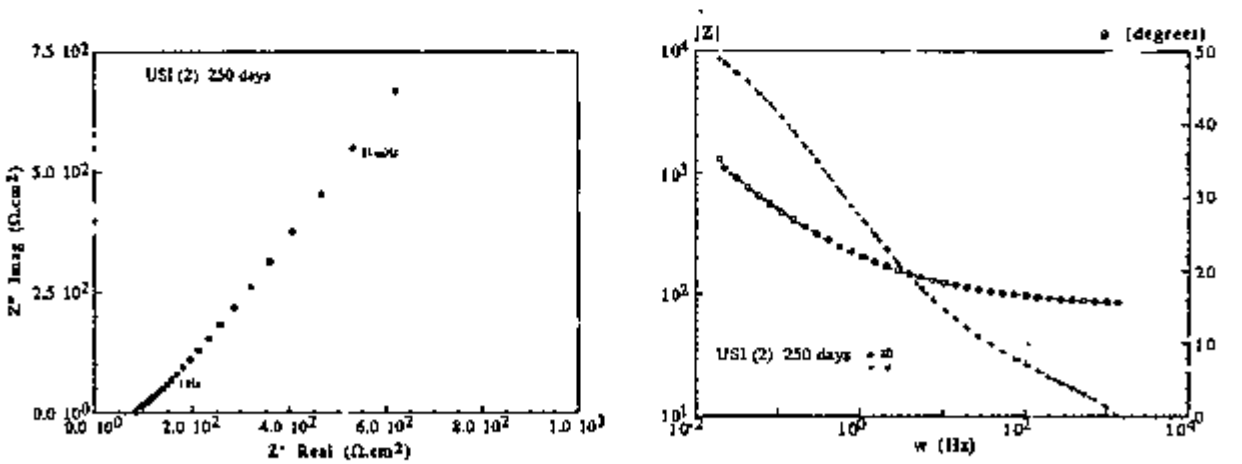

(c)

Figure 4.28 - Nyquist and Bode plots of specimen USI (2) after (a)130 and 150 days, (b) 200 and 220 days, and (c) 250 days immersion.

4.3.2.3 - Specimen USI (3)

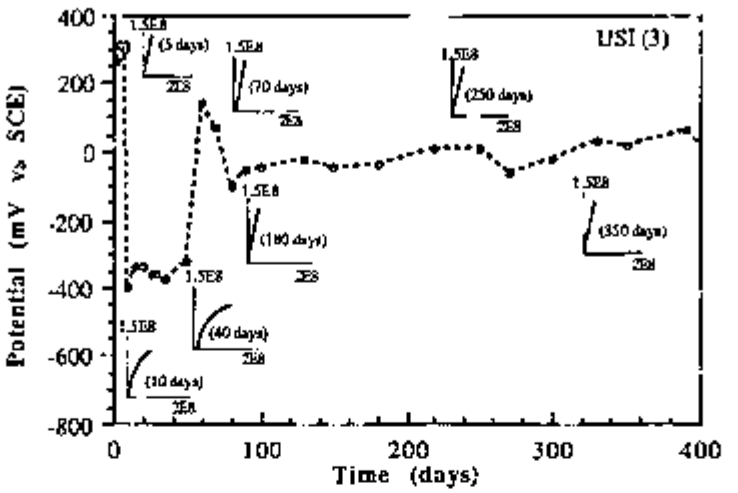

Figure 4.29 - Corrosion potential vs time and schematic Nyquist plots of specimen USI (3).

The coating resistance of this specimen was very high during the first days of immersion, and only the first part of the curve, an arc almost parallel to the Z" axis, was obtained. This arc initially bent towards the real axis from 10 until 40 days of immersion, but shifted again in the direction of the imaginary axis in the following days. This almost capacitive response was maintained until 400 days of testing. The bending of the curve towards the real axis (Nyquist plot) between 10 and 40 days was accompanied by a drop in corrosion potential. Also, after 10 days immersion a small black spot and a small blistered area were seen on the surface. These corrosion features might have been the cause of the decrease in both, R_{pf} and E_{corr}. The corrosion spot and the blistered area became gradually larger in the subsequent days. At approximately 40 days another corrosion spot was observed on the surface, and this also developed slowly. However, most of the surface was still metallic bright after 50 days exposure, Figure 4.30. Fifteen days later, yellow and blue corrosion products had formed on one of the blistered areas. At 180 days test, two black spots located at the centre of the blistered region were surrounded by brown corrosion products. No significant changes occurred from that time until the end of test (400 days). At 400 days immersion, some areas of the surface were successively covered with a

mixture beeswax:colophony resin, (ratio 1:3), in order to check if the relatively large proportion of highly protective coating was interfering with the impedance response. The results of this test are shown in Section 4.3.5.

Figure 4.30 - Specimen USI(3) after 50 days immersion.

4.3.2.4 - Specimen USI (4)

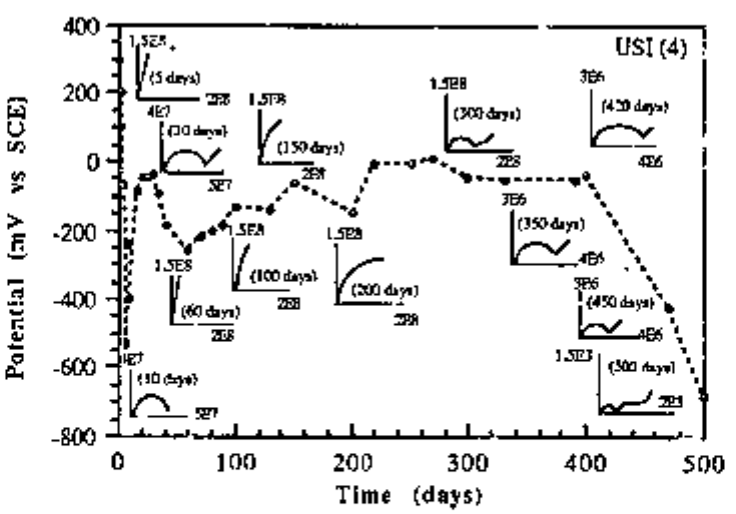

Figure 4.31 - Corrosion potential vs time and schematic Nyquist plots of specimen USI (4).

For this specimen the drop in potential in the first days immersion was accompanied by the appearance of a high frequency semi-circle in the Nyquist

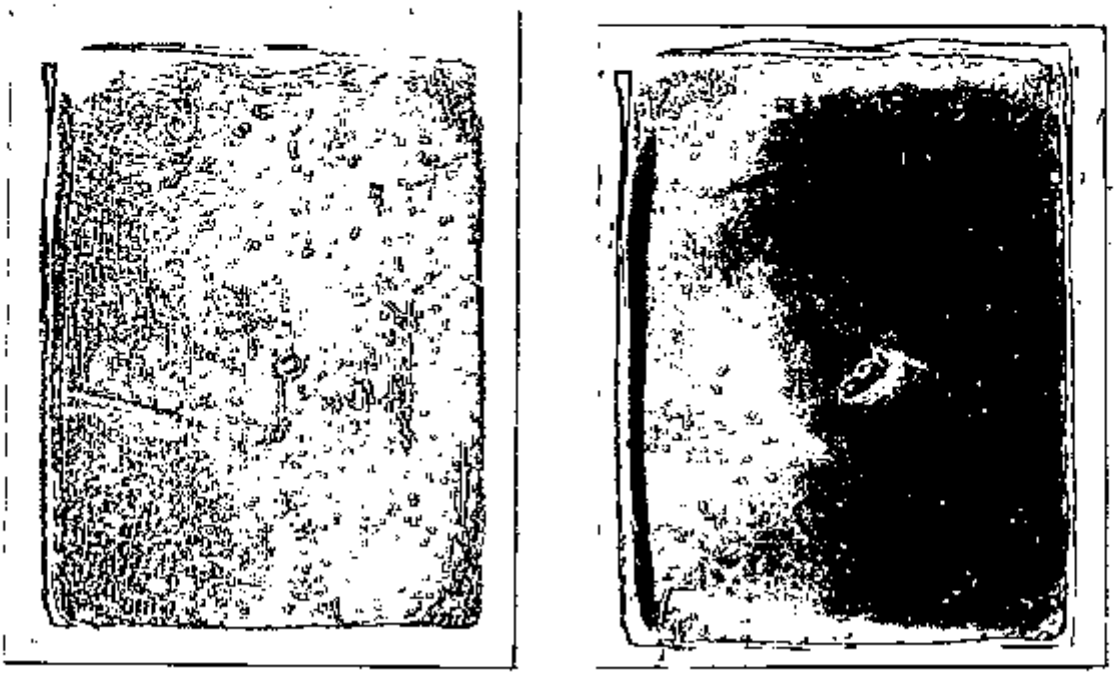

(a) (b)

Figure 4.32 - Specimen USI (4) after (a) 20 and (b) 50 days immersion

Figure 4.33 - Corrosion features of specimen USI(4) after 180 days immersion.

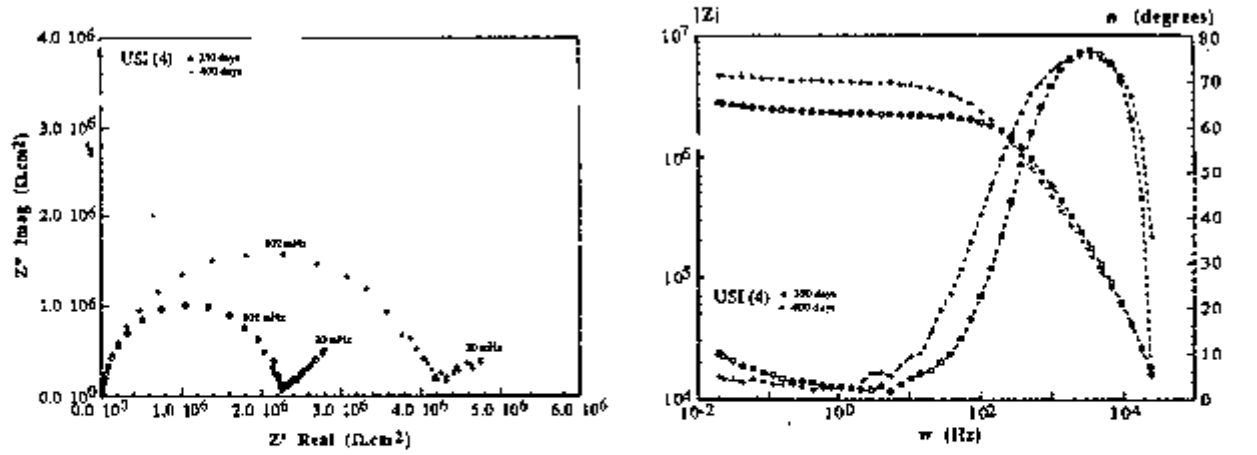

(a)

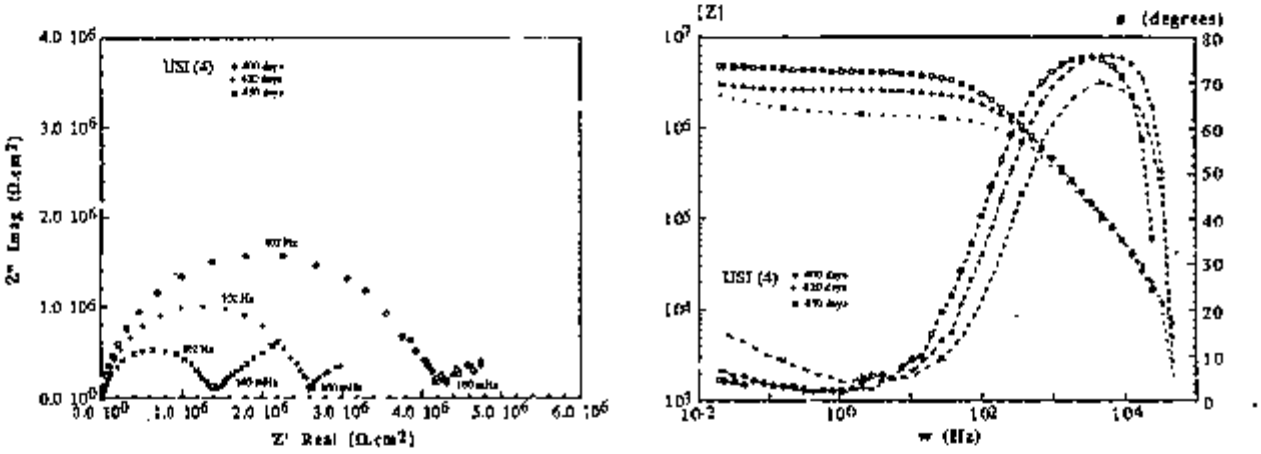

(b)

Figure 4.34 - Impedance response of specimen USI(4) after (a) 350 and 400 days, and (b) 400, 420, and 450 days immersion.

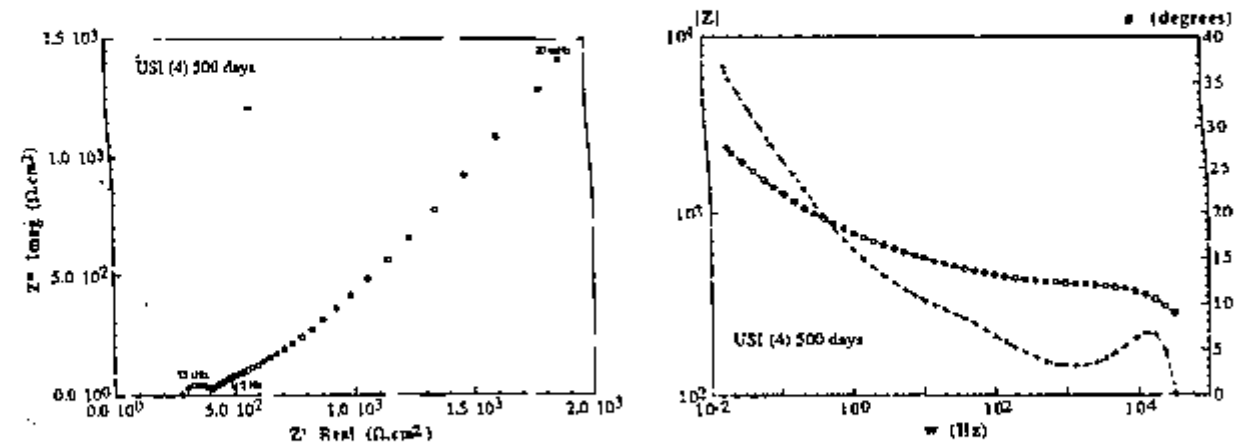

Figure 4.35 - Nyquist and Bode plots of specimen USI (4) after 500 days immersion.

4.3.2.5 - Specimen USI (5)

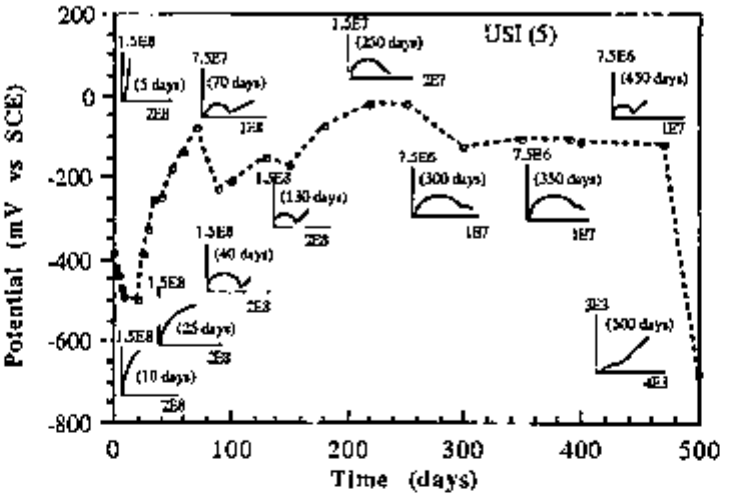

Figure 4.36 - Corrosion potential vs time and schematic Nyquist plots of specimen USI (5).

For this specimen the very small brown spots distributed all over the surface since the early days of immersion were probably associated with the characteristics of the microstructure of this steel. After 5 days immersion a small black spot was noted on the surface and two days later it was surrounded by a disbonded area. These corrosion features grew slowly with time, and 20 days after the test started, another small black spot and disbonded area were observed on the surface, Figure 4.37(a). Although the corrosion features expanded in the following days, no other corrosion features appeared until 50 days of immersion, Figure 4.37(b). It was also observed that large volumes of liquid had accumulated in one of the disbonded areas after 180 days of testing. The black corrosion product associated with that region had also become much larger. Yellow and brown corroding areas were also found on another area of the surface, at that exposure time. After 250 days immersion, most of the coating had disbonded and two large and voluminous black corrosion areas were seen on the surface. Despite the corrosion features described above, the coating resistance, R_{pf}, was still very large at that time (250 days), and had a value of around $10M\Omega.cm^2$. This started to decrease slowly soon afterwards, Figure 4.38, and at 500 days exposure the coating did not protect the substrate any longer, Figure 4.39.

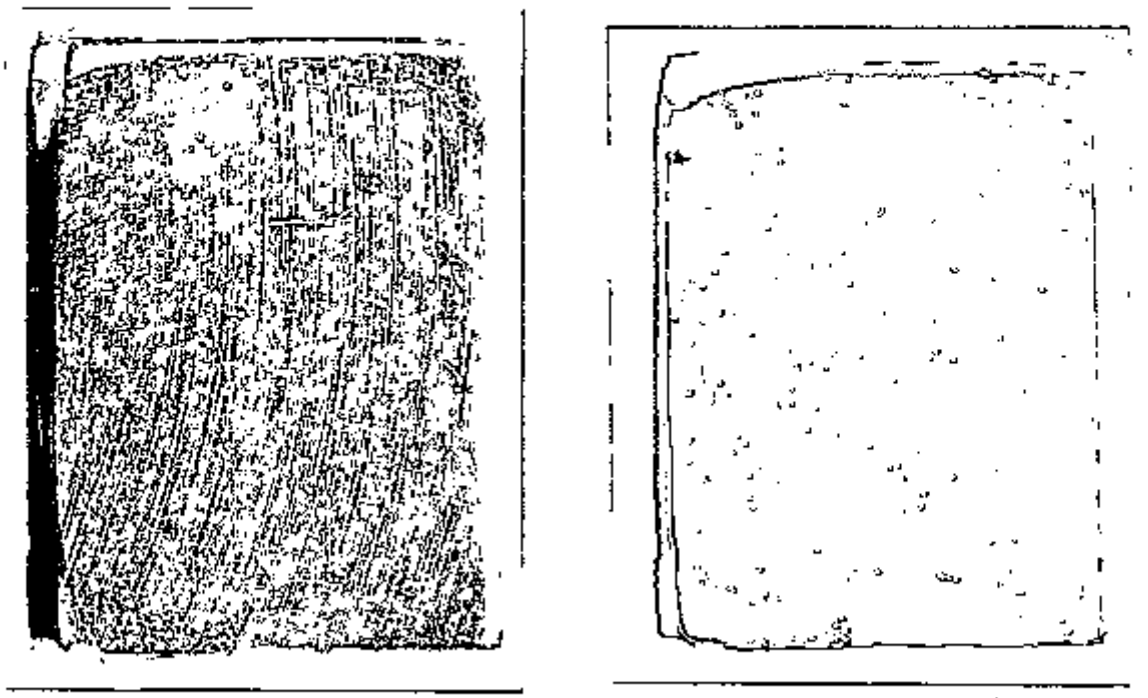

(a) (b)

Figure 4.37 - Specimen USI(5) after (a) 20 and (b) 50 days immersion.

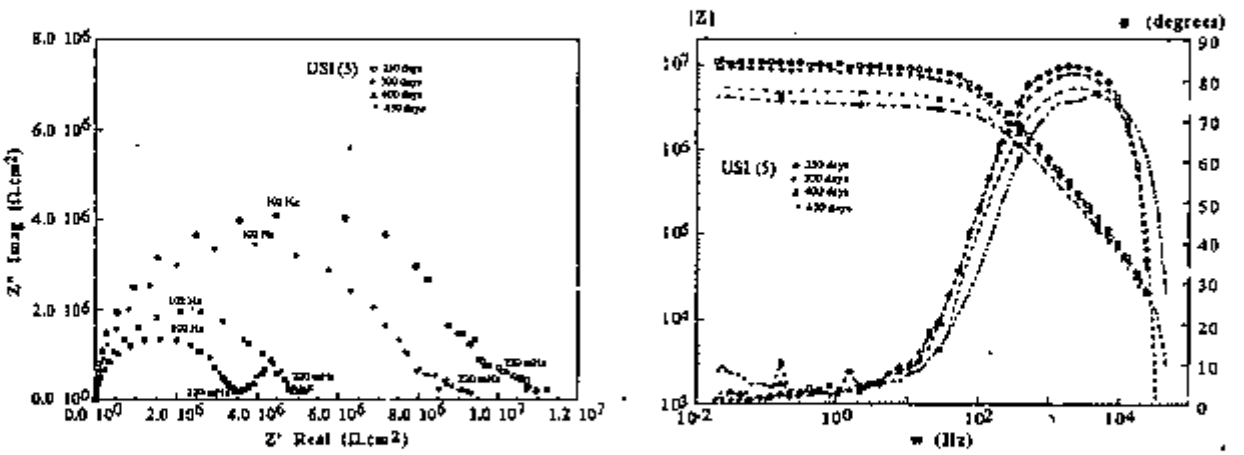

Figure 4.38 - Impedance response of specimen USI(5) after 250, 300, 400, and 450 days immersion.

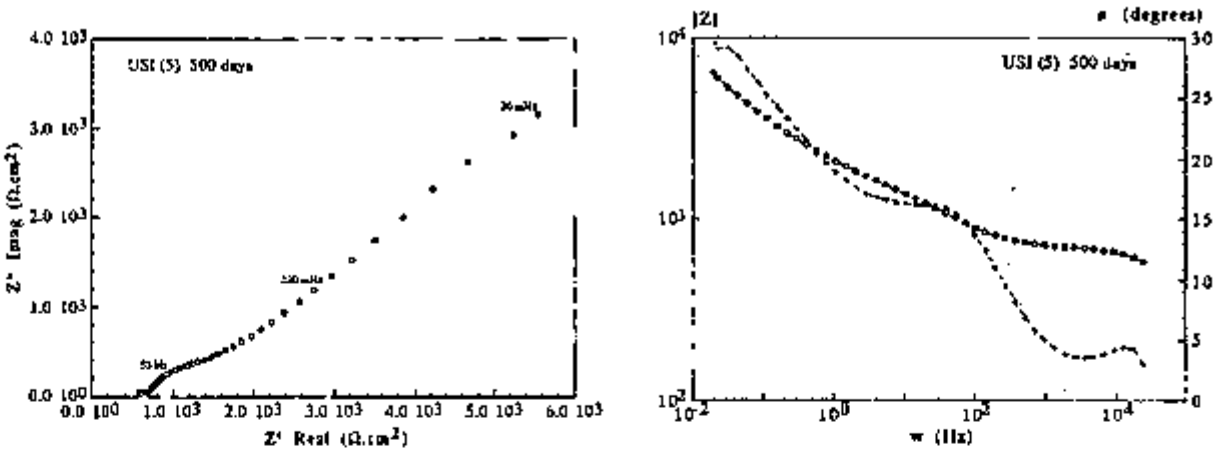

Figure 4.39 - Nyquist and Bode plots of specimen USI(5) after 500 days immersion.

4.3.3 - Substrate MS

The development of corrosion potential with time and impedance response (schematic Nyquist plots) of the specimens corresponding to this substrate are shown in Figures 4.40, 4.43, 4.46 and 4.48.

4.3.3.1 - Specimen MS (1).

This specimen showed unusual behaviour with immersion time, which was later found to be related to the lack of electrical contact between the lead wiring and the substrate. Thus, for this substrate only four specimens will be considered.

operative during that period, and finally at 350 days of testing, the coating did not exhibit any barrier properties, Figure 4.42(c).

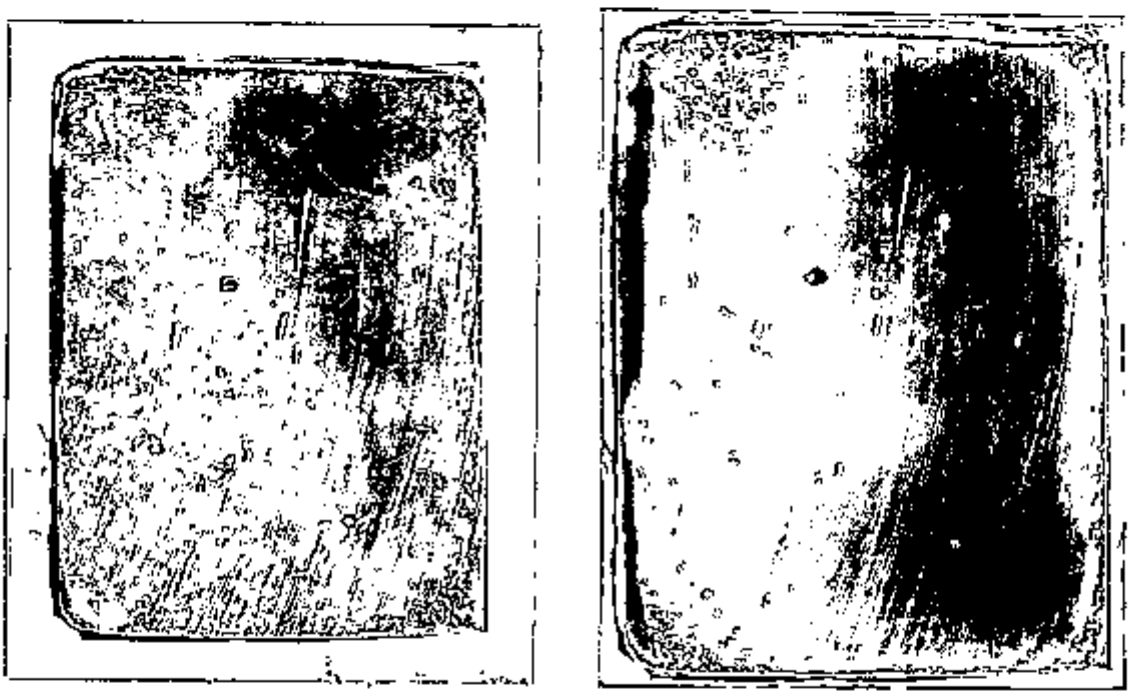

(a) (b)

Figure 4.41 - Specimen MS (2) after (a) 30 and (b) 50 days immersion.

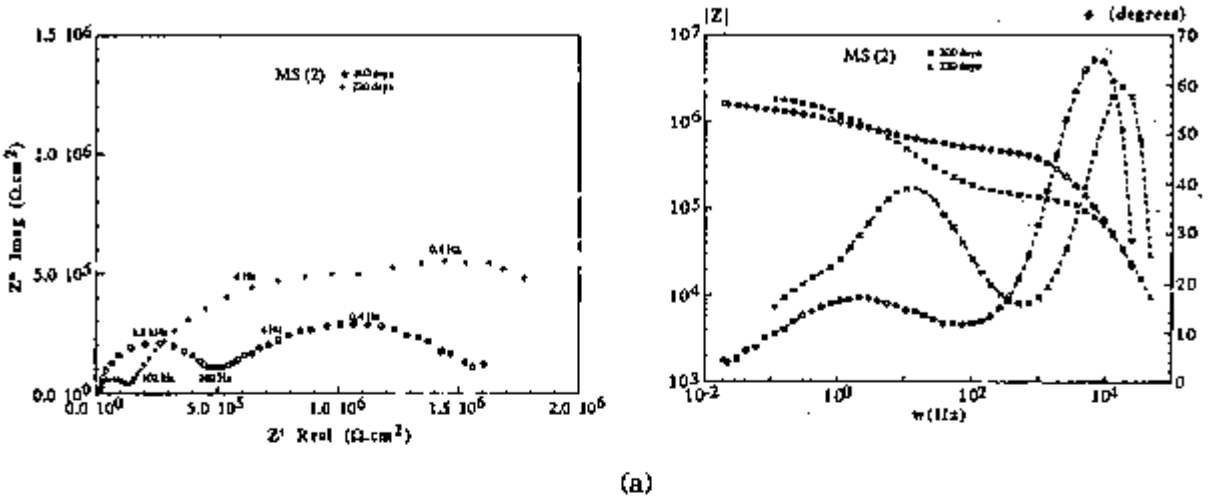

(a)

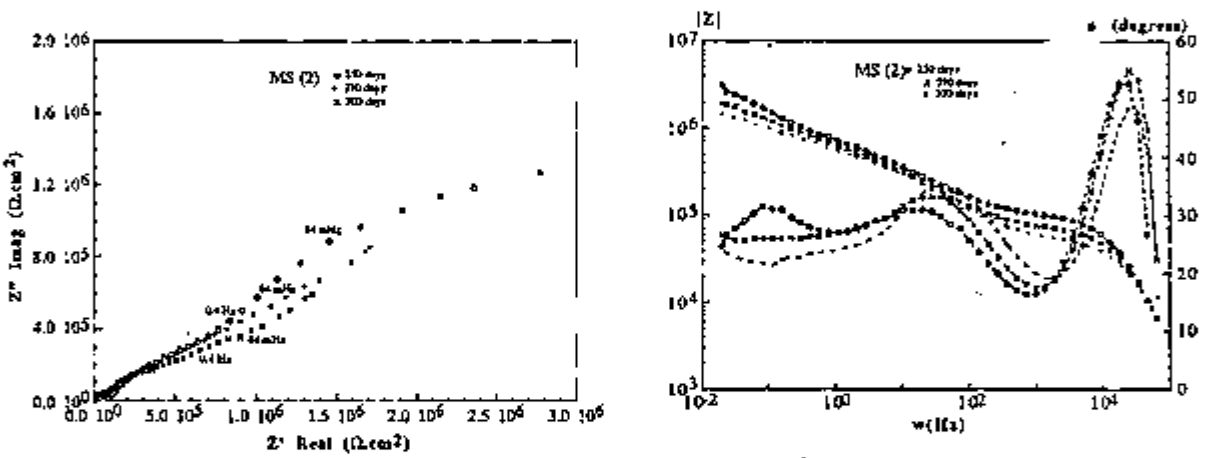

(b)

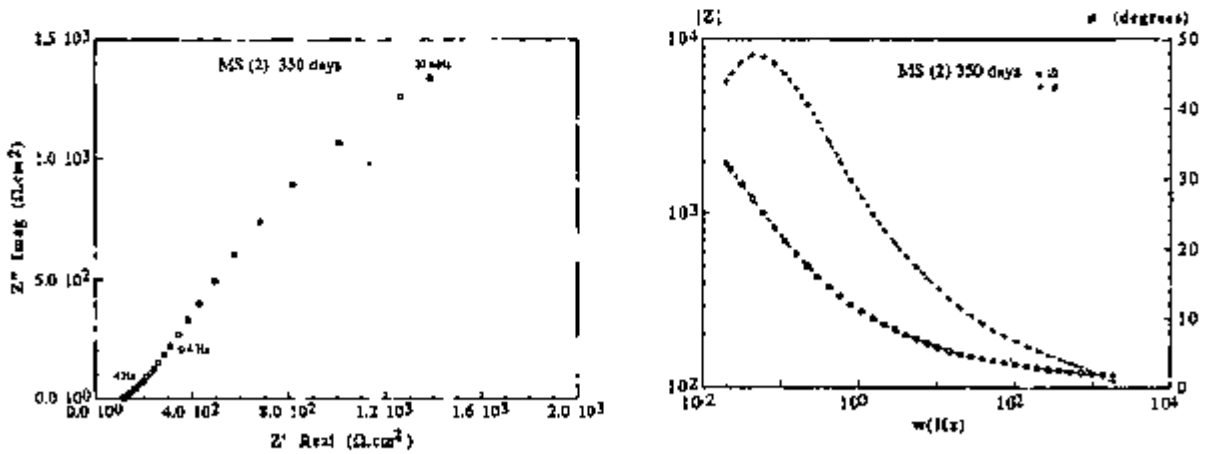

(c)

Figure 4.42 - Nyquist and Bode plots of specimen MS(2) after (a) 200 and 220 days, (b) 250, 270, and 300 days, and (c) 350 days immersion.

4.3.3.3 - Specimen MS (3)

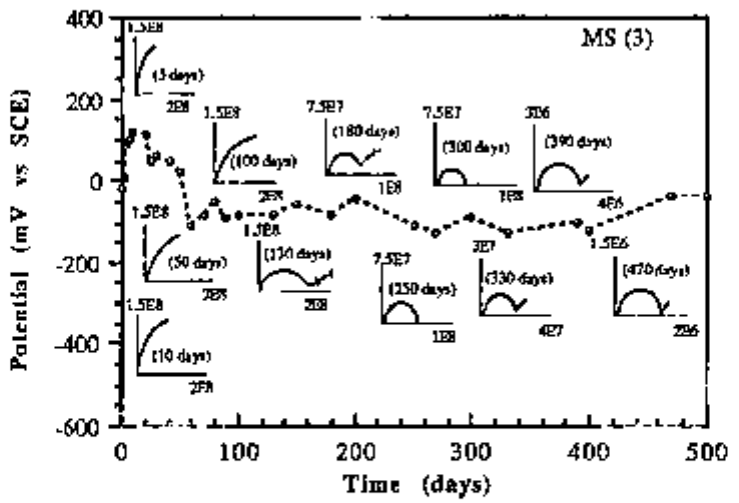

Figure 4.43 - Corrosion potential vs time and schematic Nyquist plots of specimen MS(3).

At the beginning of the test, the impedance response of this specimen produced only the initial part of the high frequency semi-circle which progressively bent towards the real axis. Only at 130 days immersion did the high frequency semi-circle become complete, which implied a slight coating deterioration. Relatively high and stable corrosion potentials were also produced by this specimen indicating that the coating was highly protective. From 150 days to 350 days exposure, R_{pf} decreased from values of around 100 MΩ.cm^2 to approximately 20 MΩ.cm^2. A larger drop in R_{pf} occurred after that time, and at 390 days immersion R_{pf} was nearly 2.5 MΩ.cm^2. From then and until the end of test, (500 days), R_{pf} varied only slightly and values close to 1.5 MΩ.cm^2 were obtained. After 330 days immersion, a low frequency impedance response was first obtained probably associated with the corrosion process occurring underneath the coating. The coating was still protective at the end of test (approximately 1 MΩ.cm^2), and also the corrosion potential was relatively noble (nearly -50 mV).

Despite the highly protective characteristics of the coating on this specimen, a small black spot and a small blister were seen on the surface after seven days of immersion. The rest of the surface, however, showed no sign of

corrosion. Both corrosion features developed slightly in the subsequent days, Figure 4.44, but it was only after 60 days immersion that a small and blue area was identified close to the black corrosion spot. Two new corrosion spots surrounded by a disbonded area were distinguished on the surface after 250 days of testing. At that time the blistered area occupied approximately half of the total exposed area. Even though corrosion was evident on the surface, R_{pf} was still too high to allow the detection of the corrosion processes by impedance measurements. The faradaic processes could be easily identified after 390 days immersion, Figure 4.45. At that time (390 days) the low frequency impedance response seemed to correspond to the initial part of a semi-circle related to the charge transfer controlled corrosion reaction which was probably occurring at relatively low corrosion rates. The diameter of the low-frequency semi-circle, R_{ct}, was observed to decreased with immersion time, and a diffusion response was seen at low frequencies. This can be seen for times corresponding to 450 days immersion in Figure 4.45.

Figure 4.44 - Specimen MS(3) after 30 days immersion.

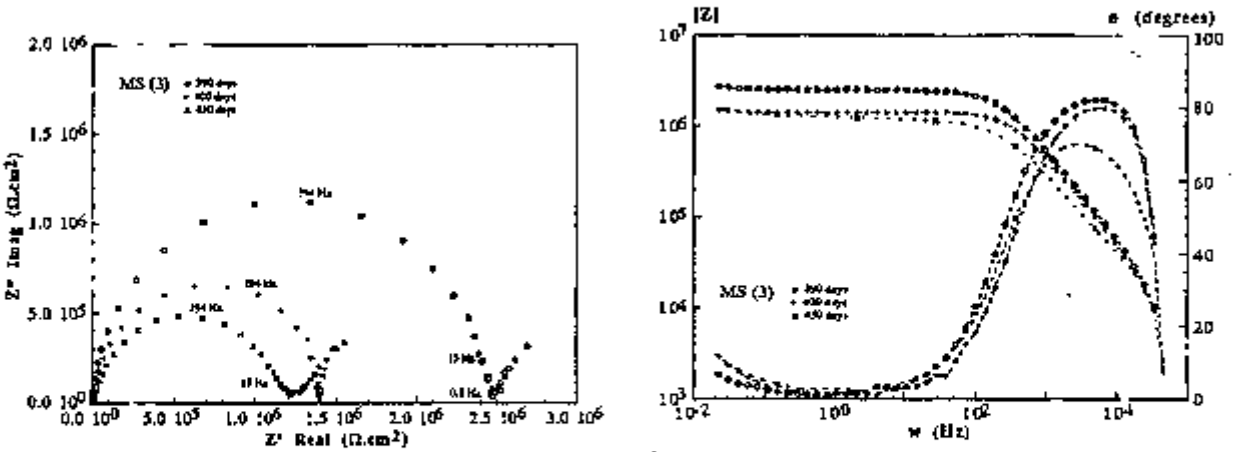

Figure 4.45 - Impedance response of specimen MS(3) after 390, 400, and 450 days immersion.

4.3.3.4 - Specimen MS (4)

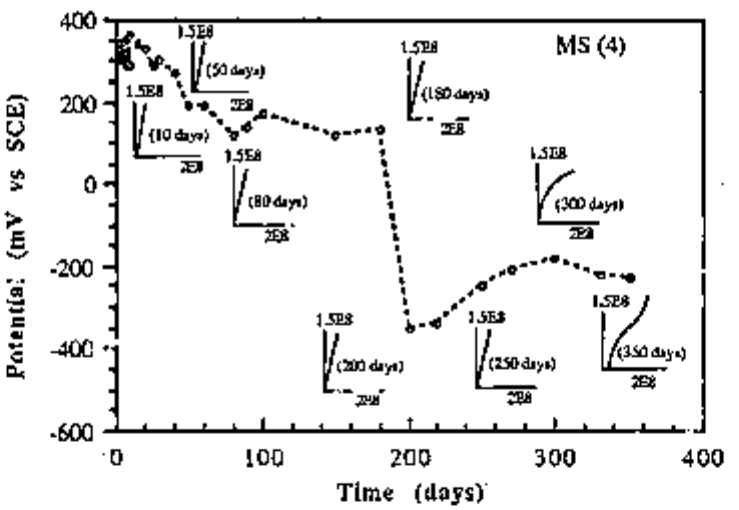

Figure 4.46 - Corrosion potential vs time and schematic Nyquist diagrams of specimen MS (4).

A very slow decrease in corrosion potential occurred from the start of the test and until 180 days immersion. During that period, the impedance response was one characteristic of a highly resistive coating. Even after a sharp drop in E_{corr} took place at approximately 200 days, the impedance response remained the same. It was only after 300 days immersion, that the arc running almost parallel to the imaginary axis started bending towards the real axis, Figure 4.47. After 350 days exposure, various areas of this specimen were successively masked with colophony:beeswax mixture in order to test the effect of the ratio between

protective and corroding areas of the coating on the impedance response of the system. The results of this test are presented in Section 4.3.5. The corrosion features identified on this specimen since the first days of immersion corresponded to two small black spots and some blistered areas. These can be seen in Figure 4.48 after 50 days immersion and were still unchanged when the test was interrupted at 350 days, confirming the good corrosion characteristics of this system.

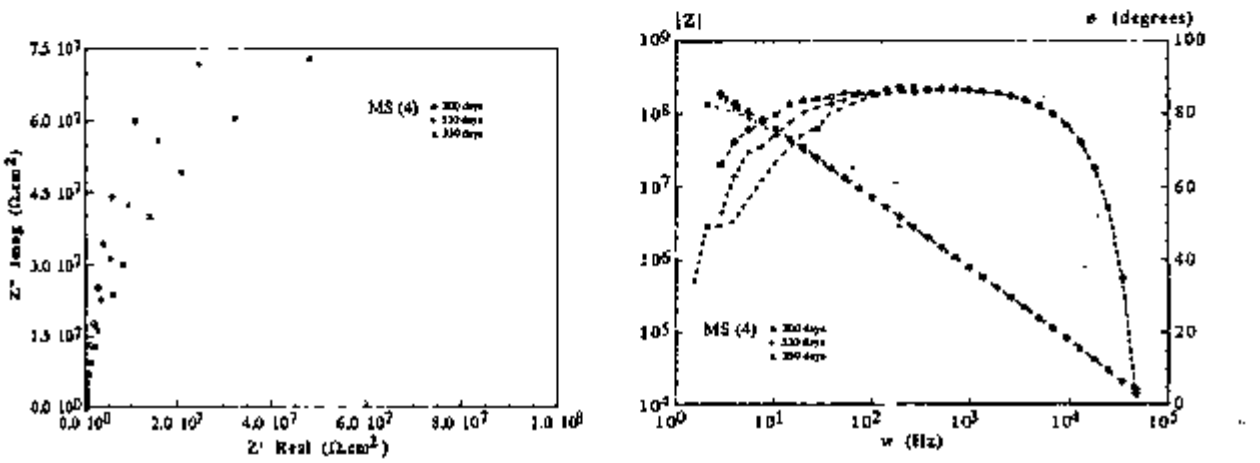

Figure 4.47 - Nyquist and Bode plots of specimen MS (4) after 300, 330, and 350 days immersion.

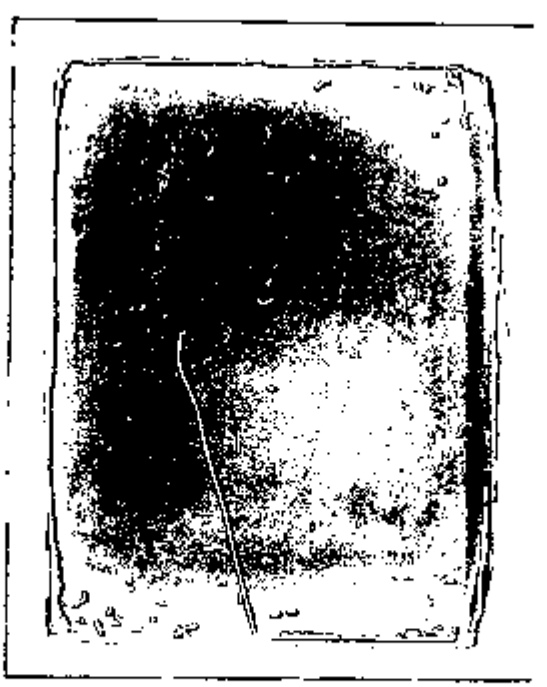

Figure 4.48 - Specimen MS (4) after 50 days immersion.

4.3.3.5 - Specimen MS (5)

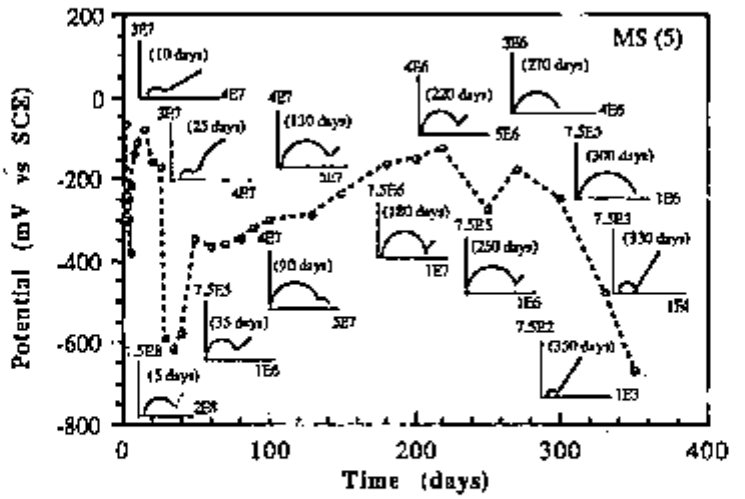

Figure 4.49 - Corrosion potential vs time and schematic Nyquist plots vs time of specimen MS (5).

For this specimen four blistered areas and a black corrosion spot were noticed on the surface as early as the fifth day of exposure, and this was probably the cause for the initial drop in corrosion potential. The impedance response also changed from an almost capacitive behaviour of coating to a definite high frequency semi-circle after 5 days immersion (R_{pf} approximately 100 $M\Omega.cm^2$). The diameter of this semi-circle decreased in the subsequent days to values of around 10 $M\Omega.cm^2$, suggesting that the coating was losing its protective qualities. This also explains the rapid development of corrosion features underneath the coating. The blistered areas spread relatively quickly in the following days, and 10 days after the start of the test, these areas were completely surrounding the corroding spots. The corroding spots also grew with immersion time, and changed colour from brown to black. Figure 4.50 (a) and (b) shows the corrosion characteristics of this specimen after 30 and 50 days immersion, respectively. The impedance data showed a large increase in R_{pf} from 25 to 30 days, but this soon decreased again. The increase in R_{pf} is possibly explained by the blockage of pores where the localized corrosion had occurred. The corrosion products grew under diffusion control, and since these were locally deposited

they hindered the access of corrosion species to the metallic matrix. Once the pore was blocked, the resistance of the system increased and corrosion processes were only detected when corrosion started in a new area of the surface. The coating resistance was relatively stable between 35 and 130 days immersion but decreased after that period, Figure 4.51(a) and (b). It should be added that R_{pf} recovered slightly to higher values between 250 and 270 days immersion, and this event was also accompanied by an increase in the corrosion potential, Figure 4.51(c). The high frequency semi-circle became depressed between 250 and 300 days immersion, Figure 4.52(a). A final decrease in both, R_{pf} and E_{corr}, started after 270 days. At 330 days, R_{pf} values of approximately 2 $k\Omega.cm^2$ were obtained, Figure 4.52(b). The test was terminated at 350 days, as it was considered that the coating was of no protective value, Figure 4.52(c).

(a) (b)

Figure 4.50 - Specimen MS (5) after (a) 30 days and (b) 50 days immersion.

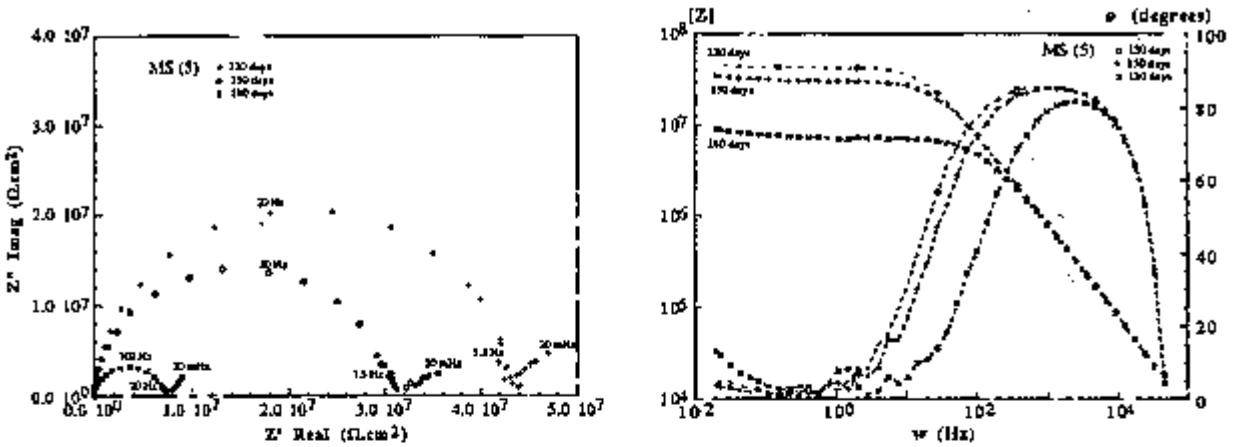

(a)

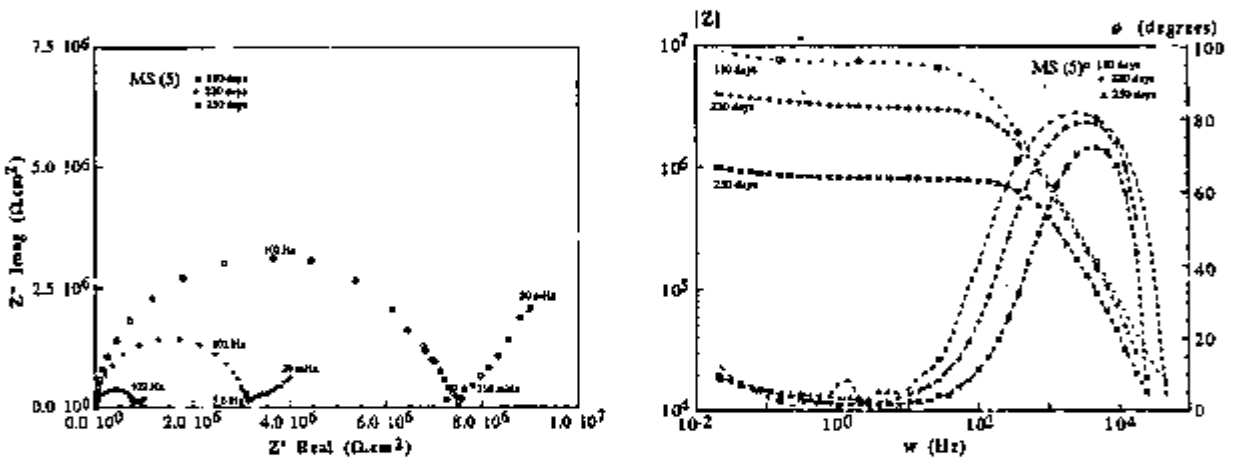

(b)

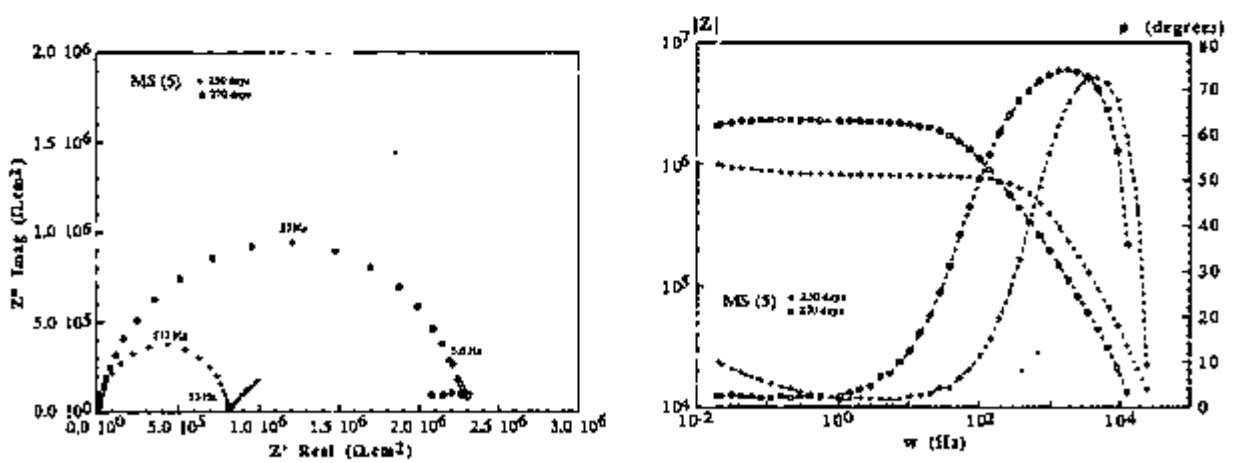

(c)

Figure 4.51 - Impedance response of specimen MS(5) after (a)130, 150, and 180, (b) 180, 220 and 250, (c) 250 and 270 days immersion.

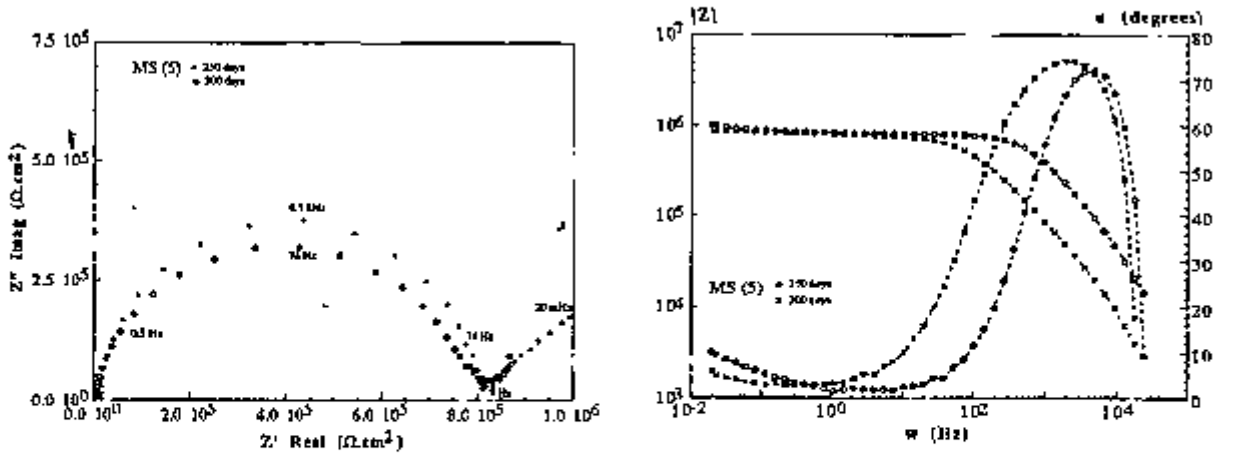

(a)

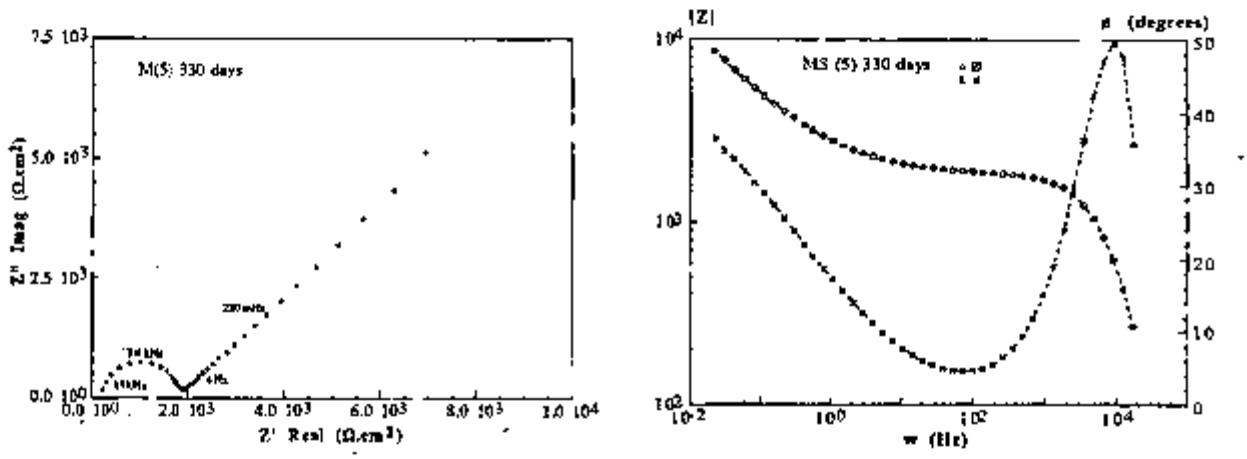

(b)

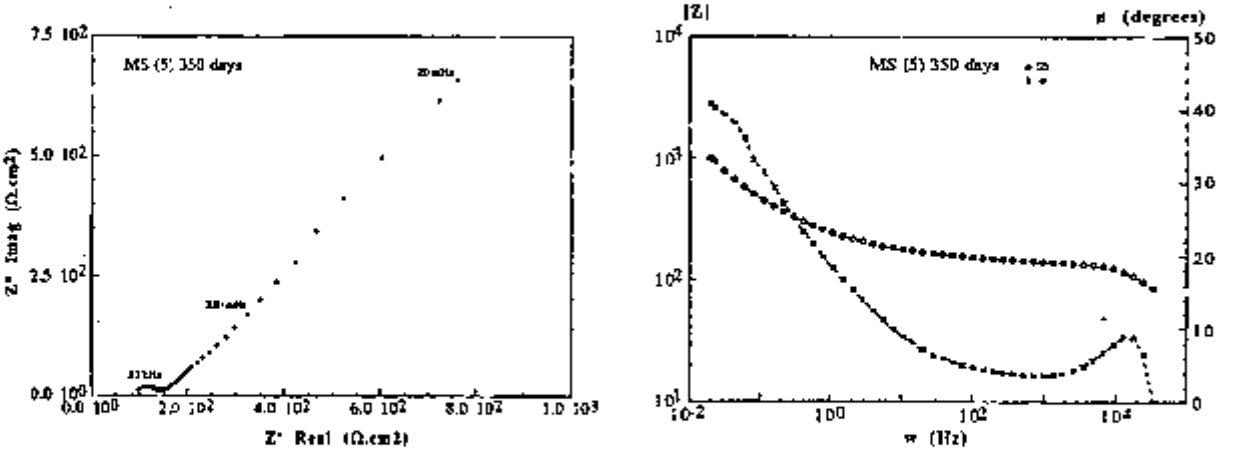

(c)

Figure 4.52 - Impedance response of specimen MS(5) after (a) 250 and 300 days, (b) 330 days and (c) 350 days test.

4.3.4 - Substrate LAS II

The evolution of corrosion potential of the coated LAS II specimens are shown in Figures 4.53, 4.55, 4.59, and 4.63, which also include schematic Nyquist plots.

4.3.4.1 - Specimen LAS II (1)

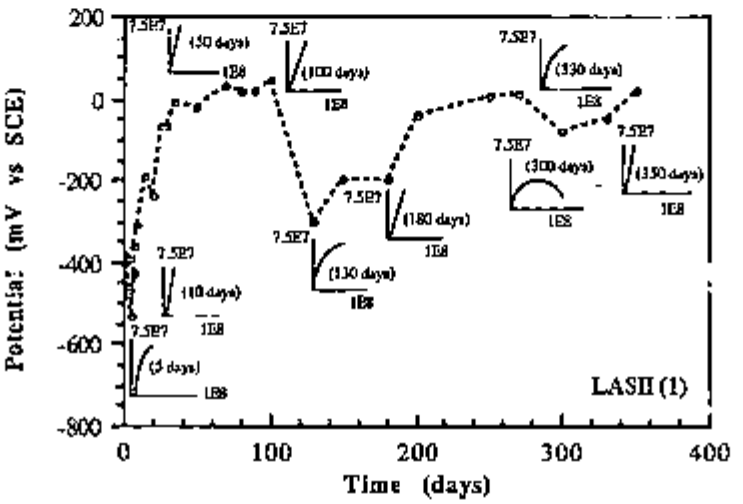

Figure 4.53 - Corrosion potential vs time and schematic Nyquist plots of specimen LAS II (1).

The corrosion features which were observed during the early stages of the immersion of this specimen, corresponded to a black corrosion spot surrounded by a disbonded area. The rest of the surface showed no visible corrosion. The disbonded area spread in the following days, and a new brown corrosion spot, located close to the black one, was seen on the surface at approximately 30 days exposure. These corrosion characteristics shown in Figure 4.54 after 50 days immersion remained unchanged in the subsequent days. From that time until the test was finished, no new corrosion features appeared on the surface. The coating resistance had a relatively large magnitude throughout the duration of experiment. Slight degradation of the coating was only indicated by the bending of the arc at times corresponding to 5 days, 130 days, and 300 days immersion. At

these times the corrosion potential also shifted temporarily to more active values. However, E_{corr} recovered to nobler values soon afterwards. The test was interrupted after 360 days immersion, when this specimen was used to investigate the effect of the ratio of the protective and corroding areas of specimen on the impedance response of the system. The results of this test are presented in Section 4.3.5.

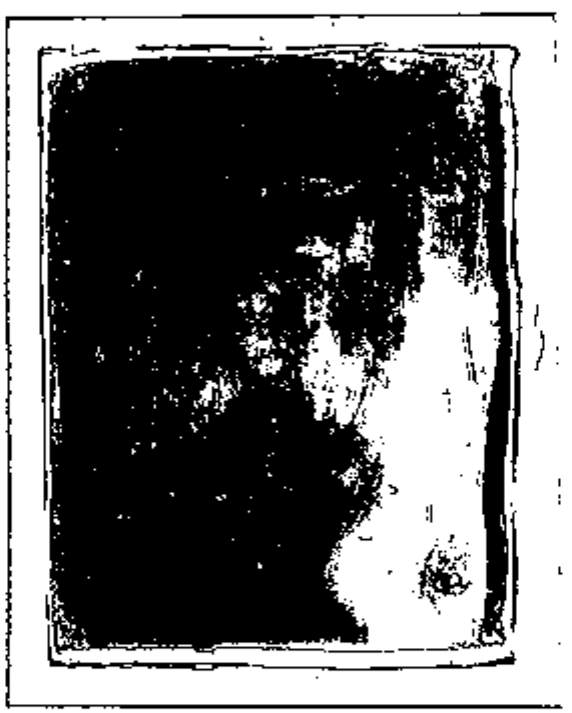

Figure 4.54 - Specimen LAS II (1) after 50 days immersion.

4.3.4.2 - Specimen LAS II (2)

This specimen produced unusual behaviour which was later found to be caused by the corrosion of the screw connecting the lead wire to the steel substrate. Thus, for this type of steel only four specimens will be considered.

4.3.4.3 - Specimen LAS II (3)

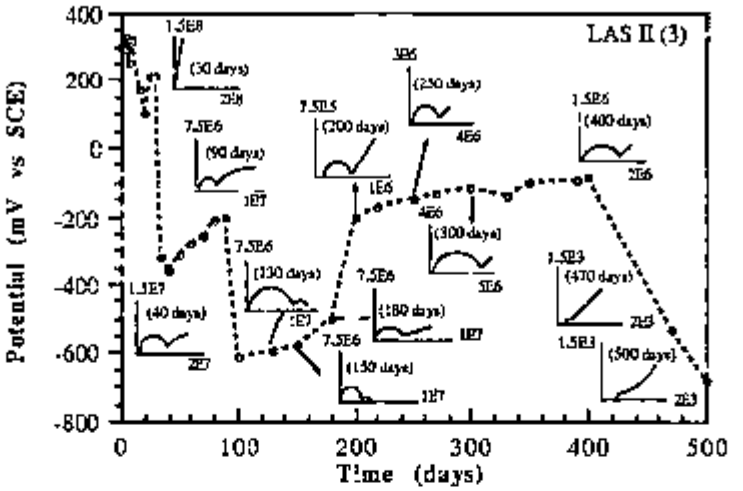

Figure 4.55 - Corrosion potential vs time and schematic Nyquist plots of specimen LAS II (3).

A minute black spot was noted on the surface of this specimen after 7 days immersion, but the remainder of the surface was still metallic bright at that time. This situation was still unchanged after 30 days immersion, but 10 days later a large blister was seen on the surface and this covered almost all the surface at 50 days immersion, Figure 4.56. In addition, large volumes of liquid accumulated under the disbonded area and were easily visible through the transparent coating. Also between 30 and 50 days a new corrosion spot showing a brown centre and black boundaries appeared on the surface. The impedance response after 40 days immersion produced a high frequency semi-circle and a low frequency response representing the corrosion process underneath the coating. A drop in corrosion potential occurred at that time. The coating resistance decreased in the period from 50 to 90 days immersion. After 50 and 180 days immersion new corrosion features developed. These corresponded to yellow, brown and black areas on the surface which was completely blistered at the end of that period. Although slight increases in R_{pf} occurred in the periods from 90-130 days and from 200-250 days, the general trend was for decreasing R_{pf} values,

Figure 4.57(a-c). At 420 days immersion, the specimen was removed from solution since it was considered that the coating no longer exhibited protective characteristics, Figure 4.58.

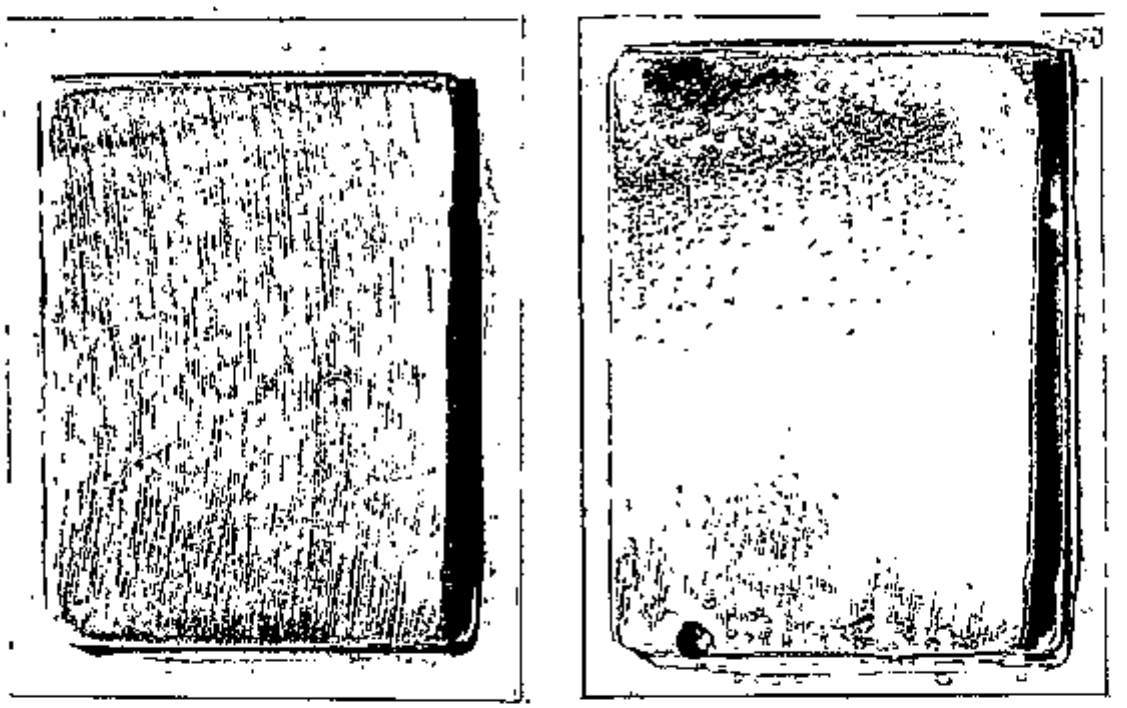

(a) (b)

Figure 4.56 - Specimen LAS II (3) after (a) 30 and (b) 50 days immersion.

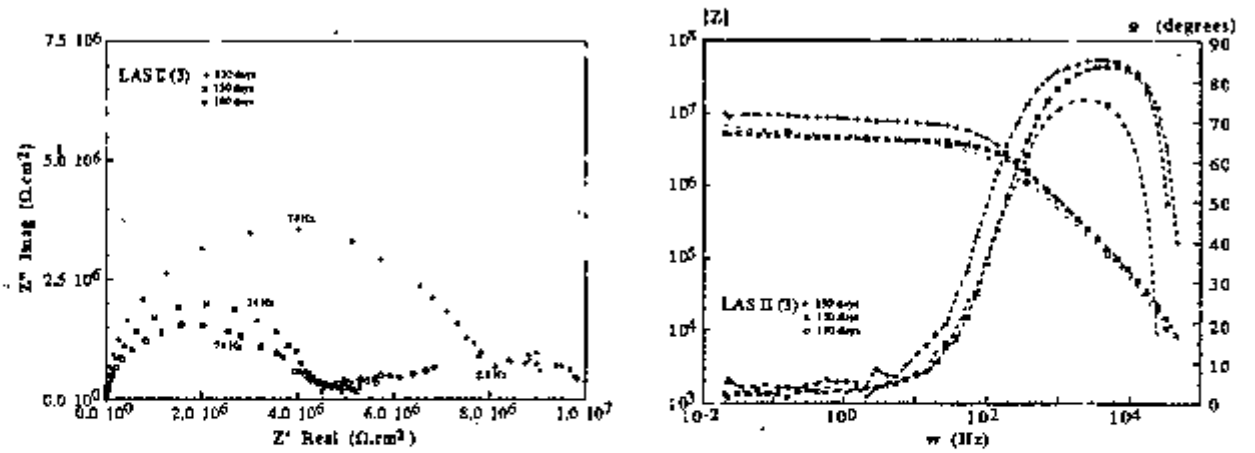

(a)

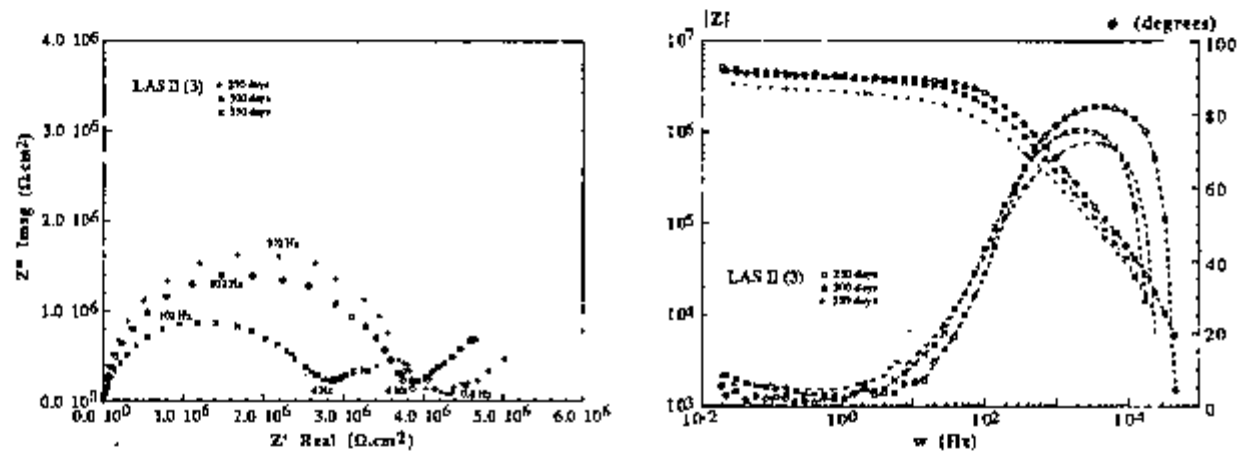

(b)

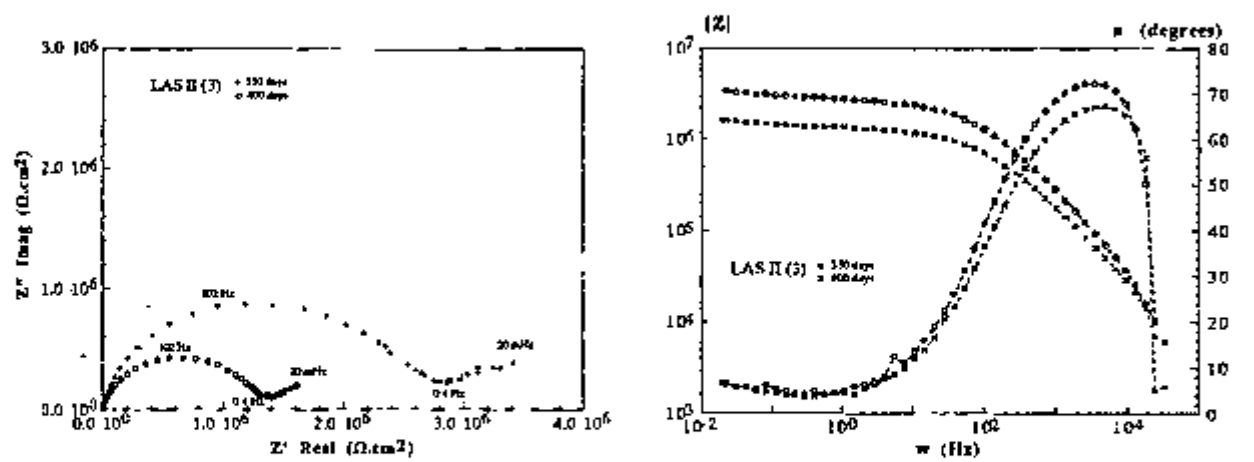

(c)

Figure 4.57 - Impedance response of specimen LAS II (3) after (a)130, 150, and 180 days, (b) 250, 300 and 350 days, and (c) 350 and 400 days.

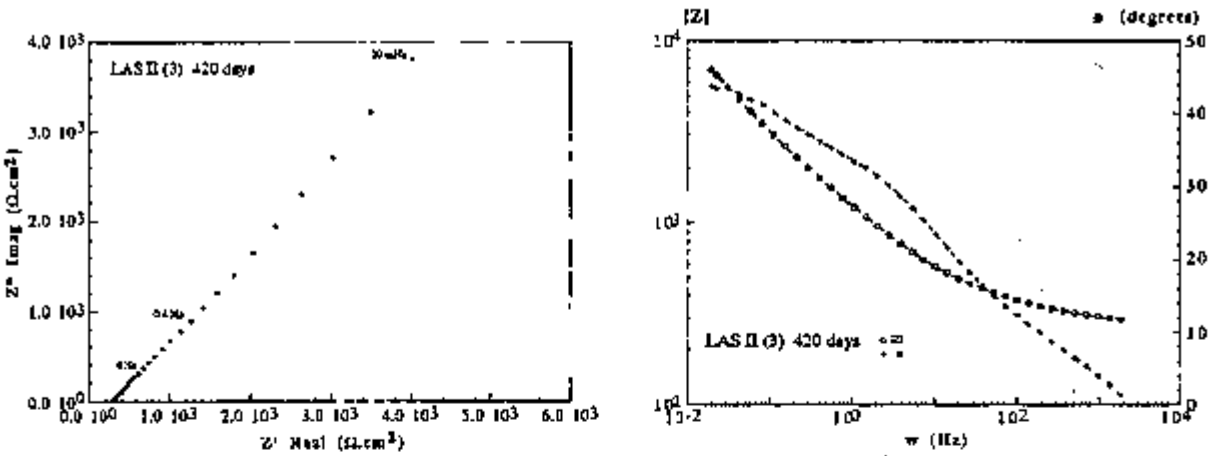

Figure 4.58 - Nyquist and Bode plot of specimen LAS II (3) at 420 days immersion.

4.3.4.4 - Specimen LAS II (4)

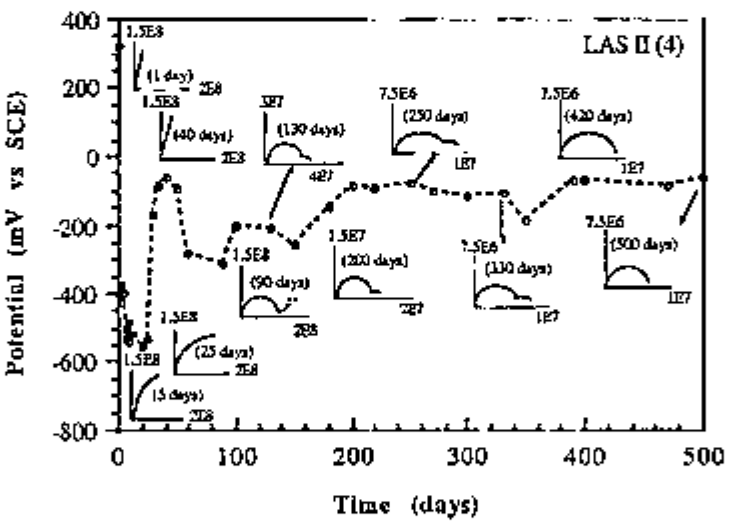

Figure 4.59 - Corrosion potential vs time and schematic Nyquist plots of specimen LAS II (4).

Corrosion features on the surface of this specimen became visible six days after starting the test. These corresponded to a small black spot and a small blister whereas the rest of the surface showed no evidence of corrosion. In the following days the corroding spot became more voluminous and two new blistered areas developed on the surface which were easily seen after 20 days exposure. Figure 4.60 shows the above corrosion characteristics after 30 and 50 days immersion, respectively. The liquid accumulated in the blister at 50 days

exposure was yellow indicating the presence of ions generated in the corrosion reaction. This same solution changed to a brownish colour after 180 days of testing, Figure 4.61. Despite the corrosion characteristics mentioned above, the coating resistance was still relatively high at 130 days (around 20 $M\Omega.cm^2$). Even though R_{pf} decreased by nearly half in the next 200 days, it was still very high, approximately 8 $M\Omega.cm^2$, when the experiment was interrupted at 500 days immersion, Figure 4.62.

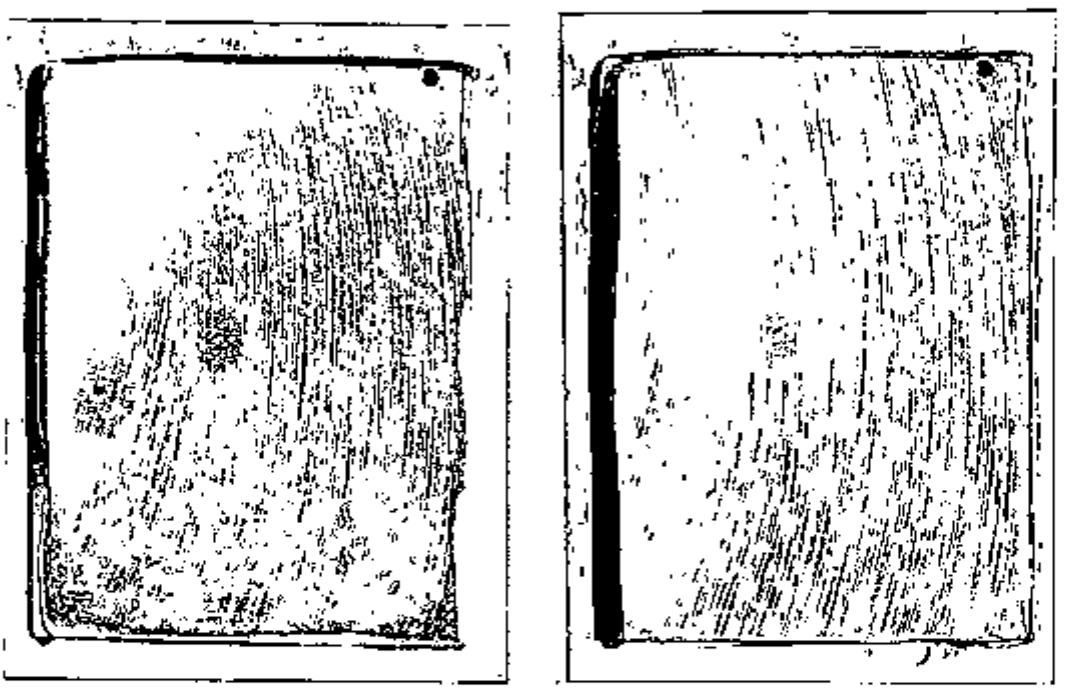

(a) (b)

Figure 4.60 - Specimen LAS II (4) after (a) 30 and (b) 50 days immersion.

Figure 4.61 - Specimen LAS II (4) after 180 days immersion.

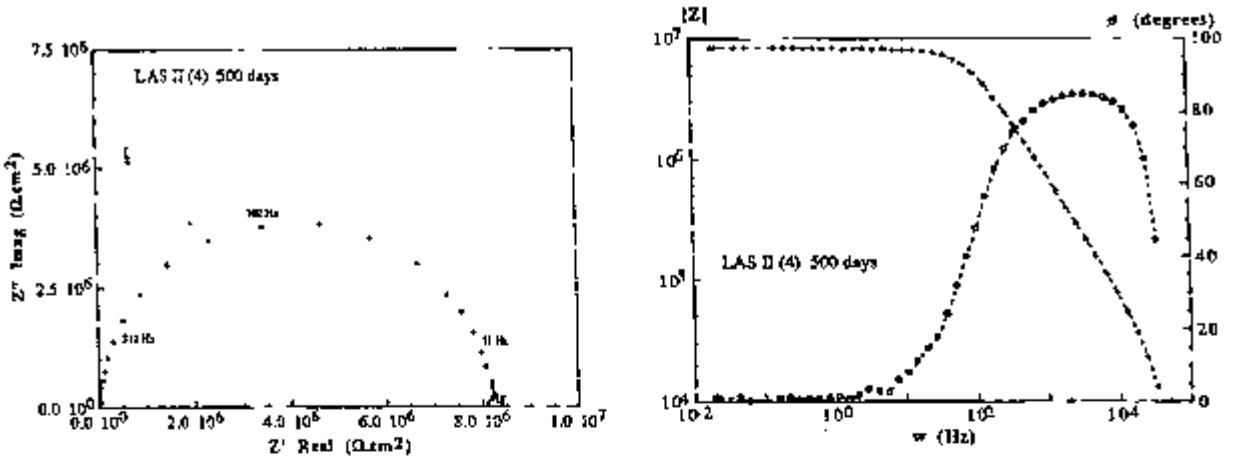

Figure 4.62 - Nyquist and Bode plots of specimen LAS II (4) after 500 days immersion.

4.3.4.5 - Specimen LAS II (5)

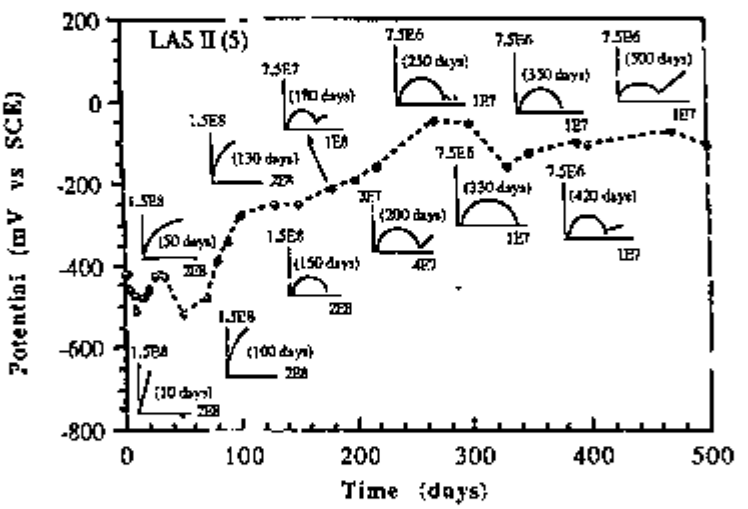

Figure 4.63- Corrosion potential vs time and schematic Nyquist plots of specimen LAS II (5).

During the first 5 days of immersion only a very small brown corrosion spot was seen on the surface. This spot grew slightly and became black with time. The surface characteristics of this specimen are shown in Figure 4.64 at 50 days immersion. Fifteen days later the corroding spot was surrounded by a disbonded area. The disbonded area and the corrosion spot enlarged slightly in the following days. These features, at 180 days immersion, are shown in Figure 4.65. The rest of the surface at that time did not show evidence of corrosion, and

the coating resistance was also very large (around 50 $M\Omega.cm^2$). The coating resistance then decreased from approximately 30 $M\Omega.cm^2$ (200 days) to nearly 7 $M\Omega.cm^2$ (420 days), but was still of that order when the experiment was terminated at 500 days immersion, Figure 4.66.

Figure 4.64 - Specimen LAS II (5) after 50 days immersion.

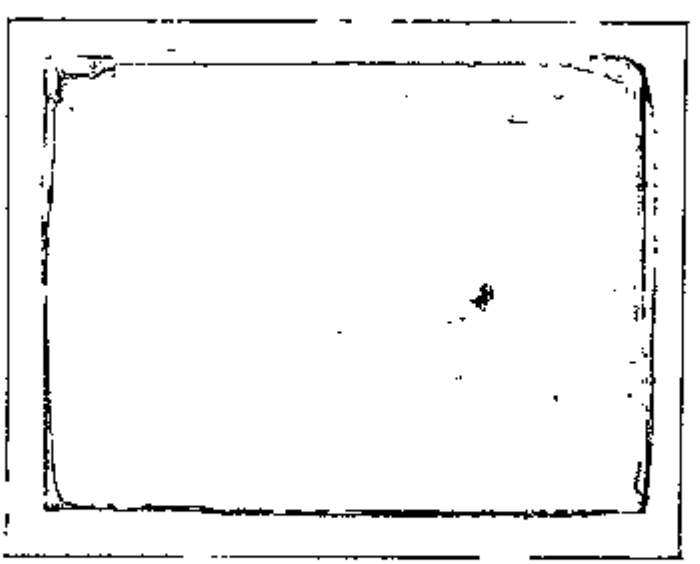

Figure 4.65- Specimen LAS II (5) after 180 days immersion.

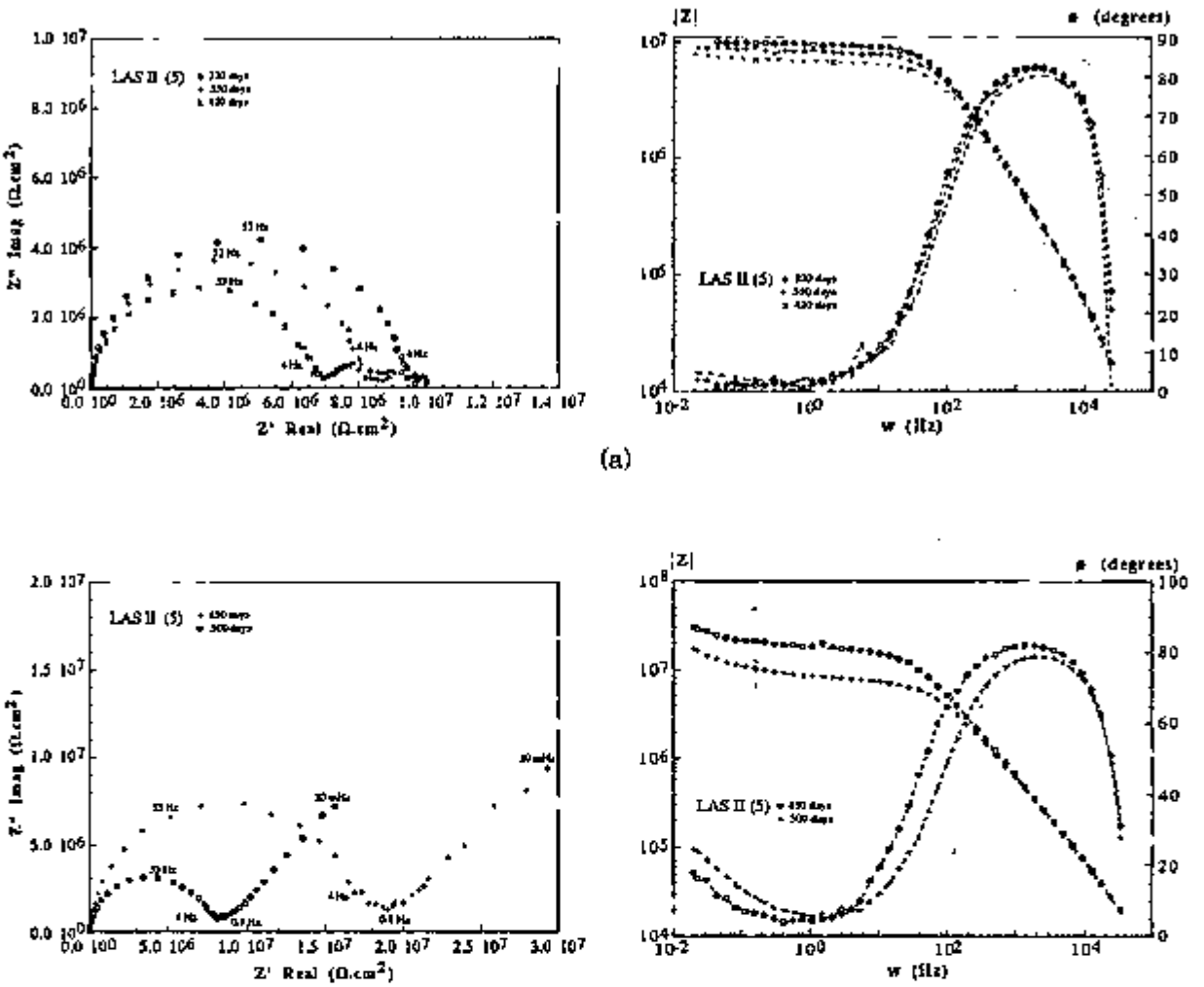

Figure 4.66 - Impedance response of specimen LAS II (5) after (a) 330, 350, and 420 days, and (b) 450 and 500 days immersion.

4.3.5 - Impedance results

A sketch of the circuit diagrams used in the electrochemical impedance measurements was presented in section 2.1.6.9.

4.3.5.1 - Changes in R_{pf} with immersion time.

The impedance measurements were carried out at the corrosion potential. The resulting electrochemical impedance data were interpreted to determine individual components of an equivalent electrical circuit that best approximates the behaviour of the coated metal-solution interface. The value of these

components such as paint film capacitance, C_{dl}, and coating resistance, R_{pf}, altered with immersion time. Table 4.2 presents a summary of the development of the coating resistance with time of the various systems used. This includes the time for the film resistance of the various coated specimens to decrease to a magnitude of the order of 1 $M\Omega.cm^2$, and the time of failure of the protective characteristics of the various systems used. A curve-fitting procedure, in which a compass was used to find the semi-circle which best fitted the experimental data, was employed for the determination of semi-circles in the Nyquist plot.

From Table 4.2 it can be noted that at least one coated specimen of each substrate did not fail during the duration of the test.

Some specimens, USI (3), MS (4) and LAS II (1), were used for testing the effect of ratio between corroded and non-corroded areas because their impedance response only showed characteristics typical of an almost perfect coating, this was despite the corrosion which was observed on the substrate. The results are presented in the next section.

Two specimens showed unusual behaviour. One, MS (1), had the connecting screw unprotected thus allowing the corrosive solution to preferentially attack the screw. The other specimen, LAS II (2), was electrically disconnected. Two other specimens, A36 (1) and USI (1), were removed from solution after 250 days immersion, and allowed to dry for 10 days in a desiccator over silica gel. Although no significant changes were observed upon re-immersion of the specimen USI (1), due to its highly resistive coating at the time of removal, re-adhesion seemed to have occurred in the case of the A-36 (1). Because of that, the time of failure for this latter specimen was delayed. Thus these two specimens were not considered to have been exposed under the same conditions for the duration of the test. For comparison purposes only specimens which were exposed at the same conditions for the whole test will be considered.

Figures 4.67 to 4.70 show the variation in R_{pf} values with immersion time for the following substrates A-36, USI, MS, and LAS II, respectively. The coating

resistance, R_{pf}, was obtained from the intersect of the high frequency semi-circle with the real axis, or as the chord AC shown in Figure 3.33, in the case of depressed semi-circles.

TABLE 4.2 - Time for coating failure and decay in resistance.

Substrate	time for $R_{pf} \leq 10^6$ Ω.cm^2 (days)	time for failure (days)	Observations
A-36 (1)	250	420	removed at 250 days and re-immersed 10 days later
A-36 (2)	40	150	
A-36 (3)	$>10^6$ Ω.cm^2	did not fail	capacitive behaviour most of the time
A-36 (4)	200	390	
A-36 (5)	100	180	
USI (1)	330	500	removed at 250 days and re-immersed 10 days later
USI (2)	90	250	
USI (3)	test of area effect at 390 days	-	did not fail
USI (4)	330	500	
USI (5)	200	500	
MS (1)	-	-	no electric connection
MS (2)	200	350	
MS (3)	390	$\geq 10^6$ Ω.cm^2	did not fail
MS (4)	test of area effect at 350 days	-	
MS (5)	180	350	
LAS II (1)	test of area effect at 360 days	-	
LAS II (2)	-	-	connecting screw corroded
LAS II (3)	35	450	
LAS II (4)	200	$\geq 10^6$ Ω.cm^2	did not fail
LAS II (5)	300	$\geq 10^6$ Ω.cm^2	did not fail

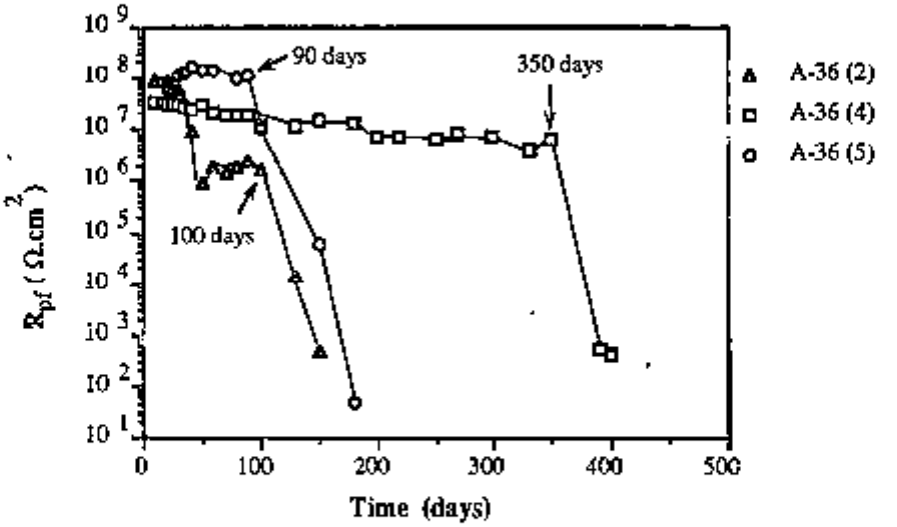

Figure 4.67 - Progress of R_{pf} with immersion time for A-36 specimens.

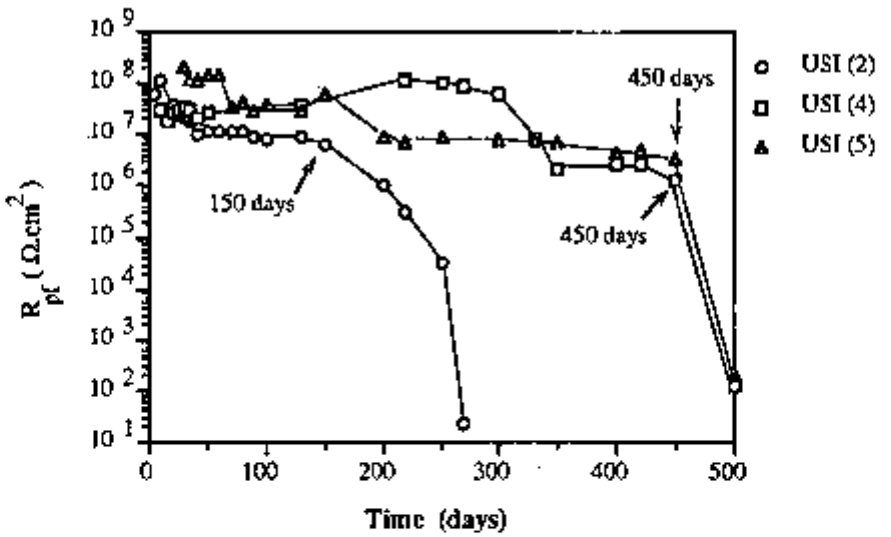

Figure 4.68 - Evolution of R_{pf} with immersion time for USI steel substrates .

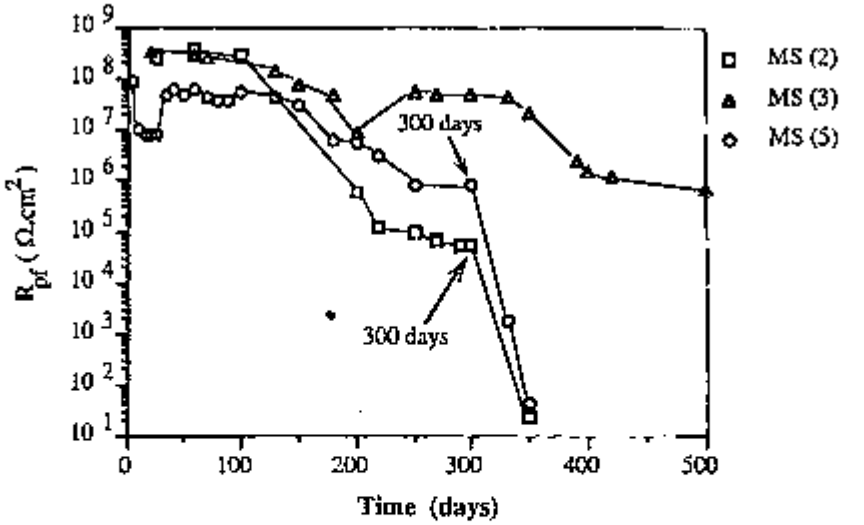

Figure 4.69 - Changes of R_{pf} with immersion time for MS specimens .

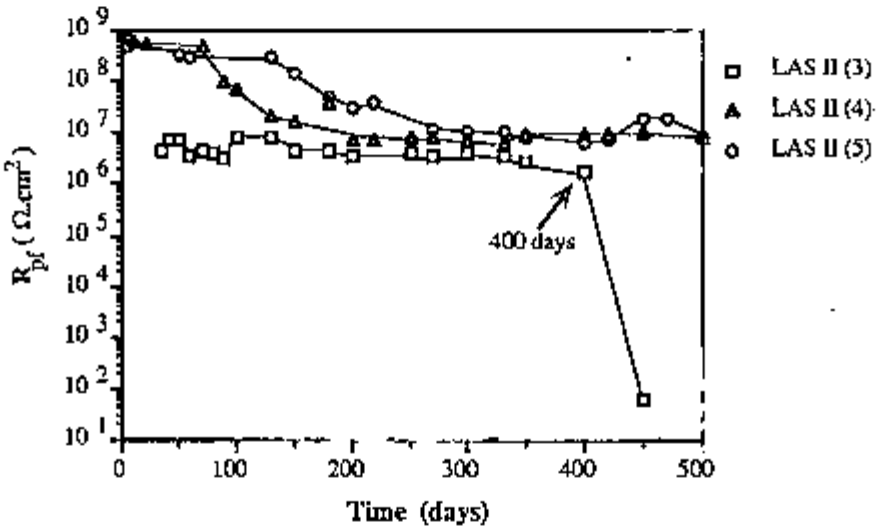

Figure 4.70 - Development of R_{pf} with immersion time for LAS II specimens .

Only a single coated LAS II substrate failed during the immersion period. The two other LAS II specimens shown in Figure 4.70 simply showed a slight decrease in R_{pf}, but the coating on these specimens was still very protective, having a R_{pf} value of the order of $10^7 \Omega.cm^2$, when the test was terminated. Comparatively, the coated system corresponding to the A-36 steel substrate showed lower failure times. All three A-36 specimens presented in Figure 4.67 failed at times less than 400 days. The coated substrates, MS and USI, produced intermediate behaviour between the two other steels, A-36 and LAS II. Two of the coated USI steel specimens, USI(4) and USI(5), failed at times of approximately

500 days and a third specimen, USI(2), failed at nearly 250 days. Even though two MS coated specimens, MS(2) and MS(5) had failed at approximately 350 days, a third specimen, MS(3), did not fail during the test period.

In general an arrest in the decrease of coating resistance occurred after a slight and initial decline was observed. A plateau in the log R_{pf} vs time curve was then obtained. The values of the plateau resistance seemed to correlate well with the extent of corrosion for long term exposure. The initial values of R_{pf}, however, did not usually show any correlation with long exposure behaviour of the coated specimen.

The time τ at which a final and steady decrease in the coating resistance to values $\leq 10^3$ $\Omega.cm^2$ started, is tabulated in Table 4.3 for the various specimens compared.

TABLE 4.3 - Time, τ, when the final drop in R_{pf} started.

Substrate	τ (days)
A-36 (2)	100
A-36 (4)	350
A-36 (5)	90
USI (2)	150
USI (4)	450
USI (5)	450
MS (2)	300
MS (3)	>500
MS (5)	300
LAS II (3)	400
LAS II (4)	>500
LAS II (5)	>500

From the Table above, it can be deduced that the substrate seems to have an effect on the behaviour of the coated system. While the coating on the LAS II

steel substrate remained very protective most of the time, relatively rapid deterioration of the protective properties of the coating occurred for the substrate A-36. The performance of the coating-substrate system seemed to be ranked in the following order, LAS II>USI>MS>A-36. The criteria used for comparing the performance of the coated substrates was the time for failure and the time for a final drop in R_{pf} to start, τ. It can also be noted that two of the LAS II coated specimens did not fail during the period of the test, eventhough the R_{pf} corresponding to these specimens had dropped to values of the order of 10^6 $\Omega.cm^2$, after 200 and 300 days immersion, which indicates that some deterioration of the system occurred. This supports the idea that even for cases when the coating is losing its protective characteristics, the lower corrosion of the LAS II substrate retarded the complete failure of the system.

4.3.5.2 - Effect of ratio between corroding and protective area of specimen on the impedance response.

Three specimens, LAS II (1), MS (4), and USI (3) were used after different immersion times for investigating the effect of the large protective area of the coating in relation to the small corroding areas on the impedance response of the system. In this experiment it was hypothetised that the active corroding area corresponded to the whole area covered by the black spot, by assuming that the real active area was only slightly different from the measured area. The reason for undertaking this test was that although corrosion was visible on the surface, the corresponding impedance response was one typical of a very protective coating with an enormous resistance. Thus, increasing areas of the specimen were successively masked with a mixture of beeswax and colophony resin, in order to increase the proportion of corroding area in relation to the intact one.

Impedance runs were carried out after each masking step, and the respective responses corresponding to the various specimens used are shown in

Figures 4.71-4.73. It is easily noted from these Figures that two of the specimens above, LAS II (1) and MS (4), produced curves which increasingly bent towards the real axis after the total exposed area was consecutively reduced from 10 cm^2 to 1 cm^2. The high frequency semi-circle for these two specimens was completed when the total area exposed was 1 cm^2. For this exposed area a diffusion tail, related to corrosion processes underneath the coating, was also obtained at the low frequency range. The coating resistance in both cases was approximately 20 $M\Omega.cm^2$, which is still very high. The corroded area for both specimens corresponded to approximately $2x10^{-2}$ cm^2. These observations suggest that the ratio of cathodic to anodic areas affects the impedance response obtained for a coated system which was showing localized corrosion.

Based upon the results obtained for the two specimens, LAS II (1) and MS (4), it can be said that only when the ratio of the cathodic and anodic areas, *r*, was around 50, that the corrosion processes were identified by the impedance response. For *r* ratios higher than that, only the response corresponding to the coating was produced. It is worthwhile mentioning that if the coating resistance is too high, as in the case of the other specimen tested, USI (3) (corroding area also corresponding to approximately $2x10^{-2}$ cm^2), only the coating response will be obtained. For this specimen even when the exposed area was reduced to approximately 0.2 cm^2, only an arc almost parallel to the imaginary axis was obtained, Figure 4.73.

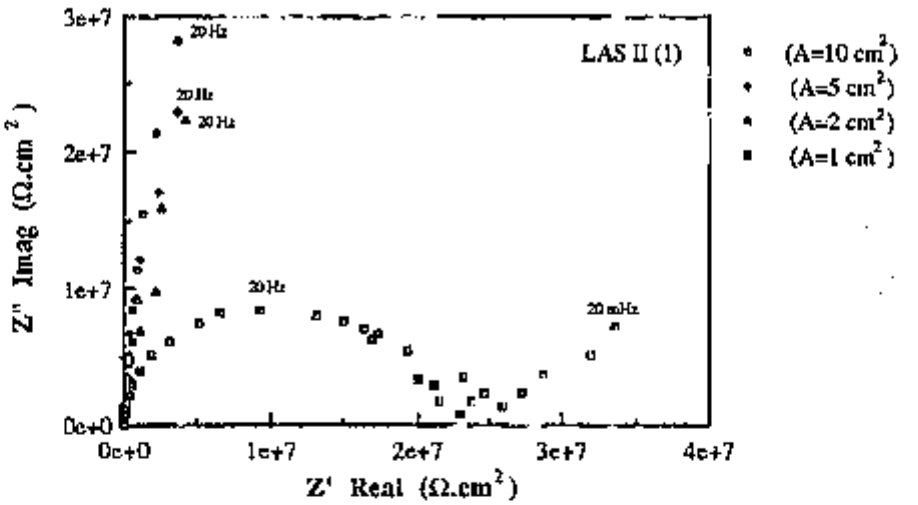

Figure 4.71 - Nyquist plots of specimen LAS II (1) after successive reductions in the exposed area.

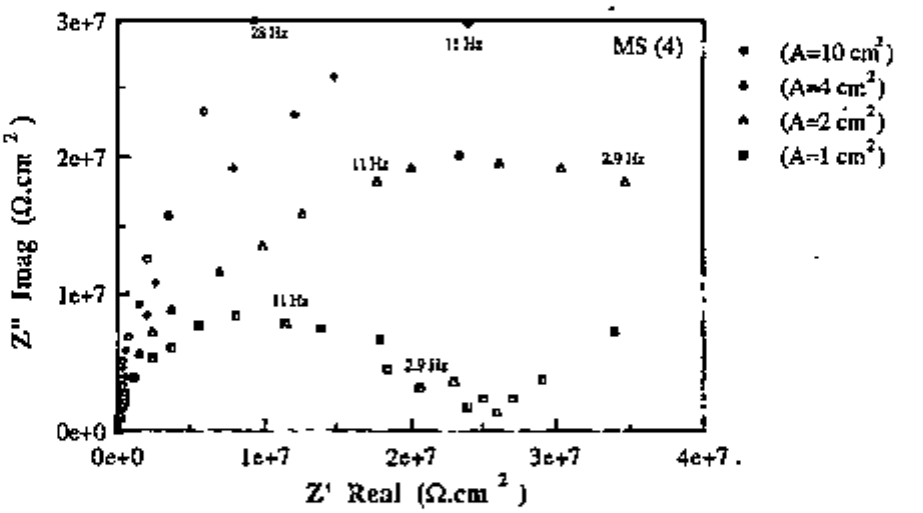

Figure 4.72 - Impedance response of specimen MS (4) after reduction in the exposed area.

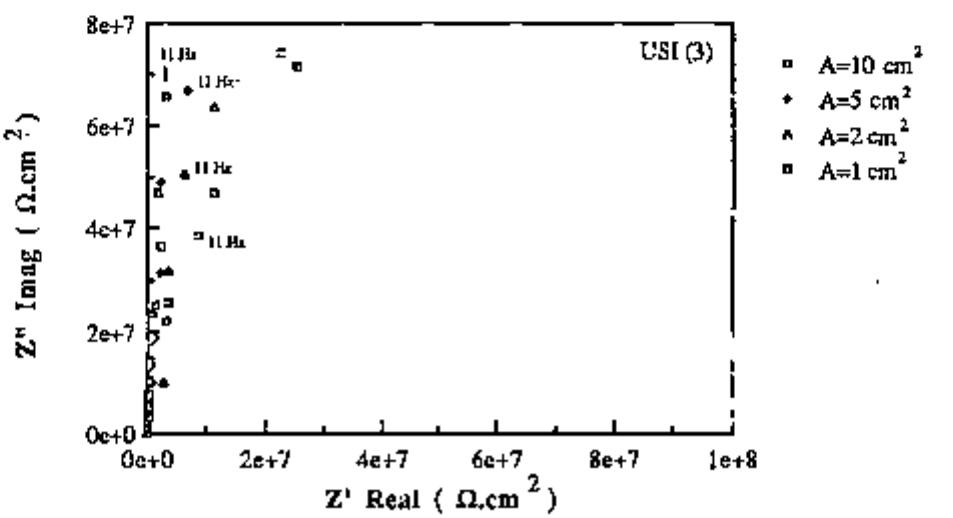

Figure 4.73 - Nyquist plots of sp. USI (3) after consecutive reductions in the exposed area.

4.3.5.3 - Coating capacitance vs time results.

The penetration of water in a coating is known to induce changes in its capacitance. The relative dielectric constant of water (e=80) is much larger than the one corresponding to an organic coating (e=4-8)[71]. Thus the incorporation of water by a coating can be monitored by measuring its capacitance, C_{pf}, using electrochemical impedance measurements. Figure 4.74 shows the coating capacitance as a function of time for the various coated steels during the first hours of immersion. Assuming that the change in coating capacitance is due to the absorption of water by the coating, it can be said that the water uptake is rapid during the first 2 hours of exposure, and a steady value is attained after that. The lack of variation of C_{pf} with time for longer periods is probably caused by the saturation of the coating with water. The fact that alkyd coatings, in general, take up water very rapidly when exposed to aqueous solutions, does not necessarily facilitate the corrosion reaction, because this water is dispersed throughout the coating. It is known that only when water condenses at the coating/substrate interface, providing a medium for the electrochemical process, that it can be considered dangerous[20]. The only information provided by capacitance measurements is regarding the total water in the system. The proportion of that water as an aqueous phase water at the coating/substrate interface, however, is not obtained from these measurements.

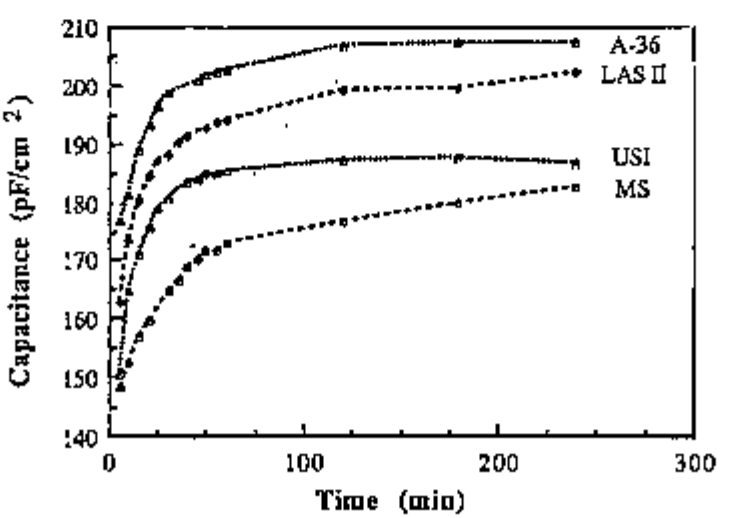

Figure 4.74 - Typical change in C_{pf} of systems used during initial exposure to 3.5% wt NaCl.

The small differences in C_{pf} observed in Figure 4.74 might be attributed to a variation in the microscopic structures of the various coatings, such as different cross-linking densities or defects introduced in the coating during application. The substrate is not supposed to affect C_{pf} in the first hours of exposure.

The values of C_{pf} depend upon both the chemical and physical nature of the coating film, particularly its thickness, chemical composition and microscopic structure[71]. The absorption of water was seen to have a marked effect on C_{pf}, but this is particularly significant in the first hours of immersion, after which steady values of C_{pf} were obtained. In this work, thicknesses and the chemical composition of the coatings used were similar, thus any small differences produced could only have been caused by different microscopic structures generated during coating application and/or curing process. The curing process affects the cross-linking characteristics of organic coatings and can lead to small differences in the coating properties. Organic coatings are usually composed of macromolecular compounds, whose molecules or their part move within certain limits of space volume[209]. The space not physically occupied by the polymer segment corresponds to a free volume or areas of low density, "holes". The "holes" or low density areas generated are probable areas through which species diffuse into the coating. Cross-linking affects significantly the movement of macromolecular units[209]. Coatings with high cross-linking density are expected to provide lesser "free volumes" or low density areas, and consequently have lower rates.

Changes in the coating capacitance of the various systems used are given in Figures 4.75-4.78 for long term immersion in 3.5% wt sodium chloride solution.

The very low values of calculated capacitance, (order of 10^{-10} F/cm^2), obtained in the first days of the test show that the high frequency semi-circle represents the effect of the coating film. Only a single specimen, MS(2), showed

an intermediate arrest in coating capacitance increase. The usual characteristic behaviour of the other specimens corresponded to a large and sharp increase in capacitance, once the protective characteristic of the coating deteriorated and corrosion became general over the substrate. The accumulation of aqueous phase water at the interface can be one of the causes of the increase in capacitance. Changes in coating capacitance after prolonged times of immersion for the various specimens might also be due to a change in the structure of the film under the action of the electrolyte which penetrates the film to the metal surface through the existing pores in the film. The penetration of the electrolyte in itself is known to induce a change in the capacitance of the coating due to the different dielectric constant of the organic coating and that of the electrolyte[14].

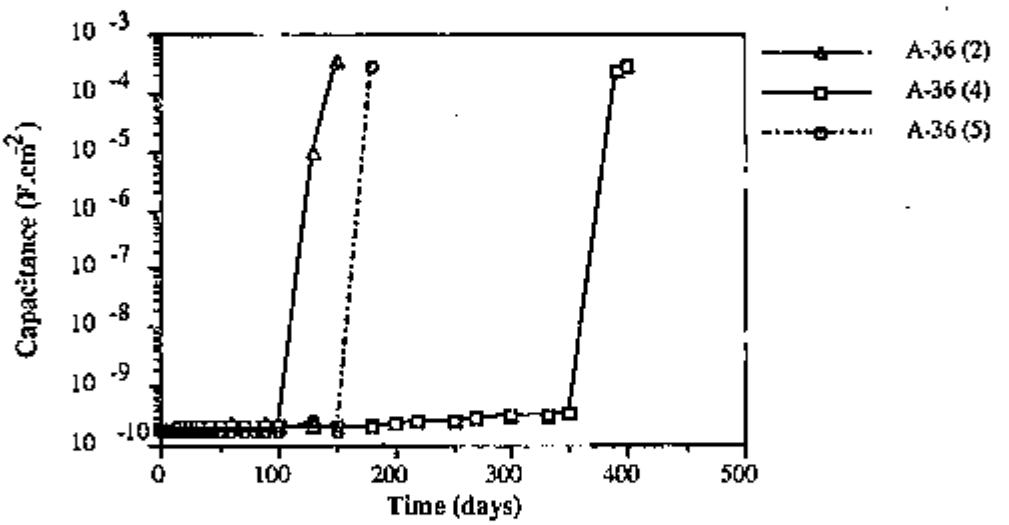

Figure 4.75 - Evolution with time of the capacitance for coatings on A-36 steel.

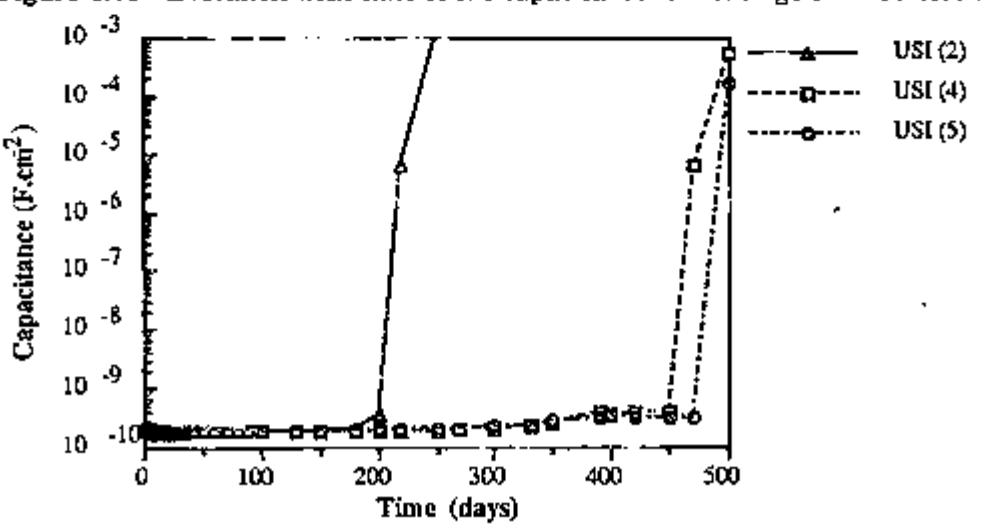

Figure 4.76 - Changes in the coating capacitance with immersion time for coated USI systems.

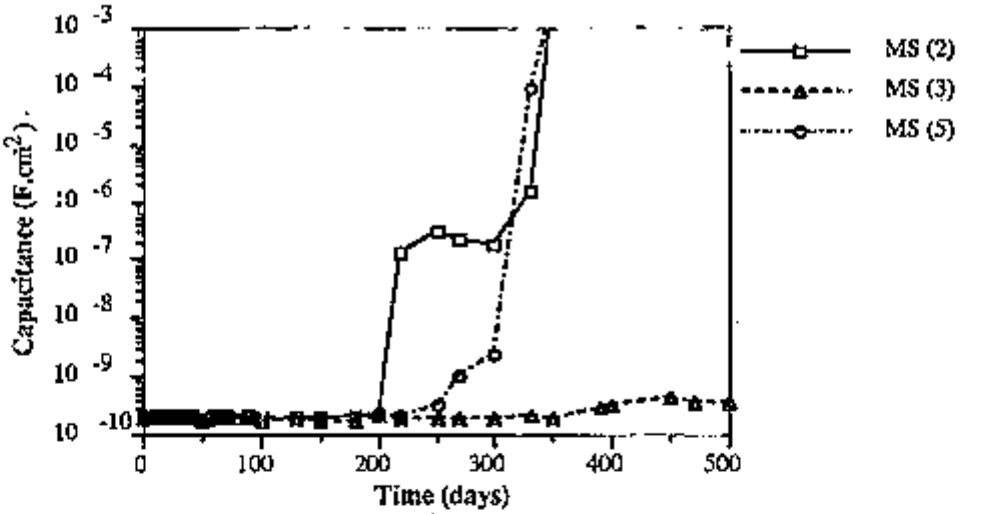

Figure 4.77 - Evolution with time of the coating capacitance on MS steel specimens.

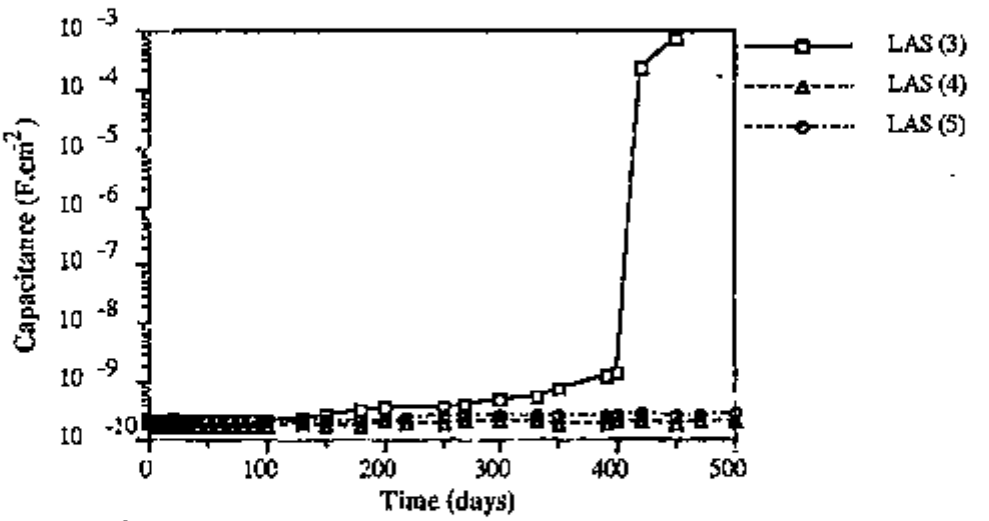

Figure 4.78 - Progress of C_{dl} with time for coated LAS II steel substrates.

If large quantities of water are introduced into the coating, its dielectric constant increases and channels are formed along the chains of the film forming macromolecules, through which large hydrated ions can penetrate[209]. This is generally followed by a large increase in the coating capacitance and the generalisation of corrosion all over the surface.

When water is not allowed to accumulate at the interface, corrosion does not spread all over the surface. This seemed to be the case with specimen A-36 (3), for which the coating capacitance was practically constant during the whole test, Figure 4.13. Values of the order of 10^{-10} F.cm^{-2} were maintained for this specimen until the end of the test.

From the data presented above it can be assumed that if the evolution with time of the coating capacitance and coating resistance are compared as a criteria for detection of deterioration of the protective characteristics of the coating, the changes in the coating/substrate system are easily and first detected by analysis of the coating resistance. However, the analysis of the coating capacitance with time seem to provide accurate coating failure times.

4.3.6 - X-Ray Photoelectron (XPS) and Auger Spectroscopy results

A coated substrate corresponding to LAS II was left for 100 days immersed in 3.5% wt NaCl. At that time, the only corrosion characteristics on that specimen corresponded to three small corrosion spots surrounded by small delaminated areas, Figure 4.79.

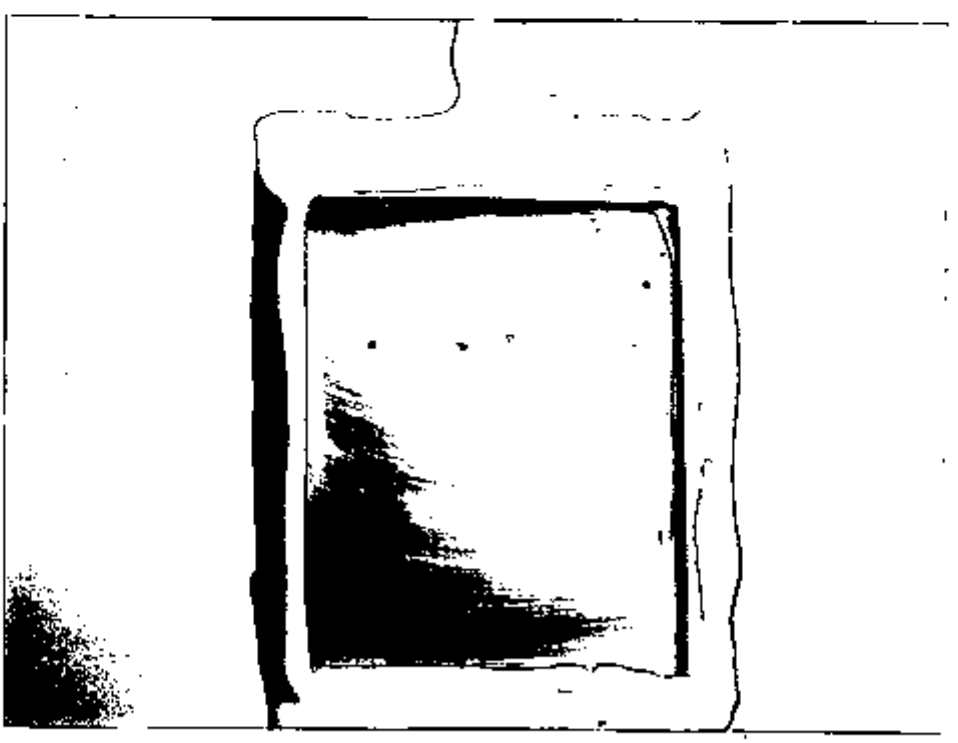

Figure 4.79 - Specimen LAS II after 100 days exposure to 3.5% wt NaCl.

After 100 days immersion the specimen was removed from solution and surface analytical techniques were applied to investigate the chemical composition of one of the corrosion spots and the interfacial regions surrounding it. For this purpose the coating was peeled off, being easily removed from the delaminated area. Figure 4.80 illustrates the regions analysed by XPS and Auger techniques. The small dark spot corresponded to the site of the anodic reaction, and the lighter coloured regions around it represent the regions where the cathodic reaction took place with the development of an alkaline environment.

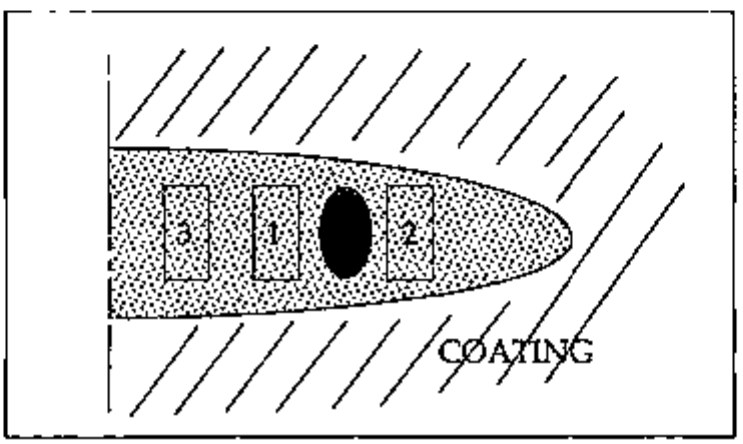

Figure 4.80 - Regions of specimen analysed by XPS and Auger Spectroscopy.

Elemental surface compositions for the regions analysed are summarized in Table 4.4 .

TABLE 4.4 - Elemental surface compositions XPS (Atomic(%)) of regions analysed.

Element Identified	Top of coating	Region (1)	Region (2)	Region (3)
C 1s	91.9	68.1	67.6	66.3
O 1s	8.1	11.3	10.0	12.6
Fe 2p	...	9.9	12.2	16.0
Na 1s	...	10.7	10.1	5.1

It is noted from the Table above that the Na content is reduced by nearly half when moving from regions (1) and (2) to region (3). This is probably

explained by the alkali generation at the cathodic regions adjacent to the corrosion area, which subsequently moves to more remote areas, leading to the spread of the disbonded area. The fact that C and O species were detected on the substrate surface after the peeling off the coating, indicates that either the resin degradation occurred near the coating/substrate interface, or the disbonding was not uniform and coating residue was left on the surface.

The peaks O 1s and C 1s corresponding to regions (1), (2), and (3), were split. This could have been caused by a chemical shift or differential charging. Auger Spectroscopy analysis undertaken over the centre of corrosion spot and the areas around it indicated much less C on the corrosion spot than on the surrounding areas. Thus differential charging was unlikely. Chemical shift, on the other hand, could be a consequence of attack of the coating by alkali. No significant differences were found among the characteristics of the O 1s and C 1s peaks in the 3 regions. The coating on the unaffected area, Figure 4.81 (a) and (b), produced only a peak for each element, C 1s or O 1s, shifted by approximately 3.5eV (C 1s) and 4.2eV (O 1s) indicating the type of coating used. A peak corresponding to Na 1s was obtained at BEs around 1072.5 eV, in the disbonded regions, also suggesting that this could be related with sodium hydroxide species. Figure 4.82 (a) and (b) illustrates the response referent to the region (1). A first peak occurred at binding energies (BE) of approximately 285 eV, generally due to carbon bound to itself and/or hydrogen[199]. A second peak was noted at BE of 289.3 eV, and this is usually associated with carboxylic acid or ester. Therefore, this second peak is probably associated with the coating. Oxygen induces shifts to higher BEs by approximately 1.5 eV per C-O bond, and thus -COOH causes a shift of nearly 4.5 eV in the C 1s BE corresponding to C-C or C-H. The O 1s XPS spectra produced a first peak at BEs of 532.2 eV typical of most oxygen functional groups, and a second one at BE values around 533.5 eV. Ester oxygen in carboxyl groups causes a shift in the O 1s peak to values around 533.5 eV, and this supports the view that the second O 1s peak refers to the coating.

Increases in the relative concentration of carboxyl groups in the coating with increasing oxidation, have been associated with enlarging shifts in the O 1s peak [199]. Peaks detected in the range 531-534 eV could also suggest a variety of forms of chemically and physically bound water, oxygen and hydroxyl.

A series of maps of the elements C, Fe, Na, and O on the corroded and the disbonded areas are shown in Figure 4.83. High concentrations of the element analysed are represented by the orange colour. It is seen from this Figure that Na was detected at the centre of the corrosion spot in relatively large concentrations. This observation indicates that corrosion in this case, might have started at a weak point in the coating film. This faulty region would represent an area of low ionic resistance, where the penetration of ions would have been easier. Since alkyd resins are cationic selective, the diffusion of Na^+ ions at weak points would be expected. Na species were also detected at the disbonded areas, meaning that the formation of alkali by the cathodic reaction was the probable cause for disbonding. The other elements identified on the corrosion spot corresponded to Fe and O from the corrosion product.

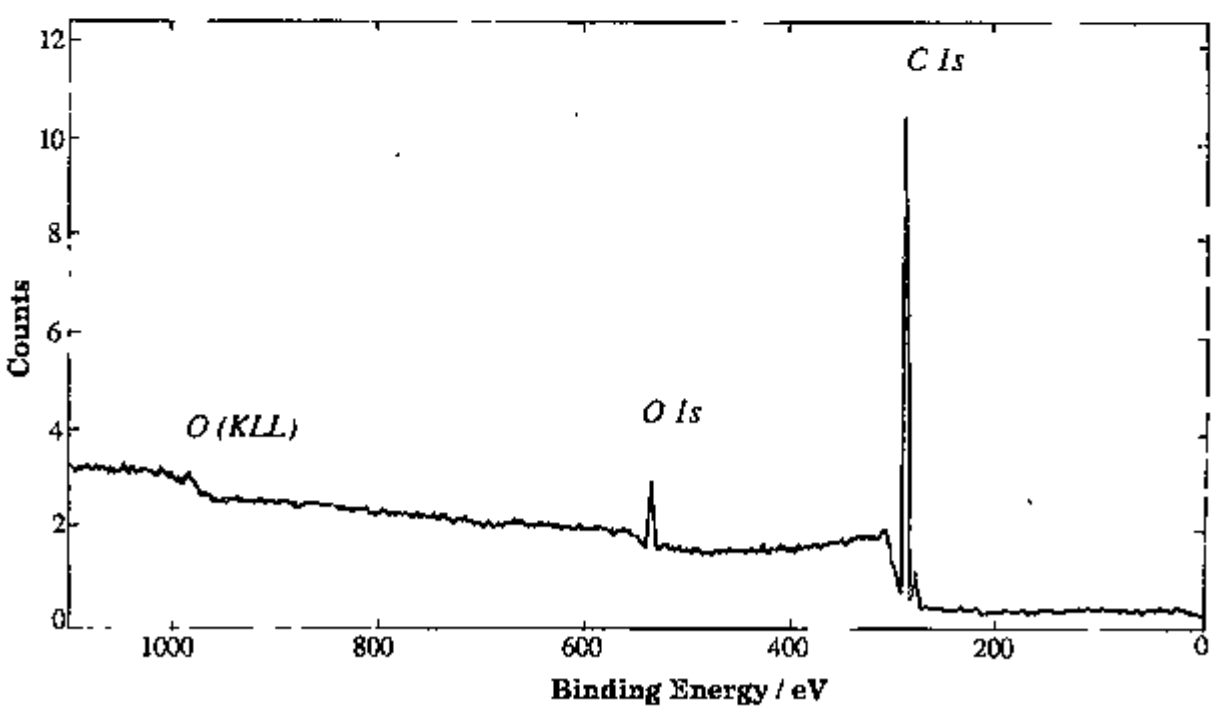

Figure 4.81 - XPS Spectra on unaffected area.

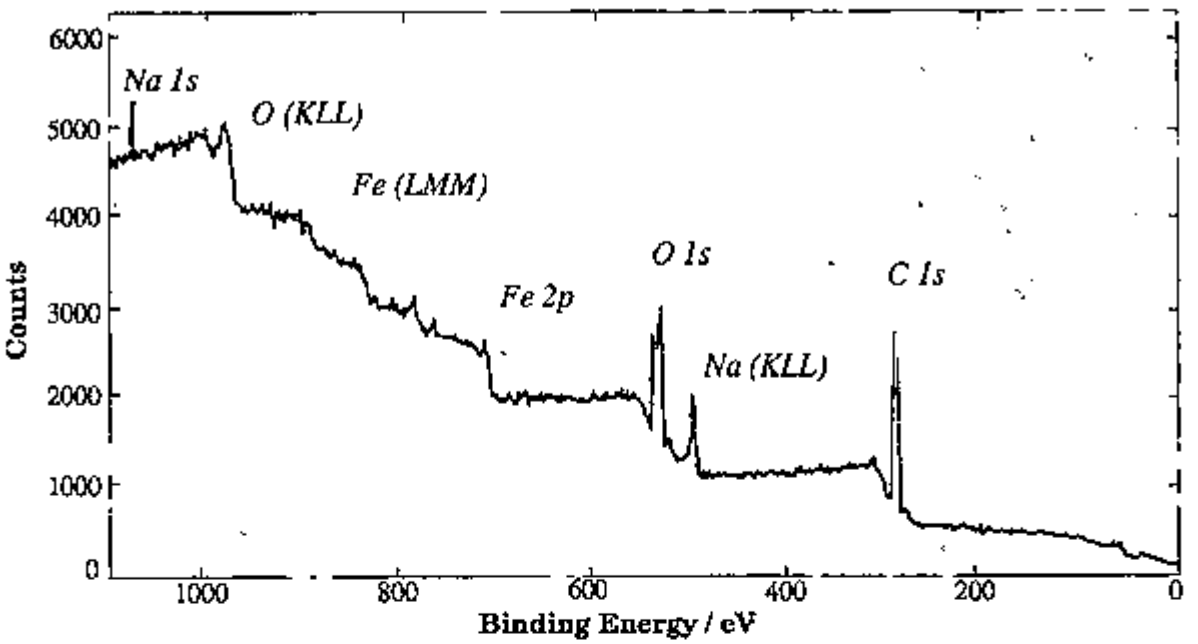

(a)

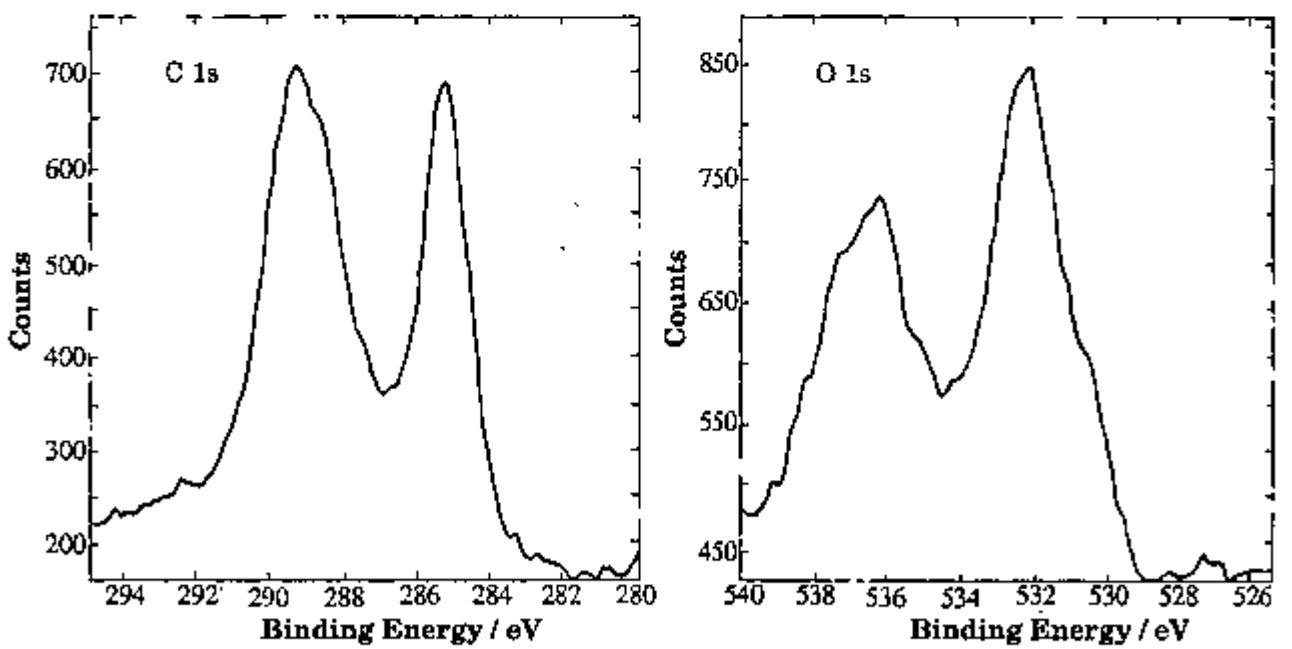

(b)

Figure 4.82 - XPS analysis on (Region-1); (a) whole spectra, (b) C 1s and O 1s spectra.

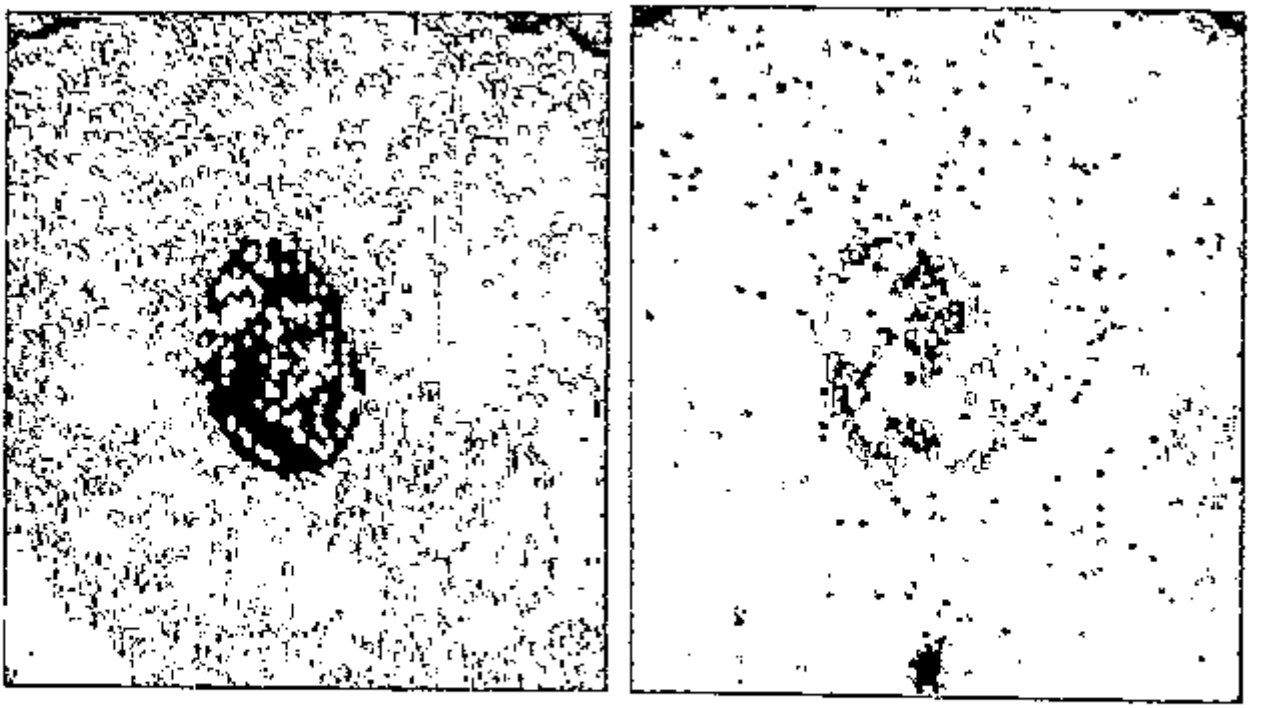

C(KLL) Fe(LMM)

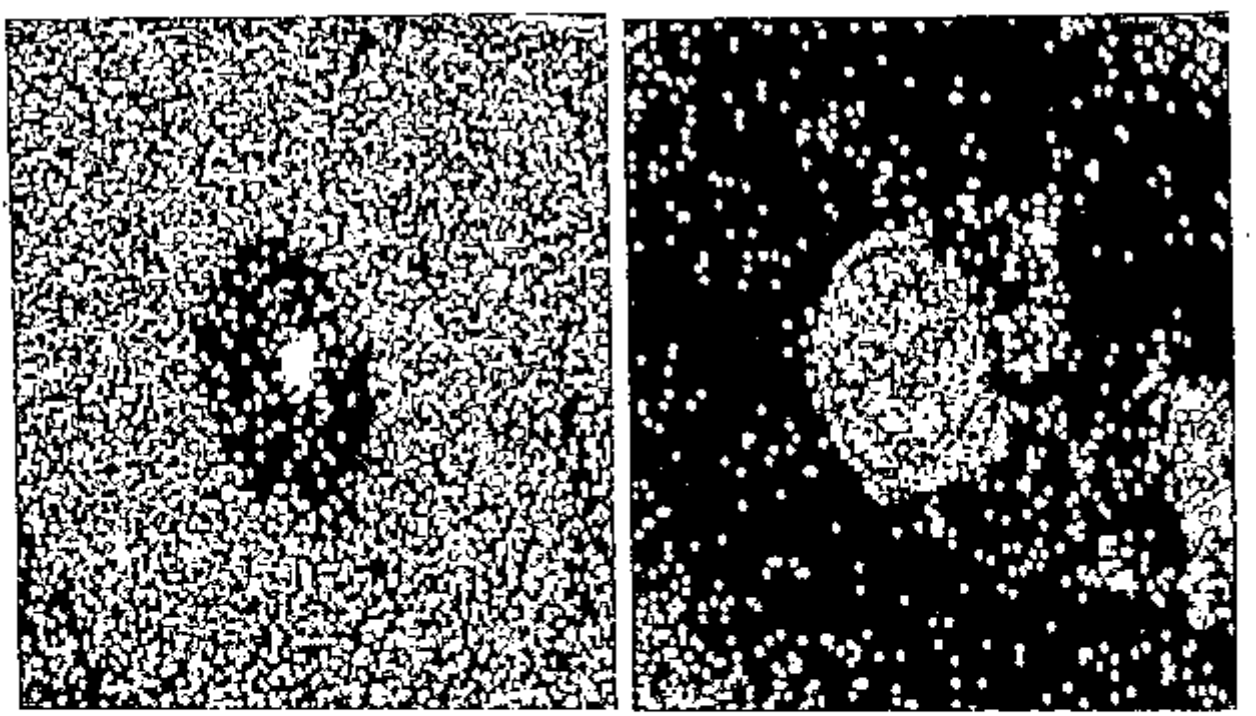

Na(KLL) O(KLL)

Figure 4.83 - Auger maps of C, Fe, Na and O on the corrosion spot and disbonded area around it.

Another specimen also corresponding to LAS II coated substrate, was analysed by XPS and Auger Spectroscopy, after immersion for 110 days in the same corrosive solution. The spot analysed is shown in Figure 4.84. The coating was peeled off before analysis and it was easily removed from the areas corresponding to the darker ring surrounding a lighter centre. The ease of removal of the coating from the darker region was a result of cathodic disbondment caused by the generation of alkali. Large concentrations of Na species were associated with that area, since Na^{2+} ions diffused to the region to neutralise the charge effect caused by the production of OH^- by the cathodic reaction, Figure 4.85(a). The removal of coating, exposed the bare metal which was protected from corrosion by the alkaline environment, Figure 4.85(b). The centre of the analysed spot corresponded to the anodic region where the formation of corrosion products occurred. Some contribution of the coating was still detected on the centre of spot, indicating that the corrosion product confered adhesion between coating and substrate, Figure 4.85(a). The presence of oxide and hydroxide was also detected by XPS analysis on the disbonded area around the corrosion spot, Figure 4.86.

Figure 4.84 - Spot analysed by XPS and Auger Spectroscopy analysis.

(a) (b)

Figure 4.85 - (a) XPS maps of carbon (red) and sodium (green) and, (b) map of Fe on the spot analysed.

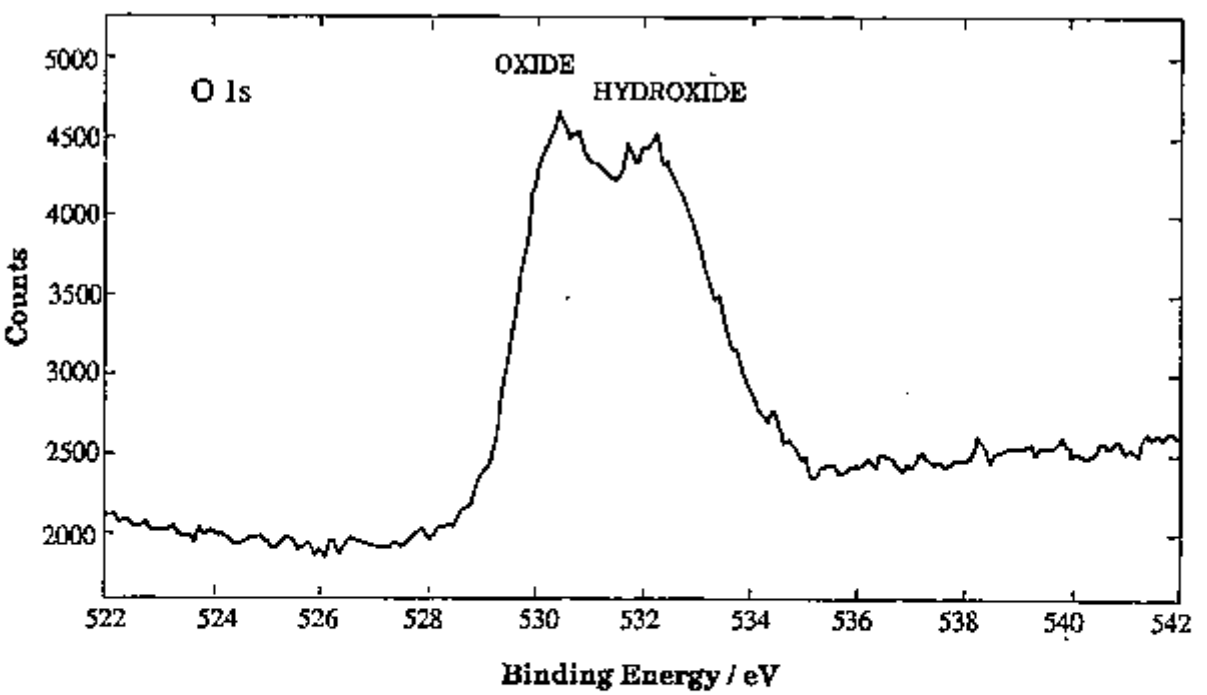

Figure 4.86 - O 1s XPS spectra at disbonded area showing the contributions of oxide and hydroxide.

4.4 - General Discussion

At the beginning of the immersion period an arc running almost parallel to the Z" axis was produced for most coated specimens indicating an initial highly protective coating. This also indicates that the coating on the specimens used was not grossly defective, and there was no significant ionic transport through the coating.

For the coatings which maintained their protective characteristics during all the test, the substrate did not seem to have affected the performance of the system. This is expected since the coating in these cases works as an almost "perfect barrier" to the corrosive environment. Unfortunately, this rarely occurs in practice and defective coatings are usually found. Defects can also develop during the service lifetime of coatings. In these common cases, "non-perfect" coated systems, the substrate electrochemical properties is believed to affect the corrosion characteristics of the system. In the cases where R_{pf} decreased with time, it is considered that the corrosion process at the interface enhanced conduction through defects in the coating. Thus, substrates more susceptible to corrosion would result in lower times for failure of the coated system.

One of the possible reasons for the excellent properties of some coatings, even after long periods of exposure, might have been their high cross-linking density resulting from a complete cure of the coating. This was supported by the great difficult in removing it from the substrate, either mechanically or chemically. Proper coating application after adequate surface preparation might have been the cause for the resulting outstanding coating characteristics obtained.

It can be said that all experiments used in testing the corrosion characteristics of the coated systems are greatly dependent on the perfection of the coating. Obtaining or preparing films without defects is always difficult. So results should always report on the reliability of the test based on their reproducibility.

Some specimens produced an increase in the values of R_{pf} at certain times, and this is attributed to pore or defect blockage by corrosion products. An increase in R_{pf} was generally seen after the disappearance of the faradaic response at the low frequency range. For cases where the low frequency response corresponded to a Warburg diffusion impedance 'tail', it suggested the growth of rust spots under diffusion control.

For most specimens tested localized corrosion was noted and these were associated with small brown and black corrosion spots. These corresponded to the location of the anodic reaction. In some cases the corrosion spot was surrounded by a delaminated area which represent the regions where the cathodic reaction took place resulting in the development of an alkaline environment. The presence of Na and hydroxide species at the disbonded areas, detected by Auger and XPS analysis, supports the view that disbonding was caused by the production of alkali.

Generally the corrosion of coated metals has its first step as the result of a galvanic effect with the anodic reaction being located at the bare metal exposed at a paint defect or 'weak' area, and the cathodic reaction underneath the intact coating. The way the corrosion product acts subsequently is treated differently by three mechanisms. A first viewpoint considers that the corrosion product behaves as inactive areas[211]. A second explanation assumes that the voluminous corrosion products affect mechanically the coating/metal bond, lifting the paint and eventually causing the breakage of the interfacial bond[220]. Finally, a third hypothesis postulates that the corrosion products actively participate in the electrochemical reactions responsible for metal substrate corrosion and subsequent delamination[221].

In fact it is believed that all the three proposed mechanisms might be operative depending on the corrosion product characteristics. When the corrosion product is compact, not voluminous and is covered by FeOOH (brown rust), it might block the access of corrosive species to the underlying metal

without disturbing the bond metal oxide-coating. Since this type of rust is not a good electronic conductor it is not possible for it to take part in the electrochemical reactions and the first mechanism is bound to be prevailing. This mechanism might have been operative in the corrosion of the specimen A-36(3). For this specimen although brown corrosion spots were observed, these still showed the same colour at the end of test (500 days immersion). Voluminous corrosion products were formed on some tested specimens resulting in the lifting off of the coating and subsequent mechanical damage of the interfacial bond. Cases were also found where the delaminated areas were surrounded by black corrosion spots. Magnetite, (Fe_3O_4),the black corrosion product is an electronic conductor and thus might have participated actively in the electrochemical reaction eventually leading to delamination. It is also believed that sulphide inclusions, which are good electronic conductors, can take part in the electrochemical reactions and contribute to the phenomenon of underfilm corrosion. On the other hand, oxide particles which are poor electronic conductors are not expected to be as effective as the sulphide types.

Differences in the general trend shown by coating-substrate systems to resist corrosion failure could only be detected because long term testing was used. The high coating resistance found at the initial period of the test resulted in long immersion periods (> 150 days) for the various systems to fail.

An attempt was made to explain the reasons for the different behaviour exhibited by the various coated substrates, based upon their microstructural characteristics. As mentioned in Section 3.3.4, the microstructure of the various steels used was analysed by Optical Microscopy and Energy Dispersive Spectroscopy. The reasoning for investigating the microstructure characteristics as a possible cause for the differences was that these features after few days immersion were easily revealed in the case of the steel A-36. They were usually associated with small brown and black corroding spots. Small brown spots were also easily identified on two of the coated USI substrate, USI(1) and USI(5). The

common characteristics of these two steels, A-36 and USI, were a relatively larger inhomogeneities content at the surface with larger inclusions compared to MS and LAS II. In fact a great number of the inhomogeneities on the A-36 and USI steels were visible to the naked eye. In the case of the steel A-36, these were aligned in the rolling direction as result of the production process and thus were easily distinguished. Much brighter surfaces were obtained after polishing the steels MS and LAS II compared to the other two steels.

The common type of inclusion for each steel varied according to the steel type. Sulphide types were usually found in the mild steels. In the case of A-36 steel most inclusions corresponded to MnS as shown in Figures 4.87 and 4.88. However, some few inclusions on this steel were also observed to contain Al, Si, Mn, and Fe, and are probably oxides of these elements. On the other hand, the usual inclusions for the low-alloy steels were of the oxide or mixed, oxide-sulphide type. Thus, a relationship seems to exist between the nature, size and content of inclusions, that is the 'cleanliness' of the steel and its performance when coated.

Inclusions or slag particles are undesirable volume defects which are introduced during the production process. They cannot be completely avoided, and can lead to a selective attack. Corrosion processes described as selective attack are localised, and thus can be very penetrating, leading to pitting[8].

Most specimens showed corroding spots and delaminated areas during the immersion time. "Weak" areas of the coating, present initially or developed during exposure to the corrosive environment, allowed localized attack of the substrate and the subsequent production of alkali at the surrounding areas to occur. In these cases the substrate seemed to have an influence on the system behaviour. Considering the value of the resistance R_{pf} as an evaluation of corrosion protection, the order in which the corrosion progressed on the different substrates was as following: LAS II>USI>MS>A-36. It is worthwhile mentioning that the uncoated steel LAS II produced comparatively better corrosion

characteristics under non polarized conditions among the four steels above, see chapter 3, sections 3.3.2 and 3.3.3.

It is therefore proposed that one of the probable reasons for the relatively lower performance of the A-36 substrate when compared to the other substrates is its larger inhomogeneity content, consisting mainly of inclusions of MnS. The presence of inclusions causes the creation of microgalvanic cells when an electrolyte is present. MnS is cathodic to ferrite and as such it works as cathodic reaction sites, and the surrounding metal is hence attacked. When water is allowed to accumulate at the interface in amounts sufficient to cause the breakage of passivity, the presence of MnS there acts as a corrosion stimulating. Sulphide inclusions are much better electric conductors than silicate slags and oxide inclusions, MnS ($k=0.1\Omega^{-1}.cm^{-1}$)[8]. Since inclusions are compositional heterogeneities on the surface, they can lead to localized corrosion. Localised attack is known to be generally initiated by metallurgical factors[200]. In the case of the coated steels used in this work localised corrosion was usually found. This was possible due to the protective characteristics of the coating, which allowed corrosion to initiate at "weak" or defective areas of the coating and be restricted to that particular area, whereas the cathodic reaction occurred at the surrounding areas.

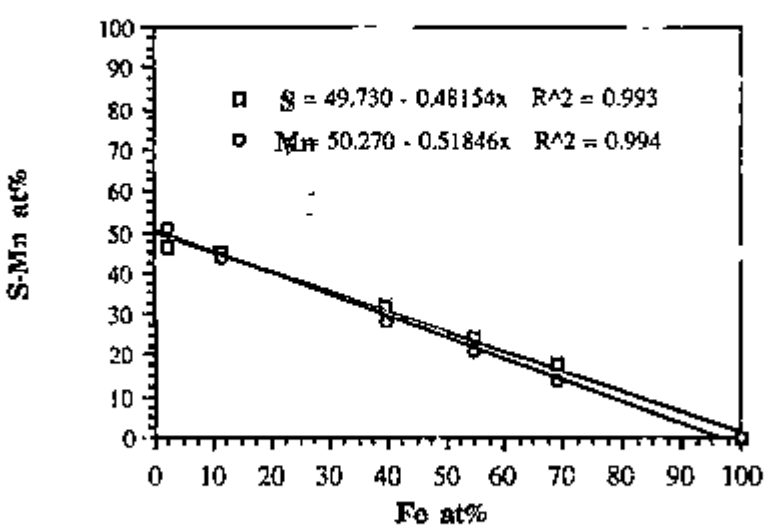

Figure 4.87- Analysis of the inclusions in A-36 type steel.

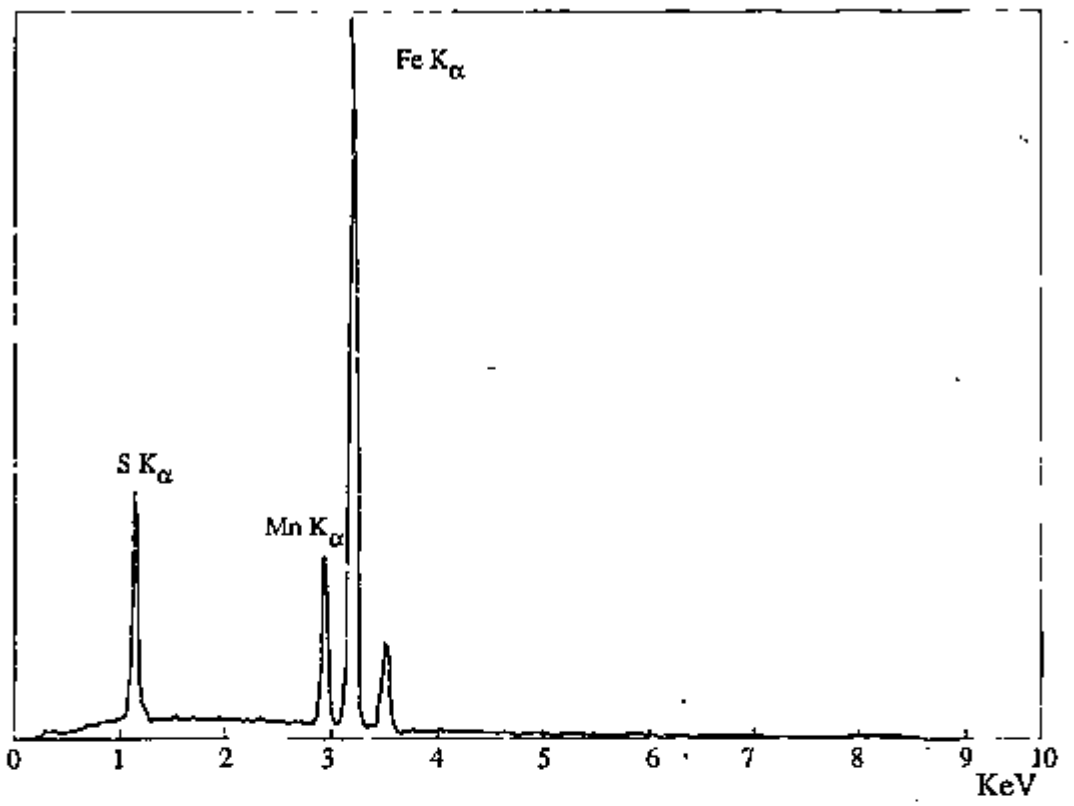

Figure 4.88 - EDX Spectra on the MnS sulphide inclusion.

The following steps have been proposed for the localised corrosion of carbon steels [200], and by analogy this can be applied to this work. The presence of MnS inclusions at the surface is believed to work as further of localized corrosion.

Initially water reaches the coating-substrate interface, and possibly when it is allowed to form a continuous layer, corrosion starts at the anodic sites[208]:

$$Fe \rightarrow Fe^{2+} + 2e^- \quad (4.3)$$

A hydrolysis reaction occurs next, resulting in an increase of the acidity at the region

$$Fe^{2+} + H_2O \rightarrow Fe(OH)^+ + H^+ \quad (4.4)$$

The presence of oxygen at the reaction site promotes the formation of iron (III) ions. The combined iron in the $Fe(OH)^+$ ion, can also be oxidised to a III state, according to:

$$2Fe^{2+} + 1/2O_2 + 2H^+ \rightarrow 2Fe^{3+} + H_2O \quad (4.5)$$

$$\text{or} \quad 2Fe(OH)^+ + 1/2O_2 + 2H^+ \rightarrow 2Fe(OH)^{2+} + H_2O \quad (4.6)$$

The solution is further acidified by more hydrolysis reactions:

$$Fe(OH)^{2+} + H_2O \rightarrow Fe(OH)_2^{+} + H^{+} \quad (4.7)$$

and

$$Fe^{3+} + H_2O \rightarrow Fe(OH)^{2+} + H^{+} \quad (4.8)$$

Magnetite (Fe_3O_4) and rust (FeO.OH), which are the two major corrosion products, are formed from the complex ionic species produced in reactions (4.7) and (4.8):

$$2Fe(OH)^{2+} + Fe^{2+} + H_2O \rightarrow Fe_3O_4 + 6H^{+} \quad (4.9)$$

and

$$Fe(OH)^{2+} + OH^{-} \rightarrow FeO.OH + H_2O \quad (4.10)$$

Corrosion products develop and rise over the corroding site and its surroundings, forming a layer or incrustation which further isolates the environment within the anodic site from the bulk electrolyte. When this occurs, the corrosion process is hindered, and in the case of coated systems, results in an increase in R_{pf}.

As mentioned previously MnS inclusions are strongly cathodic relative to the free metal, and therefore provide ideal nucleation sites for rusting[200]. Besides, manganese sulphide is also susceptible to attack by an acid environment, producing S^{2-} and HS^{-}. Thus, the increasing acidity promoted by reactions (4.8), (4.9), and (4.10) allows the formation of S^{2-} and HS^{-} ions which in turn contribute to further dissolution of iron, since they decrease the activation polarisation for this latter reaction[8]. The increased acidity can also cause the reduction of hydrogen ions by electrons originating from the oxidation reactions. Occasionally hydrogen evolution can lead to the breaking of the crust of corrosion product.

Inclusions of MnS were not detected separately on the low-alloy steels substrate. This does not mean that they are not present, but considering the number of analysis made, if they happen to exist on this type of steel, they are only present in a very minute quantities. Various other types of inclusions were however found on those particular steel, such as silica, alumina, or other oxide

types, for example titanium oxide. These were in many cases associated with MnS inclusions, and generally corresponded to a mixture of the elements Ti, Mn, Cu, S, Al, Si and Cr. It indicates that on this steel the inclusions were mainly composed of oxides, silicates, or a mixture of oxide-sulphides. Oxide inclusions are normally known as slag inclusions, and in general consist of SiO_2 and Al_2O_3, and MnO[8]. When found together, MnO and SiO_2 form manganese silicate. They are not metallic conductors, and therefore cannot act as local cathodes in corrosion cells. However, they affect the corrosion properties of steel in another way. They prevent the formation of passivating oxide films and also decrease the adhesion of protective coatings[8]. This indicates that not only sulphide type inclusions are responsible for a lower corrosion performance of coated systems, although these seem to have a particular detrimental effect. Any type of inhomogeneity at the surface can also lead to inferior corrosion performance. Thus cleaner steels are thought to result in better performance when coated and immersed in corrosive solutions.

4.5 - Summary

In this chapter the long term corrosion behaviour of coated steels under immersed conditions was presented.

The effect of the substrate type on the corrosion behaviour of coated systems was tested. The substrates consisted of four steels, MS, LAS II, A-36 and USI, and the systems on the substrate A-36 produced the lowest corrosion resistance, whereas the coated LAS II specimens showed superior protection.

Differences in the corrosion behaviour of the various coated substrates were only detected by long term testing. Tests of long duration were necessary because the coating resistance was very large at the beginning of the immersion period.

The inferior corrosion characteristics of the coated A-36 substrates were possibly caused by the larger inhomogeneities content, which consisted mainly of MnS inclusions, at the surface of this steel. This type of inclusion is cathodic relative to free metal, providing nucleation sites for rusting. On the other hand, the LAS II was the 'cleanest ' among the steels used. The effect of the higher corrosion property of the substrate LAS II upon the corrosion characteristics of the coated system was demonstrated by the fact that although a significant decrease in the coating resistance was obtained after short periods, the whole coated system exhibited a comparatively good anti-corrosion properties until the test was terminated after 500 days.

Other types of inhomogeneities, oxide or mixed (oxide + sulphide) inclusions type were associated with the low-alloy steels. Even though these are not metallic conductors, they also affect the corrosion properties of coated steels by decreasing the adhesion of protective coatings.

Localized corrosion was generally observed on the various coated specimens used. The presence of Na species on top of a corrosion spot indicates that corrosion was bound to have started at a 'weak' area of the coating, since the coating used was cationic selective.

The very localized characteristics of the corrosion on the various systems tested allowed the blockage of the 'weak' areas of the coating. Consequently an increase in the coating resistance was found after the blockage occurred. This usually took place after the disappearing of the low frequency faradaic response. It is likely that mechanical stresses produced by growing corrosion products may have enlarged defects initially present in the coating. Hence, for a given system coating and substrate, the coating-metal interface most susceptible to corrosion is bound to induce the most rapid decrease in R_{pf}.

The relation between intact and corroding area of the specimens was found to affect the impedance response of the system. For coatings with large proportion of protective area relative to the corroding area, the impedance

response was mainly that of the coating. Increasing the ratio corroding/protective area, however, leads to the appearance of the corrosion response on the impedance plots, provided that the coating resistance is not too large.

Delamination around corroding spots was seen to be caused by the generation of alkalis. This was supported by XPS and Auger Spectroscopy analysis which detected the presence of hydroxide species on those areas.

CHAPTER 5

THE CORROSION BEHAVIOUR OF COATED STEELS EXPOSED TO WET-DRY CYCLES INSIDE CABINET.

5.1 - Introduction

Atmospheric accelerated testing methods such as salt spray are usually employed to evaluate the performance of organic coatings on metal substrates in the laboratory. The outcome of these tests, however, often lack correlation with paint performance observed in real situations[201]. This is particularly true when industrial atmospheres are of concern [202,203]. The reasons for the low reliability of the salt spray tests have been attributed to the lack of species found in the natural atmosphere such as ammonium and sulphate, and to the absence of the effects of wet/dry cycling which are not reproduced in the continuous spray test[204]. Several modifications have been suggested but most of these also have been proved inappropriate for testing organic coatings, since they do not reproduce the modes of coating failure usually found in long-term atmospheric exposure[205]. A solution consisting of 3.25% wt ammonium sulphate and 0.25% wt sodium chloride was recommended by some authors [203,204,206], and these were observed to yield improved correlations with long-term outdoor exposures in industrial environments. Timmins[207] suggested that the dilution of the above mentioned solution would be even more effective. The test procedure adopted by Timmins[207], also named 'Prohesion' test, describes a philosophy which means protection by adhesion and implies that adhesion failure precedes corrosion. The test solution used in this test has been reported as providing an approximate simulation of atmospheric attack on steel[205].

Cabinet tests with controlled atmosphere are considered very useful and reliable if what is required from the accelerated test is only a comparison between various substrates. In this case, even if the simulation in the cabinet is not a good indicator of the atmospheric attack, the test is valuable provided that the results are reproducible. It was with this aim that the cabinet tests were carried out in this research.

5.2 - Experimental

5.2.1 - Specimen preparation

The surface of four steels, MS, LAS II, A-36 and USI, was prepared and subsequently coated as described in Section 4.2.1. An area of 20 cm^2 was exposed to the test environment. Dry coating thicknesses of the various specimens were measured by means of an Elcometer Minitector thickness gauge and the averages of nine readings per panel are given in Table 5.1. Next, the coating was scratched through to the bare steel (scribe marked) to permit the observation of the extent to which film breakdown and corrosion would progress from a line of exposed steel. The scribe mark (X) was done using a sharp and clean scalpel. The aim of this test was to determine whether the resistance of the organic film to undercutting differed with the diverse steel substrates used, and also to accelerate the evaluation of the coating performance on the various substrates.

TABLE 5.1 - Coating thicknesses of specimens exposed to Prohesion test.

Specimen	Coating thickness (μm)			
	MS	LAS II	A-36	USI
1	(26.0 ± 0.5)	(29.8 ± 0.2)	(25.5 ± 0.4)	(23.9 ± 0.5)
2	(25.4 ± 0.4)	(29.7 ± 0.5)	(24.5 ± 0.3)	(24.0 ± 0.4)
3	(24.3 ± 0.6)	(29.6 ± 0.3)	(20.0 ± 0.2)	(26.7 ± 1.1)
4	(20.2 ± 0.6)	(28.1 ± 0.3)	(25.4 ± 0.3)	(21.5 ± 0.6)
5	(24.7 ± 0.3)	(31.6 ± 1.0)	(49.3 ± 1.2)	(29.9 ± 0.8)

5.2.2 - Test method

The test method consisted of exposing the coated panels to an intermittent wet/dry cycle corresponding to 1-hour wet, 1-hour dry in a test cabinet. The test cabinet (~0.32 m^3) comprised a control unit, a compressed air supply, and a salt solution reservoir. Solenoid valves under the control of a time switch selected the wet (salt mist) or the dry (air draught) periods. The feed rate during misting was approximately 600 ml per hour. For reasons of reproducibility, five specimens of each substrate were tested. These were arranged around the periphery of the cabinet which was heated to 35°C during drying and cooled naturally during misting. The specimens were wet within 5 minutes from the onset of misting, and their surfaces were dry at the end of the drying cycle. The solution used was the same as used by Lyon and co-workers[205] and consisted of a mixture of 0.35% $(NH_4)_2SO_4$ + 0.05% NaCl. The test was continued until corrosion had spread over most of the surface.

A cabinet test with wet and dry cycles which employed an aggressive solution simulating the acid rain of Manchester was also carried out. The simulating solution was 10 times more concentrated than that of Manchester rain. The aim of this test was to simulate the atmospheric exposure of coated specimens in the Manchester area or areas of similar atmospheric aggressiveness and also to confer an accelerated character to the test. The composition of the artificial acid rain solution was arrived at after various analysis of the Mancunian rain by a research group at UMIST[224]. This composition is given in Table 5.2.

The pH of the artificial acid rain solution was adjusted to 3.5 with $NaHCO_3$. The wet-dry conditions applied in this test consisted of spraying the solution for 2 hours followed by an 1 hour drying period. The temperature inside cabinet was maintained at approximately 22° C. The testing duration was 35 days and during that period the corrosion features of the scribed specimens were observed. Four specimens of each substrate were tested for reasons of reproducibility. In the

results section, however, only two specimens of each substrate are presented. The specimens used were prepared as described in Section 5.2.1, and their respective dry thicknesses are shown in Table 5.3.

TABLE 5.2 - Composition of Artificial Acid Rain Solution[224].

Constituent	Concentration, mg l^{-1}
H_2SO_4 (98%)	31.85
$(NH_4)_2SO_4$	46.20
Na_2SO_4	31.95
HNO_3	15.75
$NaNO_3$	21.25
NaCl	84.83

TABLE 5.3 - Coating thicknesses of specimens exposed to wet-dry cycles with artificial acid rain solution.

Specimen	Coating thickness (μm)			
	MS	LAS II	A-36	USI
6	(22.8 ± 0.6)	(25.9 ± 0.3)	(20.9 ± 0.3)	(22.5 ± 0.5)
7	(20.6 ± 0.3)	(25.6 ± 0.3)	(21.6 ± 0.6)	(23.3 ± 0.5)
8	(21.1 ± 0.4)	(27.0 ± 0.2)	(22.9 ± 0.2)	(23.6 ± 0.2)
9	(32.5 ± 0.6)	(25.5 ± 0.3)	(29.2 ± 0.6)	(21.5 ± 0.2)

5.3 - Results and Discussion

5.3.1 - Visual observation of specimens exposed to Prohesion test.

The corrosion features of the various scribed specimens with increasing exposure time to the wet-dry mixed Prohesion tests are shown in Figures 5.1 - 5.11. The printing magnification used in these Figures was 1.6X. Although five specimens of each substrate were used for testing the reproducibility of the experiment, only the development of corrosion with time on two samples of each substrate, specimens (1) and (2), will be shown in this section.

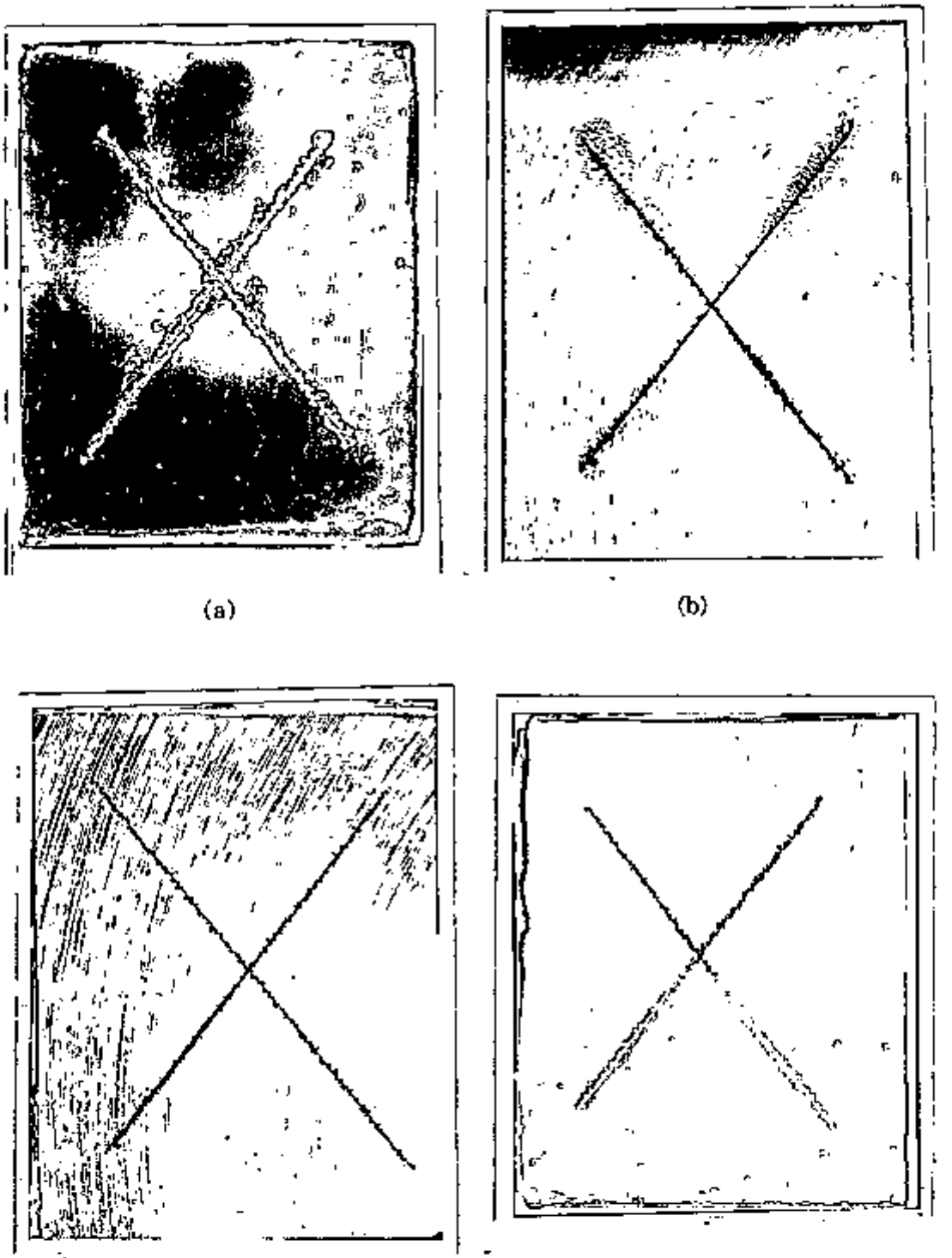

Figure 6.1 - Scribed specimens (1) exposed to cabinet (high sulphate solution) after 1 day (a) MS, (b) LAS II, (c) A-36, and (d) USI.

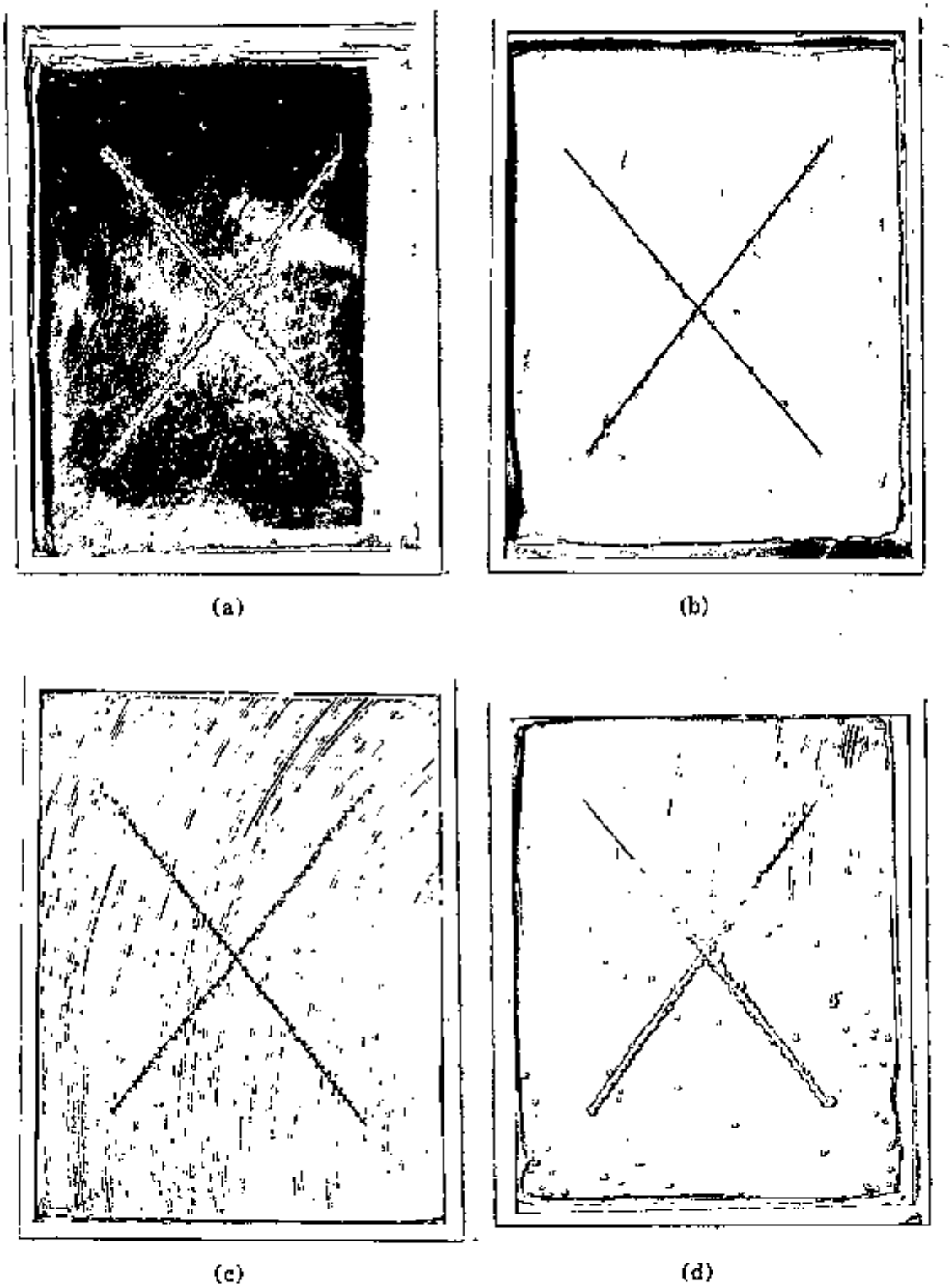

Figure 5.2 - Scribed specimens (2) exposed to cabinet (high sulphate solution) after 1 day (a) MS, (b) LAS II, (c) A-36, and (d) USI.

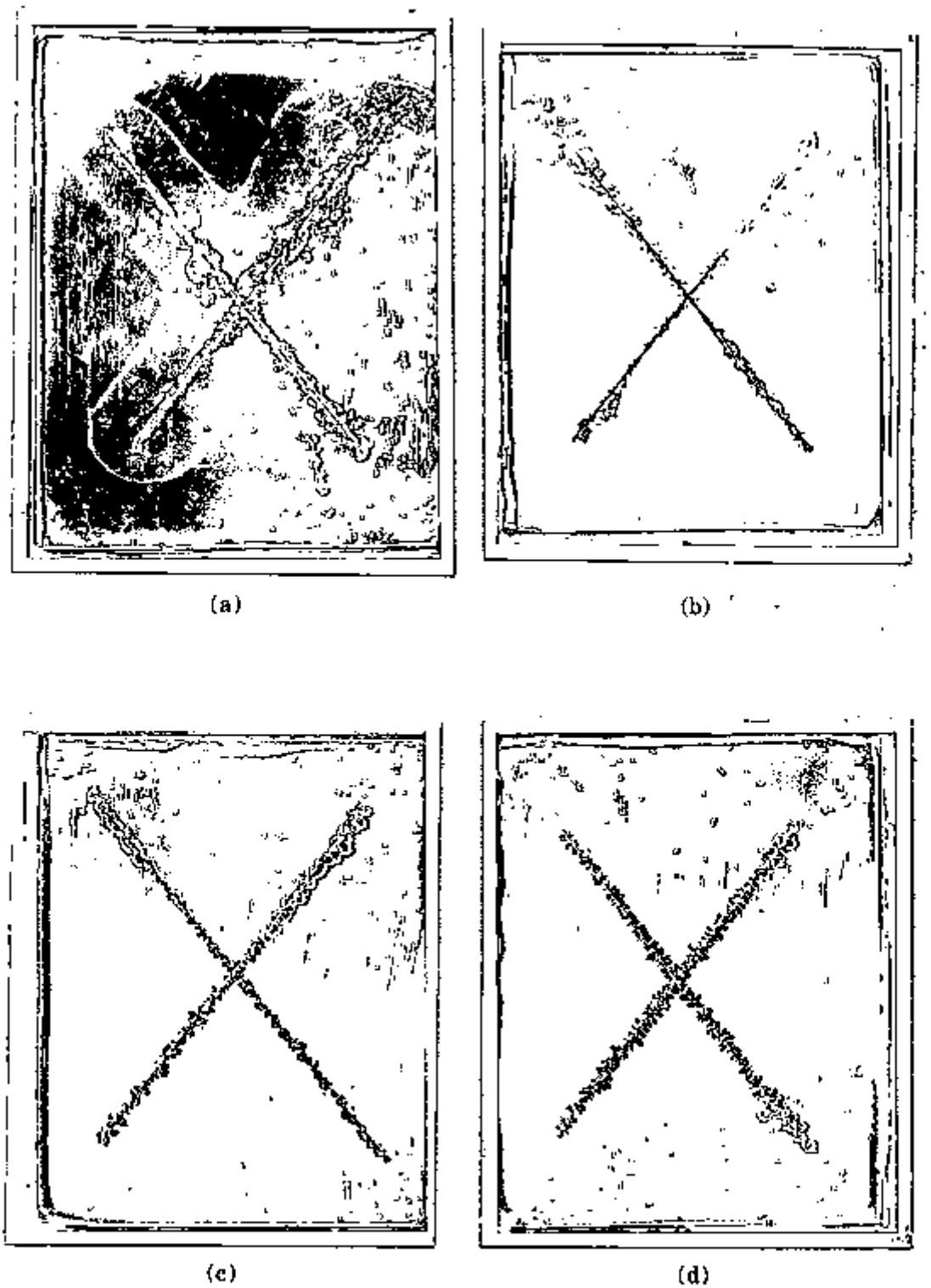

Figure 5.3 - Scribed specimens (1) exposed to cabinet (high sulphate solution) after 3 days (a) MS, (b) LAS II, (c) A-36, and (d) USI.

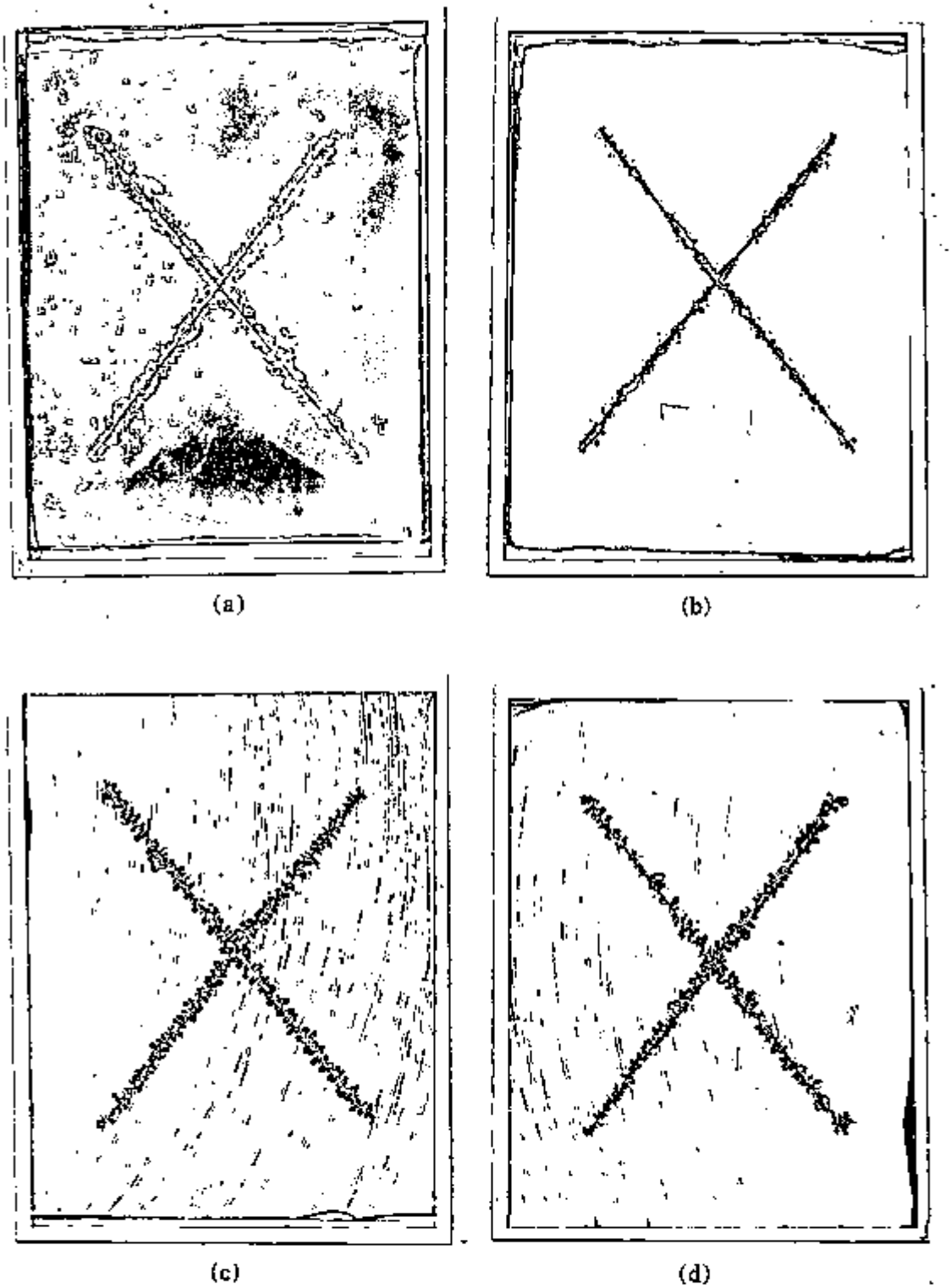

Figure 5.4 - Scribed specimens (2) exposed to cabinet (high sulphate solution) after 3 days (a) MS, (b) LAS II, (c) A-36, and (d) USI.

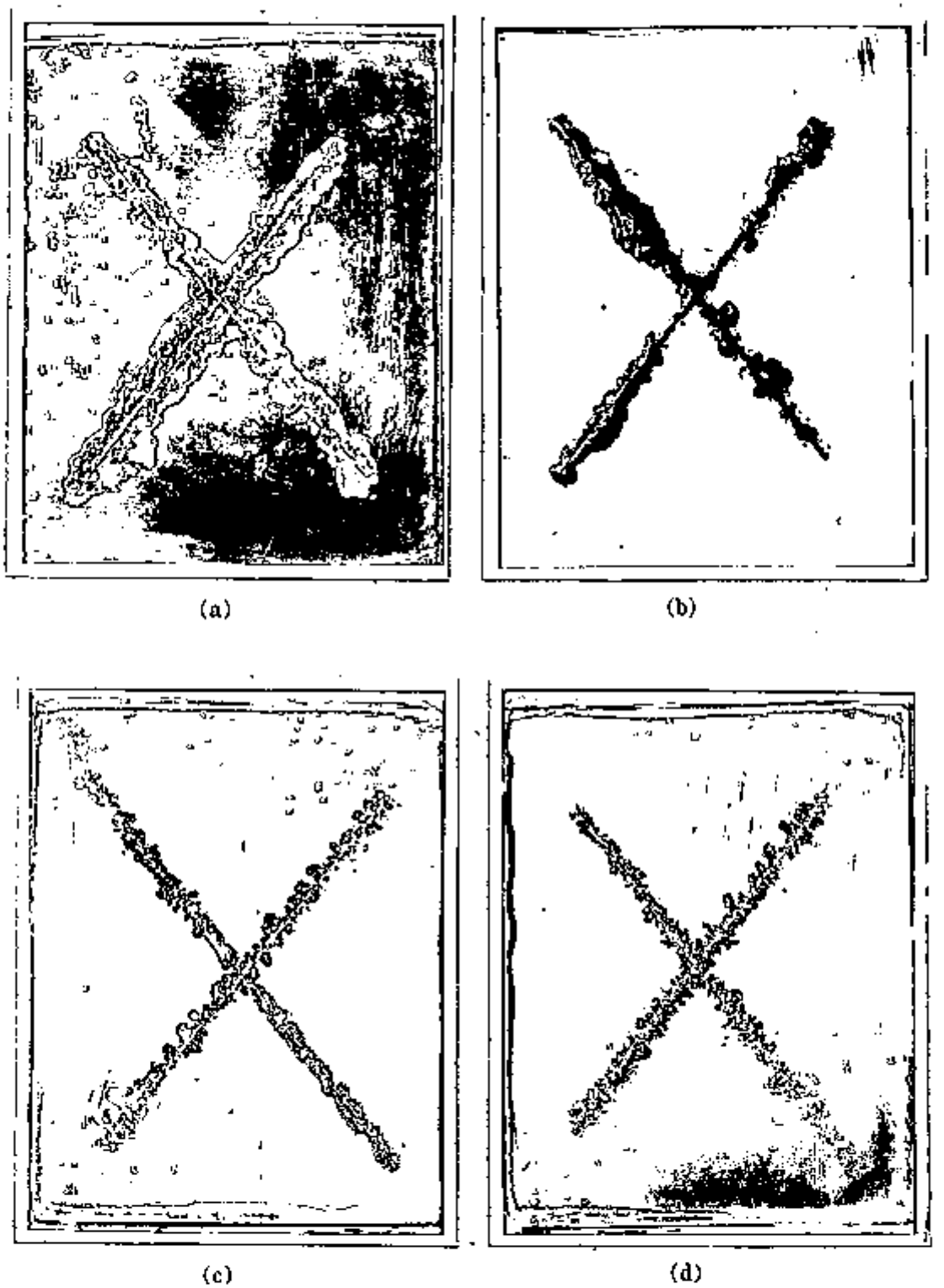

Figure 5.5 - Scribed specimens (1) exposed to cabinet (high sulphate solution) after 6 days (a) MS, (b) LAS II, (c) A-36, and (d) USL

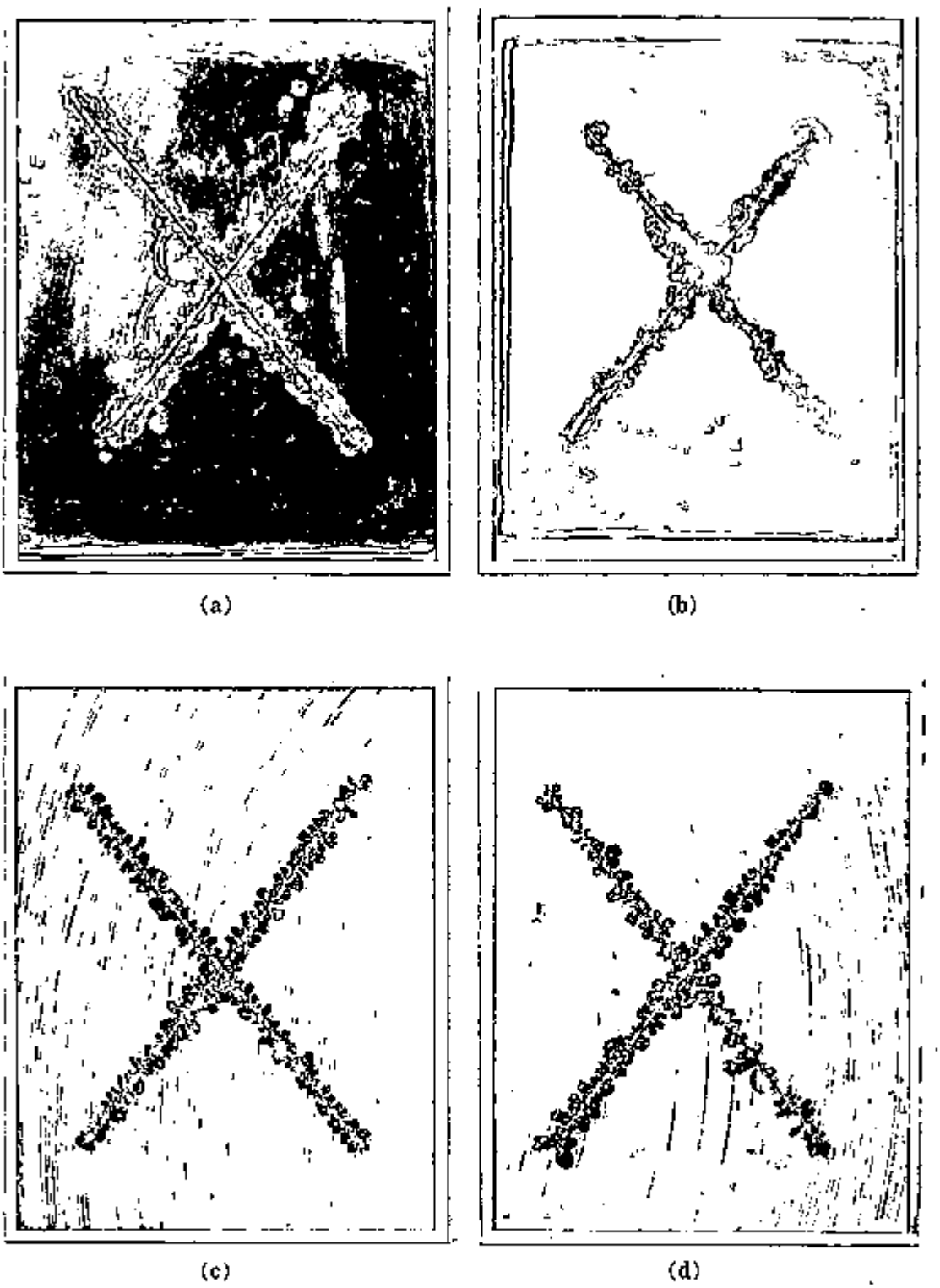

Figure 5.6 - Scribed specimens (2) exposed to cabinet (high sulphate solution) after 6 days (a) MS, (b) LAS II, (c) A-36, and (d) USI.

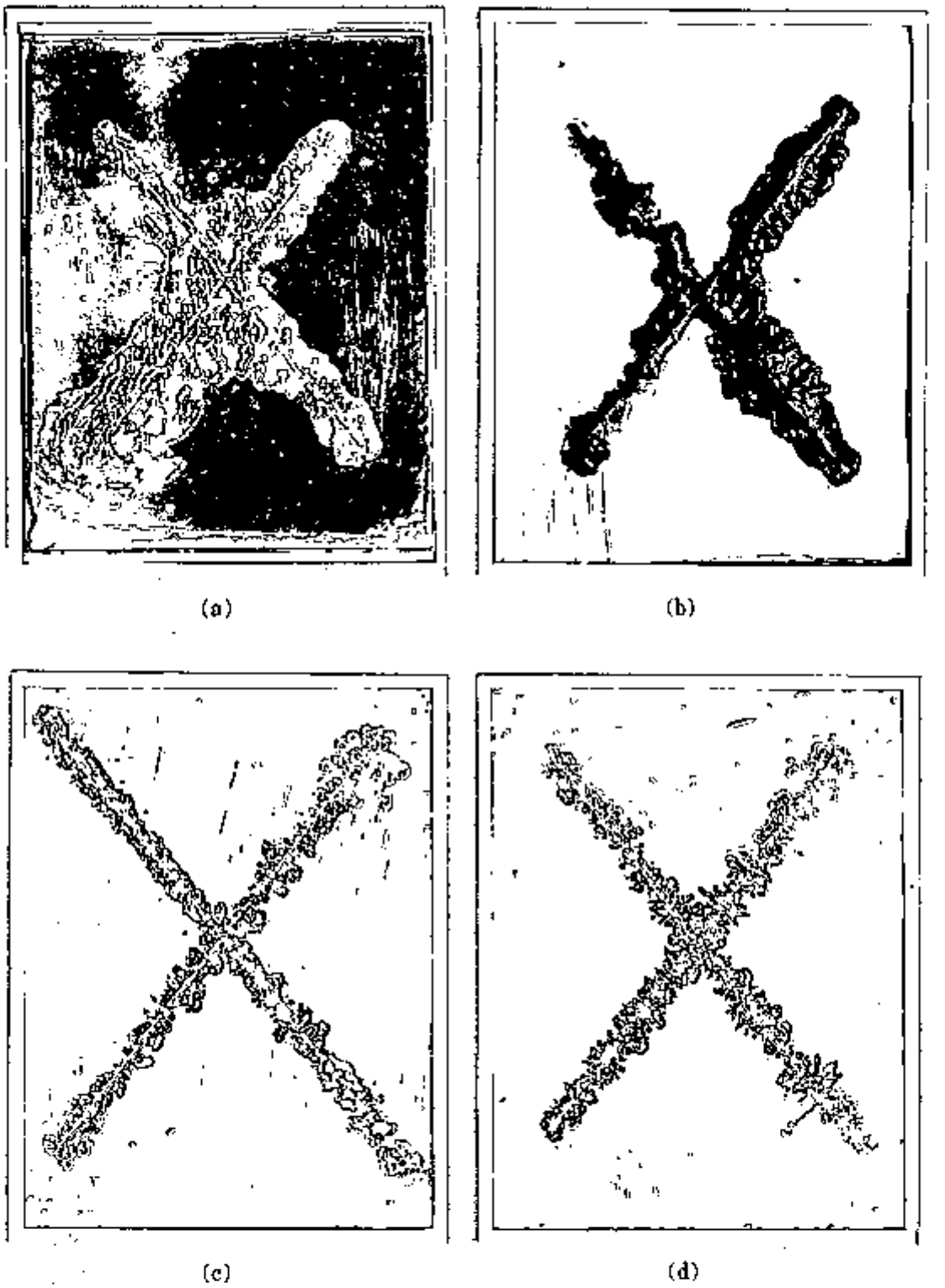

Figure 5.7 - Scribed specimens (1) exposed to cabinet (high sulphate solution) after 8 days (a) MS, (b) LAS II, (c) A-86, and (d) USI.

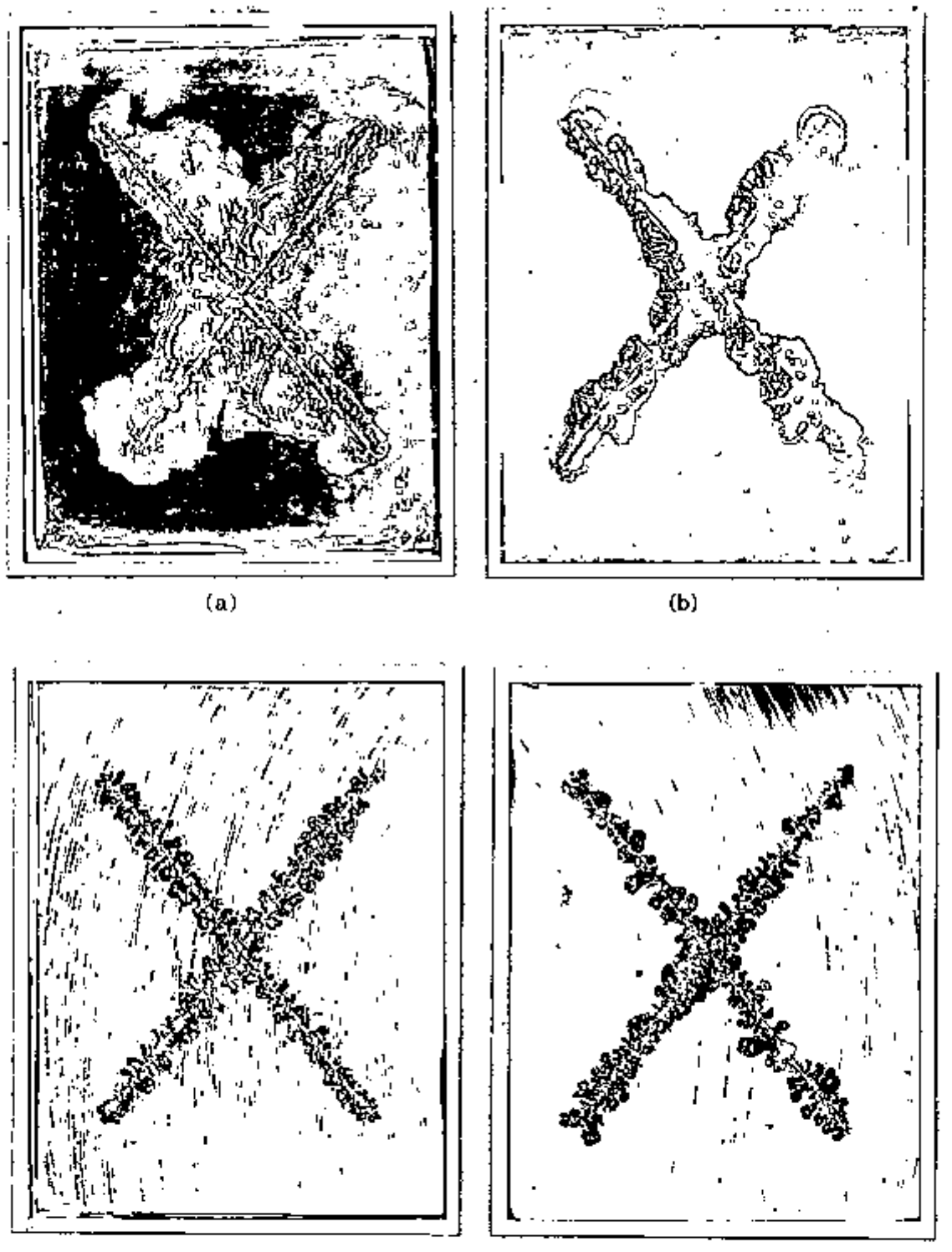

Figure 5.8 - Scribed specimens (2) exposed to cabinet (high sulphate solution) after 8 days (a) MS, (b) LAS II, (c) A-36, and (d) USI.

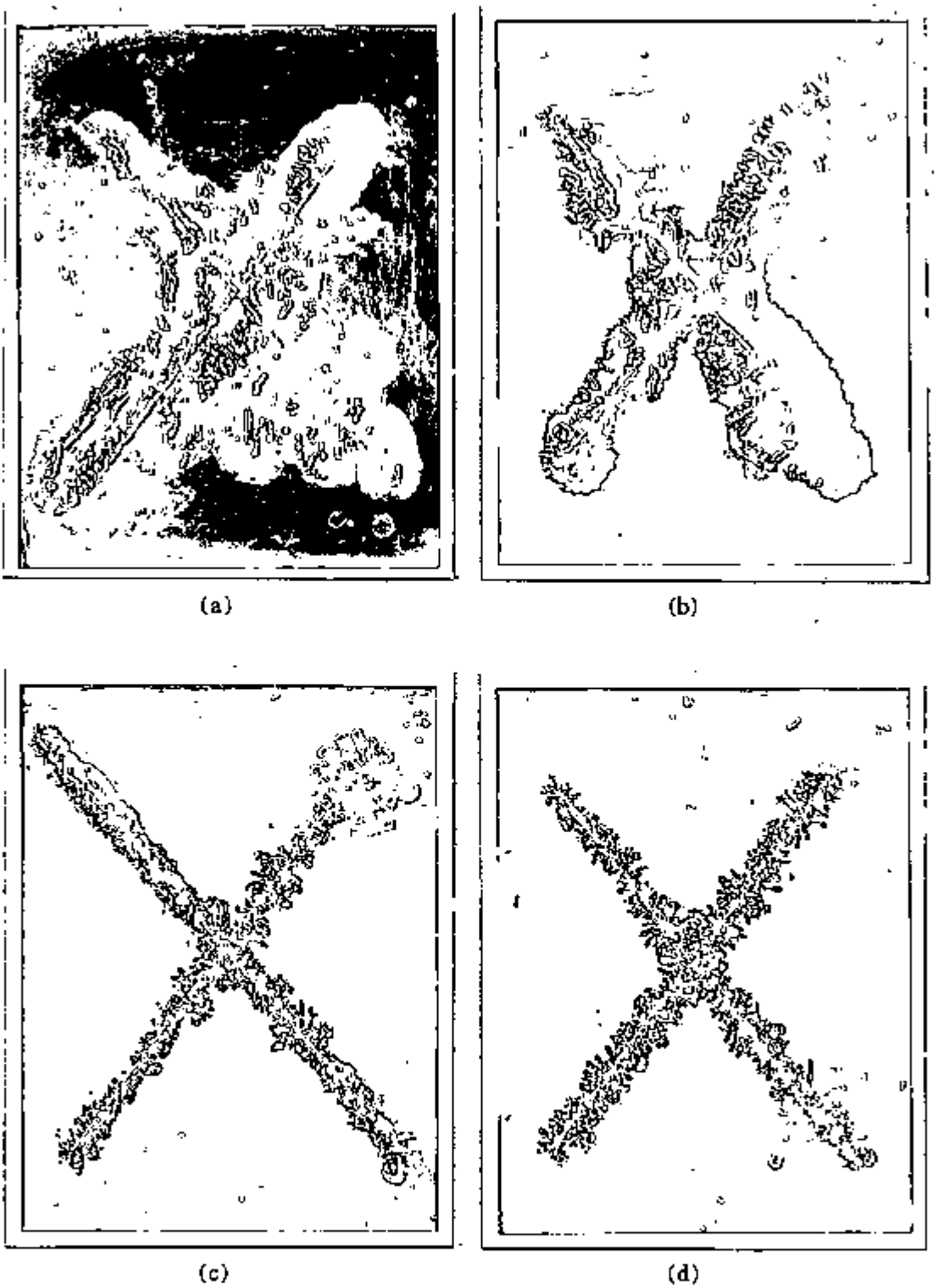

Figure 5.9 - Scribed specimens (1) exposed to cabinet (high sulphate solution) after 10 days (a) MS, (b) LAS II, (c) A-36, and (d) USI.

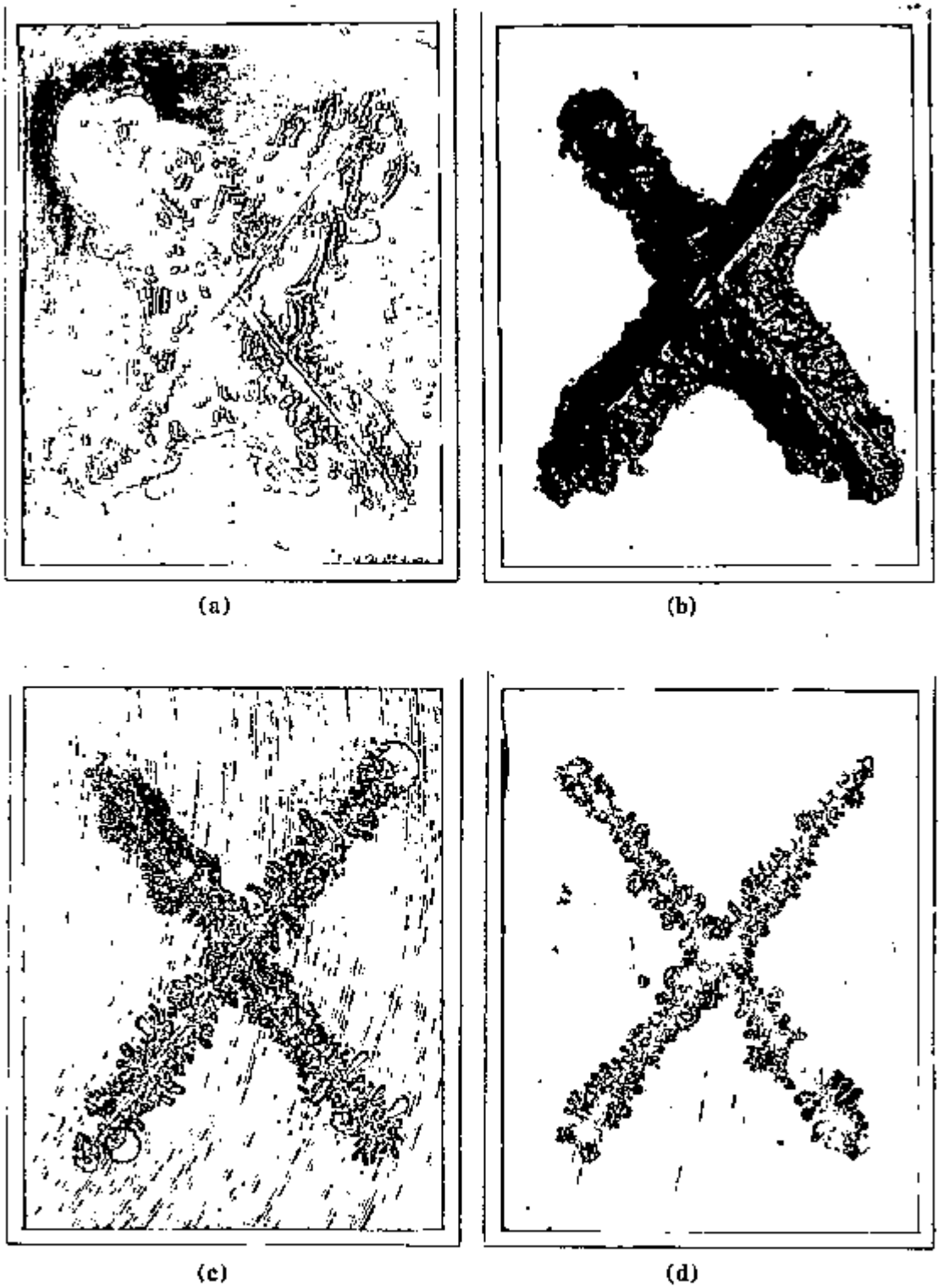

Figure 5.10 - Scribed specimens (2) exposed to cabinet (high sulphate solution) after 10 days (a) MS, (b) LAS II, (c) A-36, and (d) USI.

After 1 day exposure in the cabinet, undercutting and delamination at the scratch were already seen on the coated MS and LAS II steels. On the other hand, only slight undercutting at the scratch was produced by the two other steels, A-36 and USI, Figures 5.1 and 5.2. In the following days, the difference in performance of the coated system was even more pronounced, Figures 5.3 - 5.10.

After 10 days exposure to the wet-dry cycle, one specimen of each substrate was removed from cabinet and stored in desiccator over silica gel for subsequent XPS analysis. The results are presented in the next section. At that time the coating on the specimens corresponding to the substrates MS and LAS II had lifted from the substrate at the areas surrounding the scribe mark and large volumes of liquid had accumulated underneath the coating. The adhesion in the area surrounding the scribe was completely lost. The other coated A-36 and USI specimens remained in the cabinet for 5 additional days and their corrosion features at the end of that period are shown in Figure 5.11.

From the Figures shown earlier it can be said that the use of the scribe mark (X) to evaluate the performance of the coating on the different steel substrates may have been a too severe test in the aggressive atmosphere used since most of the paint coating deteriorated rapidly after a week's test. Extensive corrosion of the underlying steel at the scribed mark was apparent in all the cases. Table 5.2 summarises the general observations related to each coated substrate after 10 days exposure.

It is evident from the previous Figures and Table 5.2 that the modes of degradation produced were similar in the cases of the steels MS and LAS II, but the deterioration characteristics of these specimens showed some differences from the two other steels used, A-36 and USI. The degree of delamination on the specimens corresponding to the steels MS and LAS II was much larger than for the steels A-36 and USI. One possible explanation for the improved corrosion performance of the A-36 and USI steels in terms of degree of delamination is that the cathodic reaction on these latter steels could have occurred on the exposed

metal at the scratch. The larger content of inclusions of MnS or mixed, MnS + oxide, in these steels, A-36 and USI, might be responsible for this result, since these types of inclusions would favour the cathodic reaction on their surface.

Another reason for the large variation in delamination could be that nature of the rust layers formed. The corrosion product on A-36 and USI steels was observed to be more firmly attached to the substrate than the rust layer on the two other steels, MS and LAS II. A more adherent corrosion product would also tend to resist and stifle further corrosion. The differences among the steels were even more significant for longer exposure times. This is demonstrated by the corrosion features of the various specimens for times corresponding to 8 and 10 days. The retardation of the corrosion process probably occurs only when the rust formed becomes sufficiently thick and therefore acts as an effective barrier.

Heavy blistering was observed in the case of the steels MS and LAS II. It is believed that the rust on these two latter steels was more porous permitting the passage of moisture and aggressive species, and thus keeping the metal surface wet for a longer time. In fact in the case of the steels, MS and LAS II, solution was observed to accumulate underneath the coating causing the lift-off of the paint. Therefore, the superior corrosion characteristics of the steels A-36 and USI, were caused by either the location of the cathodic reaction at the scratch or the non-porosity and the higher adhesion of their corrosion products to the substrate thus providing some protection by impeding the ingress of the aggressive species to the metal substrate.

TABLE 5.2 - Modes of degradation exhibited by the various scribed specimens after 10 days exposure to high sulphate solution in wet/dry cycle test.

Substrate	Observations
MS	Substantial blistering and heavy corrosion at scratch
LAS II	Substantial blistering and heavy corrosion at scratch
A-36	Undercutting at scratch; filiform attack; adherent corrosion product
USI	Undercutting at scratch; filiform attack; adherent corrosion product

The nature of the corrosion products formed is also likely to influence the physical delamination of the coating adjacent to the damaged regions[210]. After a certain amount of rust is formed, the cathodic reduction of oxygen is shifted to the surrounding area of the rust deposit. The access of oxygen to the reaction site where it is reduced is restricted at the areas covered by the rust layer but it can easily reach the rust-free surface. Consequently a differential oxygen concentration cell is established, and a highly alkaline electrolyte is generated in the surrounding cathodic areas at the coating-steel interface. The high pH of the electrolyte at the interface, values above 12 were found in a sodium chloride environment, leads to delamination of the coating[211]. This process is known as cathodic delamination or disbonding. The driving force for cathodic delamination is provided by the separation of the anodic and cathodic half-reactions under the coating. In the cathodic delamination process the failure of the coating/substrate bond is assumed to be caused by the hydroxyl ions formed at the surrounding regions of the defective areas.

Various explanations have been given to the effect of a high pH on the interface[19,40,,47,72]. Ritter and Kruger[40] using ellipsometric techniques found

experimental evidence for the attack of the oxide as the cause for delamination. Dickie and co-workers[72] assumed that the attack of the polymer by the strong alkaline environment was the reason for the failure of the bond between the coating and the substrate. Their experimental evidence was the presence of carboxylated species at the interface which was detected by surface analysis techniques. Koehler[19] ,however, believes that the disbonding process occurs as a result of the displacement of the coating by a high pH aqueous film formed at the interface. Leidheiser[47] proposed that the solubilization of the thin oxide film at the interface is the chief mechanism for the process of delamination. According to his hypothesis, the dissolution of the oxide leads to the breakage of the coating/substrate bond, and subsequently the high pH causes the localized attack of the polymer at the interface.

Delamination was observed for all the coated substrates at the areas surrounding the corroding exposed metal. In the case of the coating used in this work, delamination may occur as a consequence of the saponification of reactive ester groups present in the coating resin, causing the breakage of the adhesive bond coating-substrate[219]. It is also possible that the other mechanisms proposed above might have an effect on the process of delamination. The degree of delamination as indicated by this work seemed to be dependent on the nature of the steel surface. The largest degree of delamination was produced by the specimens corresponding to the MS steel substrate, while the steel USI exhibited optimum cathodic delamination resistance. Since the delamination is caused by the production of OH^- as a result of the cathodic reaction $H_2O + 1/2O_2 + 2e^- \rightarrow 2OH^-$, the reactants, water, oxygen, electrons and counter ion cations must reach the reaction site[20]. The electrons reach the reaction site through the oxide film or any other heterogeneities on the metal surface. Thus, any poor electronic conductor film at the surface can limit the access of electrons to the reaction site[47].

The degree of disbonding for the various coated steels increased in the following order: USI, A-36, LAS II, and MS, as can be seen in Figures 5.7 - 5.10. It is noted in Figures 5.9 and 5.10 that the steels A-36 and USI produced higher resistance to delamination at the regions away from the scratched areas than the steels MS and LAS II. Besides the probable causes mentioned previously in this chapter, another possible reason for the larger resistance to delamination found for the USI steel might have been the presence of a large content of oxide inclusions at the interface, which are poor electronic conductor and might have hindered the access of electrons to the reaction site. The blocking of the scratch line by more adherent corrosion products, in the case of the steels A-36 and USI, may also have affected the subsequent delamination process, because the lateral diffusion of water and oxygen to the reaction site is hindered in this case.

If the steels produced by the same manufacturer are considered as a group, that is, if the steel MS is compared to the steel LAS II, and the steel A-36 is compared to the steel USI, it can be noted that the low-alloy steels in each group, USI and LAS II, produced more dense, compact and adherent rust layers, and lesee delamination than their corresponding carbon steels, A-36 and MS. This is indicated by Figures 5.9 and 5.10. Thus it seems that less damage and the tendency to rupture is diminished on the low-alloy steels in each group.

Filiform corrosion was commonly observed on the A-36 and USI steels in the region of the scribe, Figure 5.11. Filiform corrosion is a form of underfilm corrosion which generally occurs in humid environments. For it to take place some conditions must be fulfilled. These are[84]: (1) high humidity (65-95%), (2) coating permeable to water, and (3) presence of defects in the coating. It is also stimulated in the presence of impurities such as sulphur dioxide. The conditions above were met in the Prohesion test adopted in this work. Filiform corrosion has been found to be promoted by maintaining the specimens at a relative humidity in the range 70-85% after scratching through the coating to the metallic substrate[47].

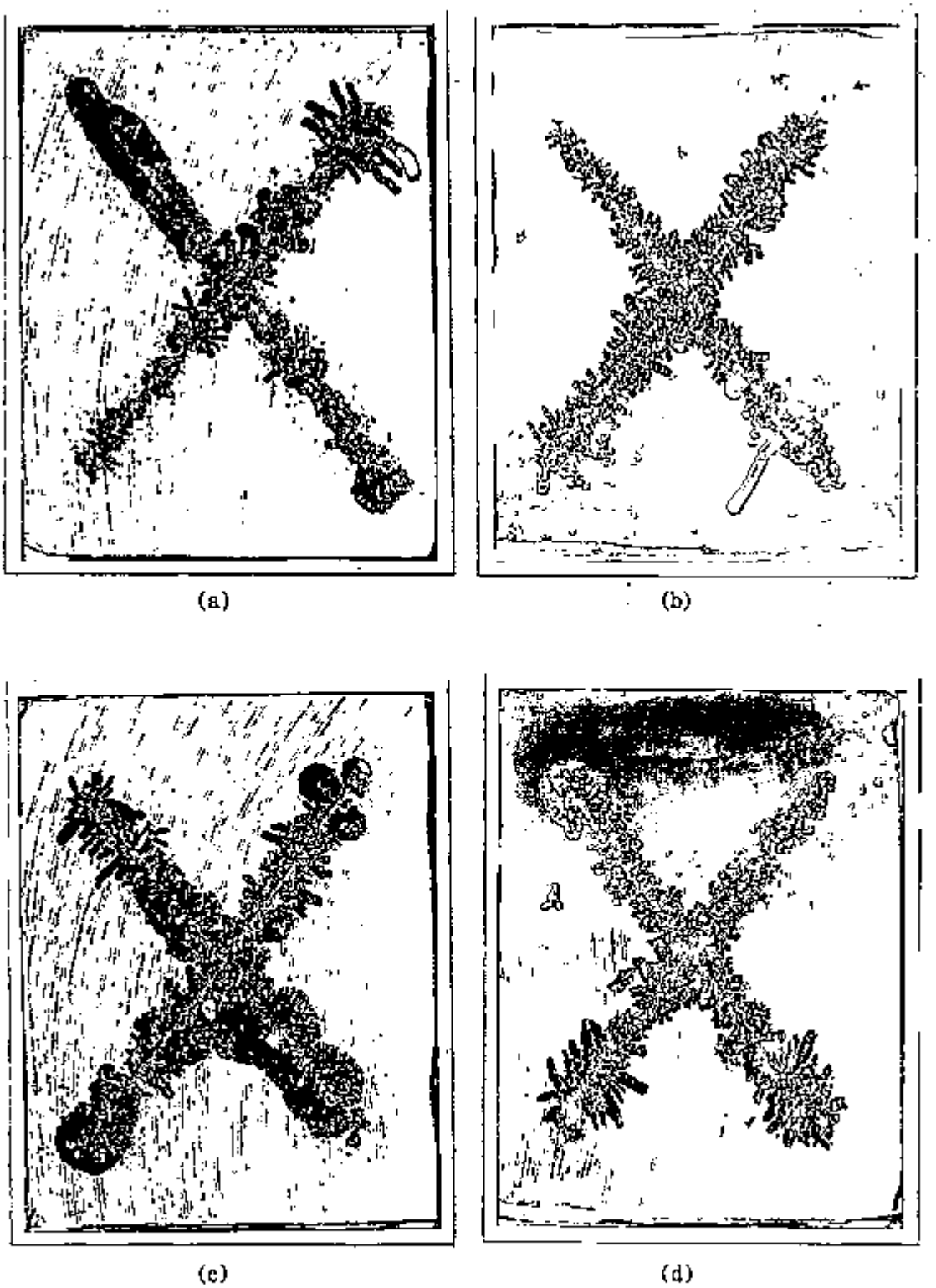

Figure 5.11 - Scribed specimens exposed in cabinet (high sulphate solution) for 15 days (a) A-36(1), (b) USI(1), (c) A-36(2), and (d) USI(2).

Studies on the character of filiform corrosion on steel[222] have observed a pH of approximately 1 at the leading edge of the filament, and a pH of 3 to 4 corresponding to the liquid immediately behind the leading edge. It is worthy mentioning that pH's of this order are expected on the basis of hydrolysis of Fe^{2+} ions.

When the steels A-36 and USI are compared, it can be said that the specimens corresponding to the substrate USI showed better corrosion characteristics than the ones shown by the A-36 steel. This is demonstrated by a relatively more adherent corrosion product for the scribed USI steels compared with that found on the A-36 specimens. In addition, larger volumes of liquid accumulated on this latter steel than on USI and consequently this resulted in the lifting of the coating. However, because more adherent corrosion products were formed on the USI steels, the corrosion reaction was slowed down by blocking off the access of aggressive species to the underlying surface.

The results above are supported by XPS analysis presented in the next section.

5.3.2 - XPS analysis of specimens exposed to Prohesion test.

XPS analysis was carried out on four scribed specimens, one of each substrate, exposed to the mixture 0.35% $(NH_4)_2SO_4$ + 0.05% NaCl inside cabinet with wet-dry cycle. The specimens corresponding to the substrates MS and USI were removed from the cabinet after 10 days exposure, but the other two, A-36 and USI remained for an additional five days. After removal from cabinet, all specimens were stored in desiccator over silica gel until the time of analysis. The coating was then peeled off next to the scribed region, and XPS analysis was carried out at the coating interface. The element composition (Atomic %) obtained for each of the specimen analysed is shown in Table 5.4.

TABLE 5.4 - Element composition obtained by XPS analysis on the coating interface of the various tested specimens

Substrate	Element (% Atomic)						
	Fe	O	C	Na	Cl	S	N
MS	15.0	49.4	25.0	2.0	1.1	4.7	3.3
LAS II	26.6	50.1	19.0	0.8	0.5	1.7	1.3
A-36	13.4	63.5	19.0	1.0	0.9	2.0	0.3
USI	24.2	45.8	29.6	0.4	...	...	...

From the above Table it is evident that the corrosive species, (Cl, S, and N), were not detected in the interface areas of the substrate USI. On the other hand, the largest contents of these elements were found in the interface region of the MS steels. It should be added that the coated system of this latter steel was also the first to exhibit deterioration of the coating and underlying steel. It is probable that the corrosive species present in the aggressive environment diffused easily in the case of the systems for which the coating was readily lifted. The largest Na concentration was also produced by the coated system of the MS steel and this might have been associated with the formation of sodium hydroxide species leading to the extensive delamination observed.

Figure 5.12 shows the XPS spectrum relative to O 1s at the coating interface of the four steels analysed. It can be seen that the O 1s spectrum corresponding to the USI substrate shows larger concentration of oxide oxygen species, O^{2-}, in comparison to the hydroxyl oxygen species OH^-. However, for the other substrates the proportion of OH^- was higher than that of O^{2-} species, and this proportion seemed to have increased in the following order: A-36, LAS II, and MS. This indicates that the OH^- concentration in the coating interface seems to be directly related to the corrosion characteristics of the system. In fact the specimens which showed larger delamination and large volumes of liquid accumulated at the

interface were also the ones which produced the highest proportion of OH^- species in the coating interface.

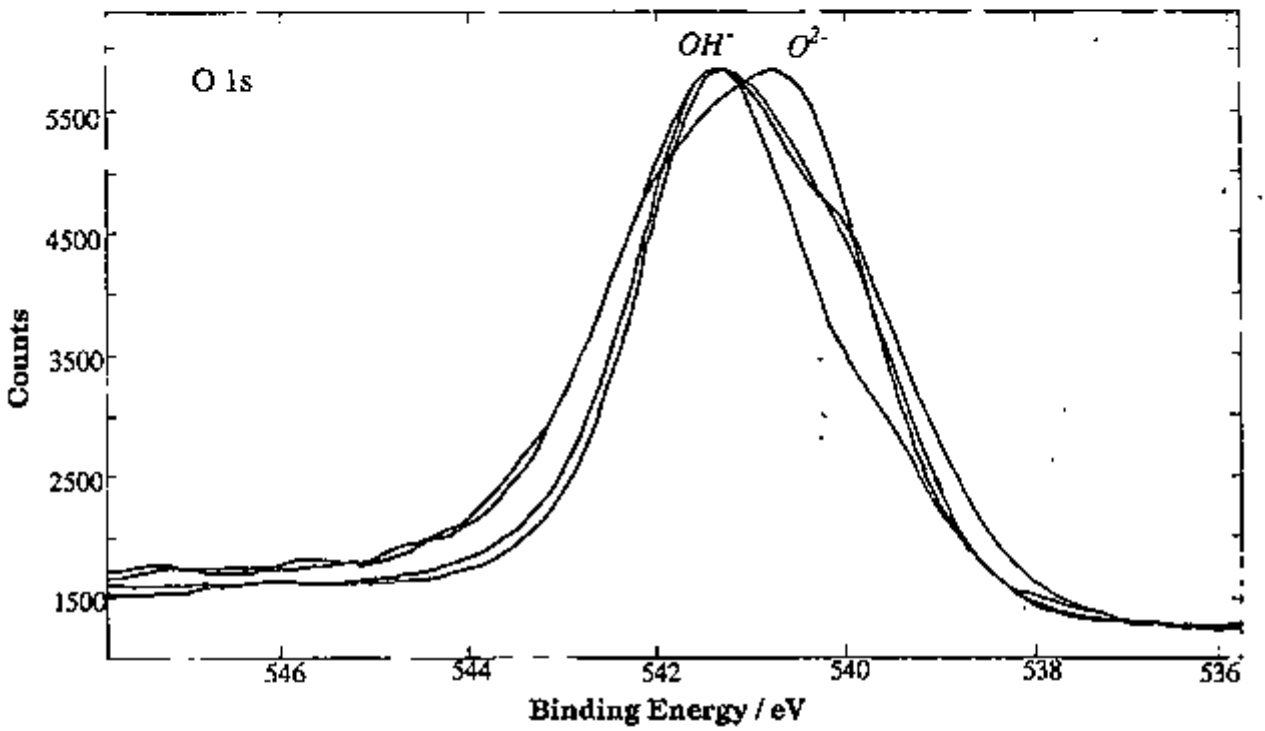

Figure 5.12 - O 1s XPS Spectrum detected on the coating interface of the four steels studied.

5.3.3 - Specimens exposed to wet-dry cycles with artificial acid rain solution

The scribed specimens tested in the artificial acid rain were maintained inside the cabinet for 35 days. The development of corrosion features on the various specimens used was followed with time, and at the end of the testing period (35 days) the corrosion characteristics around the specimens 6 and 7 were as shown in Figures 5.13 and 5.14. The printing magnification used in these Figures was 1.9X.

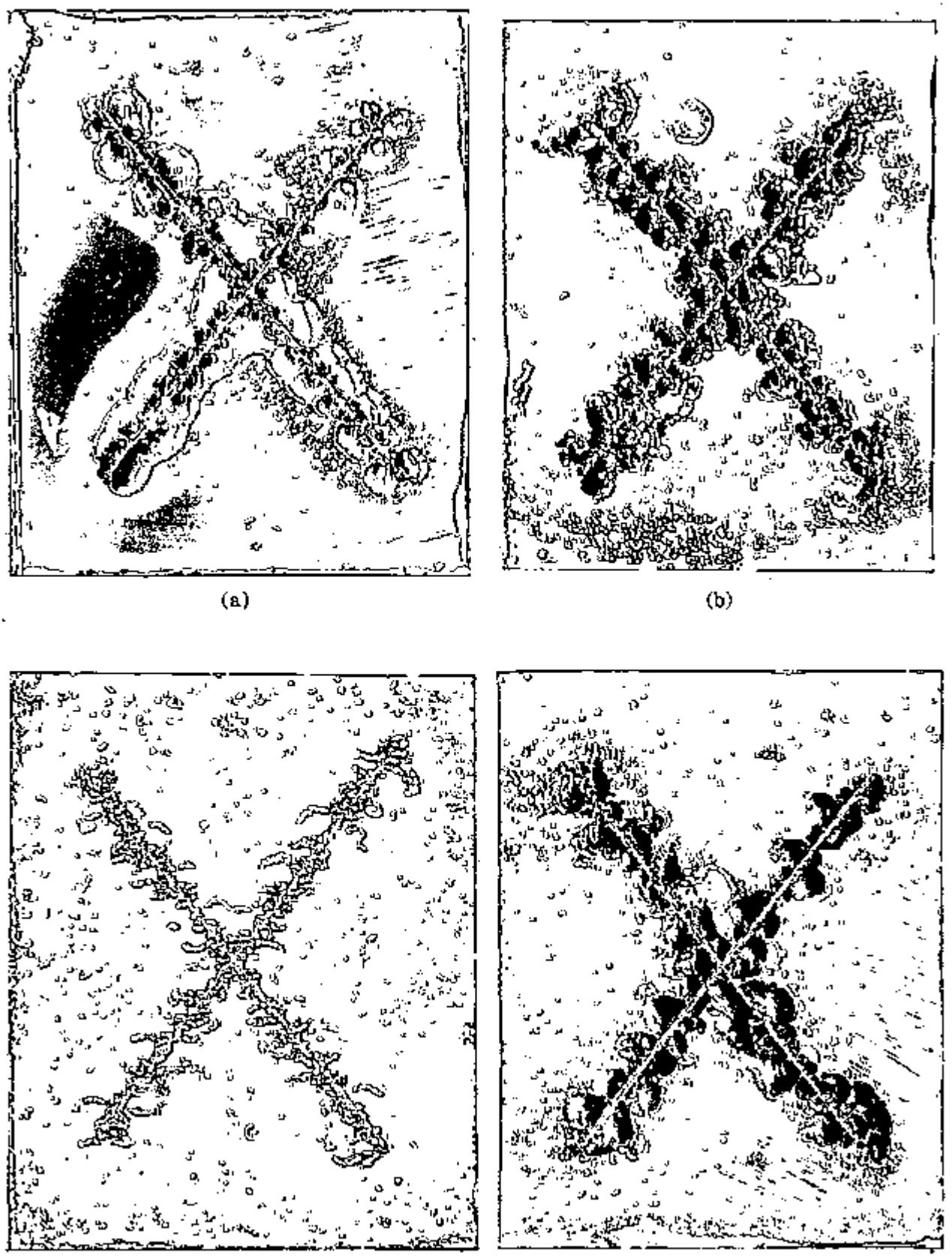

Figure 5.13 - Scribed specimens (6) exposed to artificial acid rain after 35 days (a) MS, (b) LAS II, (c) A-36, and (d) USI.

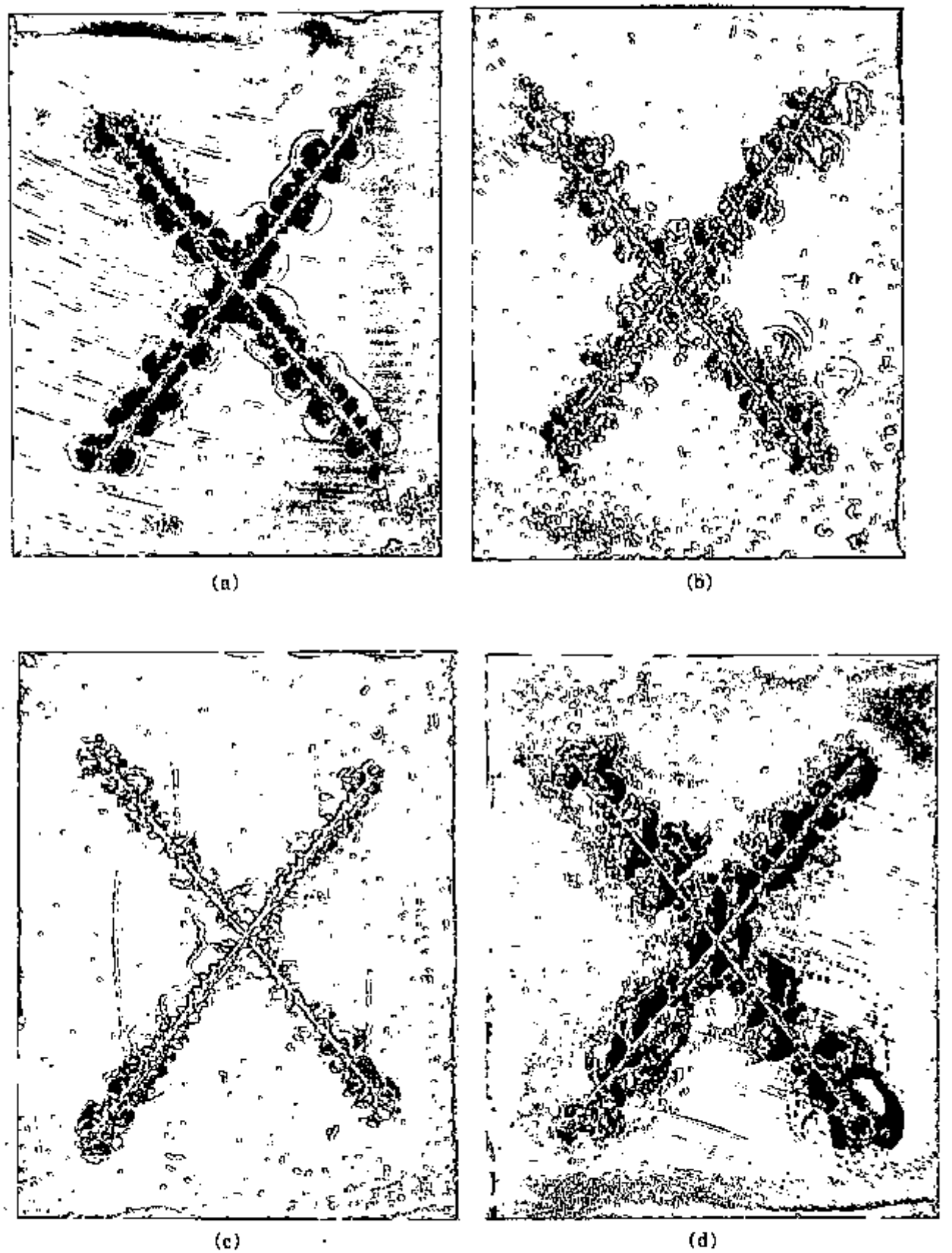

Figure 5.14 - Scribed specimens (7) exposed to artificial acid rain after 35 days
(a) MS, (b) LAS II, (c) A-36, and (d) USI.

From these Figures it is evident that similar corrosion features developed around the scribe mark of the coating on the various steel substrates used. The corrosion characteristics corresponded to blisters beside the scribe filled with black and/or brown loose corrosion products and volumes of liquid. Rust had probably formed at the scribed or exposed area of the metal substrate. The coating surrounding the scribed area had been delaminated either by the direct action of the hydroxyl ions produced by the cathodic reaction or by saponification reactions. Due the large area of unprotected metal at the scribe, it is probable that the membrane of hydrated oxide corrosion product covering it is either discontinuous or has not enough mechanical strength to resist the osmotic pressure[84]. In this case the rust formation has a dynamic character consisting of continuous rupture and healing processes. Since the rust formed at the scribe is not continuous or is broken periodically, corrosive species can easily diffuse underneath the coating leading to the spread of corrosion to the adjacent areas of the scribe. The oxygen cathodic reaction with generation of alkali is then dislodged to further areas and consequently cathodic disbondment is spread to more distant areas from the scribe. The cathodic disbonded areas surrounding the rusted ones are well defined in Figures 5.13 and 5.14.

The significant observation of this experiment was that the various steels tested could not be differentiated throughout the whole testing period under the conditions used. This proves that the conditions of an accelerated test are of major importance in ranking different coated substrates with relation to their corrosion properties.

The main difference between the two tests carried out in the cabinet was the chemical nature of the environment. The composition of the solutions differed with respect to ion concentration and pH. In the Prohesion test the medium had an ionic concentration of approximately 0.4% wt and a pH of around 5.6; whereas for the artificial acid rain solution the concentration of ions was nearly 0.023% and the pH was approximately 3.5. Considering that during the dry cycle the

concentration of ions of the two media becomes concentrated and at the saturation point eventually achieve a similar concentration, it seems that the difference in the ionic concentration between both enviroments could not have significantly influenced the results obtained. On the other hand, the distinct pHs of the two atmospheres, one corresponding to a nearly neutral medium and the other being of an acidic nature, could account for the different type of response produced.

It is possible that in the acidic environment used, the sulphide inclusions were dissolved more rapidly than in neutral media. As a consequence of this attack, the inclusions play an insignificant role on the overall corrosion of the steel substrate. Therefore, the steels used exhibited similar corrosion behaviour. The substantial cathodic delamination observed indicated that oxygen reduction might have been the dominant cathodic reaction.

5.4 - General Discussion

The steels substrates which showed similar deterioration features of their scribed systems included the two types of steels used, that is, mild steel and low-alloy steel types. The ones which presented more adherent corrosion products and lower degree of delamination were the A-36 steel and USI steel. The other two steels, MS and LAS II, produced large delamination and accumulation of solution at their interface. Thus, the type of steel can not be made responsible for the differences found in the corrosion features of the various coated substrates. Also the surface condition can be eliminated as the cause of the inferior corrosion behaviour of the steels MS and LAS II relatively to the A-36 steel and USI steel, since a similar surface finishing, (1200 μm), was adopted for all the steels.

The common characteristic of the specimens showing the same kind of deterioration was their larger heterogeneities content at the surface. As mentioned previously in this chapter, for the steels with more inclusions, the

cathodic reaction was facilitated on the uncovered metal at the scratch due to the MnS or MnS + oxide inclusions exposed at the scribe. If this occurred, less cathodic delamination at the surrounding areas of the scribe would result. A second probable explanation for the results obtained is that the heterogeneities at the steel surface might have contributed to the formation of more adherent corrosion products at the coating-substrate interface. In this situation, the anodic reaction would have been hindered by the blockage of the exposed metal by deposited corrosion products which could have isolated the metal substrate from the environment. The 'blocking' of the anodic reaction would in turn limit the cathodic reaction. Thus, the above results indicated that the larger content of heterogeneities at the surface of some steels was beneficial for improving the corrosion characteristics of the systems tested in this relatively aggressive manner.

The properties of the rust are of great importance in determining the efficiency of the protective coating. Adherent rust reduces the attack on the base metal whereas loose rust exposes fresh metal for further attack. The rust formed initially is non-protective until it becomes sufficiently thick to reduce additional attack. It should be noted that no significant differences were found among the various coated substrates in the first days of exposure.

If steels produced by the same manufacturer are considered, the low-alloy steels showed slightly improved corrosion characteristics compared to the mild steels in each set. Although the corrosion mechanism for low-alloy steels and mild steels is believed to be similar, the rust on the low-alloy steels forms a more dense and compact layer[212]. The relatively more adherent and compact layer formed on the low-alloy steels retards the anodic reaction by limiting the supply of water and corrosion stimulating ions to the steel surface. In addition, the corrosion rate might then be further decreased due to the increased electrolytic resistance of the corrosion products.

Among the added alloying elements in the low-alloy steels, copper has been assumed to be responsible for the most pronounced effect in decreasing the corrosion rate. The beneficial effects of alloying elements, mainly copper, on the characteristics of the rusting formed on the low-alloy steels, weathering type have been explained by various mechanisms[212-217]. Copson[212] proposed that some alloying addition elements to iron lead to the slowing down of the rate of rusting by the formation of insoluble compounds which inhibit cell action, either by blocking the pits even under acidic conditions, or by binding the rust more closely and consequently creating an impervious protective covering on the iron surface.

Okada[213] showed that an optically isotropic layer, consisting mainly of amorphous spinel type oxide, covers completely the surface of the weathering steels and prevents water penetration. In the case of the mild steels the major constituent of the rust layer was found to be FeOOH. On the other hand, Suzuki and co-workers[214] associated the beneficial effect of copper addition to the aggregating state of the rust layer. It was assumed that copper inhibits the growth of primary colloidal particle which has an effect on the properties of rust and consequently this would increase the protective ability of the rust layers.

Misawa and collaborators[215,216] concluded that Cu and P are concentrated at the metallic surface of the low-alloy steels and have a catalytic effect on the transformation of Fe(II) complexes to the amorphous ferric oxyhydroxide, $FeO_x(OH)_{3-2x}$. They demonstrated that the amorphous phase formed on low-alloy steels is compact and uniform and acts as a protective barrier against atmospheric corrosion. Other workers believe[215-217] that for the formation of the protective corrosion layer (patina) on the low-alloy steels, a cyclical variation between wet and dry periods is necessary. Stratmann and co-workers[217] suggested that the effect of copper upon the atmospheric corrosion of iron is limited to the period of drying out of the rust layer.

5.5 - Summary

The modes of degradation of four steels after their coating has been scribed was investigated by exposure inside a cabinet under controlled atmospheric conditions and using wet and dry cycles.

For the Prohesion tests two main types of deterioration were observed and these seemed to be associated with two sets of steels, with each set emanating from the same manufacturer. Each set included one type of steel, one low-alloy and the other mild steel. Thus, the similarities in the corrosion deterioration observed for the steels which originated from the same producer, indicated that the characteristics of the surfaces of these steels and not their composition is related to their corrosion behaviour. The steels A-36 and USI produced less degree of delamination and more adherent corrosion products than the steels MS and LAS II. The two latter steels had 'cleaner' and brighter surfaces which might have resulted in the lower corrosion performance observed upon exposure.

The anti-corrosion properties of the coated steels observed in the Prohesion test improved in the following order: MS < LAS II < A-36 < USI. Large disbonding was produced by the first two steels, and the substrate USI was the one to show improved disbonding performance. The cathodic reaction might have occurred at the scratched areas or the resultant adherent rust layer might have hindered the access of corrosive species to the corroding surface, leading to a slower corrosion rate. The ranking above was confirmed by XPS analysis, the minimum content of aggressive ions being detected at the interface layer corresponding to the steel USI, and the largest content was found for the MS substrate.

Small differences were found between the mild steel and the low-alloy steel types provided by the same manufacturer. Considering the steels manufactured by the same producer as a set, the low-alloy steel type of each set produced slightly improved corrosion performance than its mild steel match. The improved performance of low-alloy steels, weathering types, is generally correlated with the

addition of some alloying elements, mainly copper, which acts as a stimulator in the formation of more protective rust layers.

Although clear differences were found in the corrosion deterioration of the steels used in the Prohesion tests, no distinction was seen when the same steels were tested in the artificial acid rain solution. This finding is a clear evidence of the importance of the specific conditions used in ranking coated systems in terms of their corrosion characteristics.

CHAPTER 6

GENERAL DISCUSSION

6.1 - Introduction

In the previous chapters the corrosion behaviour of four steels with minor compositional differences was studied under various testing conditions. The work examined bare surfaces and coated substrates under immersed conditions, and coated and scribed specimens exposed to controlled atmosphere inside a cabinet with wet and dry cycles. The corrosion resistance characteristics of the various steels analysed, coated or uncoated, were found to be dependent on the conditions of the test.

The steels which exhibited higher corrosion resistance either bare or coated and under immersed conditions were the same to display a larger degree of deterioration when exposed to wet and dry cycles inside a cabinet in the Prohesion test. However, a direct correlation seemed to exist between the corrosion resistance behaviour of the bare steel surfaces under immersion and the anti-corrosion properties of the same steels when coated and immersed in sodium chloride solution.

In the immersion tests, the steels with lower inclusions content, or 'cleaner' surfaces, showed slightly higher corrosion resistance and their coated system had a relatively longer life. Thus, it is supposed that there is a relationship between the 'cleanliness' of the steel and its corrosion characteristics when immersed in neutral solution, either bare or coated. On the other hand, for the tests inside a cabinet with wet and dry cycles, the coated and scribed specimens which showed the least deterioration of the system also produced more adherent corrosion products in the Prohesion test. It should be added that these

steels had a larger content of heterogeneities. Contrary to the results of the other tests, the high heterogeneities content of these steels seemed to have contributed to an improved corrosion performance. Thus, the results obtained in this work indicate that the characteristics of the surface, especially the inclusions content, affect the corrosion performance of the various steels used, and this was observed under almost all the testing conditions. The only exception was the cabinet test which used artificial acid rain solution as the aggressive environment. In this latter test, no distinction was found among the various steel substrates analysed.

6.2 - Effect of minor alloying elements on the corrosion behaviour of bare and coated steels - A hypothesis

6.2.1 - Bare steel surfaces under immersed conditions

The electrochemical behaviour of bare steel surfaces did not show marked differences when the various steels were tested in neutral and aerated solutions and under low polarization conditions. This result agrees favourably with work reported in the literature which states that the corrosion reaction rate of many metals immersed in neutral and aerated solutions is mainly controlled by the diffusion of oxygen to the metal surface. Under these conditions, the composition of the steel is not expected to affect significantly the corrosion rate. For the steels used in this research, two types of rate control were observed for the corrosion reaction. These were diffusion or mixed (diffusion+activation) control. This suggests that for all the steels tested under the conditions stated above, the diffusion of oxygen to the metal interface always had a significant effect on the rate of the corrosion process.

However, it was observed that steels originating from different manufacturers exhibited slight variation in the type of rate control for the corrosion reaction. For instance, a mixed control was operative for the steels MS,

LAS I and LAS II, whereas for the other steels, A-36 and USI a diffusion control was predominant.

A possible cause for the difference in reaction control could be the content of heterogeneities, inclusions, at the surface of the steel. The steels with larger inclusions content at the surface corroded slightly faster and therefore required more oxygen for the cathodic reaction. This could have been the cause for the diffusion control shown by these steels. No significant differences were, however, noticed in the type of corrosion control of the steels produced by the same manufacturer. Thus, the content of heterogeneities in the steel is believed to affect the corrosion characteristics observed.

6.2.2 - Coated specimens under immersed conditions

The explanation given to account for the anti-corrosive properties of coated specimens, under immersed conditions, was that oxide or sulphide inclusions might have participated in the electrochemical reactions occurring on the metal surface and consequently contributed to the phenomenon of underfilm corrosion.

A model is proposed for the development of corrosion under immersion conditions for the coated steels used in this work. This model is shown schematically in Figures 6.1 to 6.4.

The following steps are believed to occur during the corrosion of coated steels under immersed conditions.

Initially, water and oxygen permeate through the coating. For high resistance coatings, it is supposed that during the early stages of immersion no significant diffusion of ionic species occurs, Figure 6.1 (a) and (b).

What occurs next depends mainly on the coating characteristics. There are two possible developments. These are:

(1) If the coating has a closely packed structure, free of defects or pinholes, water and oxygen diffuse through the coating and arrive at the interface. It is

postulated that the presence of small quantities of water at the interface can support passivation, Figure 6.1 (c). It has been reported in the literature that the arrival of water in small quantities at the coating-oxide interface can sustain passivation by acting as oxygen donors[115]. Other work found in the literature[223] suggests that the first water surface layers at the interface are tightly bound to the surface hydroxyl groups which are the result of the hydration of the outermost surface oxygen of the oxide layer. A probable passivation process aided by water was also indicated in this work by the movement of corrosion potential towards more positive values in the initial period of immersion, that is, before corrosion was seen on the surface. The high positive values were generally maintained until generalized corrosion started to spread over the surface.

However, if the amount of water at the interface exceeds the amount necessary to support passivation, it can cause the dissolution of the oxide at the interface and induce corrosion, Figure 6.1 (d) and (e). Corrosion is easily initiated at the boundary regions between metal matrix and non-metallic inclusions which act as microgalvanic cells, Figure 6.1 (f).

Two main types of inclusions were found in the steels used in this research, oxide and manganese sulphide types. Local dissolution of the oxide layer is sustained by the presence of the sulphide inclusions which act as effective cathodic sites, Figure 6.2 (a). The metal is then attacked preferentially since in carbon steels the sulphide inclusions are usually more noble than the surrounding matrix[200], Figure 6.2 (b). It should be added that dissolution of the sulphide may also occur. The solubility of sulphide inclusions have been reported as sufficient high[200], even in neutral water, to give a significant concentration of HS^- ions which will further accelerate the corrosion reaction. Also the boundary region between the oxide film and the oxide inclusions corresponds to regions of irregularities at the surface where the adhesion of the coating is decreased. At these 'free' regions water can accumulate and cause the dissolution of the oxide

film. Subsequently corrosion can start at the areas of exposed metal, Figure 6.2 (c) and (d).

The corrosion process causes the consumption of its precursors, water and oxygen, and consequently the concentration of these species decreases at the interface. If these are not replenished at a reasonable rate due to the barrier characteristic of the coating, water is not allowed to accumulate at the interface in quantities enough to sustain corrosion. Corrosion in then limited to the initial areas, and the deposition of corrosion products on these areas hinders further access of corrosive species to the underlying metal, Figure 6.3 (a) and (b). Eventually corrosion stops. Also, the cathodic reaction in these cases is restricted to a very small area surrounding the corroding spot, since it is sustained by the anodic reaction which in this situation decreases with time. On the other hand, if due to a less protective character of the coating water and oxygen are restored at the surface, corrosion is sustained and the corrosion product formed can be voluminous. If this occurs the corrosion product can exert a mechanical stress on the adhesive forces at the coating-substrate interface, and consequently lifts off the coating. Once the coating is lifted, water can accumulate at the interface and corrosion can continue. Also, if the crust formed on top of the corroding spot which isolates the environment from the corroding metal is broken periodically, corrosive species are allowed to have access to the metallic substrate and corrosion can proceed, Figures 6.3 (c) and (d). Since the dissolution process concurrently sustains the cathodic reaction, the generation of alkali will affect adversely the adhesive bonds at the coating-substrate interface leading to further loss of adhesion.

(2) If defects, pores, or 'weak' areas corresponding to free volume regions are present in the coating, or are developed during exposure time, then corrosive species will have easy access to the underlying metal, Figure 6.4 (a). Water reaching the substrate at these regions initially dissolves the oxide film and then

corrodes the metal. The corrosion of the substrate is stimulated as a result of the bare metal exposed locally at the coating defect leading to localized corrosion. In this work, localized corrosion was generally observed in the form of black and brown corrosion spots for the coated and immersed steels. Dissolution of the oxide at the interface usually precedes corrosion, Figure 6.4 (b). This causes the breakage of the bond between coating and metal oxide, and the high pH generated by the cathodic reaction leads to localized attack of the polymer. Disbonded areas were generally observed around localized corrosion spots. The separation of the anodic and cathodic corrosion half-reactions provides regions which are subject to a driving force similar to externally applied cathodic potentials.

The corrosion reaction under the coating involves a cathodic reaction, generally:

$$H_2O + 1/2O_2 + 2e^- \rightarrow 2OH^- \qquad (6.1)$$

Thus H_2O and O_2 are required at the interface and also ionic species that provide sufficient conductivity at the interfacial region to permit separation of the anodic and cathodic regions.

At the anodic area, the metal corrodes according to:

$$Fe \rightarrow Fe^{2+} + 2e^- \qquad (6.2)$$

The small volumes of liquid involved in the early stages of corrosion leads to very high and low values of pH at the cathodic areas and anodic areas, respectively.

If the interfacial bond of the coating-metal oxide does not deteriorate at areas distant from the corroding spot, corrosion is restricted to the 'defective' area leading to localized corrosion. The hydroxyl ions generated by the reaction (6.1) diffuse inwards and react with the iron ions produced by reaction (6.2) and diffusing outwards. The deposition of insoluble corrosion products around the void or localized corroding area follows. Corrosion products develop and rise over

the corroding area and its surroundings forming a layer or incrustation which isolates the environment within the cavity from the bulk electrolyte. This subsequently retards the diffusion of corrosive species, and once the defective area has been blocked by insoluble corrosion product, corrosion in many cases can stop, Figure 6.4 (c).

The propagation of corrosion to areas away from the defective zone, however, depends on the characteristics of the system. For systems with highly protective corrosion properties, corrosion is limited to the defective area and the deposition of corrosion product blocks the defect or 'pore' without causing significant lifting of the coating. This explains why in certain cases an increase in the coating resistance was measured after the onset of localized corrosion. This situation can be maintained for long times in the case of resistant coatings, until corrosion is allowed to start on other areas of the specimen.

In the case of systems with lower corrosion resistance characteristics the bond at the coating-substrate interface is disturbed and this results in the lifting off of the coating, Figure 6.4 (d). Since water can easily be replenished at these areas of the interface it forms a layer which can sustain corrosion. Once water has accumulated on large areas of the surface the corrosion characteristics of the substrate are supposed to have a significant effect on the anti-corrosion properties of the system. The boundary regions between inclusions and metallic matrix are the likely regions for corrosion initiation due to a microgalvanic effect. Inclusions can also affect the movement of water through a capillary or pore which is easier under the influence of a potential gradient, by electroendosmosis[200]. Consequently, galvanic couples at the interface may lead to a blister. In the blistered area, coating has lost its adherence and water may accumulate allowing generalized corrosion to start.

Thus it is believed that the presence of 'imperfections or heterogeneities' at the interface, such as inclusions, segregates or precipitates, associated with 'non-perfect' coatings can act as additional corrosion promoters. Galvanic cells are set-

up between the heterogeneity and the steel base. These cells are sufficient to activate the corrosion process as soon as the corrosive species reach the interface. MnS type inclusions which are cathodic relatively to bare metal can provide ideal nucleation sites for rusting. These when attacked by an acidic environment, produce HS^- and S^{2-} which in turn promote a faster dissolution rate of iron by decreasing its activation polarization[8]. Increasing acidity caused by hydrolysis reactions, leads to the reduction of hydrogen ions by electrons originating from the oxidation reactions. The evolution of hydrogen can occasionally cause the breaking of the crust of corrosion product. If this occurs, further corrosion is possible.

Summarizing, a correlation seemed to exist between the corrosion resistance of the bare steels and their corrosion performance when coated and immersed in solution of 3.5% wt NaCl. The bare steels which had relatively higher corrosion resistance produced coated systems with longer protective lifes. On the other hand, bare steels which had relatively lower corrosion resistance produced coating systems with inferior quality. The 'cleanliness' of the steel is thus proposed as the probable cause for the differences found in the corrosion performance of both coated systems.

The part of the model refering to the interaction of water at the interface substrate-coating, Figure 6.1 (c) and (d) is a modified version of the model proposed by Funke[53]. In the model proposed in this work, however, the inclusions at the surface are considered.

1) For coatings with a closely packed structure, and free of defects or pinholes:

1.1) Permeation stage

(a) initially water and oxygen permeate through the coating.

(b) water and oxygen arrive at the interface.

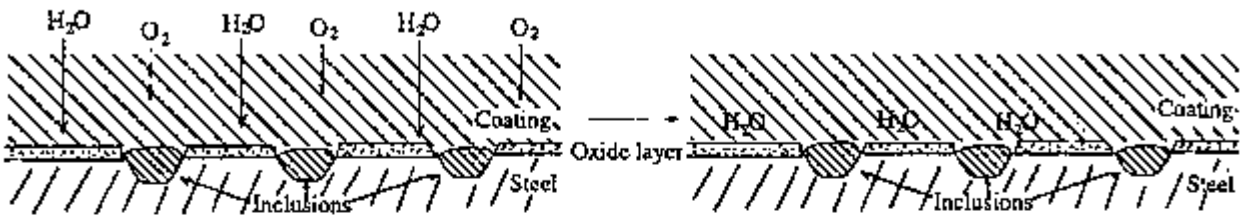

1.2) Interaction of water at the interface

(c) at low contents water may support passivation, or;

(d) at larger water concentrations lifting of the coating may occur as a result of blistering.

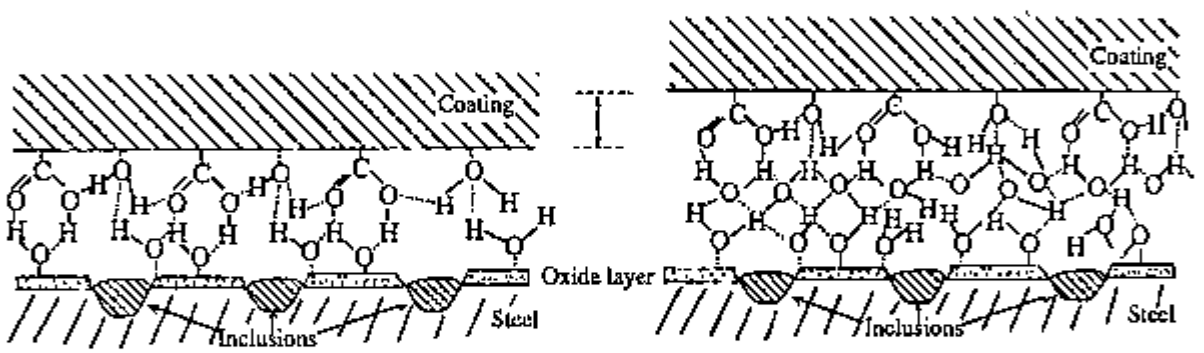

1.3) Initiation of corrosion

After the coating has lifted from substrate;

(e) water can accumulate at the interface and dissolve the oxide layer;

(f) corrosion is then started.

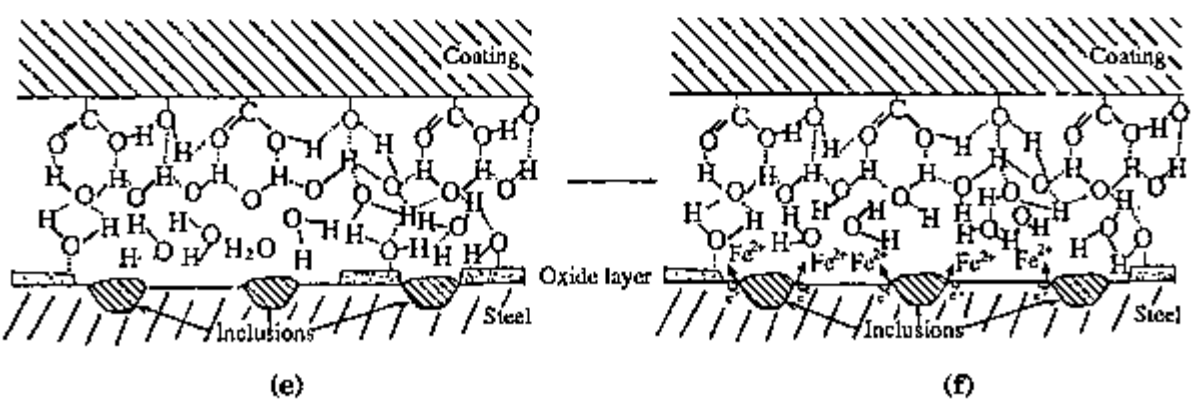

Figure 6.1 - Schematic representation of proposed model for the initiation of corrosion of coated metals under immersed conditions.

The interfacial regions between inclusions and substrate are more susceptible to the initiation of corrosion.

IN THE CASE OF SULPHIDE INCLUSIONS

The metal matrix surrounding the inclusion dissolves preferentially due to a microgalvanic effect where the sulphide inclusions are cathodic relatively to the surrounding metal.

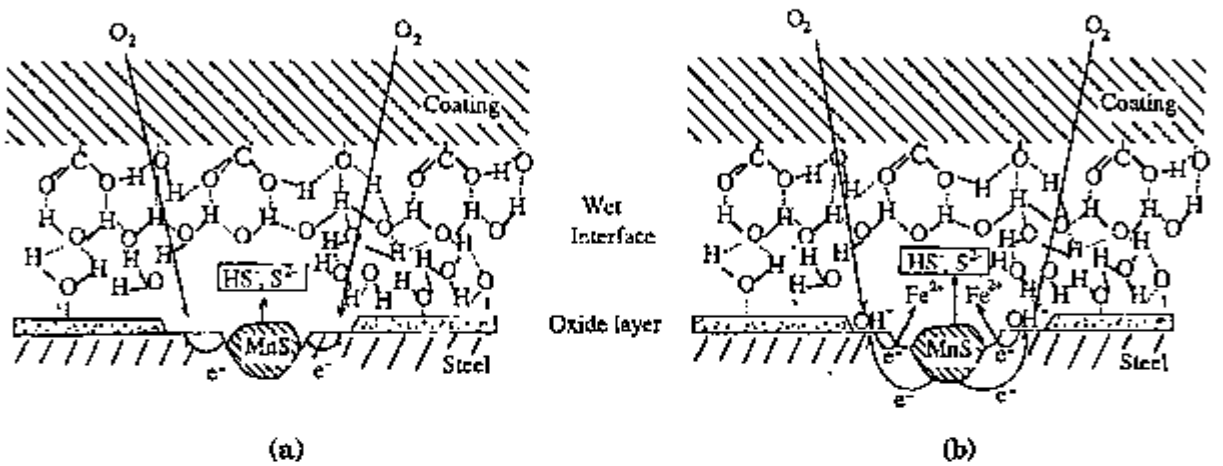

IN THE CASE OF OXIDE INCLUSIONS

The adhesion of the coating is impaired at the regions of irregularities at the surface. Water can accumulate in the 'free' spaces at the interface dissolving the air formed oxide film. Corrosion can then start at the exposed metal around the oxide inclusion.

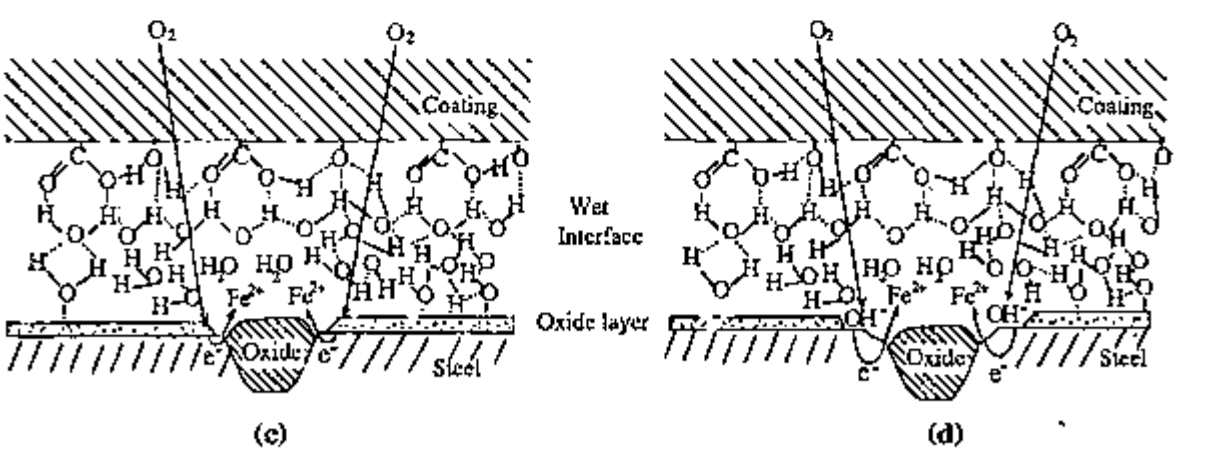

Figure 6.2 - Schematic representation of the effect of inclusions on the first stages of corrosion for the model proposed in this work.

For highly protective systems whose adhesive properties are maintained during the whole test period, the corroding site is covered by corrosion products which hinders the access of corrosive species to the metallic substrate and corrosion eventually stops.

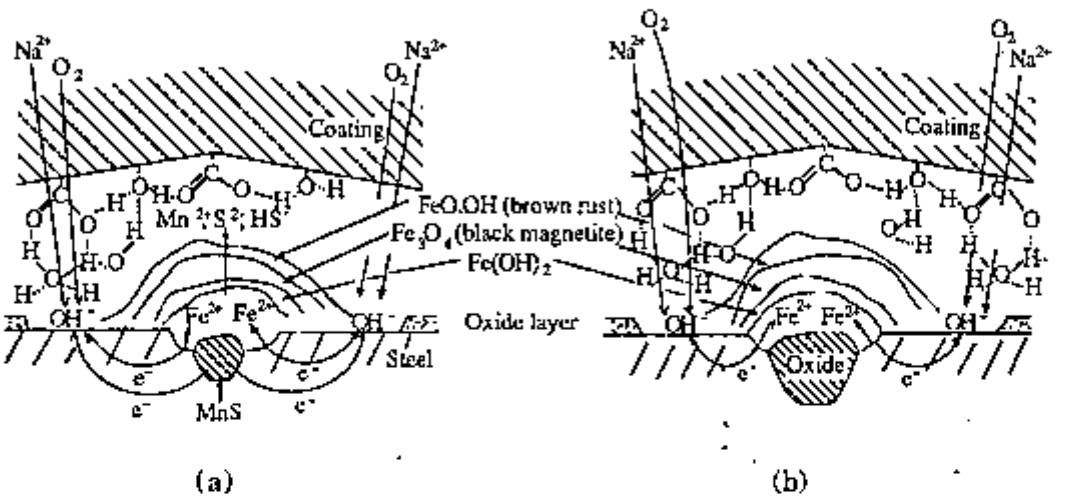

In the case of coatings whose protective characteristics are gradually lost during the duration of test , the continuation of corrosion leads to the formation of voluminous corrosion products which mechanically affect the adhesion coating-substrate and causing lift-off.

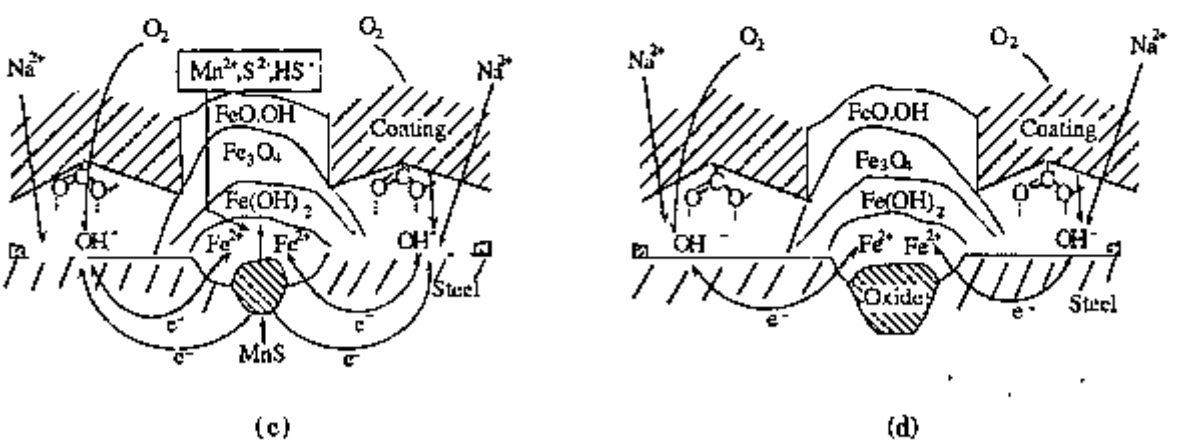

Figure 6.3 - Schematic illustration of the propagation of corrosion at areas surrounding the non-metallic inclusions for the model proposed.

2) In the case of coatings with defective areas at the beginning of the test or developed during the immersion period:

(a) water and oxygen have easy access to the metal substrate through the weak or defective areas of the coating;

(b) water locally dissolves the air formed oxide layer and corrosion then starts.

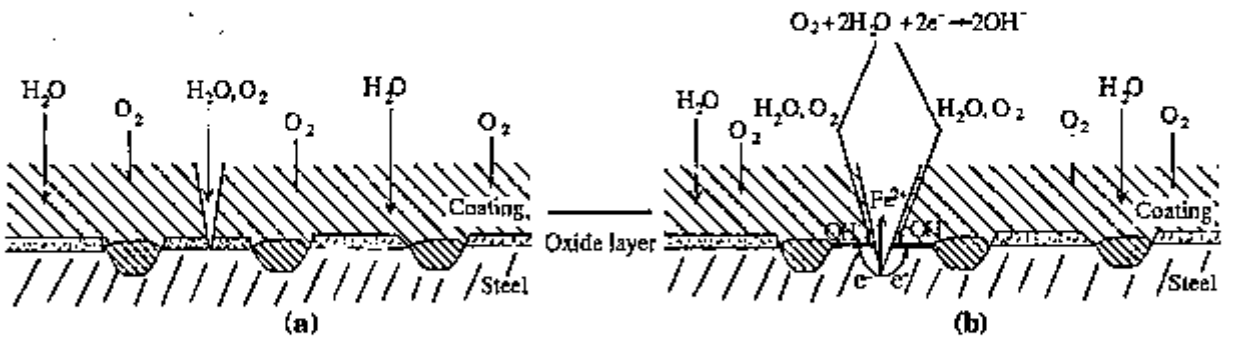

FOR HIGHLY PROTECTIVE SYSTEMS

Corrosion products are deposited on the defect or 'weak' spot and block it. The access of corrosive species to the substrate is hindered and due to the highly protective characteristics of the system, corrosion is limited to the defective area. The cathodic reaction is also limited to the areas surrounding corroding spot. Corrosion eventually stops.

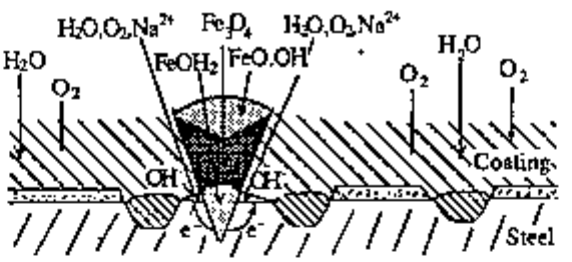

FOR LESS PROTECTIVE SYSTEMS

The coating is lifted from substrate and water can accumulate at the interface. The corrosion characteristics of the surface are believed to affect significantly the corrosion behaviour of the whole coated system.

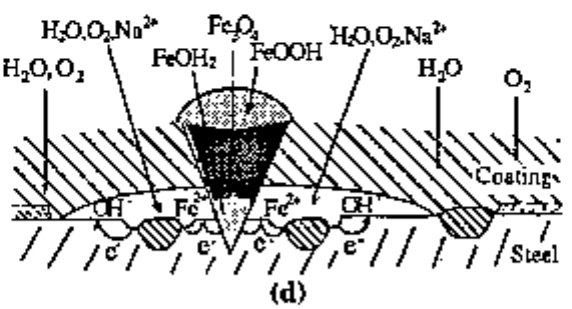

Figure 6.4 - Schematic illustration of the corrosion at defective areas of coating on steels.

6.2.3 - Coated specimens exposed to wet-dry cycles inside a cabinet

(1) Prohesion test

In this test the steels which produced the larger degree of deterioration were exactly the ones which exhibited improved corrosion performance when coated and tested under immersed conditions. This reveals that the conditions of test are of major importance in ranking the corrosion resistance properties of coated systems. However, since the steels provided by the same manufacturer produced similar deterioration features, this indicates that the microstructural similarities between these steels might have had a significant effect on their corrosion performance.

As mentioned previously, the similarities between the steels originating from the same producer were mainly their heterogeneities content. In the Prohesion test the differences in the degree and type of deterioration between the two sets of steels provided by the same maker were mainly shown as dissimilar degree of delamination and adhesion characteristics of the corrosion products formed upon cyclic exposure. It is then supposed that the different adhesion features of the corrosion products formed on the two group of steels, were primarily caused by their heterogeneity content at the surface. Larger delaminated areas and accelerated adhesion failure was associated with 'cleaner' steels, that is, steels with lesser inclusion contents. On the other hand, the steels which had relatively longer lifes also had larger inclusion contents.

It is proposed that the presence of larger heterogeneity content at the surface might have either allowed the cathodic reaction to occur on the exposed metal at the scratch or led to the initiation of localized corrosion on several points of the exposed substrate. The presence of a large number of MnS or mixed (MnS + oxide) inclusion at the exposed surface of some steels could have led to the location of the cathodic reaction on the bare metal, specifically on the inclusions surface. If the cathodic reaction occurs at the scratch less delamination results and consequently the loss of adhesion between coating and substrate is diminished.

The location of both reactions, anodic and cathodic, at the scratch leads to less damage at areas away from the exposed metal. Also, the accumulation of liquids at the interface is hindered in this case. The other possible effect of the inclusions on the corrosion performance is the stimulation of localized corrosion. The localized corrosion could have been beneficial in terms of adhesion characteristics of the corrosion products formed since these might also have been locally deposited on specific areas. The deposition of corrosion products on various localized areas might have acted as adhesion promoter by exerting an anchoring effect between the coating and the substrate. On the other hand, generalized corrosion might have contributed to the more generalized loss of adhesion found in the case of the 'cleaner' steels. Thus, it can be assumed that whereas a larger degree of steel 'cleanliness' seemed to be beneficial for the anti-corrosion properties of bare or coated steels under immersion conditions, the opposite effect was observed in the Prohesion test.

In the Prohesion test, it was also found that the mild steels produced a rust layer with slightly lower adhesion properties than its respective low-alloy steel match provided by the same manufacturer. Extensive published literature in this field[212-217] proposed that the addition of alloying elements in the low alloy steels, weathering steel types, mainly Cu, improves the protective characteristics of the rust layer formed during atmospheric exposure.

(2) Cabinet test with artificial acid rain solution

Since in this test no difference was observed between the various coated steels, it is evident that the aggressivity of the test environment has a major effect on the characteristics of the corrosion products formed. Thus, the ranking of the anti-corrosive properties of coated teelsis only valid under the specific conditions applied in the test. This is a significant shortcoming of some of the accelerated tests used for the evaluation of paints, especially when correlation with outdoor exposure is sought.

The indistinguishable results obtained by this test for the various steels analysed were supposed to have been caused by the corrosion of the steels in an acidic environment. The pH of the environment was supposed to be the main factor affecting the response which was different from the one obtained in the Prohesion test. It is known that in the acidic environment, the sulphide inclusions are easily dissolved exposing the metal matrix. If this occurred the situation was similar for all the steels tested, and the effect of the heterogeneities on the corrosion properties of the coated system was insignificant.

CHAPTER 7

CONCLUSIONS AND SUGGESTIONS FOR FURTHER WORK

7.1 - Conclusions

From the experimental results described in the previous chapters, the following conclusions can be drawn for the various tests:

7.1.1 - Bare steel surfaces

1. The two types of steels used, low-alloy steel and mild steel types, were not differentiated electrochemically under immersion and low polarized conditions.

2. Minor differences were observed between steels produced by two manufacturers. The slight differences were mainly detected by linear polarization resistance and electrochemical impedance techniques.

3. The cause for the dissimilarities was assumed to be the difference in the inclusions content of the steels produced by different manufacturers.

4. Differences were found between the two types of steels used at conditions far removed from the corrosion potential. The distinctions were related to the passivation characteristics of the two steel types used.

5. The low-alloy steel types passivated at higher polarization potentials, and at larger critical current densities than the mild steel types. Thus, the alloying elements shifted the active/passive transition towards more positive values.

6. The difference in the nature of the main inclusions on the two types of steels tested was also believed to be the cause for the dissimilar behaviour obtained in the high polarization conditions.

7. The current density at the 'passive' region, i_{pass}, increased with the Cu content of the steel. This is probably due to an enrichment of Cu at the surface during the dissolution of the metal matrix increasing the electric conductivity of the 'passive' layer, and therefore i_{pass}.

8. A distinct behaviour of the two steel types analysed was also found in the case of the steels exposed to the vapour phase of 10^{-2} M $NaHSO_3$ at 54° C. The low-alloy steels produced less voluminous and more compact corrosion products than the mild steels.

7.1.2 - Coated steels under immersed conditions

9. In the case of systems with highly resistive coatings and whose resistance was maintained throughout the testing period, the substrate did not have an effect on the corrosion behaviour of the system.

10. Differences were however found in the corrosion behaviour of the various coated steels used with fairly resistive coatings.

11. The distinction in the corrosion behaviour of the steels analysed were only detected by long term testing. This was due to the high resistance of the coating at the beginning of the immersion period.

12. An analogy seemed to exist between the corrosion behaviour of the bare and coated steels. The uncoated steel which displayed lower corrosion properties also showed faster deterioration in the corrosion properties when coated and under immersed conditions. On the other hand, the steel with longer protective

life also showed slightly higher corrosion resistance when its bare surface was electrochemically tested.

13. The substrate which had a shorter protective life when coated was the A-36, while the LAS II coated system lasted the longest. The steels A-36 and LAS II had the largest and lowest inclusions content, respectively.

14. The poor performance of the A-36 substrate when compared to the other substrates was probably due to its larger inhomogeneity content which consisted mainly of inclusions of MnS.

15. The sulphide type inclusions were assumed to take part in the corrosion processes underneath the coating and interfere with the behaviour of the coated system.

16. Large contents of oxide or mixed (oxide+sulphide) type inclusions are also believed to affect the corrosion characteristics of the steel. These correspond to regions of irregularities at the surface and are supposed to interfere with the adhesion of the coating to the substrate. Water can accumulate at these areas inducing corrosion and leading to earlier failure times than the 'cleaner' steels.

17. Steels with larger inclusions content were likely to be more susceptible to corrosion. This was the probable consequence of the larger number of corrosion nucleation sites which if associated with 'defective' areas of the coating might have allowed corrosion to continue. Consequently a larger concentration of ionic species at the interface could also have caused a larger diffusion of water due osmotic forces. The accumulation of water at the surface results in blistering and causes the loss of adhesion of the coating and subsequently corrosion can become generalized.

18. Localized corrosion was generally observed for the various systems analysed, and this was supposed to have started at 'weak' or 'defective' areas of the coating. The detection of Na species at the centre of a black corroded spot supported this observation.

19. When corrosion products grew locally, this might have led to an increasing mechanical stress at the interface and consequently to the enlargement of defects initially present in the coating.

20. The impedance response of the various systems was affected by the relation between intact and corroding area of the specimens. In the case of coatings with large proportion of unimpaired area relative to the deteriorating area, the impedance response was mainly that of the coating.

21. If the proportion between corroding and protective area is increased, and provided that the coating resistance is not too large, the effect of the corrosion on the impedance response might appear.

22. Delamination around corroding areas was caused by the high alkalinity generated by the cathodic reduction reaction. This was confirmed by XPS and Auger analysis which detected the presence of hydroxide species on the delaminated areas.

7.1.3 - Coated and scribed specimens exposed to wet and dry cycles inside cabinet

For the Prohesion test the following conclusions are put forward:

23. The steels produced by the same manufacturer which included the two types of steel used, mild steel and low-alloy steel types, showed similar deterioration features. Thus, the type of steel was not the main factor leading to

the distinct corrosion features found between the two sets of steels provided by different producers.

24. The distinguished deterioration features between two sets of steels provided by different makers was possibly caused by the variation in 'cleanliness' of these steels, that is, their inclusions content at the surface.

25. The steels A-36 and USI produced more adherent corrosion products than the steels MS and LAS II. On the other hand, the latter steels showed faster loss of adhesion and larger accumulation of solution at the interface.

26. The corrosion characteristics of the steels used improved in the following order: MS < LAS II < A-36 < USI.

27. XPS analysis on the coating side of the specimens tested confirmed the ranking above. The largest content of aggressive ions were obtained for the MS steel substrate, and the lowest, for the USI steel.

28. When steels supplied by the same maker were compared, the mild steel type of each group showed inferior corrosion characteristics than its low-alloy steel match. This was demonstrated by a faster deterioration of the system and slightly larger delaminated areas around the scratch. The presence of alloying elements, mainly copper, is thought to be the cause for the improved resistance of the low-alloy steels relatively to the mild steels under these conditions.

29. The corrosion properties of the steels analysed was dependent on the conditions of the test. The coated steels which resisted failure for longer times under immersion conditions were the same to show faster deterioration and larger loss of adhesion when tested under cyclic conditions inside a cabinet with controlled atmosphere.

30. No differentiation was found between the various steels tested inside a cabinet with wet and dry cycles and in an atmosphere simulating the acid rain of Manchester. Thus, the aggressive atmosphere of test is of major importance in ranking the anti-corrosion properties of steels as substrates for paint systems.

7.2 - Suggestions for further work

The present research raised some aspects on the effect of the substrate on the corrosion behaviour of coated systems which might require further work. These are outlined below:

1. A study of the effect of inclusions on the corrosion characteristics of bare steel surfaces is required. Surface analytical techniques such as Auger Spectroscopy should be useful to investigate the initiation sites of the corrosive attack and their relation to the inclusions at the surface.

2. Further studies on the influence of steel inclusions content on the subsequent behaviour of coated specimens under fully immersed conditions are suggested. The characteristics of the interface between the coating and the substrate should be looked at thoroughly. Methods that can be helpful in this examination are adhesion tests and surface analytical methods.

3. The inclusions sites and areas surrounding them need to be systematically analysed with immersion time. The development of corrosion on these heterogeneities and areas around them, might provide valuable information on their effect upon their correlation with the subsequent behaviour of the coated system.

4. The role of inclusions in stimulating localized corrosion and blistering by an electroendosmotic effect caused by the microgalvanic cells created requires investigation.

5. Studies examining how the steel 'cleanliness' at the surface affects the degradation behaviour of coated and scribed specimens exposed to cyclic tests in controlled atmospheres is suggested. Further work is needed to find out what is the role of the inclusions on the formation of adherent or loose corrosion products.

6. Steels with slight compositional differences and various heterogeneities content should be studied in order to correlate the inclusions content with the corrosion characteristics of coated steels, either under immersed conditions or scribed and exposed to cyclic tests inside cabinet. The Prohesion test is suggested as a good test for the ranking of coated steels with different heterogeneities content since this provided a clear distinction between the steels used in this research.

7. A further investigation might examine how an anti-corrosive pigment or a conversion coating would interact with the inclusions at the interface of the coated system.

REFERENCES

.) SCULLY, J. C.; "The Fundamentals of Corrosion", 3rd edn., Pergamon Press, 1990.

:) COPSON, H.R., and LARRABEE, C.P.; ASTM Bulletin, No. 242, (1959), 68.

:) SHREIR, L.L. ed.; "Corrosion", Vol. 1, 2nd edn., Newness-Butterworths, London, 1976.

:) BOCKRIS, J.O.M., and REDDY, A.K.N.; "Modern Electrochemistry", Vol. 2, Plenum Rosetta, New York, 1977.

:) WHITNEY, W.R.; J. Am. Chem. Soc., 25, (1903), 394.

:) TOMASHOV, N.D.; "Theory of Corrosion and Protection of Metals", Macmillan, New York, 1966.

:) POURBAIX, M.; "Atlas d'Equilibres Electrochemiques a 25° C.", Gauthier-Villar, Paris, 1963.

:) WRANGLÉN, G.; "An Introduction to Corrosion and Protection of Metals", Chapman and Hall, 1985.

:) STEWART, D., and TULLOCH, D.S.; "Principles of Corrosion & Protection" Macmillan, New York, 1968.

.0) EVANS, U.R., and TAYLOR, C.A.; Corr. Sci.; 12, (1972), 227.

.1) MANSFELD, F.; Corrosion, 44, No. 12, (1988), 856.

.2) LEIDHEISER Jr, H.; Corrosion, 38, No. 7, (1982), 374.

.3) DICKIE, R.A., and SMITH, A.G.; Chemtech., 10, (1980), 31.

4) TOMASHOV, N.D., MIKHAILOVSKII, Y.N., and LEONOV, V.V.; Corrosion, 20, (1964), 125t.

5) TOMASHOV, N.D., MIKHAILOVSKII, Y.N., and LEONOV, V.V.; ibid, 218t.

5) WALTER, G.W., Corr. Sci., 26, No.1, (1986), 27.

7) KITTELBERGER, W.W., and ELM, A.C.; Ind. Eng. Chem. Prod. Res. Dev., 38, (1946), 695.

:) MILLER, R.N.; Materials Protection, 7, (1968), 35.

(19) KOEHLER, E.L., Corrosion, 40, No. 1, (1984), 5.

(20) LEIDHEISER Jr.,H.; Corrosion, 39, No. 5, (1983), 189.

(21) FUNKE, W., LEIDHEISER Jr.,H., DICKIE, R.A., DINGER, H., FISCHER, W., HAAGEN, H., HERRMANN, K., MOSLÉ, H.G., OECHSNER, W.P., RUF, J., SCANTLEBURY, J.D., SVOBODA, M., and SYKES, J.M.; J. of Coatings Technology, 58, No. 741, (1986), 79.

(22) HOLTZMANN, K.A.; J. Paint Technol., 43, (1971), 47.

(23) KATZ, R., and MUNK, B.F.; J. Oil Colour Chem. Assoc., 52, (1969), 418.

(24) BROWNE, F.L., and FROEST, J.; Ind. Eng. Chem. Prod. Res. Dev., 4, (1954), 391.

(25) FUNKE, W.; Werkstoffe u. Korr., 20, (1969), 12.

(26) HUNT, O.L., HUFF, R.B., and SPENCER, H.G.; Off. Dig., 35, (1963), 113.

(27) CORTI, H., FERNANDEZ-PRINI, R., and GOMEZ, D.; Prog. Org. Coatings, 10, (1982), 5.

(28) FUNKE, W., and HAAGEN, H.; Ind. Eng. Chem. Prod. Res. Dev., 17, (1978), 50.

(29) FUNKE, W.; J. Oil Colour Chem. Assoc., 62, (1979), 63.

(30) D'ALKAINE, C.V., GARCIA, C., CORTI, J., and GOMEZ, D.; J. Oil Colour Chem. Assoc., 63, (1980), 23.

(31) MURRAY, J.D.; J. Oil-Colour Chem. Assoc., 56, (1973), 507.

(32) KENDIG, M., MANSFELD, F., and TSAI, S.; Corr. Sci., 23, (1983), 317.

(33) WALKER, P.; J. Oil Colour Chem. Assoc., 65, (1982), 415.

(34) WALKER, P.; ibid, 66, (1983), 188.

(35) MAYNE, J.E.O., and MILLS, D.J.; J. Oil Colour Chem. Assoc., 58, (1975), 155.

(36) LEIDHEISER Jr.,H.; and FUNKE, W.; J. Oil Colour Chem. Assoc., 5, (1987), 121.

(37) IEZZI, R.A., and LEIDHEISER Jr.,H.; Corrosion, 37, No.1, (1981), 28.

(38) SCHWAB, L.K., and DRISKO, R.W.; "Corrosion Control by Organic Coatings", (ed. LEIDHEISER Jr.,H.), NACE, (1981), 222.

(39) MANSFELD, F., LUMSDEN, J.B., JEANJAQUET, S.L.,and TSAI, S.; ibid, 227.

(40) RITTER, J.J., and KRUGER, J.; Surface Science, 96, (1980), 364.

(41) DICKIE, R.A., and FLOYD, F.; "Polymeric Materials for Corrosion Control", (eds. DICKIE, R.A., and FLOYD, F.L.,), Am. Chem.Soc., (1986).

(42) BACON, R.C., SMITH, J.J., and RUGG, F.M.; Ind. Eng. Chem. Prod. Res. Dev., 40, (1948), 161.

(43) MILLS, D.T., and MAYNE, J.E.O.; "Corrosion Control by Organic Coatings", (ed. LEIDHEISER Jr.,H.), NACE, (1981), 12.

(44) MILLS, D.T., and MAYNE, J.E.O.; J. Oil Colour Chem. Assoc., 67, (1984), 49.

(45) MAYNE, J.E.O., and MILLS, D.T.; J. Oil Colour Chem. Assoc., 65, (1982), 138.

(46) LEIDHEISER Jr.,H.; Prog. Org. Coatings, 7, (1979), 79.

(47) LEIDHEISER Jr.,H.; "Corrosion Mechanism" (ed. MANSFELD, F.,), Marcel Dekker Inc., New York, (1987), 165.

(48) GURUVIAH, S.; J. Oil Colour Chem. Assoc., 53, (1970), 669.

(49) HAAGEN, H., and FUNKE, W.; J. Oil Colour Chem. Assoc., 58, (1975), 359.

(50) BAUMANN, K.; Plaste Kautsch, 19, (1972), 694.

(51) MAYNE, J.E.O.; J. Oil Colour Chem. Assoc., 32, (1949), 481.

(52) MAYNE, J.E.O.; Research, 5, (1952), 278.

(53) FUNKE, W.; J. Oil Colour Chem. Assoc., 68, (1985), 229.

(54) PERERA, D.Y., and HEERTJES, P.M.; J. Oil Colour Chem. Assoc., 54, (1971), 313.

(55) MICHAELS, A.S.; Off. Dig., 37, (1965), 638.

(56) VALENTINE, L.; J. Polym. Sci., 27, (1958), 313.

(57) BRASHER, D.M., and NURSE, T.J.; J. Appl. Chem., 9, (1951), 96.

(58) MAYNE, J.E.O.; Trans. Inst. Met. Fin., 41, (1964), 121.

(59) KITTELBERGER, W.W., and ELM, A.C.; Ind. Eng. Chem. Prod. Res. Dev., 39, (1947), 876.

(60) GLASS, A.L., and SMITH, J.; J. Paint Technol., 38, No. 495, (1966), 203.

(61) YASEEN, M., and FUNKE, W.; J. Oil Colour Chem. Assoc., 61, (1978), 284.

(62) KITTELBERGER, W.W., and ELM, A.C.; Ind. Eng. Chem. Prod. Res. Dev., 44, (1952), 326.

(63) LEIDHEISER Jr.,H.; J. Coatings Technol., 53, No. 678, (1981), 29.

(64) MAITLAND, C.C., and MAYNE, J.E.O.; Off. Dig./ J. of Paint Technol. and Engineering, 34, (1962), 972.

(65) CHERRY, B.W., and MAYNE, J.E.O.; Proc. of 2nd Int. Cong. Met.Corr., New York, NACE, 1963, 680.

(66) KHULLAR, M., and ULFVARSON, U.; Proc. of 9th FATIPEC Congress, Brussels, 1968, Sec. 3, 165.

(67) ULFVARSON, U., and KHULLAR, M.; J. Oil Colour Chem. Assoc., 54, (1971),604.

(68) MALIK, W.U., and AGGARWAL, L.; J. Oil Colour Chem. Assoc., 57, (1974), 131.

(69) MAYNE, J.E.O., and SCANTLEBURY, J.D.; Br. Polym. J., 2, (1970), 240.

(70) PARKS, J. and LEIDHEISER Jr.,H.; Ind. Eng. Chem. Prod. Res. Dev., 25, (1986), 1.

(71) GEENEN, F.M., de WIT, J.H.W., and van WESTING, E.P.M.; Prog in Org. Coatings, 18, (1990), 299.

(72) HAMMOND, J.S., HOLUBKA, J.W., and DICKIE, R.A.; J. Coatings Technol.,51, (1979), 45.

(73) DICKIE, R.A.; "Critical Issues in Reducing the Corrrosion of Stee", (eds. LEIDHEISER Jr.,H., and HARUYAMA, S.), NACE, Nikko, Japan, 1985, 379.

(74) FUNKE, W.; Ind. Eng. Chem. Prod. Res. Dev., 24, (1985), 343.

(75) FUNKE, W.; J. Oil Colour Chem. Assoc., 69, (1986), 78.

(76) MIKHAILOVSKI, Y.N., ZUBOV, P.I., ZAVRAZHINA, V.I., NARIMOVA, S.F., SOKOLOVA, E.M., and SERAFIMOVICH, V.B.; 3rd Int. Congress Met. Corr., Moscow, 1966, Vol.3, 241.

(77) GARBER, YU, I., and ZUEV, YU, S.; Korroz. Zashch. Neftegasov Pronsti, 10, (1977), 16.

(78) WALKER, P., Off. Dig./J. of Paint Technol. and Engineering, 37, No. 491, (1965), 1561.

(79) SCHWENK, W.; 3R-International, 15, (1976), 389.

(80) RUGGERI, R.T., and BECK, T.R., "Adhesion Aspects of Polymeric Coatings", (ed. MITTAL, K.L.,) Plenum, New York, 1983, 329.

(81) BULLET, T.R., J. Oil Colour Chem. Assoc., 46, (1963), 441.

(82) McCAFFERTY, E., PRAVDIC, V., and ZETTLEMOYER, A.C.; Trans. Faraday Soc., 66, (1967), 1720.

(83) REINHARD, G.; Prog. Org. Coatings, 15, (1987), 125.

(84) FUNKE, W.; Prog. Org. Coatings, 9, (1981), 29.

(85) LECKIE, H.P.; "Process Industries Corrosion", NACE, 1975 , 90.

(86) LARRABEE, C.P., Corrosion, 9, (1953), 259.

(87) WIESTER, H.J., and TERNES, H.; Stahl und Eisen, 87, (1967), 746.

(88) SCHRAMM, G.N., TAYLERSON, E.S., and LARRABEE, C.P., Railway Age, 101, (1936), 780.

(89) JONES, J.A.; J. Iron and Steel Inst., 135, No.1, (1937), 137.

(90) LAQUE, F.L.; Proc. of Am. Soc. Testing Mats., 51, (1951), 495.

(91) LARRABEE, C.P., and COBURN, S.K.; 1st Int. Cong. on Metallic Corrosion, London, 1961, 276.

(92) HUDSON, J.C.; J. Iron and Steel Inst., 135, No.1, (1937), 137.

(93) HUMBLE, H.A.; Corrosion, 5, (1949), 292.

(94) SPELLER, F.N.; "Corrosion Causes and Prevention", McGraw-Hill Book Co., New York, 1951, 322.

(95) EVANS, U.R.; "An Introduction to Metallic Corrosion", Edwards Arnold & Co., New York, 3rd edn, 1981.

(96) LAQUE, F.L., and BOYLAN, J.A.; Corrosion, 9, (1953), 237.

(97) THE AMERICAN SOCIETY FOR METALS, Metal Progress, 88, August, 1965, 141.

(98) SCHMITT, R.J., and MATHAY, W.L.; Materials Protection, 6, No. 9, (1967), 37.

(99) FANCUTT, F., and HUDSON, J.C.; Corrosion, 8, (1952), 366.

(100) CLEARY, H.J., and GREENE, N.D.; Corr. Science, 7, (1967), 821.

(101) de SOUZA, J.G.; MSc. Thesis, UMIST, 1980.

(102) POURBAIX, M.; Corr. Sci., 5, (1965), 677.

(103) BANNISTER, L.C., and EVANS, U. R.; J. Chem. Soc., (1930), Part I, 1361.

(104) HARING, H.E., and GIBNEY, R.B.; Trans. Electr. Soc., 76, (1939), 287.

(105) WHITBY, L.; Paint Research Association, Technical Paper No. 125, 1939.

(106) ZAHN, H.; Corrosion, 3, (1947), 233.

(107) WORMWELL, F., and BRASHER, D.M.; J. Iron and Steel Inst., 162, (1949), 129.

(108) WORMWELL, F., and BRASHER, D.M.; J. Iron and Steel Inst., 164, (1950), 141.

(109) GREENE, N.D.; "Experimental Electrode Kinetics", Rensselaer, New York, 1965, 43.

(110) MAYNE, J.E.O.; Chem. Ind., (1951), 293.

(111) YAKUBOVITCH, S.V., NITSBERG, L.V., and KARYAKINA, M.I.; Proc. of 6th Int. Conf. on Electrodepos. and Metal Finishing, London, 1964, 321.

(112) WINKLER, K., and TASCHOW, H.J.; Plaste Kautsch., 11, (1964), 381.

(113) GRUBITSCH, H., HECKEL, K., and MONSTAD, O.; Farbe Lacke, 70, (1964), 167.

(114) WOLSTENHOLME, J.; Corr. Sci., 13, (1973), 521.

(115) FAIDI, S.E., COSTA, I., HEPBURN, B.J., and SCANTLEBURY, J.D.; "Advances in Corrosion Protection by Organic Coatings", (eds. Scantlebury, J.D., and Kendig, M.), Cambridge, 1989, 212.

(116) SIEBERT, O.W., "Laboratory Corrosion Tests and Standards", ASTM STP 866, (eds. HAYNES, G.S., and BABOIAN, R.), ASTM, Philadelphia, 1985, 65.

(117) DEAN, S.W., FRANCE, W.D., and KETCHAM, S.J.; "Handbook on Corrosion Testing and Evaluation, John Wiley & Sons, New York, 171.

(118) STERN, M., and GEARY, A.L.; J. Electrochem. Soc., 104, (1957), 56.

(119) BANDY, R.; Corr. Sci., 20, (1980), 1017.

(120) IJSSELING, F.P.; Br. Corros. J., 21, No.2, (1986), 95.

(121) MANSFELD, F.; Corrosion, 29, (1973), 397.

(122) DEARNALAY, G.; Corrosion, 34, No. 1, (1978), 20.

(123) MANSFELD, F.; Corrosion, 32, (1976), 143.

(124) WOLYNECK, S., and ESCALANTE, E.; Corrosion, 36, No. 7, (1980), 327.

(125) AZZERI, N., BRUNO, R., and SPLENDORINI, L.; Corr. Sci., 21, No. 11, (1981), 781.

(126) CLAY, H.F.; J. Oil Colour Chem. Assoc., 48, (1965), 356.

(127) CALLOW, L.M., RICHARDSON, J.A., and DAWSON, J.L.; Br. Corros. J., 11, No. 3, (1976), 123.

(128) CHANCE, R.L., SCHREIBER, T.P., and FRANCE Jr., W.D.; Corrosion, 31, 1975, 296.

(129) LIZLOVS, E.A., and BOND, A.P.; J. Electrochem. Soc., 122, (1975), 719.

(130) MacDONALD, D.D.; "Critical Issues in Reducing the Corrosion of Steel", (eds. LEIDHEISER Jr.,H., and HARUYAMA, S.), NACE, Nikko, Japan, 1985, 326.

(131) MacDONALD, D.D.; Corrosion, 46, No.6, (1990), 229.

(132) LEDERMAN, W.; "Complex Numbers", Routledge and Kegan, London, 1962.

(133) BROPHY, J.J.; "Basic Electronics for Scientists", MacGraw-Hill, New York, 1977.

(134) RANDLES, J.E.B.; Discuss. Faraday Soc., 1, (1947), 11.

(135) SLUYTERS-REBACH, M., and SLUYTERS, J.H.; Electroanalytical Chem., Vol 4, Ch.1, Dekker, New York, 1969.

(136) EPELBOIN, I., and KEDDAM, M.; J. Electrochem. Soc., 117, (1970), 1052.

(137) EPELBOIN,I., and KEDDAM, M.; Electrochim. Acta, 17, (1972), 177.

(138) COLE, K.S., and COLE, R.H.; J. Chem. Phys., 9, (1941), 341, ibid, 10, (1942) 98.

(139) SCANTLEBURY, J.D., and HO, K.N.; J. Oil Colour Chem. Assoc., 62, (1979), 89.

(140) MANSFELD, F., KENDIG, M.W., and TSAI, S.; Corrosion, 38, (1982), 478.

(141) BEAUNIER, L., EPELBOIN, I., LESTRADE, J.C., and TSAI, S.; Surface Technol., 4, (1976), 237.

(142) MIKHAILOVSKII, Y.N., LEONOV, V.V., and TOMASHOV, N.D.; Korr. Met. and Spanov. British Lending Library Translation, (1965), 202.

(143) WALTER, G.W.; J. Electroanal. Chem., 118, (1981), 259.

(144) WALTER, G.W.; Corr. Sci., 26, No.9, (1986), 681.

(145) BURSTEIN, G.T., GAO, G., and MAYNE, J.E.O.; J. Oil Colour Chem. Assoc., 72, 10, (1989), 407.

(146) JOHN, D.G; PH.D Thesis, UMIST, 1979.

(147) MANSFELD, F., and KENDIG, M.; Proc. of 9th. Int. Cong. on Metallic Corrosion, Vol III, Toronto, Canada, June, 1984, 85.

(148) SZAUER, T.; Prog. Org. Coatings, 10, (1982), 171.

(149) van MEIRHAEGHE, R.L., DUTOIT, E.C., CARDON, F., and GOMES, W.P.; Electrochim. Acta, 20, (1975), 995.

(150) LORENZ, W.J., and MANSFELD, F.; Corr. Sci., 21, (1981), 647.

(151) SUSSEX, G.A.M., and SCANTLEBURY, J.D.; Proc. of 9th Int. Cong. on Met. Corr.; Vol 3, Toronto, Canada, 1984, 85.

(152) HUBRECHT, J., VEREECKEN, J., and PIENS, M.; J. Electrochem. Soc., 131, (1984), 2010.

(153) SATO, Y.; Prog. Org. Coatings, 9, (1981), 85.

(154) HEPBURN, B.J., GOWERS, K.R., and SCANTLEBURY, J.D.; Br. Corros. J., 21, No. 2, (1986), 105.

(155) CALLOW, L. M., and SCANTLEBURY, J. D.; J. Oil Colour Chem. Assoc., 64, (1981), 119.

(156) BEAUNIER, L., EPELBOIN, I., LESTRADE, J.C., and TAKENOUTI, H.; Surf. Technol., 4, (1976), 4.

(157) SCANTLEBURY, J.D., and SUSSEX, G.A.M.; Proc. of Conf. on Corrosion Control by Organic Coatings; Bethlehem, Pa, 1980, 235.

(158) HEPBURN, B.J., CALLOW, L.M., and SCANTLEBURY, J.D.; J. Oil Colour Chem. Assoc., 67, (1984), 193.

(159) MANSFELD, F., JEANJAQUET, S.L., and KENDIG, M.W.; Corr. Sci., 26, (1986), 735.

(160) HUBRECHT, J., and VEREECKEN, J.; J. Electrochem. Soc., 132, (1985), 2886.

(161) PICAUD, Th., DUPRAT, M., and DABOSI, F.; "Electrochemical Methods in Corrosion Research", (ed. DUPRAT, M.), Materials Science Forum, Vol.8, 1986, 303.

(162) TITZ, J., WAGNER, G.H., SPÄHN, H., EBERT, M., JÜTTNER, K., and LORENZ, W.J.; Corrosion, 46, No.3, (1990), 989.

(163) FELIU, S., GALVAN, J.C., and MORCILLO, M.; Corr. Sci., 30, No.10, (1990), 989.

(164) FAIDI, S.E., and SCANTLEBURY, J.D.; J. Electrochem. Soc., 136, No.4, (1989), 990.

(165) GHOSH, P.K.; "Introduction to Photoelectron Spectroscopy", John Wiley & Sons, 1983.

(166) BAKER, A.D., and BETTERIDGE, D.; "Photoelectron Spectroscopy - Chemical and Analytical Aspects", Pergamon Press, 1972.

(167) BRUNDLE, C.R., and BAKER, A.D.; "Electron Spectroscopy: Theory, Techniques and Applications, Academic Press, 1977.

(168) BALLARD, R.E.; "Photoelectron Spectroscopy and Molecular Orbital Theory", Adam Hilger Ltd., 1978.

(169) CASTLE, J.E.; Surface Science, 68, (1977), 586.

(170) BAER, D.R.; Applications of Surface Science, 20, (1985) 382.

(171) FLEWITT, P.E.J., and WILD, R.K.; "Microstructural Characterisation of Metals and Alloys", The Institute of Metals, 1986, 136.

(172) HAMMOND, J.S., HOLUBKA, J.W., deVRIES, J.E., and DICKIE, R.A.; Corr. Sci., 21, No.3, (1981), 239.

(173) DICKIE, R.A., HAMMOND, J.S., and HOLUBKA, J.W.; Ind. Eng. Chem. Prod. Res. Dev., 20, (1981), 339.

(174) STOCKBRIDGE, C.D., SEWEL, P.B., and COHEN, M.; J. Electrochem. Soc., 108, (1961), 928.

(175) NAGAYAMA, M., and COHEN, M.; J. Electrochem. Soc., 109, (1962), 781.

(176) GILROY, D., and MAYNE, J.E.O.; Br. Corrosion J., 1, (1965), 102.

(177) OKADA, H., HOSOI, U., and NAITO, H.; Corrosion, 26, (1970), 429.

(178) UHLIG, H.H.; "Corrosion and Corrosion Control", John Wiley & Sons, New York, 3rd Printing, 1965, 144.

(179) KESTERNICH, W.; Stahl U. Eisen, 71, (1951), 587.

(180) KUTZELNIGG, A.; Werkstoffe und Korrosion, 14, (1963) 181.

(181) EDWARDS, J.; Trans. Inst. Met. Finishing, 35, (1958), 55.

(182) BARTON,K., and MAREK, V.; Werkstoffe und Korrosion, 21, (1970) 182.

(183) LEGAULT, R.A., MORI, S., and LECKIE, H.P.; Corrosion, 29, No.5, (1973), 169.

(184) JUETTNER, K., LORENZ, W.J., KENDIG, M.W., and MANSFELD, F.; J. Electrochem. Soc., 135, (1988), 332.

(185) FAIDI, S.E., MSc.Thesis, UMIST, 1986.

(186) MUNGER, C.G., in "Corrosion Prevention by Protective Coatings", NACE, Houston, 1985, 92.

(187) Federation Series on Coating Technology, Unit Five, Alkyd Resins.

(188) LAMBOURNE, R., "Paint and Surface Coatings: Theory and Practice", Ellis Horwood Ltd, 54.

(189) MARTENS, C.R.; "Alkyd Resins", Reinhold Publishing Corporation, New York, 1961.

(190) NACE Technical Report Commitee, Materials Protection, 4, No.9, (1965), 82.

(191) VERNON, W.H.; J. Iron Steel Inst., 196, (1960), 333.

(192) MISAWA, T.; Corr. Sci., 14, (1974), 279.

(193) SUZUKI, I., HISAMATSU, Y., and MASUKO, N.; J. Electrochem. Soc., 127, No.10, (1980), 2210.

(194) FUKUSHIMA, T., SATO, N., and MATSUSHIMA, I.; Proc. of Symp. on Atm. Corr., Florida, USA, 1980, 563.

(195) ROSALES, B.M., AYLLON, E.S., BONARD, R.T., GRANESE, S.L., and IKEHARA, J.; Proc. of 8th Int. Congress on Metallic Corrosion, Mainz, 1981, 317.

(196) EKLUND, G.; "Localized Corrosion"; (eds. STAEHLE, R.W., BROWN, B.F., KRUGER, J., and AGRAWAL, A.), NACE-3, (1971), 477.

(197) WRANGLÉN, G.; idem, 462.

(198) MANSFELD, F.; "Electrochemical Techniques for Corrosion", (ed. BABOIAN, R.), NACE, Technical Committee T-3L, 1976, 18.

(199) McINTYRE, N.S.; "Practical Surface Analysis by Auger and X-Ray Photoelectron Spectroscopy", (eds. BRIGGS, D. and SEAH, M.P.), John Wiley & Sons, 1983, 397.

(200) WRANGLÉN, G.; Corr. Sci., 14, (1974), 331.

(201) ELLINGER, M.L.; J. Oil Colour Chem. Assoc., 62, (1979), 136.

(202) BARRACLOUGH, J., and HARRISON, J.B.; J. Oil Colour Chem. Assoc., 48, (1965), 341.

(203) WILLIAMS-WYNN, D.E.A.; J. Oil Colour Chem. Assoc., 60, (1977), 263.

(204) LYON, S. B., THOMPSON, G. E., JOHNSON, J. B., WOOD, G. C., and FERGUSON, J.M., Corrosion, 43, No.12, (1987), 719.

(205) LYON, S.B., and GUEST, N., "Advances in Corrosion Protection by Organic Coatings", (eds. SCANTLEBURY, J.D., and KENDIG, M.), Cambridge, 1989, 129.

(206) HARRISON, J.B., and TICKLE, T.C.K.; J. Oil Colour Chem. Assoc., 45, (1962), 571.

(207) TIMMINS, F.D., J. Oil Colour Chem. Assoc., 62, (1979), 131.

(208) TRETHEWEY, K.R., and CHAMBERLAIN, J.; "Corrosion for students of Science and Engineering", Longman Scientific & Technical, 273.

(209) SVOBODA, M., and MLEZIVA, J.; Prog. Org. Coatings, 2, (1973/74), 207.

(210) SKERRY, B.S., ALAVI, A., and LINDGREN, K.I.; J. of Coat. Tech., 60, No.765, (1988), 97.

(211) WIGGLE, R.R., SMITH, A.G., and PETROCELLI, J.V.; J. Paint Technol., 40, (1968), 174.

(212) COPSON, A.R.; Proc. Am. Soc. Test. Mater., 45, (1945), 554.

(213) OKADA, H., HOSOI, Y., YUKAWA, K., and NAITO, H.; Proc. of 4th Int. Cong. on Met. Corros., Extended Abstracts, Amsterdam, Sept., 1969, 69

(214) SUZUKI, I., HISAMATSU, Y., and MASUKO, N.; J. Electrochem. Soc., 127, No. 10, (1980), 2210.

(215) MISAWA, T., KYUNO, T., SUETAKA, W., and SHIMODAIRA, S.; Corr. Science, 11, (1971),35.

(216) MISAWA, T., ASAMI, K., HASHIMOTO, K., and SHIMODAIRA, S.; Corr. Science, 14, (1974), 131 and 279.

(217) STRATMANN, M., BOHNENKAMP, K., and RAMCHANDRAN, T.; Corr. Science, 27, No. 9, (1987), 905.

(218) BARTON, K., KUCHYNKA, D., and BERANEK, E.; Werkstoffe und Korrosion, 29, (1978), 199.

(219) HOSPADARUK, V., HUFF, J., ZURILLA,R.W., and GREENWOOD, H.T.; SAE Technical Paper Series 780186

(220) STANDISH, J.V.; Ind. Eng. Chem. Prod. Res. Dev., 24, (1985),357.

(221) JORDAN, D.L., in "Advances in Corrosion Protection by Organic Coatings", (eds. SCANTLEBURY, J.D., and KENDIG, M.), Cambridge, 1989, 30.

(222) HOCH, G.M.; in "Localized Corrosion", (eds. STAEHLE, R.W.,BROWN, B.F., KRUGER, J., and AGRAWAL, A.), NACE, Houston, 1974, 117.

(223) BOLGER, J.C., and MICHAELS, A.D.; in "Interface Conversion for Polymer Coatings", (eds. WEISS, P., and CHEEVER, G.D.), Elsevier, New York, 1968, 12.

(224) JOHNSON, J.B., et al., European Cultural Heritage, EEC, 2 (4), August 1988, 13.